CELLULAR AND MOLECULAR FOUNDATIONS OF MAMMARY BRANCHING MORPHOGENSIS

By
Robert J. Huebner

A dissertation submitted to Johns Hopkins University in conformity with the requirements for the degree of Doctor of Philosophy

Baltimore, Maryland
May 2015

Abstract

Epithelial tubes provide the compartmentalization required for processes such as fluid and gas exchange, nutrient absorption, secretion, and waste elimination. Decades of study have provided insight into the genetic and molecular regulators of mammalian tube formation, but internal development left us with an incomplete understanding of how cells respond to these signals to build epithelial organs. Using organotypic culture of primary mouse mammary epithelium and time-lapse microscopy we were able to study mammalian epithelial morphogenesis in real-time at subcellular resolution. This allowed us to identify the cellular and molecular mechanisms that underlie epithelial stratification and elongation.

Mammary ducts transition from a simple polarized state to low-polarity stratified architecture at the onset of development. The low-polarity stratified epithelium then functions as the elongation front during mammary branch elongation. We determined that stratification was initiated by a novel vertical cell division of apically localized epithelial cells in culture and in vivo. The vertical divisions also directly resulted in the polarity-loss that is associated with the stratified epithelium. We then showed that this developmental mechanism of stratification could be hijacked in response to acute oncogene activation during the initial steps of tumor formation.

To determine the cellular mechanism of mammary duct elongation we tracked the migration of individual cells within the epithelium. We found that cells at the elongation front displayed a significant increase in cell motility. When we decreased cell motility by

inhibition of Rac we found that branches stopped elongating. The high motility cells were specifically enriched for high levels of mitogen-activated protein kinase (MAPK) signaling and MAPK signaling was required for branching. Mosaic expression of an activated mitogen-activated protein kinase kinase (MEK), a member of the MAPK cascade, was sufficient to induce branch elongation in the absence of external stimulation. We concluded that mammary branches are elongated by a subset of actively migrating epithelial cells and that the increase in cell motility is driven by MAPK signaling. Finally it is worth noting that collective cell migration through aberrant MAPK signaling is a key feature of tumor progression and here we show that MAPK signaling also drives collective cell migration in normal epithelium.

Acknowledgments

First I would like to acknowledge the 2009 Biochemistry, Cell and Molecular Biology (BCMB) graduate class. It has been great to be associated with this group of students; we studied for orals together, attended each other's weddings, and now text pictures of our kids. You have made graduate school fun and will be lifelong friends.

I want to thank my thesis committee for their time and insightful comments on my research. My committee has included chair Deborah Andrews as well as Carolyn Machamer, Takanari Inoue, Denise Montell, and Steven Leach. I am including a special thanks to Carolyn who is the BCMB director and has spent a tremendous effort on the success of the program and its students. Carolyn has also found time to attend my thesis meetings, review my CV, write recommendations, and read this thesis.

During my time in the Ewald Lab I have had the opportunity to work with a number of great colleagues. Kim-Vy Nguyen-Ngoc, known as Vy, and I drove to our BCMB interview together, were accepted to Hopkins and were Andy's first two graduate students (Vy was first). Shortly after Vy and I joined the lab Eliah Shamir and Kevin Cheung, M.D. joined and the four of us were the first class of researchers to cycle through the Ewald lab. With a combination of scientific enthusiasm, competitiveness, and drive the four of us pushed each other to a level of success that could not have been achieved without each of our personalities and presence.

As the first four of us are moving to our next positions Andy has collected a new contingent of great students. Neil Neumann, Dan Georgess, Ph.D., Vanesa Silvestri, Orit Katarina Sirka, and Veena Padmanaban are the second class of Ewald researchers and they clearly will continue to do awesome research. We have had two outstanding lab managers, Jenifer Beck and Amanda Fairchild, who are the true hero's of the lab as they provided the foundation that the rest of our research is built on. I also have to thank Ryan Gray, a temporary postdoc and friend, who taught Vy, Eliah, Kevin, and I when we joined Andy's lab.

Andy has been a great mentor and I credit most of my graduate success to his guidance, scientific intelligence, and motivational abilities. Andy has a keen aptitude for developing individual mentorship approaches for each of his students. In my case this involved moderate to severe berating every few months and the expectation that I would produce work well beyond my own expectations. This approach worked and resulted in a needed boost in my self-confidence as I learned what I was capable of. Because of Andy I feel prepared and capable to pursue a career in scientific research.

I would not have made it to college without a tremendous effort from my mother who was a single parent raising two boys after the untimely passing of my father. My mother pushed academics and when she found out I am learning disabled she worked hard to make sure I had the proper tutors, testing, and educational environment to succeed. During times when I clearly gave up on school my mom kept pushing me down the correct track. My finishing grad school is a true credit to her as a loving parent. I also

have to thank my brother Justin for being a good mentor and now for being one of my best friends. There is no better person than Justin and I love the fact that he pretends to be interested in my research.

My final thanks goes to my wife Meredith. Meredith has allowed me to pursue my career goals despite major inconvenience to her own life. She has put up with crazy work hours, little income, bad apartments, and sometimes an overly stressed and under involved husband. In return Meredith has been the breadwinner, commuted hours to and from work, kept me sane and has also given me two beautiful sons. Now she is allowing me to drag our family halfway across the country for the next phase of my carrier. I do not deserve such a wonderful wife and hope someday I can repay her for sacrificing so much so that I can pursue my passion for science.

Table of Contents

List of Figures

Chapter 1

Introduction: Cellular Foundations of Mammary Tubulogenesis

(Modified form Huebner and Ewald, Semin. Cell Dev. Biol. 2014)

Abstract:

The mammary gland is composed of a highly branched network of epithelial tubes embedded within a complex stroma. The mammary epithelium originates during embryonic development from an epidermal placode. However, the majority of ductal elongation and bifurcation occurs postnatally, in response to steroid hormone and growth factor receptor signaling. The process of pubertal branching morphogenesis involves both elongation of the primary ducts across the length of the fat pad and a second wave of secondary branching that elaborates the ductal network. The architecture of the mammary epithelium during periods of active morphogenesis is stratified, with extensive proliferation and incomplete apico-basal polarity. In this review we discuss recent advances in our understanding of the relationship between epithelial architecture, epithelial polarity, and ductal elongation.

Introduction

The mammary gland is composed of bilayered tubes embedded within an adipocyte rich stroma. The epithelial cells that constitute these tubes are connected to each other by extensive intercellular junctions and have a high degree of apico-basal polarity. This polarity is manifested both by morphological specializations, such as apically-localized microvilli, and by segregated membrane domains containing distinct apical and basal polarity complexes[1,2,3]. These adhesive junctions must be remodeled for either individual or collective cell movement to occur. The strong apico-basal polarity also places constraints on tubulogenesis, as many of the molecular determinants of epithelial polarity serve distinct roles in migratory cells[1]. In this review, we will focus on the cellular mechanisms used by the mammary epithelium to build and elaborate the ductal network during puberty. Other authors have reviewed the genetic requirements for mammary gland formation[4] and the cellular steps in embryonic mammary development[5,6].

1.1 Embryonic origins of the mammary epithelium

Mammary ducts in the adult have a bilayered organization, with keratin-14+ (K14+) myoepithelial cells positioned basally relative to the K8+ luminal epithelial cells. In contrast, the embryonic mammary epithelium originates as an epidermal placode and invades into the mesenchyme with a stratified organization and without a morphologically evident lumen[7] (Figure 1A). Both the cell type specific gene expression and relative positioning of myoepithelial and luminal epithelial cells are late features that are acquired progressively during fetal and early postnatal development[8,9,10]. As the mammary bud initiates elongation, many of the epithelial cells are K8+K14+ and K14+ cells are detected in both basal and interior positions[8,11]. It is only late in fetal

development that a mature lumen forms, lined with K8+ luminal epithelial cells and surrounded by basally positioned K14+ cells[7,11]. Myoepithelial cells are named for their contractile properties, which are regulated by genes such as smooth muscle actin (SMA). This contractile gene expression program is activated postnatally and so the mature myoepithelial phenotype of K8-K14+SMA+ is not established until the onset of puberty[9]. Taken together, the embryonic mammary epithelium during morphogenesis is stratified, lacks a contiguous lumen, and is composed of cells with combinations of "cell type specific" gene expression that are uncommon in adult ducts. While the result of embryonic mammary development is a small network of polarized simple ducts, the organization of the epithelium during morphogenesis is neither simple nor polarized[7] (Figure 1-1A).

1.2 Postnatal branching morphogenesis of the mammary epithelium: Figure 1B

The mammary epithelium finishes fetal development as fully polarized bilayered ducts[7]. These simple tubes are then essentially quiescent until the rise in steroid hormones that triggers the onset of puberty[12,13] (Figure 1-1B). Before puberty the mammary ducts are all simple (Figure 1-2A,A') and they then stratify to produce stratified terminal end buds[14,15,16] (TEBs) (Figure 1-2B,B'). Terminal end buds have multiple layers of epithelial cells, referred to as body cells, surrounded by a basally positioned cap cell layer[15,16]. Most body cells stain positive for luminal epithelial markers, such as K8 and E-cadherin[17]. However, there are basal marker positive body cells as well[18,19]. Cap cells stain positive for basal cytokeratins and P-cadherin[17]. Consistent with the organization of the embryonic mammary epithelium, the body cells exhibit high levels of proliferation,

have few intercellular junctions, and incomplete apico-basal polarity[19,20]. Many body cells lack contact with either the main lumen or the basement membrane and isolated microlumens are observed within the body cell region[19,20], similar to the microlumens observed in the early fetal mammary ducts[7] (Figure 1-1A vs. 1-2C'). TEBs form in response to iterative signals exchanged between the epithelium and surrounding mesenchymal cells, mediated through both steroid hormone receptors and growth factor receptors[4,12,13].

TEBs begin elongating at the onset of puberty, 3 weeks of age in mice. These stratified TEBs build centimeters of ducts as they cross the mammary fat pad and there is an abrupt transition from the stratified organization of the TEB to the simple organization of the trailing duct (Figure 1-2C,C')[16,19]. A secondary wave of side branching initiates a couple of weeks later and fills in the complexity of the network (Figure 1-1B). The details of the branching pattern are highly variable and can be quite distinct even when comparing different glands in the same mouse. Common themes emerge at a more global level: TEBs stop elongating and revert to simple epithelial architecture when they reach the edges of the mammary fat pad. The result is a similar openness in the branching pattern across mice of the same strain. Classic experiments inferred a characteristic avoidance of TEBs from each other and also demonstrated that implanted beads soaked in TGF-β1 would locally inhibit TEB elongation[21]. Taken together these data suggest the existence of a diffusible negative cue that locally represses branching and that the signal could be TGF-β1 mediated. Modern investigations into the nature of intercellular communication among mammary epithelial cells revealed that their geometric organization predicted new

sites of growth and that regions of repression of growth were dependent on TGF-β1 signaling[22]. Genetic analysis of dozens of different alleles has demonstrated a rich molecular network regulating both the initiation and elongation of mammary ducts. We often conceptualize of cellular decisions being regulated by single "master regulators". However, both the pubertal and lactational differentiation of the mammary gland are regulated by both the levels and timing of hormones, including estrogen, progesterone, prolactin, and growth hormone[23,24]. Genetic experiments have also demonstrated a requirement for FGFR1, FGFR2, ErbB1, ErbB2, ErbB3, Met receptor, and IGF-1R[4,25]. It remains unclear exactly how mammary epithelial cells integrate signals from such diverse receptors or why so many seemingly similar receptors are needed to coordinate branching morphogenesis.

2. Cellular basis of mammary tubulogenesis

Careful histologic analysis revealed many of the key features of mammary epithelial development, such as the iterative transitions between simple polarized and stratified unpolarized architecture[7,15,18,19,20]. Thorough in vivo genetic analysis has elaborated an impressive description of the molecular components required for normal mammary development and the utilization of these components in breast cancer[4,26]. However, the optical inaccessibility of the mammary gland has typically limited the analysis of the genetic manipulations to histologic readouts, such as mitotic and apoptotic indices. This limitation has made it difficult to understand how the TEB functions as a multicellular machine for ductal elongation. It has also limited the precision of genetic analyses as

many manipulations yield quantitatively similar reductions in, for example, ductal elongation.

2.1 Technical foundations for real-time analysis of mammary tubulogenesis.

In the absence of real-time information about mammary ductal elongation, we rely heavily on analogies to other biological models. Our conceptual framework for understanding cell motility in general is founded on studies of mesenchymal and amoeboid cell migration[27,28,29]. Migratory single cells polarize in a direction, extend actin based protrusions in response to that polarity, exert force on the substratum, and move in the direction of protrusion[27,28] (Figure 1-3A). These concepts naturally led to the hypothesis that collective cell migration would involve a similar polarization of the front of the leading cells and actin-based protrusions into the surrounding environment (Figure 1-3B). This concept works well to explain the migration of Drosophila border cells[30], Drosophila salivary gland elongation[31], the zebrafish lateral line[32], and multiple types of collective cancer invasion[33].

The most direct way to determine how TEBs elongate ducts would be to image the process in vivo. Since TEB elongation occurs over weeks, within an adipocyte-rich mammary fat pad, this requires long-term intravital imaging deep inside optically scattering tissue. Two-photon microscopy has enabled intravital imaging of stromal dynamics around TEBs[34] but no publications to date have imaged the cellular basis of TEB elongation in vivo. To model this process in a more experimentally and optically convenient format, diverse 3D culture assays have been developed. Mammary epithelial

cells can be cultured on top of thin ECM gels[35,36], cultured within geometrically defined ECM environments[22], or alternately pieces of primary mammary epithelium can be explanted within 3D ECM gels[19,37,38]. To date, primary organoid assays have produced the most organotypic branching programs in either Matrigel[19] or mixtures of Matrigel and collagen I[37]. We focus on describing results obtained with these primary organoid assays as they model the in vivo events of stratification, initiation of new epithelial buds, duct elongation, and bifurcation[14,19,20].

2.2 Mammary epithelial buds initiate and elongate without ECM-directed protrusions.

Mammary TEBs in vivo lack obvious cellular protrusions into the ECM even in high-resolution confocal images[18,19] and are enclosed within an intact basement membrane[15]. However, it remained possible that the cap cells extended either fine or transient protrusions into the ECM that were difficult to detect in histologic sections. Accordingly, we optimized a 3D primary tissue organoid assay for long-term timelapse imaging[19,38]. We did not observe ECM directed protrusions using cytoplasmic or actin-GFP based timelapse imaging, by phalloidin staining, or by transmission electron microscopy[19,20] (Figure 1-3C-D'). The border between the epithelial cells and the ECM was strikingly smooth both in 3D culture and in vivo[19,20] (Figure 1-3D,D'). Despite the robust localization of E-cadherin and β-catenin to points of cell-cell contact within the stratified epithelium, we observed few intercellular junctions connecting cells in the interior of the multilayer[20]. We did observe abundant, interdigitating membrane protrusions, extending into the space between these interior cells[20]. However, the lack of ECM-directed protrusions appears to limit the extent to which TEB cells can explore the space in front

of them before migrating. This limitation suggests that TEBs may not migrate as directionally as, for example, growth cones on a neuron. Alternately, the TEB may sense soluble guidance cues collectively across a multicellular ensemble.

2.3 Asymmetric division of luminal cells initiates stratification and loss of polarity.

Cells within the TEB exhibit fewer intercellular junctions and reduced apico-basal polarity when compared to the polarized mammary ducts they are generating[19,20] (Figure 1-4A). At the molecular level, simple epithelial cells maintain segregated apical domains within the plasma membrane, enriched in the Par-3/Par-6/Cdc42 polarity complex[39] (Figure 1-4B). This apical domain is separated by tight junctions from the basolateral domain, which is enriched in the Scribble/Lethal Giant Larvae/ Discs Large complex[39] (Figure 1-4B). Immunofluorescent staining for these polarity proteins in vivo revealed that both simple organization and molecularly distinct membrane domains are absent in the TEB during ductal elongation[20]. We sought to determine the cellular mechanism that initiated the formation of the TEB and the relationship between stratification and loss of polarity.

Given that the starting point was a bilayered tube, with apically positioned luminal epithelial cells and basally positioned myoepithelial cells, we reasoned that stratification could initiate within either or both of these cellular populations. We analyzed the orientation of cell division during stratification in real-time in the organoid assay and the plane of mitosis in tissue sections collected during TEB formation in vivo[14]. In both cases, we exclusively observed stratification intitiate from asymmetric divisions within

the luminal population[14] (Figure 1-4C), consistent with the emerging concept that ductal elongation during puberty is driven by unipotent stem and progenitor cells[40]. Our real-time analysis of the dynamics of ZO1-GFP revealed that tight junctions are maintained in the mother cell during this asymmetric cell division, while the daughter cell did not form tight junctions or segregated membrane domains (Figure 1-4D). This asymmetric cell division could therefore explain both stratification and loss of polarity, two early features of epithelial cancers.

We next demonstrated that expression of either constitutively activated ErbB2 or phosphomimetic MEK1DD was sufficient to induce stratification by this mechanism. Importantly, stratified epithelial tissues such as the epidermis have been shown to initiate stratification from basally positioned cells, in contact with a basement membrane[41]. We believe our data are the first to report developmental stratification from the apical compartment, driven by cells out of contact with the basement membrane. Our data reveal a cellular mechanism for transient developmental stratification that can be readily co-opted during malignant progression through activation of receptor tyrosine kinase signaling.

2.4 Mammary tubulogenesis is driven by changes in epithelial organization and cell behavior.

Synthesizing the real-time analysis in 3D culture with the histology of the TEB during elongation, the concept that emerges is of ductal elongation driven by changes in epithelial architecture (Figure 1-5A). The simple bilayered tube stratifies in response to

steroid hormone and growth factor receptor signaling, creating a population of low polarity, highly proliferative, epithelial cells between the polarized luminal epithelial and myoepithelial cell layers. While the internal epithelial cells continue to express epithelial cytokeratins (e.g. K8) and cell adhesion molecules (e.g. E-cadherin), they have fewer intercellular junctions and incomplete apico-basal polarity. These internal epithelial cells then drive the elongation of the tube and ultimately resolve back to a simple tube.

A reasonable question is why are these transitions are necessary? It is easy to conceive of mechanisms of tube elongation that don't require major changes in epithelial architecture. However, mammary development occurs iteratively and initiates from a highly polarized, junctionally connected epithelium. This question of epithelial motility and cell migration has been addressed by multiple labs. An early study used timelapse imaging to reveal active cell migration within non-invasive, stratified epithelial acinii[42]. We observed vigorous migration and dynamic cell rearrangements during branching of primary mammary organoids[19]. Mammary epithelial cells within geometrically defined matrix environments displayed MMP-14 dependent differential persistence of migration within the epithelium and these differences determined their contribution to elongating branches[43]. Finally, multiple groups have demonstrated coherent angular motions of mammary epithelial cells within multicellular groups[44] and have related these rotations to the organization of the basement membrane[45].

Despite differences in cellular inputs and culture formats, all of these studies support the idea that mammary epithelial cells within stratified groups are highly migratory. Indeed,

when individual epithelial cells within an elongating duct are labeled with cytoplasmic GFP and imaged using timelapse confocal microscopy, they are actively migrating within the tissue[20] (Figure 1-5B). Without the Cell Tracker Red staining for tissue contrast, it would be easy to imagine that this was a mesenchymal cell migrating through the ECM. Instead, it is an epithelial cell migrating between other epithelial cells (Figure 1-5B). We speculate that this phenomenon of active migration confined within an epithelial multilayer represents an efficient solution to the dual need to enable dramatic remodeling of the postnatal mammary epithelium while still minimizing the likelihood of epithelial cells migrating to distant organs.

3. Relationship of normal mammary morphogenesis to breast cancer metastasis.

The large majority of cancers arise in epithelial cells, and among epithelial malignancies both morbidity and mortality are driven by metastasis to distant organs[46]. The resting configuration of a mammary duct is a highly polarized, highly adherent, essentially non-proliferative epithelium. With this quiescent state defining our sense of "normal" epithelial biology, it is tempting to view the problem of metastasis as a question of how the cancer "invents" epithelial motility from such stationary cells (Figure 1-6A). However, every real-time analysis has revealed that normal mammary epithelial cells have a high migratory potential, even when arranged in stratified epithelia and connected by intercellular junctions[19,20,22,43,44,45]. The most important question might instead be: why don't these normal migratory epithelial cells leave (Figure 1-6B)? The key cell behavioral difference is that when normal cells reach the tissue compartment boundary they stop migrating, while metastatic cells ignore the boundary and migrate to distant organs.

We sought to understand the molecular regulation of tissue compartment boundaries and used mammary organoid as an observable, manipulable model system in which to explore this phenomenon. Our first surprise was when we explanted tumor organoids from genetically engineered mouse models of breast cancer. In vivo, the MMTV-PyMT mouse model will metastasize to the lungs in 95% of mice on the FVB background[47,48]. Yet, when tumor organoids from this model were placed into Matrigel culture, essentially no cells disseminated into the ECM[49]. We repeated these experiments with primary human breast tumors and found the same result: even organoids isolated from tumors that had metastasized in the patient did not disseminate into Matrigel[49]. However, the microenvironment around a breast tumor is deficient in laminin I and collagen IV, the major protein constituents of Matrigel, and rich in fibrillar collagen I[50]. When organoids from the same tumor were explanted into different ECM gels, they were indolent in Matrigel and disseminative into collagen I[49]. This experiment demonstrated that the ECM is a potent regulator of invasive and disseminative behavior in tumor tissue. We next tested the response of normal organoids to direct contact with collagen I. We observed the same initial response: protrusions and dissemination into the collagen I[49], specifically into collagen I gels with a high fibrillar content[37]. However, normal epithelium rapidly reestablished basement membrane coverage, ceased protrusive activity, and reinitiated a program of branching morphogenesis[49]. These experiments reveal a conserved response of invasion and dissemination following direct contact with fibrillar collagen I, and a robust capacity of normal epithelial cells to cease invasion and reestablish epithelial organization.

We next tested whether we could identify molecular interventions that could induce dissemination of normal epithelial cells into the ECM. We decided to contrast deletion of the cell adhesion gene, E-cadherin, with induced expression of the transcription factor, Twist1, a protein frequently associated with metastatic cell behaviors. We observed that deletion of E-cadherin induced loss of simple epithelial organization, apical movement of E-cadherin$^-$ cells into the lumen, basal invasion of E-cadherin$^-$ cells into the ECM, but not single cell dissemination[51]. In contrast, expression of Twist1 induced dissemination of epithelial cells into the ECM within 24-72 hours[51]. Twist1+ cells retained epithelial specific gene expression and membrane localized E-cadherin and b-catenin. Surprisingly, knockdown of E-cadherin in Twist1 expressing cells reduced single cell dissemination and resulted in a more collective form of invasion. RNA expression analysis revealed significant changes in cell-matrix adhesion and extracellular compartment genes, consistent with an epithelial motility program in which the cells optimize their gene expression to match the environment through which they will be migrating. We believe that this assay will allow us to identify the molecular programs that enable epithelial cells to bypass compartment boundaries and exit the epithelium. More generally, the molecular techniques developed in this study can be utilized to understand the consequences of genetic interventions on both cell behavior and tissue level function.

4. Conclusions and Future Directions.

This is a tremendously exciting time in mammary epithelial biology. There are many groups bringing together innovative combinations of genetics, cell biology, and imaging

to generate an understanding of epithelial structure and function at cellular resolution. The iterative nature of mammary development throughout reproductive life provides the opportunity to study cycles of morphogenesis and quiescence in a normal context. There are many fascinating open questions that remain to be elucidated in the coming years. How do epithelial cells cooperate (or compete) to accomplish ductal elongation? What is the cellular mechanism by which the stratified TEB resolves back to simple epithelial organization? How do TEBS bifurcate? Are the cellular and molecular mechanisms employed to elongate TEBs recapitulated during side branching and lactational differentiation? These questions have fascinated generations of mammary gland biologists and the innovative tools available today should enable answers to each of these classic questions over the next decade.

References

1 Nelson, W. J. Remodeling epithelial cell organization: transitions between front-rear and apical-Basal polarity. Cold Spring Harb Perspect Biol 1, a000513, (2009).

2 O'Brien, L. E., Zegers, M. M. & Mostov, K. E. Opinion: Building epithelial architecture: insights from three-dimensional culture models. Nat Rev Mol Cell Biol 3, 531-537, (2002).

3 Bilder, D. Epithelial polarity and proliferation control: links from the Drosophila neoplastic tumor suppressors. Genes Dev 18, 1909-1925, (2004).

4 McNally, S. & Martin, F. Molecular regulators of pubertal mammary gland development. Ann Med 43, 212-234, (2011).

5 Veltmaat, J. M., Mailleux, A. A., Thiery, J. P. & Bellusci, S. Mouse embryonic mammogenesis as a model for the molecular regulation of pattern formation. Differentiation 71, 1-17, (2003).

6 Hens, J. R. & Wysolmerski, J. J. Key stages of mammary gland development: molecular mechanisms involved in the formation of the embryonic mammary gland. Breast Cancer Res 7, 220-224, (2005).

7 Hogg, N. A., Harrison, C. J. & Tickle, C. Lumen formation in the developing mouse mammary gland. J Embryol Exp Morphol 73, 39-57, (1983).

8 Sun, P., Yuan, Y., Li, A., Li, B. & Dai, X. Cytokeratin expression during mouse embryonic and early postnatal mammary gland development. Histochem Cell Biol 133, 213-221, (2010).

9 Deugnier, M. A., Moiseyeva, E. P., Thiery, J. P. & Glukhova, M. Myoepithelial cell differentiation in the developing mammary gland: progressive acquisition of smooth muscle phenotype. Dev Dyn 204, 107-117, (1995).

10 Faraldo, M. M. *et al.* Myoepithelial cells in the control of mammary development and tumorigenesis: data from genetically modified mice. J Mammary Gland Biol Neoplasia 10, 211-219, (2005).

11 Moumen, M. *et al.* The mammary myoepithelial cell. Int J Dev Biol, (2011).

12 Sternlicht, M. D. Key stages in mammary gland development: the cues that regulate ductal branching morphogenesis. Breast Cancer Res 8, 201, (2006).

13 Sternlicht, M. D., Kouros-Mehr, H., Lu, P. & Werb, Z. Hormonal and local control of mammary branching morphogenesis. Differentiation 74, 365-381, (2006).

14 Huebner, R. J., Lechler, T. & Ewald, A. J. Developmental stratification of the mammary epithelium occurs through symmetry-breaking vertical divisions of apically positioned luminal cells. Development 141, 1085-1094, (2014).

15 Williams, J. M. & Daniel, C. W. Mammary ductal elongation: differentiation of myoepithelium and basal lamina during branching morphogenesis. Dev Biol 97, 274-290, (1983).

16 Hinck, L. & Silberstein, G. B. Key stages in mammary gland development: the mammary end bud as a motile organ. Breast Cancer Res 7, 245-251, (2005).

17 Daniel, C. W., Strickland, P. & Friedmann, Y. Expression and functional role of E- and P-cadherins in mouse mammary ductal morphogenesis and growth. Dev Biol 169, 511-519, (1995).

[18] Mailleux, A. A. *et al.* BIM regulates apoptosis during mammary ductal morphogenesis, and its absence reveals alternative cell death mechanisms. Dev Cell 12, 221-234, (2007).
[19] Ewald, A. J., Brenot, A., Duong, M., Chan, B. S. & Werb, Z. Collective epithelial migration and cell rearrangements drive mammary branching morphogenesis. Dev Cell 14, 570-581, (2008).
[20] Ewald, A. J. *et al.* Mammary collective cell migration involves transient loss of epithelial features and individual cell migration within the epithelium. J Cell Sci 125, 2638-2654, (2012).
[21] Daniel, C. W., Robinson, S. & Silberstein, G. B. The role of TGF-beta in patterning and growth of the mammary ductal tree. J Mammary Gland Biol Neoplasia 1, 331-341, (1996).
[22] Nelson, C. M., Vanduijn, M. M., Inman, J. L., Fletcher, D. A. & Bissell, M. J. Tissue geometry determines sites of mammary branching morphogenesis in organotypic cultures. Science 314, 298-300, (2006).
[23] Trott, J. F., Vonderhaar, B. K. & Hovey, R. C. Historical perspectives of prolactin and growth hormone as mammogens, lactogens and galactagogues--agog for the future! J Mammary Gland Biol Neoplasia 13, 3-11, (2008).
[24] Hovey, R. C., Trott, J. F. & Vonderhaar, B. K. Establishing a framework for the functional mammary gland: from endocrinology to morphology. J Mammary Gland Biol Neoplasia 7, 17-38, (2002).
[25] Pond, A. C. *et al.* Fibroblast growth factor receptor signaling is essential for normal mammary gland development and stem cell function. Stem Cells 31, 178-189, (2013).
[26] Huang, L. & Muthuswamy, S. K. Polarity protein alterations in carcinoma: a focus on emerging roles for polarity regulators. Curr Opin Genet Dev 20, 41-50, (2010).
[27] Devreotes, P. N. & Zigmond, S. H. Chemotaxis in eukaryotic cells: a focus on leukocytes and Dictyostelium. Annu Rev Cell Biol 4, 649-686, (1988).
[28] Lauffenburger, D. A. & Horwitz, A. F. Cell migration: a physically integrated molecular process. Cell 84, 359-369, (1996).
[29] Ridley, A. J. *et al.* Cell migration: integrating signals from front to back. Science 302, 1704-1709, (2003).
[30] Montell, D. J., Yoon, W. H. & Starz-Gaiano, M. Group choreography: mechanisms orchestrating the collective movement of border cells. Nat Rev Mol Cell Biol 13, 631-645, (2012).
[31] Andrew D. J., E., A. J. Morphogenesis of epithelial tubes: Insights into tube formation, elongation, and elaboration. Dev. Biol. 341, 34-55, (2010).
[32] Lecaudey, V. & Gilmour, D. Organizing moving groups during morphogenesis. Curr Opin Cell Biol 18, 102-107, (2006).
[33] Friedl, P. & Gilmour, D. Collective cell migration in morphogenesis, regeneration and cancer. Nat Rev Mol Cell Biol 10, 445-457, (2009).
[34] Ingman, W. V., Wyckoff, J., Gouon-Evans, V., Condeelis, J. & Pollard, J. W. Macrophages promote collagen fibrillogenesis around terminal end buds of the developing mammary gland. Dev Dyn 235, 3222-3229, (2006).

[35] Debnath, J., Muthuswamy, S. K. & Brugge, J. S. Morphogenesis and oncogenesis of MCF-10A mammary epithelial acini grown in three-dimensional basement membrane cultures. Methods 30, 256-268, (2003).
[36] Debnath, J. & Brugge, J. S. Modelling glandular epithelial cancers in three-dimensional cultures. Nat Rev Cancer 5, 675-688, (2005).
[37] Nguyen-Ngoc, K. V. & Ewald, A. J. Mammary ductal elongation and myoepithelial migration are regulated by the composition of the extracellular matrix. J Microsc 251, 212-223, (2013).
[38] Ewald, A. J. Practical considerations for long-term time-lapse imaging of epithelial morphogenesis in three-dimensional organotypic cultures. Cold Spring Harb Protoc 2013, (2013).
[39] Feigin, M. E. & Muthuswamy, S. K. Polarity proteins regulate mammalian cell-cell junctions and cancer pathogenesis. Curr Opin Cell Biol 21, 694-700, (2009).
[40] Rios, A. C., Fu, N. Y., Lindeman, G. J. & Visvader, J. E. In situ identification of bipotent stem cells in the mammary gland. Nature 506, 322-327, (2014).
[41] Lechler, T. & Fuchs, E. Asymmetric cell divisions promote stratification and differentiation of mammalian skin. Nature 437, 275-280, (2005).
[42] Pearson, G. W. & Hunter, T. Real-time imaging reveals that noninvasive mammary epithelial acini can contain motile cells. J Cell Biol 179, 1555-1567, (2007).
[43] Mori, H., Gjorevski, N., Inman, J. L., Bissell, M. J. & Nelson, C. M. Self-organization of engineered epithelial tubules by differential cellular motility. Proc Natl Acad Sci U S A, (2009).
[44] Tanner, K., Mori, H., Mroue, R., Bruni-Cardoso, A. & Bissell, M. J. Coherent angular motion in the establishment of multicellular architecture of glandular tissues. Proc Natl Acad Sci U S A 109, 1973-1978, (2012).
[45] Wang, H., Lacoche, S., Huang, L., Xue, B. & Muthuswamy, S. K. Rotational motion during three-dimensional morphogenesis of mammary epithelial acini relates to laminin matrix assembly. Proc Natl Acad Sci U S A 110, 163-168, (2012).
[46] Siegel, R., Naishadham, D. & Jemal, A. Cancer statistics, 2013. CA Cancer J Clin 63, 11-30, (2013).
[47] Guy, C. T., Cardiff, R. D. & Muller, W. J. Induction of mammary tumors by expression of polyomavirus middle T oncogene: a transgenic mouse model for metastatic disease. Mol Cell Biol 12, 954-961, (1992).
[48] Lin, E. Y. *et al.* Progression to malignancy in the polyoma middle T oncoprotein mouse breast cancer model provides a reliable model for human diseases. Am J Pathol 163, 2113-2126, (2003).
[49] Nguyen-Ngoc, K.-V. *et al.* ECM microenvironment regulates collective migration and local dissemination in normal and malignant mammary epithelium. Proceedings of the National Academy of Sciences of the United States of America 109, E2595-2604, (2012).
[50] Egeblad, M., Rasch, M. G. & Weaver, V. M. Dynamic interplay between the collagen scaffold and tumor evolution. Curr Opin Cell Biol 22, 697-706, (2010).
[51] Shamir, E. R. *et al.* Twist1-induced dissemination preserves epithelial identity and requires E-cadherin. J Cell Biol 204, 839-856, (2014).

Figure 1-1

A. Mammary development begins at embryonic day 12 when the mammary placode invades the mammary mesenchyme. The epithelium then elongates and hollows to form a rudimentary duct that remains relatively quiescent until puberty. Modified from Hogg et al, 1983.

B. Mammary ducts are elaborated during puberty to form the functional ductal network. Puberty, in the mouse, begins during postnatal week 3. Pubertal development initiates with the formation of terminal end buds (TEBs) which function as the elongation front of developing ducts. Over the next 7 weeks primary ducts elongate across the mammary fat pad and secondary branching completes the ductal network.

Figure 1-1

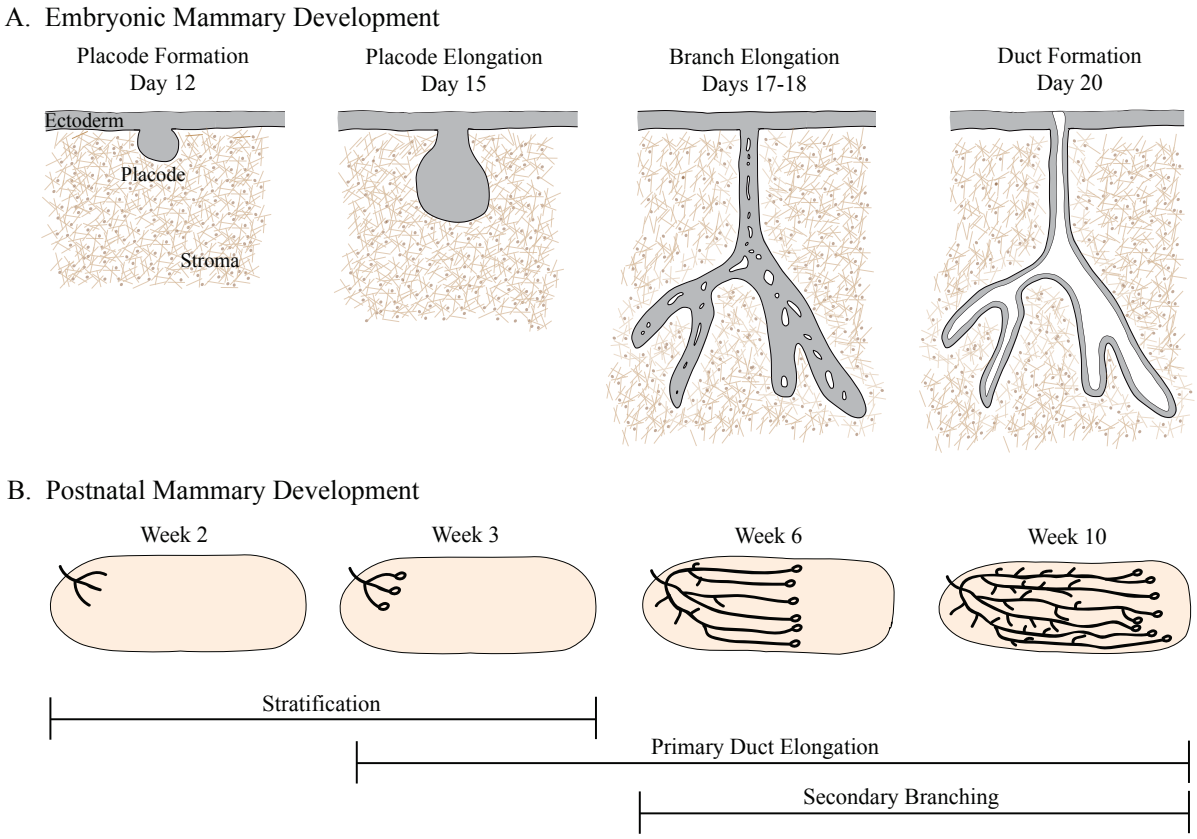
A. Embryonic Mammary Development
Placode Formation
Day 12
Placode Elongation
Day 15
Branch Elongation
Days 17-18
Duct Formation
Day 20
Ectoderm
Placode
Stroma
B. Postnatal Mammary Development
Week 2
Week 3
Week 6
Week 10
Stratification
Primary Duct Elongation
Secondary Branching

Figure 1-2

(A) Mammary epithelium consists of a rudimentary ductal network prior to puberty. (A') Duct from a 2-week-old mouse stained for F-actin (red) and nuclei (green). All mammary ducts are bilayered before pubertal development (modified from[14]). (B) TEBs form at ductal tips at the onset of puberty. (B') TEB from a 4-week-old mouse stained for F-actin (red) and nuclei (green). TEBs consist of a stratified epithelium with more than two cell layers (modified from[14]). (C) TEBs function as the elongation front of the mammary epithelium during pubertal development. (C') TEB stained for the basolateral polarity marker ß-catenin (red), the tight junction protein zona occludins 1 (ZO-1), (green) and nuclei (blue). TEBs have incomplete apico-basal polarity with ß-catenin present on nearly all cellular membranes and tight junctions present primarily at the apical-most membrane facing the luminal space. Aside from the primary luminal space, TEBs also have micro-lumens, highlighted with arrows, which are positive for tight junctions (modified from[20]).

Figure 1-2

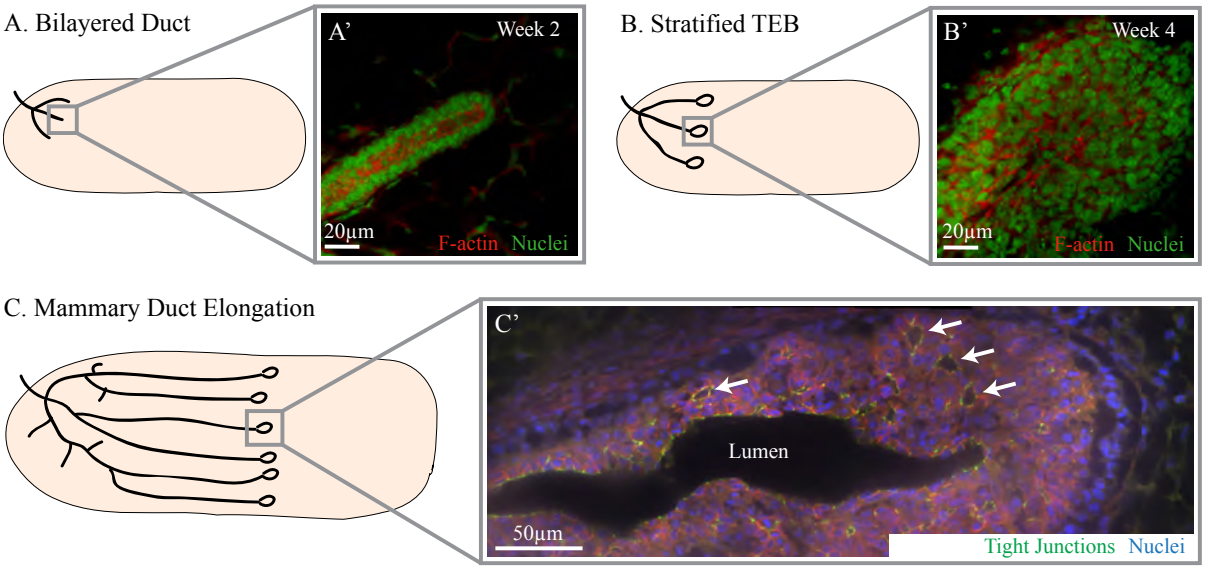
A. Bilayered Duct
A'
Week 2
20μm
F-actin Nuclei
B. Stratified TEB
B'
Week 4
20μm
F-actin Nuclei
C. Mammary Duct Elongation
C'
Lumen
50μm
Tight Junctions Nuclei

Figure 1-3

(A) Migration of single cells involves front-rear polarization and actin-based protrusions at the leading edge. (B) A possible mechanism for ductal elongation is migration of a subset of polarized protrusive leader cells. (C) Organoid bud stained for F-actin (green) and nuclei (red). (C') Zoomed image of the elongation front of the bud shown in C. Actin-based protrusions are noticeably absent from the leading edge of elongating mammary branches (modified from[19]). (D) Electron micrograph of an elongating mammary bud. (D') Leading edge of the bud shown in D. Elongating mammary branches have a smooth leading edge when viewed at the ultrastructural level (modified from[20]).

Figure 1-3

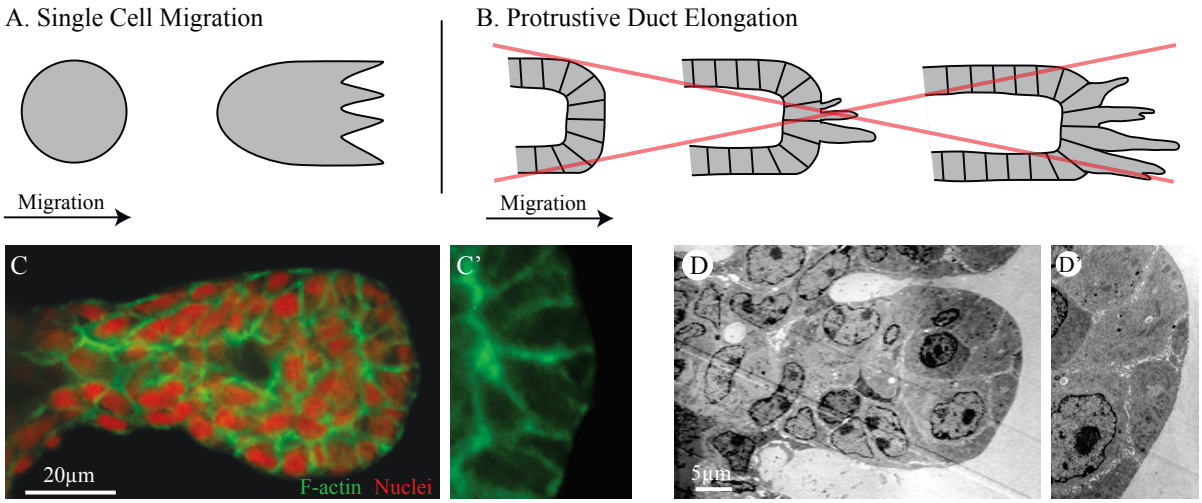
A. Single Cell Migration
B. Protrustive Duct Elongation
Migration
Migration
C
20µm
F-actin Nuclei
C'
D
5µm
D'

Figure 1-4

(A) Model of mammary duct and TEB structure. Ducts are a bilayered epithelium with apical luminal epithelial cells (gray) and basal myoepithelial cells (brown). Luminal cells have tight junctions (green) at the apical-most point of cell-cell contact. Desmosomes (blue) are cell adhesion complexes that connect luminal cells to each other and to the myoepithelial cell layer. TEBs are composed of a low-polarity internal cell population (light blue) that is bounded by the basal myoepithelial layer (brown) and apical luminal cells (gray). Internal cells have a diminished number of desmosomes and loose cell-cell contacts by electron microscopy. Tight junctions are absent from internal cells except at microlumens. Mammary ducts and TEBs are surrounded by basement membrane (red). (B) Schematic showing the apico-basal polarity of luminal epithelial cells. The polarity protein par-3 (orange) is localized to the apical membrane and scribble (red) is localized to the basolateral membrane. ZO-1 (green) marks the tight junction, which partitions the apical and basolateral membranes. (C) Model of the cellular mechanism of mammary duct stratification. Stratification is initiated by vertical proliferation of apically localized luminal epithelial cells, and the vertical divisions result in asymmetric localization of tight junctions and polarity loss for internal cells. Stratification is non-clonal, as multiple vertical divisions are observed within a single organoid. Low-polarity internal cells are proliferative, further driving stratification (modified from[14]). (D) Vertical divisions resulted in asymmetric localization of par-3 (orange) ZO-1 (green) and scribble (red) in the apical mother cell and the internal daughter cell. This asymmetry directly results in polarity loss for the internal daughter cell. The cell fate marker numb (blue) is

asymmetrically localized to the basal daughter cell during vertical divisions (modified from[14])

Figure 1-4

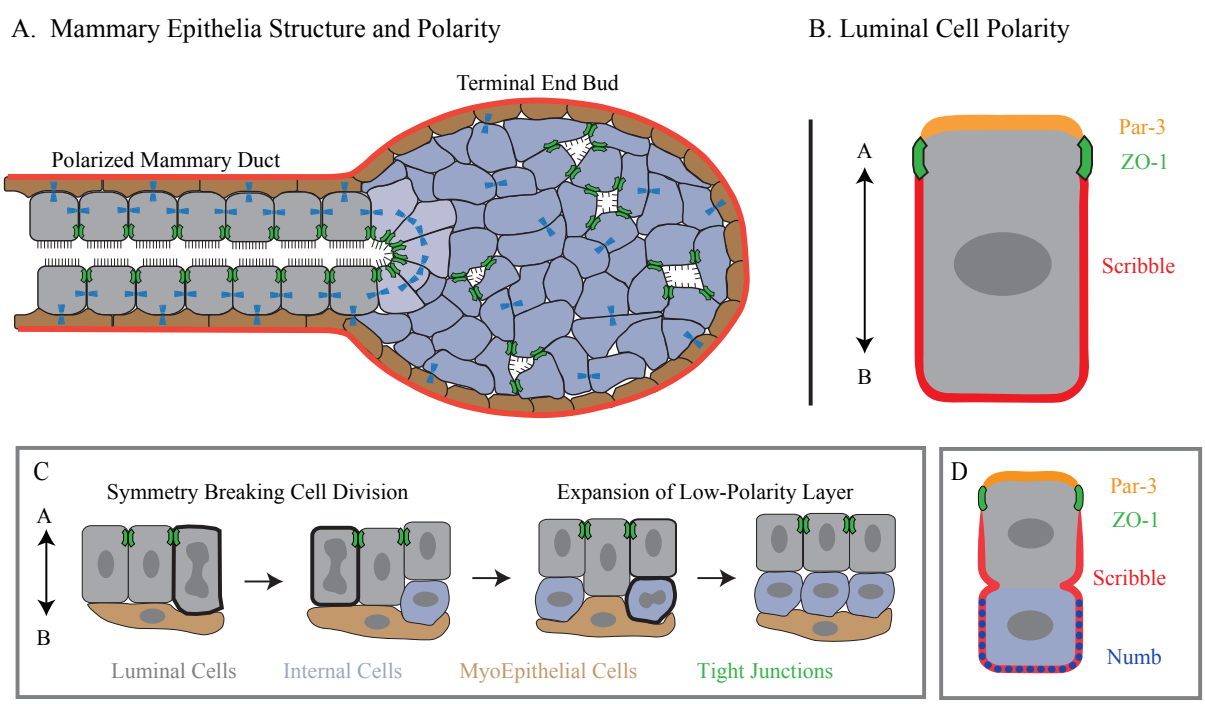
A. Mammary Epithelia Structure and Polarity
B. Luminal Cell Polarity
Terminal End Bud
Polarized Mammary Duct
A
B
Par-3
ZO-1
Scribble
C
A
B
Symmetry Breaking Cell Division
Expansion of Low-Polarity Layer
Luminal Cells
Internal Cells
MyoEpithelial Cells
Tight Junctions
D
Par-3
ZO-1
Scribble
Numb

Figure 1-5

(A) Schematic showing each stage of mammary branching morphogenesis. Prior to development, ducts are bilayered with apical luminal epithelial cells (gray) and basal myoepithelial cells (brown), and the entire duct is surrounded by basement membrane (red). The epithelium then stratifies, forming a low-polarity internal cell population (light blue). Low-polarity TEBs then elongate the epithelial ducts, and finally the epithelium polarizes back to a bilayer. (B) Still images from a movie of an organoid mosaically labeled with cytosolic GFP to visualize single cells within the epithelium. Cells are labeled green, the membranes are red, and the dashed line shows the elongation front. Cells were protrusive and migratory within the organoids. The arrow highlights a cell that moves to the basal surface and then back into the body of the elongating branch (modified from[20]).

Figure 1-5

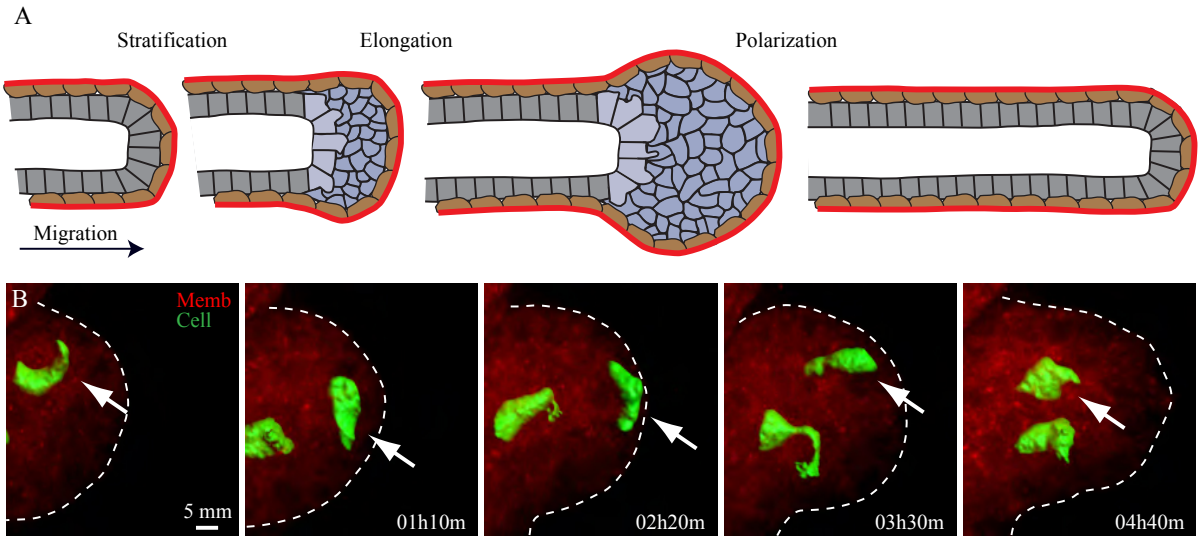
A
Stratification
Elongation
Polarization
Migration
B
Memb
Cell
5 mm
01h10m
02h20m
03h30m
04h40m

Figure 1-6

(A) Cartoon depiction of epithelial cell dissemination past the basement membrane (modified with permission from a schematic by Eliah Shamir). (B) Schematic questioning why normal motile cells within the epithelium do not invade past the basement membrane.

Figure 1-6

A. How do metastatic tumors "invent" epithelial motility?

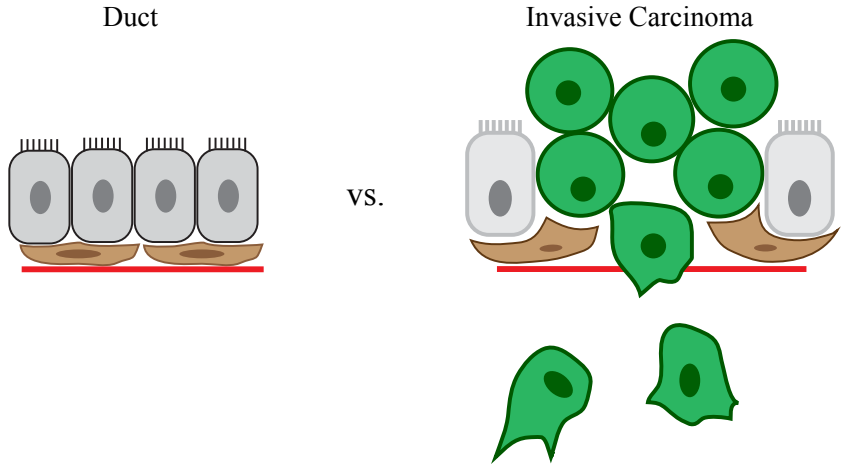

B. Why don't normal migratory cells leave?

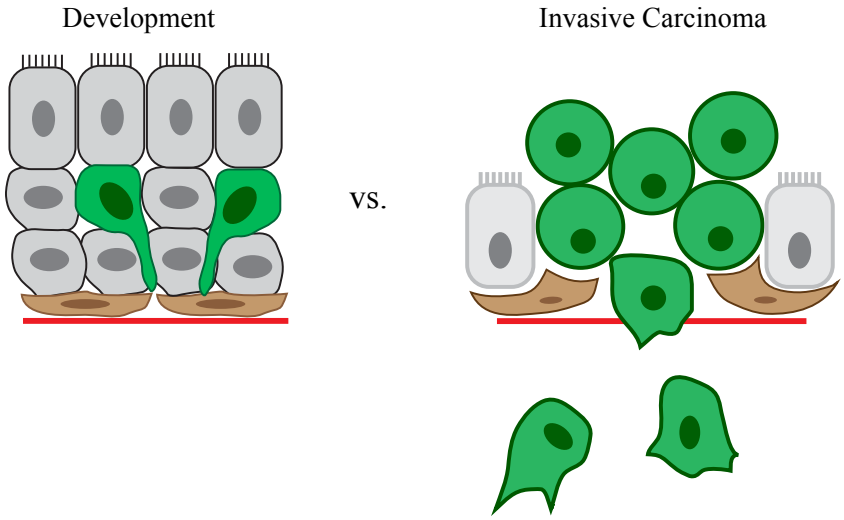

Chapter 2

3D culture assays of murine mammary branching morphogenesis and epithelial invasion

(Modified from Nguyen-Ngoc et al., Methods Mol. Biol. 2015)

Abstract

Epithelia are fundamental tissues that line cavities, glands, and outer body surfaces. We use three-dimensional (3D) embedded culture of primary murine mammary epithelial ducts, called "organoids," to recapitulate in days in culture epithelial programs that occur over weeks deep within the body. Modulating the composition of the extracellular matrix (ECM) allows us to model cell- and tissue-level behaviors observed in normal development, such as branching morphogenesis, and in cancer, such as invasion and dissemination. Here, we describe a collection of protocols for 3D culture of mammary organoids in different ECMs and for immunofluorescence staining of 3D culture samples and mammary gland tissue sections. We illustrate expected phenotypic outcomes of each assay and provide troubleshooting tips for commonly encountered technical problems.

1 Introduction

Mammary gland development occurs postnatally from a simple epithelial rudiment[1,2]. During puberty, this rudiment undergoes stratification and initiates branching morphogenesis to form a network of epithelial tubes. The functional unit of elongation is a proliferative, multilayered front called the terminal end bud (TEB)[3,4]. Behind the TEB, repolarization to a mature duct reestablishes a simple, bi-layered architecture, characterized by an inner layer of luminal epithelial cells and an outer layer of myoepithelial cells. These fundamental programs involve concurrent changes in cell proliferation, migration, polarity, and tissue architecture and are modulated by signaling cues from stromal cells and the extracellular matrix (ECM)[5].

Because mammary epithelium develops within a fat pad with limited optical accessibility, various groups have used 3D culture to facilitate direct observation and manipulation of epithelial cell behaviors[6–14]. Cultures of primary mammary tissues were first developed half a century ago[15, 16], but the past decade has seen significant improvements in and increasing utilization of 3D culture models[17–20]. While many conventional methods rely on immortalized cell lines or primary single cells, we use freshly isolated, murine mammary epithelial ducts, which we term "organoids." The organoid assay arose from a series of papers published in the Bissell and Werb Labs[17–19, 21]. There are technical differences among the papers, but all involve mechanical disruption, enzymatic digestion, and differential centrifugation to separate mammary epithelial organoids from surrounding adipocytes and stromal cells. Purified organoids can be embedded in various ECMs to model distinct epithelial programs.

Our recent studies have revealed many of the cellular mechanisms driving epithelial morphogenesis and demonstrated that the ECM microenvironment regulates the migration and dissemination of mammary epithelial cells[17, 22–24]. Normal development in vivo occurs within a basement membrane, and we use Matrigel, a basement membrane-rich ECM, as an experimentally convenient model for the normal ductal microenvironment. Culture of organoids in basal medium, without supplemental growth factors, induces formation of simple, bi-layered cysts, while culture with growth factor induces a stereotyped program of branching morphogenesis. In contrast, cancer progression involves breaks in the basement membrane, and the microenvironment around a tumor is enriched in collagen I[25–30]. We demonstrated that collagen Irich microenvironments induce a conserved program of invasion and dissemination in normal and malignant mammary epithelium[23]. Conversely, defined mixtures of Matrigel and collagen I can reproduce a more physiological organization of the elongating TEB[24].

Building on our previously published methods[17, 22, 23, 31, 33–35], this protocol seeks to provide a comprehensive guide to utilizing the mammary organoid assay (Fig. 2-1A). We introduce several variations on the assay in different ECMs and growth conditions that model different aspects of epithelial development and disease. We also provide optimized protocols for immunofluorescence staining of organoids in 3D embedded culture and of tissue sections of whole mammary glands.

2 Materials

2.1 Mice

We have successfully isolated and cultured organoids from mice ranging in age from E18.5 through 1.5 years. There are variations in response to growth factors with age and strain. All protocols below are optimized for FVB mice between 8 and 12 weeks of age. Once euthanized, mammary tissue is optimally isolated and cultured immediately, but successful organoid cultures have been established from mice sacrificed and then kept at 4 C overnight.

2.2 Reagents

1. Collagenase solution in DMEM/F12: 2 mg/mL collagenase, 2 mg/mL trypsin, 5 % v/v fetal bovine serum (FBS), 5 μg/mL insulin, and 50 μg/mL gentamicin. (a) Collagenase from Clostridium histolyticum (Sigma C2139): Dissolve 1 g in 10 mL DMEM/F12, and make 200 μL aliquots. Store at -20^{o}C. (b) Trypsin: Dissolve 1 g in 10 mL DMEM/F12, and make 200 μL aliquots. Store at -20^{o}C.

2. Dulbecco's phosphate-buffered saline (DPBS, with Ca2+, Mg2+).

3. Phosphate-buffered saline (PBS, without Ca2+, Mg2+).

4. BSA solution: 2.5 % bovine serum albumin (BSA) in DPBS.

5. 2,000 U DNase (Sigma D4263): Dissolve in 1 mL of PBS, and make 40 μL aliquots. Store at 20 C.

6. Organoid medium in DMEM/F12: 1 % penicillin/streptomycin and 1 % insulin-transferrin-selenium-X (ITS) (GIBCO 51500).

7. FGF2, 25 μg (Sigma F0291): Dissolve in 250 μL of PBS, and make 20 μL aliquots. Store at -20^{o}C.

8. Growth Factor Reduced Matrigel (Corning 354230).

9. Rat tail collagen I (Corning 354236).

10. DMEM 10x, low glucose.

11. 1.0 N NaOH.

12. 4 % paraformaldehyde (PFA) in DPBS.

13. Tissue-Tek optimal cutting temperature (OCT) compound.

14. 0.5 % Triton X-100 in DPBS.

15. 10 % FBS in DPBS.

16. Mounting Medium (Sigma F4680-25ML).

17. Primary antibodies.

18. Secondary antibodies conjugated to fluorescent probes.

2.3 Instructions for preparing solutions

Prepare solutions as follows:

1. Collagenase solution (10 mL per mouse): Combine 9 mL DMEM/F12, 500 µL FBS, 5 µL insulin (10 mg/mL stock), 10 µL gentamicin (50 mg/mL stock), 200 µL collagenase (100 mg/mL stock), and 200 µL trypsin (100 mg/mL stock) in a 15 mL tube. Filter sterilize through a 0.2 µm filter into a new tube (Do not filter collagenase and trypsin stocks, the filter will get clogged). This solution should be made fresh for each experiment.

2. BSA solution: Combine 46 mL DPBS and 4.1 mL BSA (30 % stock solution). Filter sterilize, and store at 4 C. This solution can be reused for several experiments if kept sterile but should be monitored for contamination.

3. Organoid medium: Remove 10 mL of DMEM/F12 from a 500 mL bottle of medium. Add 5 mL penicillin/streptomycin (10,000 units penicillin and 10 mg streptomycin/mL stock) and 5 mL ITS. For the branching morphogenesis assays (Subheadings 3.10.2 and 3.10.3) and the invasion assay (Subheading 3.10.4), supplement organoid medium with growth factor at the desired concentration. Diverse growth factors induce branching in the 1–10 nM range, including EGF ligands (EGF, TGF-α, amphiregulin, heregulin, neuregulin), FGF ligands (FGF2, FGF7), and HGF. We typically use 2.5 nM FGF2 for 8–12-week-old FVB mice. It is necessary to optimize the growth factor concentration for the specific age and strain of mouse.

2.4 Tools and instruments

1. One Spencer Ligature scissors, delicate pattern (Fine Science Tools (FST) 14028–10): For mouse exterior.

2. One standard forceps, narrow pattern (FST 11003–12): For mouse exterior.

3. One Iris scissors, straight pattern (FST 14060–09): For mouse interior (sterile).

4. One Graefe forceps (FST 11051–10): For mouse interior (sterile).

5. Sterile scalpel, #10 blade.

6. Polystyrene Petri dish.

7. Benchtop incubator orbital shaker (Thermo Scientific MaxQ 4450).

8. Incublock™ microtube incubator with two blocks set to 37 C (Denville Scientific Inc. I0540).

9. Ice bucket.

10. Centrifuge tubes, 15 and 50 mL. 3D Mammary Organoid Culture 139

3 Methods

3.1 Collecting mouse mammary glands

Mice have five pairs of mammary glands located beneath the skin and outside the peritoneum. This section describes how to collect glands #3, #4, and #5 for organoid isolation and how to limit contamination by other tissues.

1. Generally, use female mice between 8 and 12 weeks old.

2. Sterilize the dissecting area with 70 % ethanol.

3. Sterilize the dissecting tools by heat in a glass bead sterilizer.

4. Euthanize the mouse in a CO2-saturated chamber for 3–5 min followed by cervical dislocation.

5. Pin the mouse face up to a protected Styrofoam board.

6. Wet the mouse thoroughly with 70 % EtOH. Use the back of the standard forceps to smooth down the fur. Wipe away any feces with a 70 % EtOH-damp Kimwipe.

7. Use the standard forceps to grasp the skin above the groin.

8. Use the Spencer Ligature scissors to cut along the ventral midline from the groin to the chin (Fig. 2-1B). Be careful to cut only the skin and not the peritoneum underneath.

9. Make four incisions from the midline cut towards the four legs (Fig. 2-1B).

10. Use the standard forceps to pull back the skin one side at a time to expose the mammary glands (Fig. 2-1C). Use the dorsal side of the Graefe forceps to help separate the skin from the peritoneum (Fig. 2-1D).

11. Push back a thin yellow layer of muscle located on top of gland #3 to expose the mammary gland (Fig. 2-1E–E').

12. Use the Graefe forceps to remove the inguinal lymph node located at the intersection of three blood vessels in gland #4 (Fig. 2-1F–F').

13. Use the Graefe forceps and Iris scissors to grasp and pull out mammary glands #3, #4, and #5 from both right and left sides. Pool glands in a sterile Petri dish (Fig. 2-2A) (see Note 1).

3.2 Isolating mammary epithelial organoids

Mammary epithelium is embedded inside a fat pad containing adipose tissue and collagen-rich stroma. This section describes how to purify fragments of mammary epithelium ("organoids") using enzymatic and mechanical digestion. All centrifugation speeds refer to a Sorvall Legend X1R benchtop swinging bucket centrifuge (1,500 rpm, 1,250 rcf). We have achieved similar results with 1,500 rpm spins in similar benchtop centrifuges from other manufacturers.

1. In a sterile hood, mince mammary glands with a scalpel, ~25–50 times per mouse, until the tissue relaxes (Fig. 2-2A, A'). Use a separate scalpel for each mouse type.

2. Use the scalpel to transfer the minced glands to collagenase solution in a 15 or a 50 mL tube (Fig. 2-2B). We use 10 mL of collagenase solution per mouse.

3. Shake the suspension at 110–150 rpm for 30–40 min (see Note 2) at 37 C until the tissue breaks up into smaller pieces and is relatively dispersed (Fig. 2-2B') but not overdigested (Fig. 2-2B''). We typically use a Thermo Scientific MaxQ 4450 for this purpose.

4. Spin the tube in a centrifuge at 1,500 rpm for 10 min at room temperature. The tube will have three layers: a fatty layer on top, an aqueous layer in the middle, and a red pellet of epithelium on the bottom (Fig. 2-2C).

5. Precoat (Fig. 2-3A) (see Note 3) a 15 mL tube with BSA solution. Use one tube per mouse type. For all subsequent steps, precoat all pipette tips and tubes with BSA solution prior to contact with mammary tissue (Fig. 2-3A).

6. To recover additional epithelial tissue, use a BSA-coated pipette (Fig. 2-3B) to transfer the opaque fatty layer into the BSA-coated 15 mL tube. Add DMEM/F12 up to 10 mL. Pipette up and down vigorously to disperse the fatty layer (Fig. 2-2D). Spin the tube at 1,500 rpm for 10 min at room temperature. Aspirate the fat and supernatant, and save the pellet (Fig. 2-2E).

7. Aspirate (see Note 4) the aqueous layer in the tube with the original pellet.

8. Add 10 mL DMEM/F12 to the tube with the original pellet, and transfer to the 15 mL "fatty layer" tube (step 6). Pipette up and down vigorously to resuspend and combine the two pellets.

9. Spin the tube at 1,500 rpm for 10 min at room temperature.

10. Aspirate the supernatant, and add up to 4 mL DMEM/F12 to the combined pellet (Fig. 2-2F). At this stage during isolation, the suspension contains small clusters of organoids and stromal cells attached to one another (Fig. 2-2F–F'').

11. Add 40 μL DNase (2 U/μL) into the 4 mL organoid suspension, and gently invert by hand for 2–5 min at room temperature to break up the clusters and detach organoids from single cells (Fig. 2-2G' –G'').

12. Add 6 mL of DMEM/F12, and pipette up and down thoroughly.

13. Spin the tube at 1,500 rpm for 10 min at room temperature. The pellet should now appear red and more compact (Fig. 2-2H–H'). Next perform differential centrifugation to wash out enzymes and separate single stromal cells from the epithelial organoids. The protocol suggests aspiration of the supernatant assuming that the stromal cells will be

discarded. If recovery of mammary stromal populations is desired, then transfer the supernatant after each spin to a 50 mL tube.

14. Aspirate the supernatant to the 0.5 mL mark.

15. Resuspend the pellet in 10 mL DMEM/F12, and mix thoroughly.

16. Pulse to 1,500 rpm, and stop the centrifuge 3–4 s after it reaches speed.

17. Repeat steps 14–16 three more times (see Note 5).

18. The final pellet should be off-white and consist mostly of organoids, without single cells (Fig. 2-2I-I'', J). However, the organoid suspension may be contaminated with other tissue types, most commonly fiber bundles (Fig. 2-2K) and muscle (Fig. 2-2I).

3.3 Organoid density determination

This section describes how to determine the density of the organoid suspension and the overall yield.

1. Resuspend the pellet in 10 mL DMEM/F12 to form a homogeneous mixture (see Note 6).

2. Mix thoroughly (e.g., by rocking the tube by hand), and transfer 50 µL of the suspension to a 30 mm Petri dish. Count the number of organoids in this sample volume under a microscope (Fig. 2-2I', J).

3. Calculate the total number of organoids collected according to the following formula. For example, if 20 organoids were counted in a 50 µL sample removed from a 10 mL

total volume (9,950 μL remaining), then the total number of organoids would be (20/50) x 9,950 = 3,980 organoids.

4. Calculate the organoid density (see Note 7), and readjust to 1,000 organoids/mL to simplify allocation to ECM gels.

5. Calculate the number of organoids and the respective volume of suspension required for each experiment.

6. Aliquot the required volumes of organoid suspension into BSA-coated 1.5 mL microcentrifuge tubes (Fig. 2-3C), and spin the tubes at 1,500 rpm for 5 min at room temperature.

7. Carefully remove the supernatant so as not to disturb the pellet (see Note 8).

8. Calculate the volume of ECM solution required to reach a final density of two organoids/μL (see Note 9).

3.4 Plating mammary organoids in matrigel

Mammary epithelium develops in vivo within a basement membrane. 3D culture in Matrigel, a basement membrane-rich gel, recapitulates important features of epithelial development[17, 19, 22, 23]. This section describes how to embed organoids in 3D Matrigel.

1. Thaw Matrigel at 4 C for 3–4 h prior to plating. If the Matrigel is put at 4 C to thaw at the start of the prep, it will be ready to use by the end of the prep. During plating, always keep Matrigel on ice.

2. Use a plate with a cover glass bottom for time-lapse imaging.

3. Preincubate the plate at 37 C for 5 min.

4. Set up the tissue culture hood in preparation for plating (Fig. 2-4A).

5. Set the heating block to 37 C, and place the plate in direct contact with the block (Fig. 2-4B–C') (see Note 10).

6. Add the required volume of liquid Matrigel to a microcentrifuge tube with organoids. Since Matrigel is quite viscous, first pipette up and down slowly a few times to coat the tip and ensure an accurate volume.

7. Keep the Matrigel-containing tube on ice or in a cold block. Resuspend the organoid pellet gently to avoid introducing air bubbles. Do not try to take up the entire volume into the pipette tip while mixing.

8. Plate the appropriate volume of Matrigel/organoid suspension into the wells according to the following table (Fig. 2-5A). Pipette up and down to resuspend the organoids before plating each sample, and pipette out only until the first stop.

9. Keep the plate on the heating block for several minutes to allow further gelation before returning it to the incubator.

10. Incubate the plate at 37 C, 5 % CO2, for 30–60 min.

11. Gently add pre-warmed organoid medium to the wells. For the cyst formation assay (Subheading 3.10.1), use basal medium without supplemental growth factors. For the branching morphogenesis assay (Subheading 3.10.2 and 3.10.3), supplement the medium with nanomolar concentrations of growth factor. A variety of growth factors may be

used, including EGF ligands (EGF, TGF-α, amphiregulin, heregulin, neuregulin), FGF ligands (FGF2, FGF7), and HGF. We most commonly use 2.5 nM FGF2.

12. Add sterile water or PBS to the empty wells to prevent desiccation.

13. Label the wells. Return the plate to the incubator.

14. If the plate will be used for DIC imaging, use a glass plate cover for better image quality.

3.5 Preparing collagen 1 solution

Collagen I solubilized from rat-tail is commonly used to study 3D migration of many cell types[32]. However, the properties of collagen I gels vary depending on multiple factors during preparation, such as temperature, pH, and collagen concentration. We demonstrated that the extent of collagen fiber assembly correlated strongly with invasive behavior[24]. This section describes how we prepare collagen I (Fig. 2-5B).

1. Rat tail collagen I is used to prepare a collagen solution according to the following formula. The steps below describe how to make a 250 µL solution. Scale up the volume as needed:

Total volume (µL)	250	500	1,000	2,000	5,000
1.0 N NaOH (µL)	8	16	32	64	160
DMEM 10x (µL)	25	50	100	200	500
Collagen I stock (µL)	217	434	868	1,763	4,340

2. Perform all steps on ice. To work with a large volume of collagen solution, use a 1,000 µL extra long pipette tip to avoid the collagen solution getting stuck to the filter barrier during pipetting.

3. First, combine 25 µL DMEM 10x and 8 µL NaOH, and mix well. The solution will turn a dark pink color (Fig. 2-5C1).

4. Add 217 µL collagen I (Fig. 2-5C2) (see Note 11). Since collagen I is quite viscous, pipette up and down slowly a few times to coat the pipette tip.

5. Mix the solution well until the color remains stable. When the pH changes from acidic → neutral → basic, the color changes from light green/yellow → light pink/orange → dark pink, respectively (Fig. 2-5C3–7). The desired color is light pink or salmon, which corresponds to a pH of 7.0–7.5 (Fig. 2-5C6) (see Note 12). The pH can be tested using pH strips.

6. Use DMEM 1x to adjust the neutralized collagen I solution to the desired collagen concentration (see Note 13). For the invasion assay (Subheading 3.10.4), we use a collagen concentration of 3 mg/mL.

3.6 Plating mammary organoids in collagen 1

Fibrillar collagen I, the most abundant structural protein in mammary glands, plays an important role in normal development as well as in breast cancer. Our previous studies have demonstrated that collagen I induces a conserved response of protrusive invasion in both normal and tumor organoids[23]. This section describes how to properly prepare preassembled collagen I and embed mammary organoids in a 3D gel.

1. Use a plate with a glass bottom for time-lapse imaging.

2. Use 20–30 μL of neutralized collagen to make a thin underlay on the cover glass of the well at room temperature (Fig. 2-5E). The underlay helps the top collagen/organoid suspension attach better to the cover glass.

3. Incubate the plate with the underlays at 37 C until ready for plating.

4. Preincubate the neutralized collagen I solution (used for the top gel) at 4 C for 60–120 min for preassembly[24] (see Note 14). The collagen I solution will turn cloudy and fibrous (Fig. 2-5D1–6) (see Note 15), a state we term preassembled collagen I.

5. Set up the tissue culture hood in preparation for plating (Fig. 2-4A).

6. Set the heating block to 37 C, and place the plate on top, in direct contact with the block (Fig. 2-4B–C') (see Note 10).

7. Always keep the collagen I solution on ice. Add the desired amount of preassembled collagen I to the organoid pellet in a microcentrifuge tube. Since collagen I is quite viscous, first pipette up and down slowly a few times to coat the tip and ensure an accurate volume.

8. Keep the tube on ice or in a cold block. Resuspend the organoid pellet gently to avoid introducing air bubbles. Do not try to take up the entire volume into the pipette tip while mixing.

9. Plate the appropriate volume of collagen/organoid suspension (see table in Subheading 3.4) on top of the underlay (Fig. 2-5E'). Pipette up and down to resuspend the organoids before plating each sample, and pipette out only until the first stop.

10. Keep the plate on the heating block for several minutes to allow further gelation before returning it to the incubator (see Note 16).

11. Incubate the plate at 37 C, 5 % CO2, for 45–60 min. After gelation, collagen I fibrils are visible under the microscope at 10x and 40x (Fig. 2-5F–F').

12. Gently add pre-warmed organoid medium supplemented with growth factor to the wells. A variety of growth factors may be used, including EGF ligands (EGF, TGF-α, amphiregulin, heregulin, neuregulin), FGF ligands (FGF2, FGF7), and HGF. We most commonly use 2.5 nM FGF2.

13. Add sterile water or PBS to the empty wells to prevent desiccation.

14. Label the wells. Return the plate to the incubator.

15. If the plate will be used for DIC imaging, use a glass plate cover for better image quality.

3.7 Plating mammary organoids in a mixture of matrigel and collagen 1

A mixture of Matrigel and collagen I represents a more physiological ECM microenvironment for mammary branching morphogenesis. The presence of collagen I significantly improves epithelial ductal elongation and myoepithelial coverage[24]. We do not observe epithelial protrusions into mixed Matrigel/collagen I gels[24]. This section describes how to properly prepare a mixture of Matrigel and preassembled collagen I and how to embed mammary organoids in this mixed matrix.

1. Prepare collagen I solution as described in Subheading 3.5.

2. Repeat steps 1–4 in Subheading 3.6 to make underlays and prepare preassembled collagen I.

3. Combine Matrigel and preassembled collagen I at the desired ratio. Gently pipette up and down a few times to form a homogeneous solution (Fig. 2-5B').

4. Always keep the mixed matrix solution on ice. Add the desired amount to the organoid pellet in a microcentrifuge tube.

5. Plate the mixed matrix/organoid suspension as described in steps 5–15 in Subheading 3.6 (Fig. 2-5E').

3.8 Immuno-fluorescence staining of 3D culture samples

The thickness of 3D gels and the multicellular structure of mammary organoids often result in reduced antibody accessibility for immuno-fluorescence (IF) staining and poor visualization during imaging. This section describes two methods for performing IF staining in 3D culture samples. First, fix gels as follows:

1. Remove organoid medium from the wells.

2. Fix samples with 4 % PFA for 10–15 min at room temperature (see Note 17) on an orbital shaker at 20 rpm.

3. Remove PFA, and wash samples 2–3x 10 min with DPBS.

From here, you can perform antibody staining directly in intact 3D gels or on cut sections on slides. The whole-gel staining works well with high-quality antibodies and probes

such as phalloidin (stains for F-actin), smooth muscle actin (SMA), and keratin 14. For many other antibodies, staining sections on slides is preferable.

3.8.1 Staining whole gels

1. Permeabilize the gel with 0.5 % Triton X-100 for 30–60 min.

2. After permeabilization, immediately block samples with 10 % FBS (see Note 18) for 1–3 h at room temperature or overnight at 4 C.

3. Remove the blocking solution, add primary antibody in 10 % FBS (see Note 18) at the desired ratio, and incubate for 2–3 h at room temperature or overnight at 4 C.

4. Remove the primary antibody solution, and wash samples 3x 10 min with 10 % FBS in DPBS at room temperature.

5. Optional: Block the samples again with 10 % FBS for 30–60 min at room temperature.

6. Add secondary antibody in 10 % FBS (see Note 18) at the desired ratio, and incubate for 1–2 h at room temperature.

7. Wash 3x 10 min with DPBS at room temperature.

8. Store samples in DPBS at 4 C, but remove DPBS before imaging. If the gel has detached from the cover slip, leaving the DPBS in the well causes the gel to wiggle or float and go out of focus.

3.8.2 Staining sections on slides

1. Gently detach the gel from the culture plate and transfer to a small disposable base mold (15 x 15 x 5 mm) filled with a thin layer of OCT.

2. Freeze the mold at -80^{o}C for 5–10 min.

3. Fill up the mold with OCT to cover the sample, and return to -80^{o}C for long-term storage.

4. During sectioning, store molds on dry ice. Set up the cryostat with OT at -20^{o}C and CT at -20^{o}C.

5. Remove an OCT block from its mold, and cut sections at 20–100 μm thickness.

6. Transfer sections to slides using a fine camel hair-brush or a pair of forceps.

7. Keep slides at -80^{o}C for long-term storage.

8. For antibody staining, thaw slides at room temperature (see Note 19).

9. Wash slides 2–3x 10 min with DPBS to remove OCT.

10. Permeabilize with 0.5 % Triton X-100 for 30–60 min (see Note 20).

11. Wash 2x 10 min with DPBS to remove Triton.

12. Block slides with 10 % FBS for 2 h at room temperature or overnight at 4^{o}C.

13. Remove the blocking solution, add primary antibody in 10 % FBS, and incubate for 2–3 h at room temperature or overnight at 4^{o}C (see Note 21).

14. Wash 3x 10 min with 10 % FBS or DPBS.

15. Add secondary antibody in 10 % FBS, and incubate for 2 h at room temperature or overnight at 4^{o}C.

16. Wash 3x 10 min with DPBS.

17. Mount slides with mounting medium and 50 x 22 mm coverslips. Let the slides dry at room temperature in a dry StainTray or in a dark drawer before imaging.

3.9 Immuno-fluorescence staining of mammary gland tissue section

The opacity and thickness of the mammary fat pad limit the accessibility of mammary epithelium to whole-gland staining and imaging. This section describes how to perform IF staining in mammary gland tissue sections.

1. Collect mouse mammary glands #3 and/or #4, as described in Subheading 3.1, taking care to keep the entire gland intact (see Note 22). Spread out the gland on the bottom of a 1- or a 2-well chambered cover glass.

2. Fix the tissue with 4 % PFA for 4 h at room temperature or overnight at 4 C.

3. Wash 3x15 min with DPBS to remove PFA.

4. Transfer the gland to a medium (24 x 24 x 5 mm) or a large (30 x 24 x 5 mm) disposable base mold filled with a thin layer of OCT.

5. Freeze the mold at -80^{o}C for 5–10 min.

6. Fill up the mold with OCT to cover the gland, and return to -80^{o}C for long-term storage.

7. During sectioning, store molds on dry ice. Set up the cryostat with OT at -40°C and CT at -30°C.

8. Remove an OCT block from its mold, and cut sections at 50–200 μm thickness.

9. Transfer sections to slides using a fine camel hair brush or a pair of forceps.

10. Keep slides at -80°C for long-term storage.

11. Repeat steps 8–17 in Subheading 3.8.2 for IF staining (see Note 23).

3.10 Assays

In vivo, mammary epithelium develops within a basement membrane surrounded by collagen-rich stromal tissue. The ability to manipulate the ECM microenvironment in 3D organotypic culture allows us to isolate the effects of individual matrix components on mammary epithelial cell behaviors. This section describes four assays that use different ECM compositions or growth conditions to model distinct epithelial programs (Fig. 2-6A).

3.10.1 Cyst Formation Assay

In 3D Matrigel in basal medium, mammary organoids reorganize from a multilayered fragment to establish a simple bi-layered epithelium with an internal lumen, termed a cyst (Figs. 2-6B and 2-7A). The extent of lumen formation varies with the initial size of the organoid and with the mouse strain (Fig. 2-7A1–A4). The resulting morphologies include a minimal or a barely detectable lumen (Fig. 2-7A1), a partial lumen (Fig. 2-7A2), a complete lumen in a small cyst (Fig. 2-7A3), and a complete lumen in a large cyst (Fig. 2-7A4). Epithelial cells in the cyst always maintain a smooth basal surface with the ECM (Fig. 2-7A4). We have observed that C57BL6 organoids form cysts with complete

lumens (Fig. 2-6B) more efficiently than FVB organoids. Although the appearance of the lumen varies by light microscopy, immunofluorescence staining for SMA and F-actin can confirm the establishment of a simple bi-layered structure of internal luminal epithelial cells and basal myoepithelial cells (Fig. 2-8A). We use this assay to model the formation of mammary epithelial ducts in vivo (Fig. 2-8D).

3.10.2 Branching Morphogenesis Assay in Matrigel

In 3D Matrigel, nanomolar concentrations of growth factor induce mammary organoids to undergo branching morphogenesis (Fig. 2-6C). The branching program includes sequential steps of lumen clearing, stratification, bud initiation, and bud elongation (Fig. 2-6C)[17]. We observe variation in morphology depending on the extent of progression through this program. Organoids that only complete stratification or bud initiation (Fig. 2-7B1), or that form fewer than three buds (Fig. 2-7B2–B4), are not scored as "branched" (Fig. 2-7B). Only organoids with three or more elongated buds are scored as "branched" (Fig. 2-7C). However, the morphology of branched organoids varies based on the initial size of the organoid, the mouse strain, and the types of growth factors added. Here, we present four examples of branching in Matrigel (Fig. 2-7C1–C4). The first two show organoids with multiple multilayered, elongating buds without any regions of repolarization (Fig. 2-7C1–C2). In contrast, the second two show organoids that have reestablished simple epithelial architecture in the central lumen (Fig. 2-7C3) or within buds (Fig. 2-7C4). During bud elongation in Matrigel, the leading front of the bud is always non-protrusive (Fig. 2-7B40, C40). Notably, these buds lack or are incompletely covered by myoepithelial cells (SMA^+, Fig. 2-8B). These gaps in myoepithelial coverage

can be observed in vivo, particularly in side branches of the mammary ductal tree (Fig. 2-8E).

3.10.3 Branching Morphogenesis Assay in a Mix of Matrigel and Collagen I

In a mixture of Matrigel and collagen I, mammary organoids undergo a similar program of branching morphogenesis to that in Matrigel alone, with several notable differences[24] (Fig. 2-6D). Branched organoids in the mixed matrix generally have fewer buds, but the buds elongate much further into the ECM. We have demonstrated that ratios of 5:5 and 3:7 Matrigel to collagen I induce the highest average bud lengths[24]. Here, we present four examples of branching in the mixed matrices. Organoids may contain both short and long buds, without repolarization (Fig. 2-7D1) or with partial repolarization (Fig. 2-7D2, D4). We also observe bifurcation at the ends of elongated buds (Fig. 2-7D3). As in Matrigel alone, the leading front of the bud is always nonprotrusive (Fig. 2-7D40). Importantly, a mix of 3:7 Matrigel to collagen I yields a high percentage of epithelial buds that maintain complete myoepithelial coverage throughout bud initiation and elongation (Fig. 2-8C). This phenomenon more closely models elongation of the terminal end bud in vivo (Fig. 2-8F).

3.10.4 Invasion Assay

Collagen I induces a conserved protrusive response in mammary epithelium (48 h, Fig. 2-6E). Organoids invade collectively into collagen I, with branches varying in shape and length, from short and thin (Fig. 2-7E1–E2) to elongated and wide (Fig. 2-7E3–E4). Initially, we observe extensive subcellular protrusions. However, these protrusions cease, and the epithelium reestablishes a smooth basal surface upon formation of a basement membrane between the epithelium and ECM (Fig. 2-6E)[23]. The extent of invasion and

epithelial reorganization varies, even within the same organoid. At day 5 in culture, we observe both protrusive (violet arrowheads, Fig. 2-7E40) and non-protrusive, round tips (violet filled arrowheads, Fig. 2-7E1–E4) at the ends of multicellular invasive structures. We also observe single cell dissemination into collagen I (blue arrowheads, Fig. 2-7E1,E4).

3.11 Technical Issues

Here we present several technical problems that we commonly encounter during 3D culture. First, epithelial organoids located very close to the cover glass tend to lose their 3D structure and spread out in 2D as sheets of cells (Fig. 2-7F1–F2). Second, organoids may be surrounded by protrusive or stringy cells, which likely results from stromal or other non-epithelial cells attaching to organoids during their isolation (Fig. 2-7F3). Non-epithelial contaminating species appear distinct and behave differently from organoids. We have observed groups of dead cells (Fig. 2-7F4), clusters of protrusive stromal cells (Fig. 2-7F5), and nerve bundles (Fig. 2-7F6), which tend to locally disseminate cells into the matrix.

4 Notes

1. Mammary gland #1 is very small. Mammary gland #2 is located in the neck and is hard to distinguish from other tissues. Generally, do not collect these glands so as to avoid contamination by other tissues (e.g., muscle or other epithelial glands) (Fig. 2-2I).

2. Incubation in collagenase solution can require up to 60 min to adequately break up the fat pad. Check the status of the suspension after 30 min of shaking. We have observed that inappropriate incubation times increase the amount of contaminating tissues in the

final organoid suspension (Fig. 2-2K). If shaking is done in an incubator that is also used for bacterial cultures, wipe the outside of the tube with 70 % ethanol before bringing it into the tissue culture hood.

3. Always precoat new pipette tips and tubes with BSA solution to prevent organoids from sticking to the plastic. This precoating (Fig. 2-3) is critical to achieving a high final yield of organoids, especially with mice at younger ages or mice on a C57BL6 background.

4. Never aspirate the supernatant completely to avoid sucking up the pellet.

5. Carefully examine the pellet after each quick spin before aspirating the supernatant. If the organoids are not well pelleted, mix the suspension thoroughly again, and increase the centrifugation time.

6. The appropriate volume of DMEM/F12 to use for counting varies depending on the estimated yield. If the yield is low, add less medium. If the yield is high, dilute the suspension further 2–10x.

7. The yield varies significantly with mouse strain and age. We generally obtain 2,000–4,000 organoids per FVB mouse and 500–2,000 organoids per C57BL6 mouse.

8. Always check the pellet after every centrifugation. Be careful not to disturb the pellet when removing the supernatant. Use small pipette tips if necessary.

9. The optimal density of organoids in the gel differs for different ECMs and mouse strains. For example, C57BL6 organoids tend to be more contractile than FVB organoids

when embedded in collagen I, resulting in contraction of the gel and detachment from the glass bottom if plated too densely.

10. In a 24-well plate, the glass bottom is slightly recessed from the edge of the plastic wall. When both blocks are present in the heating block (Fig. 2-4B), there is a small gap between the plate and the heating block surface, resulting in a temperature at the glass bottom less than 37^{o}C. To establish direct contact between the glass bottom and the heating block, remove one of the blocks, and set up the plate as in Fig. 2-4C–C'.

11. When preparing the collagen I solution, always wait for the solution to come down to the tip, and pipette it out completely. This is particularly important during collagen I neutralization to ensure an accurate volume and concentration of collagen.

12. Since the concentration and pH of rat tail collagen I vary among batches, adjust the pH using small volumes of collagen stock (up to 30 μL) or small amounts of 1.0 N NaOH (calculation of the final concentration of neutralized collagen solution. (b) If you find that your collagen I stock is more basic, prepare the collagen solution with 7.0–7.5 μL of 1.0 N NaOH per 250 μL, and then adjust the final pH with small volumes of 1.0 N NaOH. This will avoid the need to add large volumes of collagen I stock to achieve the appropriate pH.

13. If you are concerned about the accuracy of the final collagen concentration, try to use the same pipette tip for mixing throughout neutralization and pH adjustment to limit the loss of collagen solution inside the pipette tip.

14. The preincubation time will determine the density of preassembled collagen fibrils. Due to batch variability in collagen stocks, the time required to obtain a gel with visible

collagen fibrils varies considerably from 45 to 120 min. To examine the extent of fibril formation during preincubation, plate 30 μL of collagen solution onto a small Petri dish, let it gel for several minutes, and examine under the microscope.

15. If the neutralized collagen I solution is preincubated for more than 3–4 h on ice, it will become very cloudy and fibrous (Fig. 2-5D6), and the resulting gel will be less transparent, impairing visibility during imaging.

16. Collagen I gels tend to detach from the cover glass when kept too long on the heating block. Therefore, if you have Matrigel and collagen I gels on the same plate, plate the Matrigel samples first and the collagen I samples last.

17. In PFA, Matrigel becomes very fragile, especially after more than 4 days in culture. To avoid disintegration of the gel, reduce the PFA concentration to 2 % with lighter shaking or incubate the gel with 4 % PFA for 8–10 min.

18. In our lab, we have identified two successful approaches for performing antibody staining that use slightly different solutions and incubation times. The first one, described in Subheadings 3.8 and 3.9, uses 10 % FBS in DPBS as both the blocking buffer and the dilution buffer for antibodies. The other method uses 10 % FBS and 1 % BSA in DPBS as a blocking buffer and 1 % FBS and 1 % BSA in DPBS as the dilution buffer for antibodies.

19. From this step on, slides are kept in a StainTray with a black lid filled with a shallow layer of water to prevent desiccation and photo-bleaching of fluorescent probes.

20. If you plan to stain for extracellular proteins, such as basement membrane components, permeabilize the samples before embedding into OCT and sectioning. Direct permeabilization on slides can extract too many of these proteins.

21. To conserve primary antibodies, especially ones that require a high concentration, use a PAP pen to draw a hydrophobic border around the section, and add primary antibody solution within this area.

22. For mice less than 4 weeks of age, we typically use only gland #4 and remove the fat pad distal to the lymph nodes. Since the glands at this age are very small, pool several glands into one OCT block for sectioning.

23. To improve antibody staining in mammary gland tissue sections, it is sometimes useful to significantly increase the incubation times. For example, we sometimes permeabilize with Triton X-100 for 1 h at room temperature; incubate with primary antibody for 48 h at 4 C; and incubate with secondary antibody for 6 h at room temperature or overnight at 4 C. In addition, for incubation with antibodies, it is preferable to draw a hydrophobic border around the tissue with a PAP pen to reduce the volume of solution required and to ensure that the tissue is always immersed in solution. Do not let samples air-dry.

References

1. Sternlicht MD (2006) Key stages in mammary gland development: the cues that regulate ductal branching morphogenesis. Breast Cancer Res 8:201
2. Hogg NA, Harrison CJ, Tickle C (1983) Lumen formation in the developing mouse mammary gland. J Embryol Exp Morphol 73:39–57
3. Williams JM, Daniel CW (1983) Mammary ductal elongation: differentiation of myoepithelium and basal lamina during branching morphogenesis. Dev Biol 97:274–290
4. Hinck L, Silberstein GB (2005) Key stages in mammary gland development: the mammary end bud as a motile organ. Breast Cancer Res 7:245–251
5. Sternlicht MD, Kouros-Mehr H, Lu P, Werb Z (2006) Hormonal and local control of mammary branching morphogenesis. Differentiation 74:365–381
6. Mroue R, Bissell MJ (2012) Three-dimensional cultures of mouse mammary epithelial cells. Methods Mol Biol 945:221–250
7. Vidi PA, Bissell MJ, Lelievre SA (2012) Three-dimensional culture of human breast epithelial cells: the how and the why. Methods Mol Biol 945:193–219
8. Griffith LG, Swartz MA (2006) Capturing complex 3D tissue physiology in vitro. Nat Rev Mol Cell Biol 7:211–224
9. Gudjonsson T, Ronnov-Jessen L, Villadsen R, Bissell MJ, Petersen OW (2003) To create the correct microenvironment: three-dimensional heterotypic collagen assays for human breast epithelial morphogenesis and neoplasia. Methods 30:247–255
10. Nelson CM, Bissell MJ (2005) Modeling dynamic reciprocity: engineering threedimensional culture models of breastarchitecture, function, and neoplastic transformation. Semin Cancer Biol 15:342–352
11. Nelson CM, Inman JL, Bissell MJ (2008) Three-dimensional lithographically defined organotypic tissue arrays for quantitative analysis of morphogenesis and neoplastic progression. Nat Protoc 3:674–678
12. Wozniak MA, Keely PJ (2005) Use of three-dimensional collagen gels to study mechanotransduction in T47D breast epithelial cells. Biol Proced Online 7:144–161
13. Provenzano PP, Eliceiri KW, Inman DR, Keely PJ (2010) Engineering three-dimensional collagen matrices to provide contact guidance during 3D cell migration. Curr Protoc Cell Biol Chapter 10:Unit 10 17
14. Debnath J, Muthuswamy SK, Brugge JS (2003) Morphogenesis and oncogenesis of MCF-10A mammary epithelial acini grown in three-dimensional basement membrane cultures. Methods 30:256–268
15. Ichinose RR, Nandi S (1964) Lobuloalveolar differentiation in mouse mammary tissues in vitro. Science 145:496–497
16. Ichinose RR, Nandi S (1966) Influence of hormones on lobulo-alveolar differentiation of mouse mammary glands in vitro. J Endocrinol 35:331–340
17. Ewald AJ, Brenot A, Duong M, Chan BS, Werb Z (2008) Collective epithelial migration and cell rearrangements drive mammary branching morphogenesis. Dev Cell 14:570–581

18. Simian M, Hirai Y, Navre M, Werb Z, Lochter A, Bissell MJ (2001) The interplay of matrix metalloproteinases, morphogens and growth factors is necessary for branching of mammary epithelial cells. Development 128:3117–3131
19. Fata JE, Mori H, Ewald AJ, Zhang H, Yao E, Werb Z, Bissell MJ (2007) The MAPK(ERK- 1,2) pathway integrates distinct and antagonistic signals from TGFalpha and FGF7 in morphogenesis of mouse mammary epithelium. Dev Biol 306:193–207
20. Nelson CM, Vanduijn MM, Inman JL, Fletcher DA, Bissell MJ (2006) Tissue geometry determines sites of mammary branching morphogenesis in organotypic cultures. Science 314:298–300
21. Sternlicht MD, Sunnarborg SW, Kouros-Mehr H, Yu Y, Lee DC, Werb Z (2005) Mammary ductal morphogenesis requires paracrine activation of stromal EGFR via ADAM17- dependent shedding of epithelial amphiregulin. Development 132:3923–3933
22. Ewald AJ, Huebner RJ, Palsdottir H, Lee JK, Perez MJ, Jorgens DM, Tauscher AN, Cheung KJ, Werb Z, Auer M (2012) Mammary collective cell migration involves transient loss of epithelial features and individual cell migration within the epithelium. J Cell Sci 125:2638–2654
23. Nguyen-Ngoc KV, Cheung KJ, Brenot A, Shamir ER, Gray RS, Hines WC, Yaswen P, Werb Z, Ewald AJ (2012) The ECM microenvironment regulates collective migration and local dissemination in normal and malignant mammary epithelium. Proc Natl Acad Sci U S A 109:E2595–E2604
24. Nguyen-Ngoc KV, Ewald AJ (2013) Mammary ductal elongation and myoepithelial migration are regulated by the composition of the extracellular matrix. J Microsc 251 (3):212–223
25. Provenzano PP, Eliceiri KW, Campbell JM, Inman DR, White JG, Keely PJ (2006) Collagen reorganization at the tumor-stromal interface facilitates local invasion. BMC Med 4:38
26. Provenzano PP, Inman DR, Eliceiri KW, Knittel JG, Yan L, Rueden CT, White JG, Keely PJ (2008) Collagen density promotes mammary tumor initiation and progression. BMC Med 6:11
27. Conklin MW, Eickhoff JC, Riching KM, Pehlke CA, Eliceiri KW, Provenzano PP, Friedl A, Keely PJ (2011) Aligned collagen is a prognostic signature for survival in human breast carcinoma. Am J Pathol 178:1221–1232
28. Egeblad M, Rasch MG, Weaver VM (2010) Dynamic interplay between the collagen scaffold and tumor evolution. Curr Opin Cell Biol 22:697–706
29. Paszek MJ, Zahir N, Johnson KR, Lakins JN, Rozenberg GI, Gefen A, Reinhart-King CA, Margulies SS, Dembo M, Boettiger D, Hammer DA, Weaver VM (2005) Tensional homeostasis and the malignant phenotype. Cancer Cell 8:241–254
30. Levental KR, Yu H, Kass L, Lakins JN, Egeblad M, Erler JT, Fong SF, Csiszar K, Giaccia A, Weninger W, Yamauchi M, Gasser DL, Weaver VM (2009) Matrix crosslinking forces tumor progression by enhancing integrin signaling. Cell 139:891–906
31. Ewald AJ (2013) Isolation of mouse mammary organoids for long-term time-lapse imaging. Cold Spring Harb Protoc 2013

32. Wolf K, Alexander S, Schacht V, Coussens LM, von Andrian UH, van Rheenen J, Deryugina E, Friedl P (2009) Collagen-based cell migration models in vitro and in vivo. Semin Cell Dev Biol 20:931–941
33. Cheung KJ, Gabrielson E, Werb Z, Ewald AJ, "Collective invasion in breast cancer requires aconserved basal epithelial program," Cell. 2013 Dec 19;155(7):1639–51
34. Shamir ER, Papallardo E, Jorgens DM, Coutinho K, Tsai WT, Aziz K, Auer M, Tran PT, Bader JS, Ewald AJ, "Twist1-induced dissemination preserves epithelial identity and requires E-cadherin," The Journal of Cell Biology. 2014 Mar 3;204(5):839–56.
35. Huebner RJ, Lechler T, Ewald AJ, "Mammary epithelial stratification occurs through symmetry breaking vertical divisions of luminal cells," Development. 2014 Mar;141(5):1085–94.

Figure 2-1: Collection of mouse mammary glands for organoid isolation and 3D culture.

(a) Schematic description of isolation and 3D culture of mouse mammary organoids. (b) Scheme for surgically accessing the mammary glands. Numbers indicate the order of cuts. (c) Locations of the ten mammary glands. (d) Expose glands #3, #4, and #5 by pushing back the abdomen (blue dotted line) with the back of the Graefe forceps. (e–e') A thin layer of muscle partially covers gland #3 (e) and should be pushed back before dissection (e'). Dotted line in (e') indicates the region of gland #3 to be collected. (f) Use the Graefe forceps to pluck out the lymph node in gland #4. Dotted line in (f ') indicates the approximate region of glands #4 and #5 to be collected.

Figure 2-1

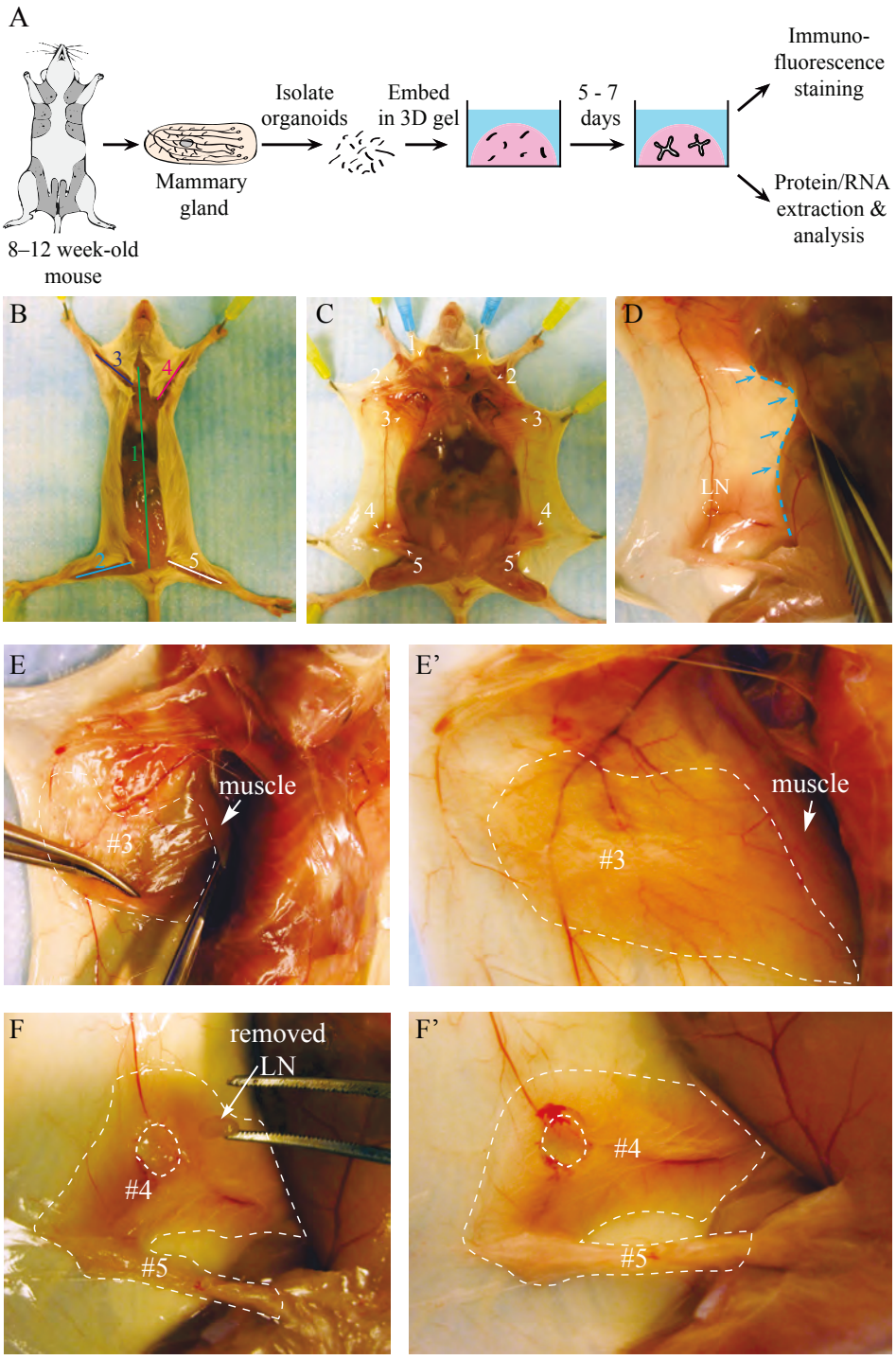
A
8–12 week-old mouse
Mammary gland
Isolate organoids
Embed in 3D gel
5 - 7 days
Immuno-fluorescence staining
Protein/RNA extraction & analysis
B
C
D
LN
E
muscle
#3
E'
muscle
#3
F
removed LN
#4
#5
F'
#4
#5

Figure 2-2: Mammary organoid isolation.

(a–a') Collected mammary glands are pooled in a Petri dish (a) and minced until the tissue relaxes, typically 25–50 cuts (a'). (b–b'') Incubation in collagenase solution breaks up the fat pad (b) into smaller pieces that are relatively dispersed (b'). Too long of a digestion (b'') will cause organoids to be too small and not grow well. (c) Following incubation in collagenase solution, centrifugation separates the suspension into three layers, with a top opaque layer of fat and a pellet (#1) of epithelium and stroma. (d) The fatty layer is transferred to a new tube and resuspended in 10 mL DMEM/F12. (e) Centrifugation of the dispersed fatty layer recovers additional epithelium in the pellet (#2). (f–f'') The combined pellets from (c) and (e) are resuspended in 4 mL DMEM/F12 with DNase (f). Before DNase treatment, organoids (pink arrowheads) are loosely attached to each other and to stromal cells (f '), forming visible clusters in the tube (f''). (g–g'') DNase treatment causes organoids (pink arrowheads) to detach from one another (g') and the clusters to disappear (g''). (h–h') Centrifugation of the suspension in (g) results in a compact red pellet (h'). (i–I'') Differential centrifugation removes single cells from the suspension (I') and results in an off-white pellet of purified epithelial organoids (I''). Organoids (pink arrowheads) may appear rounded and small or more elongated and even branched (I'). Larger organoids typically survive and branch more efficiently in our assays. (j) Close-up view of an organoid. (k–l) Non-epithelial tissues can be observed in the final suspension, including nerve bundles (k) and muscle (l) (Color figure online)

Figure 2-2

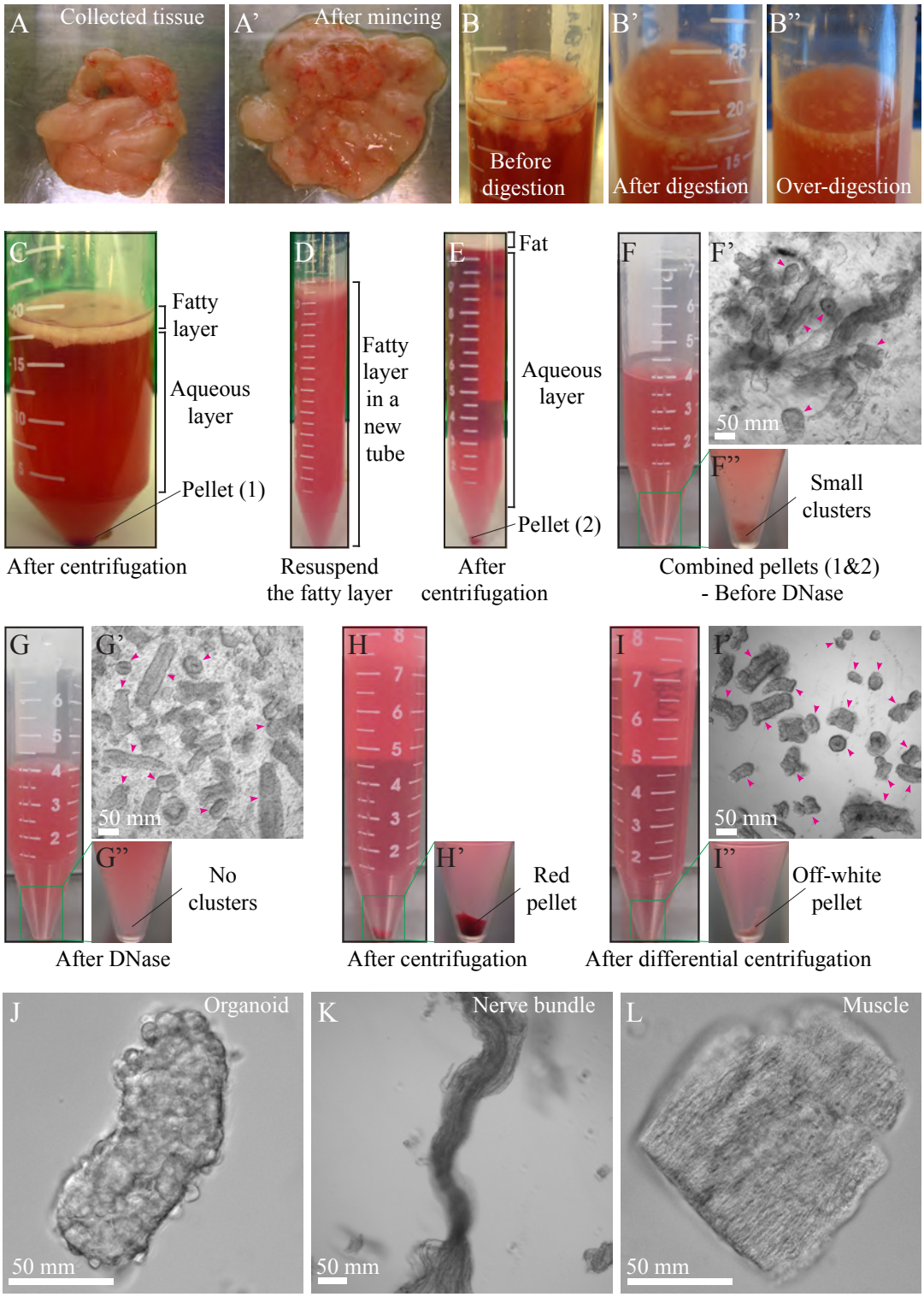
A
Collected tissue
A'
After mincing
B
Before digestion
B'
After digestion
B''
Over-digestion
C
Fatty layer
Aqueous layer
Pellet (1)
After centrifugation
D
Fatty layer in a new tube
Resuspend the fatty layer
E
Fat
Aqueous layer
Pellet (2)
After centrifugation
F
F'
50 mm
F''
Small clusters
Combined pellets (1&2) - Before DNase
G
G'
50 mm
G''
No clusters
After DNase
H
H'
Red pellet
After centrifugation
I
I'
50 mm
I''
Off-white pellet
After differential centrifugation
J
Organoid
50 mm
K
Nerve bundle
50 mm
L
Muscle
50 mm

Figure 2-3: Precoating tubes and pipette tips with BSA.

Fresh tissue can adhere to uncoated plastic surfaces, and this protocol involves many pipetting steps. Accordingly, it is essential to precoat the plastic surfaces with BSA solution to maximize final organoid yield. (a) Precoat a 15 mL tube by filling the tube with BSA solution, inverting the tube to precoat the cap, and removing the BSA solution. (b) Precoat a 10 mL pipette tip by taking up BSA solution to fill the entire pipette and ejecting back out. (c, d) Use the same approach to precoat a microcentrifuge tube (c) and a small pipette tip (d) with BSA solution

Figure 2-3

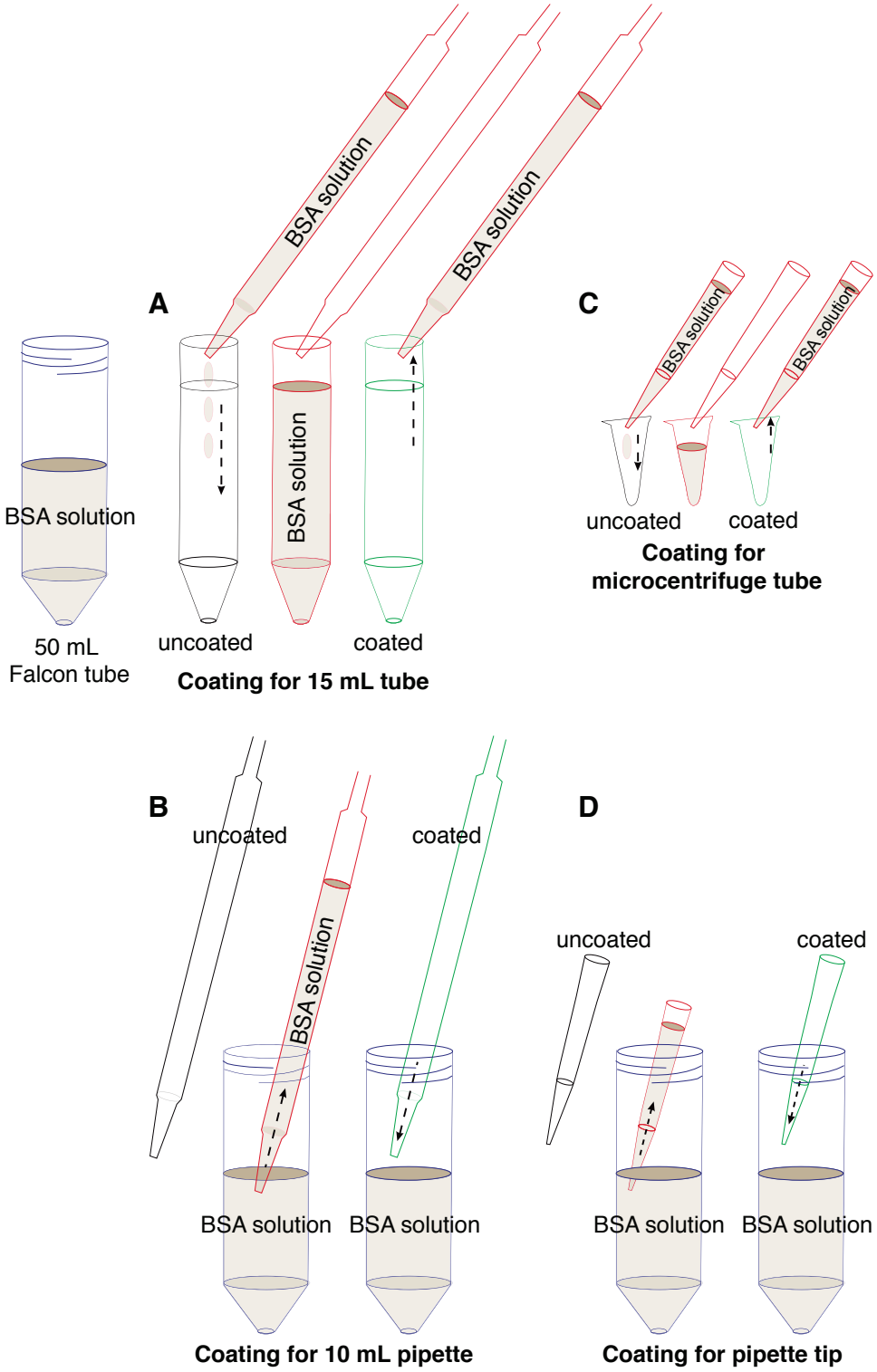
A
BSA solution
BSA solution
BSA solution
BSA solution
50 mL
Falcon tube
uncoated
coated
Coating for 15 mL tube
C
BSA solution
BSA solution
uncoated
coated
Coating for
microcentrifuge tube
B
uncoated
coated
BSA solution
BSA solution
BSA solution
Coating for 10 mL pipette
D
uncoated
coated
BSA solution
BSA solution
Coating for pipette tip

Figure 2-4: Setting up the tissue culture hood for plating.

(a) Sample layout of reagents, tools, and equipment used for plating 3D culture samples. (b) Heating block setup for plating in 2-well or 4-well chambers. (c, c') To plate in a 24-well dish, remove one of the blocks from the heating block (c) to establish direct contact between the remaining block and the plate bottom (c')

Figure 2-4

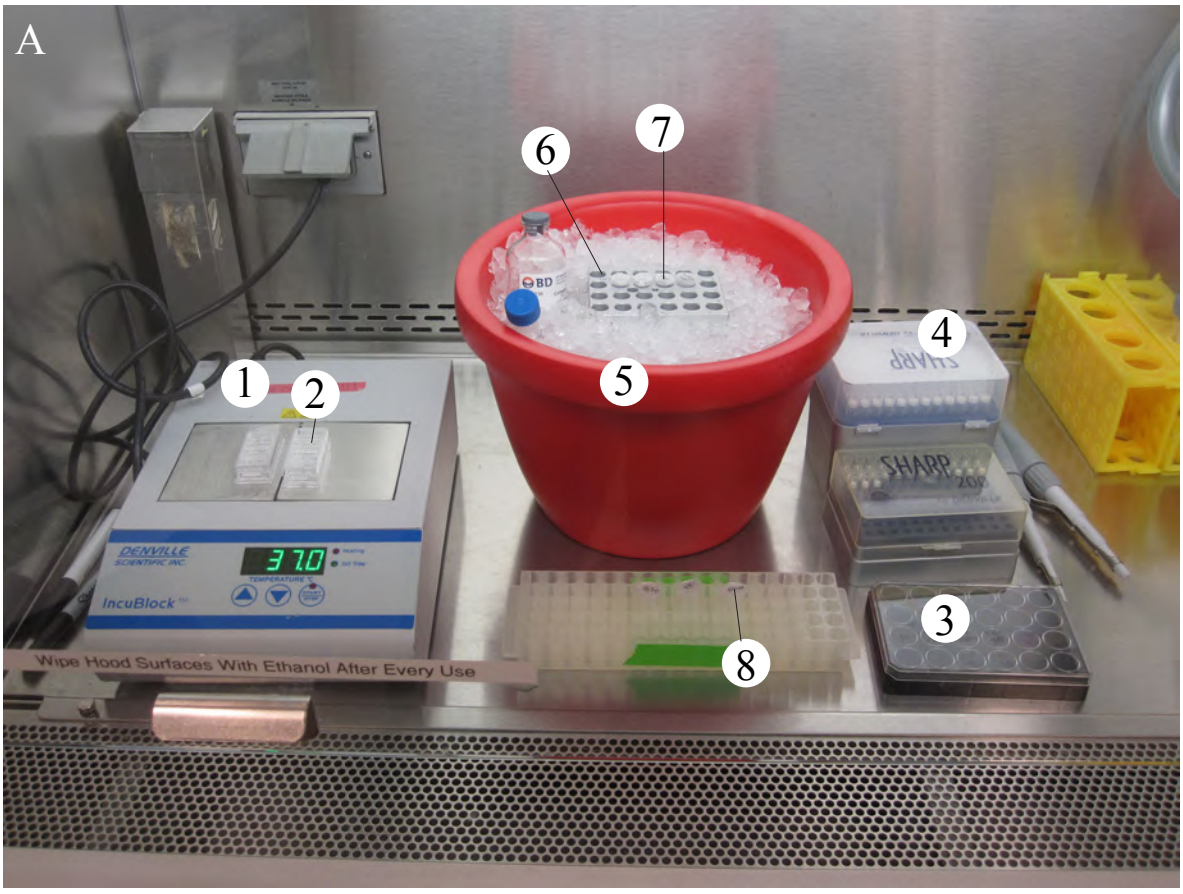

1. Heating block	4. 1 mL extra long tips	7. Collagen I solution being preincubated
2. 4-well chamber	5. Ice bucket	
3. 24-well plate	6. Cold block	8. Organoid samples

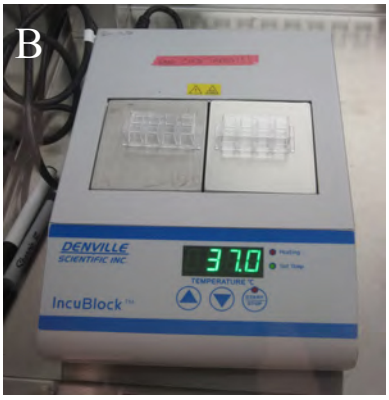

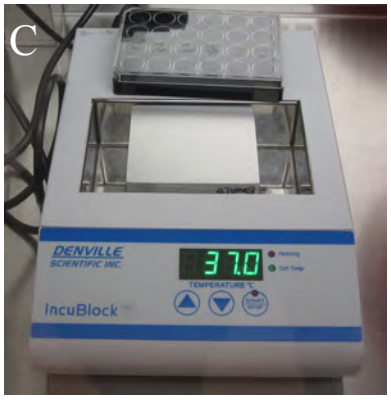

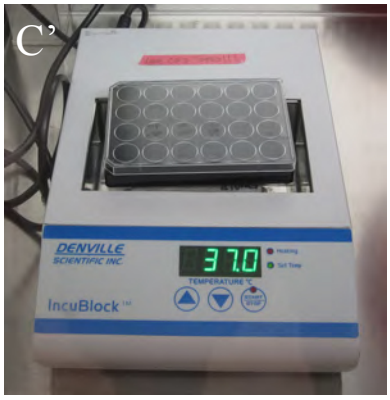

Figure 2-5: Plating organoids in 3D Matrigel and collagen I.

(a) Schematic description of plating organoids in Matrigel. (b–b') Schematic description of preparing preassembled collagen I (b), which can be used alone or mixed with Matrigel (b'). (c1–c7) Color indicators for the pH of the collagen I solution during neutralization. (d1–d6) Decreasing transparency of the collagen I solution during preincubation on ice. (e–e') Schematic description of plating organoids in 3D collagen I or in a mixture of Matrigel and collagen I. (e) Shows a top view for making an underlay on the cover glass. (e') Shows a side view of how to plate the organoid/collagen I suspension on top of the gelled underlay. (f–f ') Representative DIC images of collagen I fibers at low (f) and high (f ') magnification

Figure 2-5

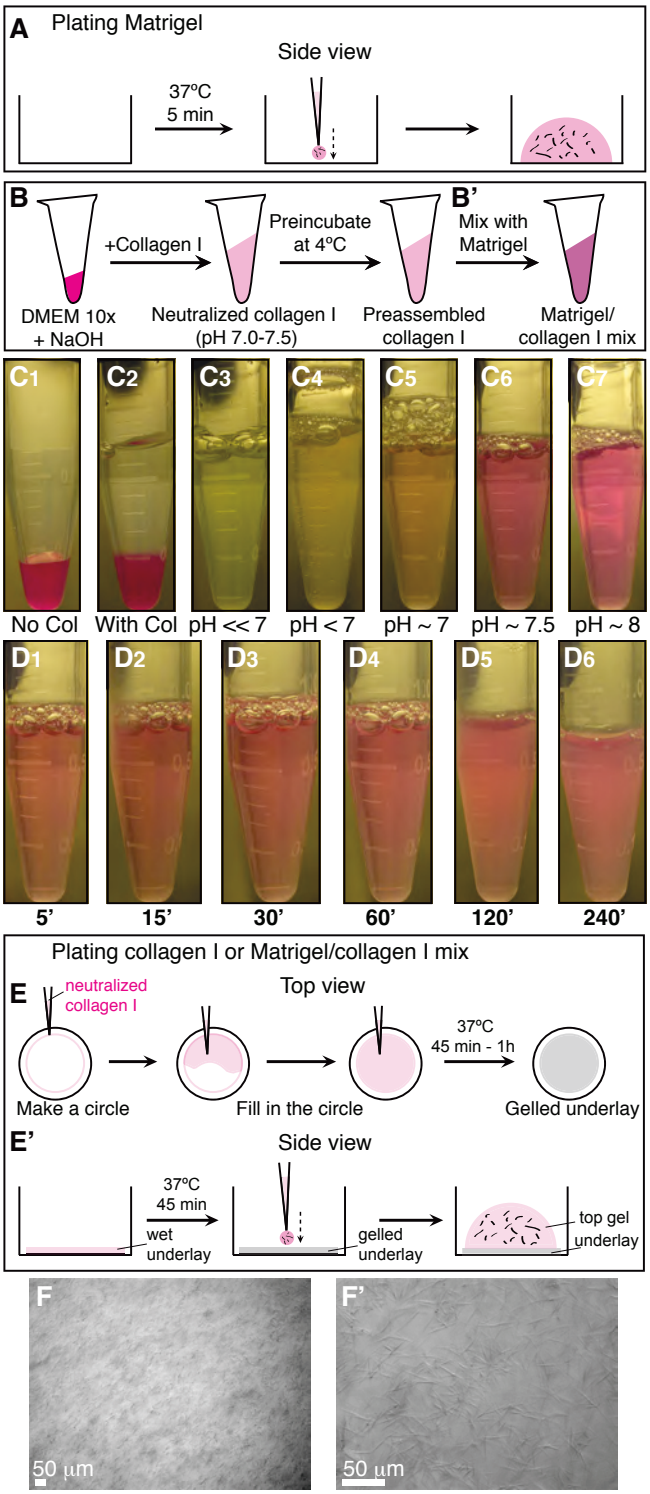
A
Plating Matrigel
Side view
37ºC
5 min
B
+Collagen I
Preincubate
at 4ºC
B'
Mix with
Matrigel
DMEM 10x
+ NaOH
Neutralized collagen I
(pH 7.0-7.5)
Preassembled
collagen I
Matrigel/
collagen I mix
C1
C2
C3
C4
C5
C6
C7
No Col
With Col
pH << 7
pH < 7
pH ~ 7
pH ~ 7.5
pH ~ 8
D1
D2
D3
D4
D5
D6
5'
15'
30'
60'
120'
240'
Plating collagen I or Matrigel/collagen I mix
E
neutralized
collagen I
Top view
37ºC
45 min - 1h
Make a circle
Fill in the circle
Gelled underlay
E'
Side view
37ºC
45 min
wet
underlay
gelled
underlay
top gel
underlay
F
50 µm
F'
50 µm

Figure 2-6: 3D organotypic culture assays.

(a) Schematic description of four assays that use different extracellular matrix compositions to model specific epithelial behaviors. (b–e) Representative frames of DIC time-lapse movies showing cyst formation in Matrigel in basal medium (b), branching morphogenesis in Matrigel induced by FGF2 (c), branching morphogenesis in a mixture of Matrigel and collagen I induced by FGF2 (d), and epithelial cell invasion into pure collagen I induced by FGF2 (e)

Figure 2-6

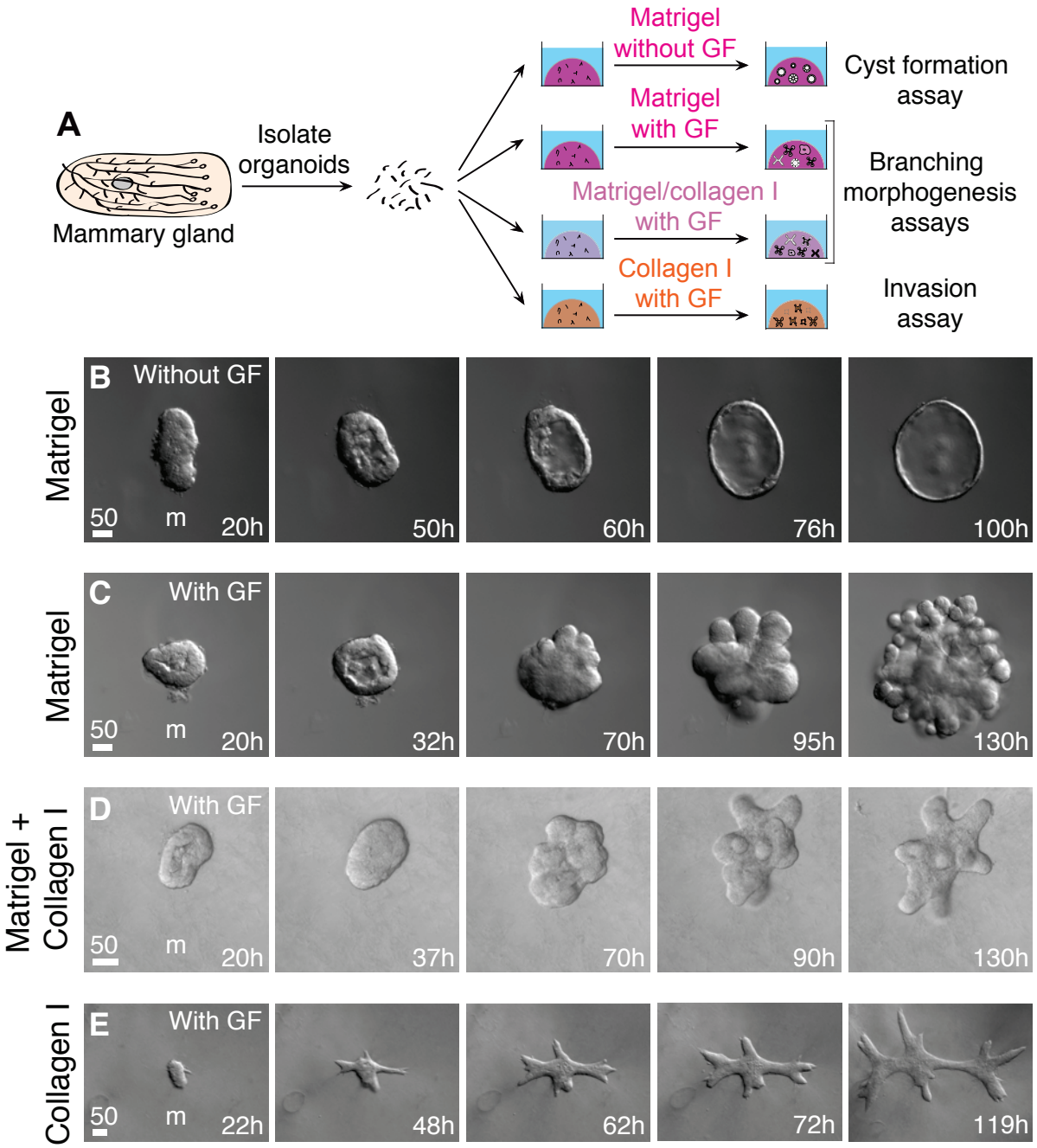
A
Mammary gland
Isolate organoids
Matrigel without GF
Cyst formation assay
Matrigel with GF
Matrigel/collagen I with GF
Branching morphogenesis assays
Collagen I with GF
Invasion assay
Matrigel
B Without GF
50 m
20h
50h
60h
76h
100h
Matrigel
C With GF
50 m
20h
32h
70h
95h
130h
Matrigel + Collagen I
D With GF
50 m
20h
37h
70h
90h
130h
Collagen I
E With GF
50 m
22h
48h
62h
72h
119h

Figure 2-7: Phenotypic variability in assay outcomes.

(a) Schematic description of a cyst. (a1–a4) DIC images showing variation in cyst morphology. (a4') An inset of (a4) showing a smooth basal surface with Matrigel. (b) Schematic description of a stratified, unbranched organoid. (b1–b4) DIC images showing examples of stratified, unbranched organoids in Matrigel. (b4') An inset of (b4) showing a smooth basal surface with Matrigel. (c) Schematic description of a branched organoid in Matrigel. (c1–c4) DIC images showing variation in branching morphology. (c4') An inset of (c4) showing a smooth basal surface with Matrigel. (d) Schematic description of a branched organoid in a mixture of Matrigel and collagen I. (d1–d4) DIC images showing variation in branching morphology. (d4') An inset of (d4) showing a smooth basal surface with the mixed matrix. (e) Schematic description of an organoid with protrusive tips in collagen I. (e1–e4) DIC images showing variation in protrusive invasion. (e4') An inset of (e4) showing protrusive tips into collagen I. (f) DIC images showing commonly observed technical issues. (f1–f2) Organoids lose their 3D organization in Matrigel (f1) and collagen I gels (f2) when they make contact with the cover glass. (f3) Non-epithelial species (red arrowheads) attached to organoids may appear elongated and mesenchymal (ECM: Matrigel). (f4) A group of dead cells beside a branching organoid (ECM: collagen I). (f5) A cluster of elongated, non-epithelial cells (ECM: Matrigel). (f6) A nerve bundle disseminating single cells into the surrounding matrix (ECM: Matrigel)

Figure 2-7

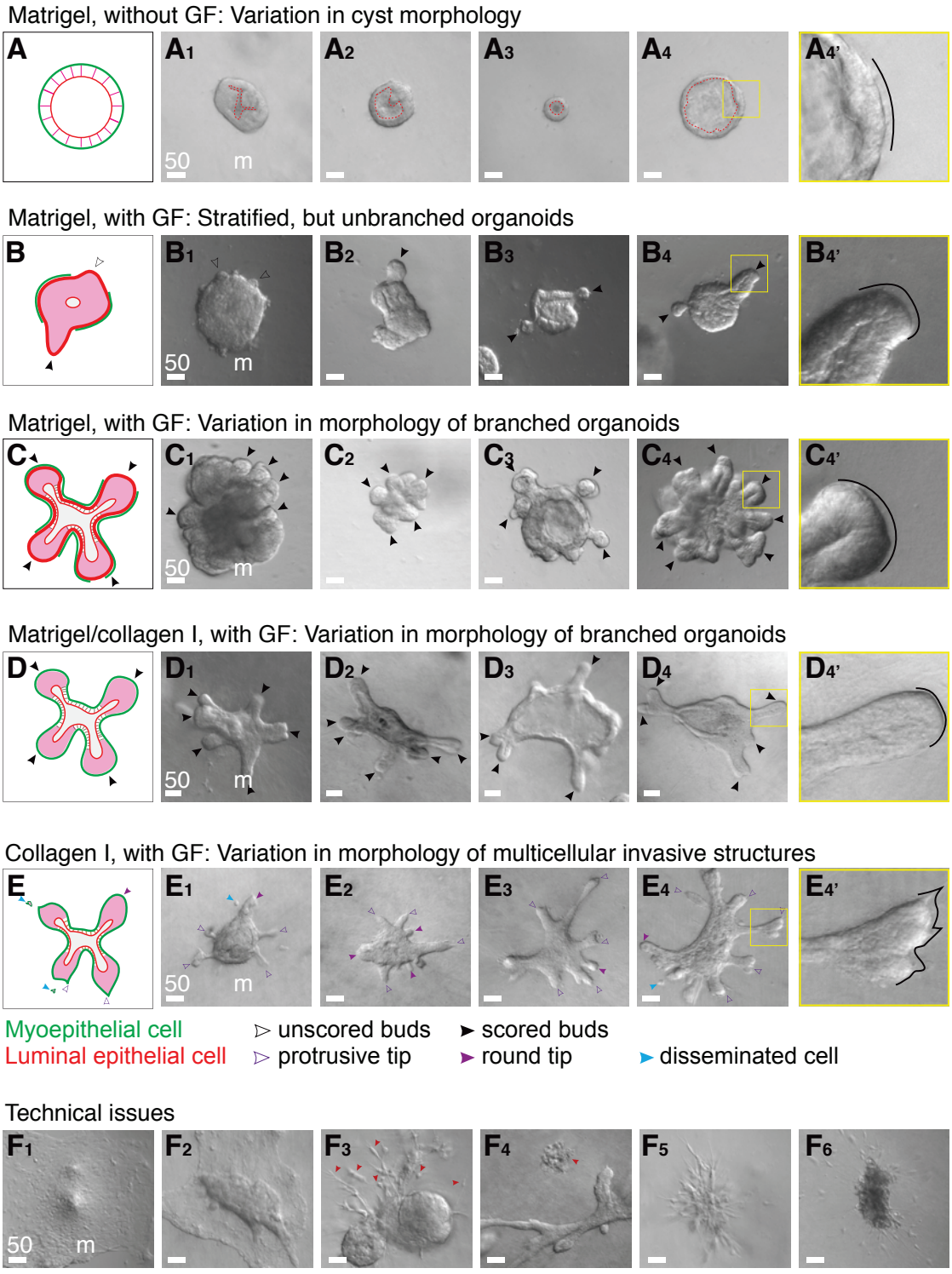
Matrigel, without GF: Variation in cyst morphology
A
A1
A2
A3
A4
A4'
50 m
Matrigel, with GF: Stratified, but unbranched organoids
B
B1
B2
B3
B4
B4'
50 m
Matrigel, with GF: Variation in morphology of branched organoids
C
C1
C2
C3
C4
C4'
50 m
Matrigel/collagen I, with GF: Variation in morphology of branched organoids
D
D1
D2
D3
D4
D4'
50 m
Collagen I, with GF: Variation in morphology of multicellular invasive structures
E
E1
E2
E3
E4
E4'
50 m
Myoepithelial cell
Luminal epithelial cell
unscored buds
protrusive tip
scored buds
round tip
disseminated cell
Technical issues
F1
F2
F3
F4
F5
F6
50 m

Figure 2-8: Correlation between epithelial morphologies in 3D organotypic assays and in vivo.

(a–c) Representative confocal images of a cyst in Matrigel (a), branched buds in Matrigel (b), and a stratified, elongating bud in a mixture of Matrigel and collagen I (c). (d–f) Representative confocal images from mammary gland tissue sections of a bilayered duct (d), a side branch (e), and a terminal end bud (f).

Figure 2-8

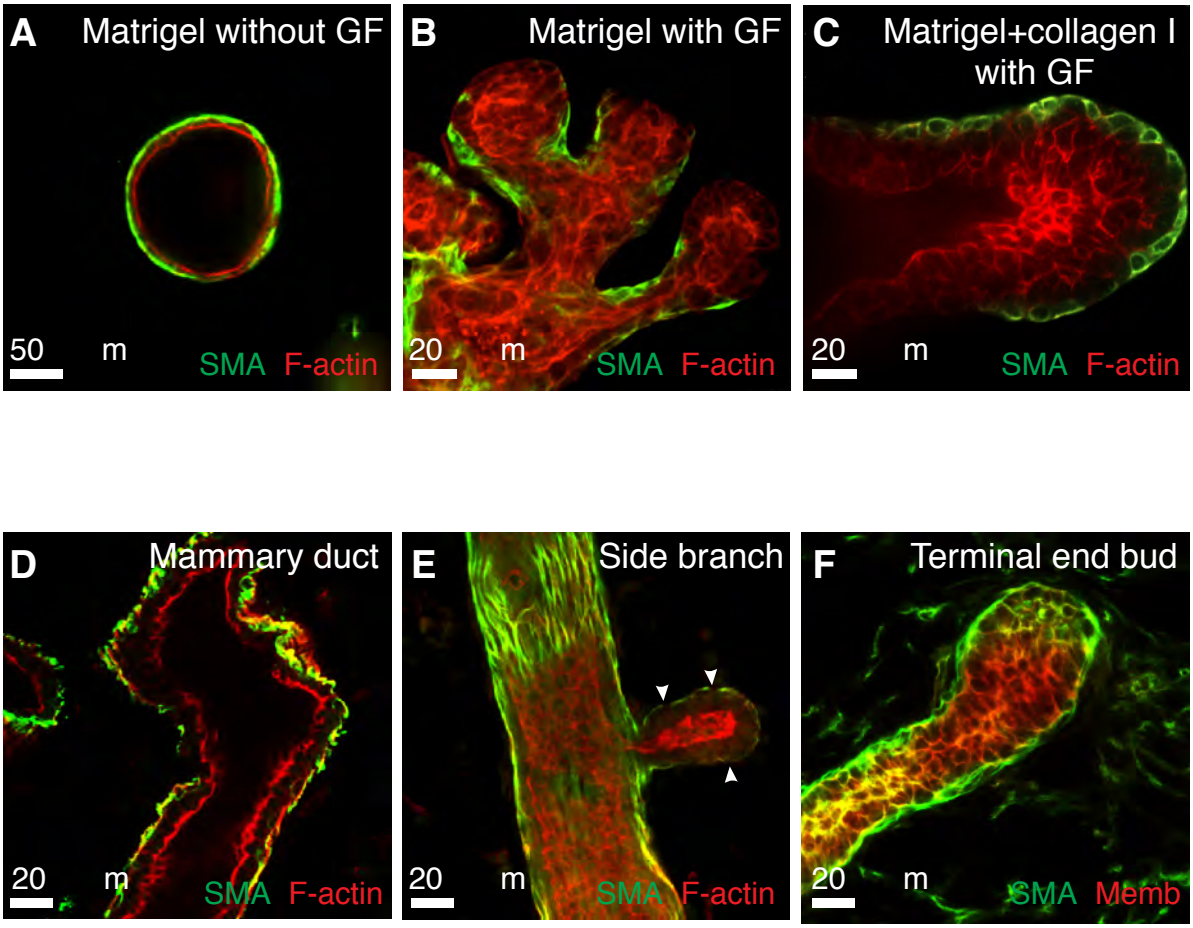
A
Matrigel without GF
50 m
SMA F-actin
B
Matrigel with GF
20 m
SMA F-actin
C
Matrigel+collagen I with GF
20 m
SMA F-actin
D
Mammary duct
20 m
SMA F-actin
E
Side branch
20 m
SMA F-actin
F
Terminal end bud
20 m
SMA Memb

Chapter 3

Mammary collective cell migration involves transient loss of epithelial features and individual cell migration within the epithelium

(Modified from Ewald et al., JCS. 2012)

Abstract

Normal mammary morphogenesis involves transitions between simple and multilayered epithelial organizations. We used electron microscopy and molecular markers to determine whether intercellular junctions and apico-basal polarity were maintained in the multilayered epithelium. We found that multilayered elongating ducts had polarized apical and basal tissue surfaces both in three dimensional culture and in vivo. However, individual cells were only polarized on surfaces in contact with the lumen or extracellular matrix. The basolateral marker scribble and the apical marker atypical protein kinase C zeta localized to all interior cell membranes, whereas PAR3 displayed a cytoplasmic localization, suggesting that the apico-basal polarity was incomplete. Despite membrane localization of E-cadherin and β-catenin, we did not observe a defined zonula adherens connecting interior cells. Instead, interior cells were connected through desmosomes and exhibited complex interdigitating membrane protrusions. Single-cell labeling revealed that individual cells were both protrusive and migratory within the epithelial multilayer. Inhibition of Rho kinase (ROCK) further reduced intercellular adhesion on apical and lateral surfaces but did not disrupt basal tissue organization. Following morphogenesis, segregated membrane domains were re-established and junctional complexes re-formed. We observed similar epithelial organization during mammary morphogenesis in organotypic culture and in vivo. We conclude that mammary epithelial morphogenesis involves a reversible, spatially limited, reduction in polarity and intercellular junctions and active individualistic cell migration. Our data suggest that reductions in polarity and adhesion during breast cancer progression might reflect partial recapitulation of a normal developmental program.

Introduction

Simple epithelial tissues are composed of a single layer of cells connected to each other through intercellular anchoring junctions, including tight junctions, adherens junctions and desmosomes. Epithelial morphogenesis therefore presents a conceptual puzzle, as adhesive junctions and strong apico-basal cell polarity are difficult to reconcile with models of motility derived from the study of isolated fibroblastic cells migrating over flat surfaces[1,2]. A major barrier to the understanding of mammalian epithelial morphogenesis is that the development occurs deep inside the animal. The mammary gland poses a particular challenge because the developing ductal network is embedded within an adipocyte-rich stroma that scatters light and limits high-resolution imaging. Consequently, mammary ductal morphogenesis has not been directly observed in vivo and the basic events are inferred from analysis of fixed specimens. The mammary ductal epithelium originates from a multilayered epithelial placode during embryonic development[3]. The epithelium internalizes and elongates into the embryonic mesenchyme as a solid, multilayered cord of cells from embryonic days 12–15. Although the mammary cells make extensive cell–cell contacts, they lack many features of mature epithelium, such as tight and adherens junctions[3]. During embryonic days 16–20 the epithelium elongates, bifurcates and establishes polarized epithelial architecture with a central lumen and mature junctional complexes[3]. This rudimentary ductal network is then essentially inactive until the increase in steroid hormone levels at the onset of puberty. The majority of mammary branching morphogenesis occurs during puberty (Fig. 3-1A). At the end of embryonic development and at the end of puberty, mammary ducts consist of a highly polarized luminal epithelial cell layer surrounded by myoepithelial cells (Fig. 3-1B,C). However, ductal elongation during puberty is accomplished by a specialized structure known as the terminal end bud (TEB; Fig. 3-1D). The TEB contains many luminal epithelial cell

layers[4], and these cells display incomplete apico-basal polarity as determined by light microscopy[5,6,7]. We developed an ex vivo culture system to enable direct observation of the cell dynamics driving mammary epithelial morphogenesis[8,9,10,11,7]. In the 'organoid' assay we isolate primary mammary epithelial ducts and embed them inside gels of extracellular matrix proteins. Epithelial organoids in three-dimensional (3D) culture initiate, elongate and bifurcate new ducts in a growth-factor-dependent fashion[11,7]. We used immunofluorescence to verify that the organization and polarity of the epithelium during morphogenesis in 3D culture is highly similar to that in the TEB in vivo[7]. We next developed microscopy techniques to visualize the cell dynamics driving mammary morphogenesis in 3D culture[12]. In time-lapse movies we observed a proliferation-dependent transition from a simple to a multilayered epithelial organization and dynamic cell rearrangements within the epithelial layer[7]. We did not observe any actin- or membrane-based protrusions extending into the extracellular matrix (ECM). Luminal epithelial buds initiate and elongate as a multilayered epithelium, with active cell rearrangements and without persistent leader cells. As elongation ceases, the epithelium returns to a simple bilayered organization[7]. We conclude that the mammary epithelium during morphogenesis in 3D culture is both multilayered and highly dynamic at the cellular level. Studies in kidney and salivary gland have revealed that epithelial cells exhibit high levels of motility and extensive cell rearrangements during morphogenesis[13,14]. However, those organs accomplish branching morphogenesis during embryonic development and these cell dynamics are essentially absent by birth[13]. Similarly, at the end of puberty all of the TEBs disappear and the mammary ductal network again has a simple bilayered organization and extensive intercellular junctions. However, mammary epithelial fragments isolated from mice of any age will reform TEBs and re-establish a

complete ductal epithelial network when transplanted into a cleared mammary fat pad in a host mouse[15]. Consistent with these in vivo observations, mammary ducts isolated from embryonic, adolescent and mature mice all branch in 3D organotypic culture and display fundamentally similar cellular dynamics. Mammary epithelial ducts elongate through the action of a multilayered TEB and the epithelium retains the potential to reform TEBs throughout the lifespan. We therefore became specifically interested in determining the extent to which intercellular adhesive junctions and apicobasal polarity are maintained in this transient epithelial multilayer. The major adhesive junctions in epithelial cells are the tight junctions, adherens junctions and desmosomes. Tight junctions are composed of claudins and occludins and they serve both to control paracellular permeability and to partition the plasma membrane into apical and basolateral domains[16]. Adherens junctions directly connect cells through classical cadherins and then link cell contacts to the actin cytoskeleton through intracellular catenins[17]. Desmosomes link cells through desmosomal cadherins and connect these cell contacts to the intermediate filament cytoskeleton[18]. In addition to the structural polarity imposed by the localization of the adhesive junctions, epithelial cells also receive molecular polarity information from the apical complex of PAR3, PAR6 an atpical protein kinase C f (aPKC-f) and basolaterally localized scribble, discs large (DLG) and lethal giant larva (LGL)[19]. Cancer in general, and breast cancer in particular, involves a characteristic loss of apico-basal polarity, changes in cell–cell adhesion, and a transition away from a simple highly polarized epithelia to a multilayered incompletely polarized epithelia[20,19,21]. Cell adhesion genes can act as tumor suppressors in mouse models of mammary carcinoma and are frequently mutated in human breast tumors[22,23,24,25,26,27,28]. Similarly, cell polarity genes can act as tumor suppressors, their loss can cooperate with oncogene function in model

systems and their expression and localization is frequently disrupted in human cancers[29,30,31,19,21]. However, it is unclear whether the changes in cell–cell adhesion and loss of apico-basal polarity observed in cancer are specific features of neoplastic growth or whether normal epithelial morphogenesis also requires reduced polarity and adhesion. In the present study, we sought to determine whether apico-basal polarity and junctional adhesion were preserved in the multilayered epithelium characteristic of mammary branching morphogenesis. We analyzed the fine structure of mammary epithelium during growth in a 3D organotypic culture model and then the in vivo organization of TEBs during pubertal development. We complemented this ultrastructural analysis with time-lapse microscopy of cell and protrusion dynamics within the epithelial multilayer during morphogenesis in 3D culture

Results

Mammary epithelial cells can form highly polarized bilayers in Matrigel

We previously established culture conditions sufficient for survival and differentiation of primary mammary epithelium explanted into Matrigel (simple medium: DMEM with F12, insulin-transferrin-selenium and penicillin-streptomycin) in which essentially all epithelial fragments ('organoids') will form bilayered cysts[11,7]. Addition of nanomolar concentrations of growth factor induces a complex multi-day program of branching morphogenesis[11,7]. We selected FGF2 for this study as it induces branching morphogenesis with high efficiency (80–95% of organoids) in 3D culture and FGFR2 is required in the TEB during puberty[32]. We first sought to define the normal ultrastructural organization of bilayered mammary epithelium in Matrigel. We examined 75 sections from five mammary cysts in simple medium and observed simple epithelial organization by ultrastructure (Fig. 3-1E). The lumens were electron dense and contained secretory material (black arrows in Fig. 3-1E–E''). Cells lining the lumen had microvilli (Fig. 3-1E') and were connected by tight junctions (Fig. 3-1E''). We also observed desmosomes connecting luminal–luminal (Fig. 3-1E'), luminal–myoepithelial (Fig. 3-1E'') and myoepithelial–myoepithelial cells (not shown). The basal tissue surface was smooth and we detected no protrusions into the ECM. Morphological polarity can be assessed with transmission electron microscopy (TEM), but molecular polarity is most readily assayed with immunofluorescence. Simple epithelial polarity is associated with apical localization of the PAR3– PAR6–aPKC-ζ complex and basolateral localization of scribble. Consistent with the high degree of morphological polarity observed by TEM, the molecular polarity complexes were also segregated into distinct apical and basolateral domains. PAR3 was apically localized on the lumen-facing surface of the luminal

epithelial cells (Fig. 3-1F), whereas scribble was basolaterally localized in the luminal epithelial cells (Fig. 3-1G). The protein numb is involved in cell polarity, adhesion[33] and asymmetric cell division in multiple systems[34]. In polarized bilayers its localization is confined to the basolateral domain (Fig. 3-1H). We therefore conclude that our epithelial isolation and culture conditions in Matrigel are compatible with simple epithelial organization, complete apical junctional complexes and fluid-filled lumens, consistent with the in vivo organization of mammary ducts in the mouse[35] and human mammary glands[36,37].

Mammary morphogenesis in 3D culture is accomplished via a transiently stratified epithelium

Mammary epithelium in 3D culture forms a multilayered epithelium that initiates, elongates and bifurcates new mammary buds[7]. Apico-basal polarity is well defined in simple epithelia[36,35,2], but the extent of polarity within the interior of a transiently multilayered epithelium was unclear. We have previously shown that aPKC-ζ localizes to all interior contact surfaces within the multilayer suggesting that interior cells lack segregated apical and basolateral membrane domains (Fig. 3-2A)[7]. Following morphogenesis, the localization of aPKC-ζ f in the re-established simple epithelium is restricted to the apical surface (Fig. 3-2A')[7]. We have also shown that E-cadherin and β-catenin localize to all interior contact surfaces within the multilayer, both in vivo and in vitro (Fig. 3-2B–C')[7]. Because E-cadherin and β-catenin are major components of the adherens junction these data motivated us to assay for junctional complexes directly. Here, we used TEM and further molecular marker analysis to test our hypothesis that mammary morphogenesis involves a transient reduction in apico-basal polarity and junctional adhesion in interior cells.

Mammary epithelium during morphogenesis lacks protrusions into the ECM

A newly discovered feature of mammary collective epithelial migration is the absence of forward-oriented actin protrusions in advance of elongating ducts[7]. However, it was possible that fine protrusions extended into the ECM that could not be detected by light microscopy. To test for fine protrusions, we fixed organoids during active branching and identified regions of active ductal elongation on the basis of the organization of the epithelium. We examined 95 sections from 12 samples. We typically observed ducts elongating simultaneously in multiple directions (Fig. 3-2A–D). We then examined the basal surface of elongating ducts in 3D culture at high resolution by TEM. We saw no evidence of forward-oriented protrusions into the ECM (0 of 95 sections, Fig. 3-2D–F). We instead observed a smooth and organized basal tissue surface. Individual cells showed polarized basal surfaces at the tissue–ECM interface, but little morphologically evident polarity on interior surfaces (Fig. 3-2F–F’’’).

Mammary epithelial morphogenesis in 3D culture involves a reduction in intercellular junctions

Because cells in the interior of the multilayer did not have conventional epithelial cell morphologies, we next sought to determine the extent to which intercellular junctions are maintained during normal branching morphogenesis. We observed well-defined apical tissue surfaces, with electrondense lumens, microvilli and extensive secretory material (Fig. 3-2D,G–G’’’). Tight junctions only connected cells lining electron-dense luminal spaces (TJ in Fig. 3-2G’’,G’’’). We observed an electron-dense luminal space and an electron-lucid intercellular space between cells in the multilayered region (Fig. 3-2G’’,G’’’). By contrast, cells within the interior of the multilayered epithelium lacked most features of simple epithelial organization or apico-basal polarity. We did not observe a zonula adherens at points of interior cell–cell contact. However, E-cadherin and β-catenin were still membrane

localized in interior cells and so we cannot rule out the possibility of small E-cadherin-based adhesive complexes that would be difficult to detect by TEM. Cell–cell contact in the interior appeared loose and was characterized by extensive frequently interdigitating membrane extensions (Fig. 3-2F''). Interior cells displayed a variety of cell shapes and sizes and frequently included round cells with minimal cell–cell contacts (Fig. 3-2F''').

Interior cells lack membrane-associated PAR3 and are unpolarized

Because the interior cells lacked morphological polarity, we next used antibodies to visualize the localization of molecular markers for apico-basal polarity during each stage of morphogenesis in 3D culture. Interior cells within the multilayered epithelium displayed a diffuse cytoplasmic localization of PAR3 (Fig. 3-3A). By contrast, scribble was membrane-associated on all interior cell surfaces in the multilayer and was absent only from lumen-facing surfaces (Fig. 3-3B). Similar to the localization of scribble, numb was localized to all lateral surfaces at the complex cyst stage. In the multilayered epithelium of elongating ducts, PAR3 localized to all lumen-facing membranes, but was diffusely localized to the cytoplasm in interior cells (Fig. 3-3D). Scribble and numb instead localized to all interior cell surfaces and were excluded from lumen-facing surfaces (Fig. 3-3E,F). After morphogenesis, the reformed simple epithelium had PAR3 that was localized to the apical surface of luminal cells and scribble and numb to basolateral surfaces (Fig. 3-3D',E',F').

Isolated microlumens exist between interior cells in the multilayered epithelium in 3D culture

We have previously observed small isolated zona occludens protein 1 (ZO-1; also known as TJP1)-lined spaces within the multilayered epithelium of elongating mammary buds both in 3D culture and in vivo[7]. We sought to distinguish whether these represent small lumens or accumulations of apical molecular markers without corresponding ultrastructural features.

We first used confocal microscopy to collect optical sections and generate 3D reconstructions of the multilayered mammary epithelium during 3D culture. We discovered that the ZO-1-lined microlumens were isolated from the main lumen of the organoid (Fig. 3-4A–A''). Following morphogenesis, individual ducts had single simple lumens (Fig. 3-4B,B'). Using TEM we observed both empty (electron lucid) intercellular regions (Fig. 3-4C') and isolated lumens filled with electron-dense material (Fig. 3-4C''–D'''). The electron-lucid intercellular regions had extensive membrane protrusions but no evidence of tight junctions or secretory material (Fig. 3-4C', white arrow). Desmosomes were the only junctions that we observed connecting cells surrounding the electron-lucid intercellular spaces. By contrast, isolated microlumens had microvilli, as well as tight junctions at points of apical intercellular contact and accumulated electron-dense material (Fig. 3-4C''–D'''). Isolated lumens extended several microns into the multilayer (Fig. 3-4E).

Epithelial organization is highly variable during morphogenesis in 3D culture

Our expectation was that cells at the basal tissue surface would remain columnar throughout branching. Strikingly, this was not the case and we observed considerable heterogeneity in the shape of basally located cells (Fig. 3-5A), with 'islands' of high local order (Fig. 3-5A') and disorder (Fig. 3-5A'') located in the same branching structure. Even in actively branching structures with highly variable cell shapes, there were frequently locations with a single luminal epithelial cell layer and highly polarized ultrastructural organization. Following branching the transiently stratified epithelium returned to a simple epithelial organization, with mature apico-basal polarity at the morphological level.

Regions with few intercellular junctions display extensive 3D membrane protrusions

During active morphogenesis in 3D culture, we observed few intercellular junctions connecting interior cells, but extensive membrane protrusions. Some of these protrusions had the morphological appearance of interdigitating microvilli (Fig. 3-5B,B'). However, membrane protrusions were observed at some distance from the apical surface and were frequently intermixed with desmosomes. Membrane protrusions were several microns in length (Fig. 3-5C,C') and branched multiple times (Fig. 3-5D). The uniform thickness along the protrusions, as well as the tendency for the protrusions to appear continuous over long distances, led us to analyze whether they were thin microvillar-like individual membrane protrusions or whether they were complex 3D membrane extensions. Accordingly, we collected a series of consecutive 90-nm sections and imaged each by TEM (Fig. 3-5E,E'). Protrusions extended through 5–10 sections and changed continuously from branched to unbranched (Fig. 3-5E', arrowheads). To confirm the 3D structure of these newly discovered membrane protrusions we next collected continuous image series using serial block face scanning electron microscopy (SFB-SEM) and focused ion beam scanning electron microscopy (FIB-SEM). In both cases, a thin layer of material was removed from the surface of the embedded sample and the block face was then imaged. The procedure was repeated to produce a 3D image series. Serial block face and focused ion beam imaging both prevent warping artifacts associated with transfer of a thin section to a solid support. We observed transitions from thin to thick protrusions and from linear to branched protrusions (Fig. 3-5F). We conclude that these membrane elements are interdigitating 3D membrane extensions (Fig. 3-5G– H''). By contrast, we did not observe complex 3D extensions in regions of simple epithelial organization.

Interior cells exhibit apparently migratory polarity during morphogenesis in 3D culture

As ductal elongation ceases, the multilayered duct reorganizes to a simple epithelium[7]. In electron micrographs, this corresponded with a transition from largely non-junctional cell adhesion with loose cell–cell contact to a simple epithelial organization with extensive intercellular junctions. One possible mechanism for a transition from a multilayered to simple organization is radial intercalation, in which cells move between layers to give a thinner tissue[38,39]. We observed elongated cells within the multilayered epithelium whose morphology was consistent with individualistic cell migration (Fig. 3-6A–D). Despite the absence of actin-based protrusions extending into the ECM, we observed long extensions at the front of these elongated cells (Fig. 3-6A,B). One cell that appeared to have recently arrived at the basal surface displayed an intermediate polarity between elongated and apico-basal (Fig. 3-6D–D'').

Desmosomes are frequently observed in the interior of the multilayered epithelium

We have demonstrated that a subset of cells in the interior of the multilayered epithelium lack molecular apico-basal polarity and appear to have a migratory polarity and forward-oriented protrusions. However, we did not observe spontaneous dissemination of luminal epithelial cells in 3D culture in the hundreds of movies we collected in our previous study[7]. We therefore sought to identify persistent intercellular junctions that might limit the dissemination of luminal epithelial cells. The only intercellular junctions that we regularly observed connecting interior cells during morphogenesis were desmosomes (Fig. 3-6B'–C',E–H). We observed desmosomes connecting apparently migratory cells to their neighbors in close proximity to the ECM (Fig. 3-6B–C'). We also observed desmosomes connecting columnar cells at the ECM border (Fig. 3-6E–F') and interior cells within the multilayer (Fig. 3-6G,H). Desmosomes in the interior were small and did not accumulate extensive

intracellular plaques to the degree observed in highly polarized epithelial cells (compare Fig. 3-6G,H with Fig. 3-1E',E'').

Interior cells are protrusive and migratory within the multilayered epithelium

Our electron micrographs revealed extensive protrusions and apparent migratory polarity in cells within the epithelial multilayer. However, it is difficult to infer cell movements accurately from a series of fixed specimens. We therefore labeled small numbers of cells using adenovirally delivered cytoplasmic GFP and imaged their behavior using time-lapse confocal microscopy. We tracked 21 cells from 10 movies collected over three independent experiments. All 21 cells were protrusive and motile. Cells had a mean speed of 5.5 + 1.8 μm per hour (S.D.).

We observed individual cells migrating over multiple cell diameters within the multilayered epithelium (Fig. 3-7A). Round cells in the interior extended and retracted long cytoplasmic protrusions (Fig. 3-7B). We also directly observed radial intercalation of front–rear-polarized migratory cells into the tissue basal surface (Fig. 3-7C). The forward extensions in these cells immediately flattened out as the cells made contact with the extracellular matrix. Cells just inside from the tissue basal surface extended and retracted protrusions over most of their cellular surface area (Fig. 3-7D). Cells bridging tissue apical and tissue basal surfaces also extended and retracted protrusions along their lateral surfaces (Fig. 3-7E). We did not observe protrusions into the ECM or the lumen. We conclude that mammary epithelial cells display extensive protrusions during morphogenesis in 3D culture on all interior cell surfaces and that individual cells appear to migrate actively in the interior of the multilayer.

Inhibition of MLCK or Rac blocks duct initiation but results in different architectural states

Pharmacological inhibition of either Rac or myosin light chain kinase (MLCK) results in a dose-dependent block of ductal initiation[7]. In both cases, when we added the inhibitor at the start of culture the lumens fill as normal, but new ducts do not initiate. However, inhibition of Rac results in a persistently multilayered epithelium, whereas MLCK-inhibited structures eventually clear their lumens to form a simple epithelial organization[7]. Accordingly, we examined organoids treated with 100 mM Rac inhibitor and collected electron micrographs to determine whether these structures were well polarized (two samples, 220 sections imaged). We observed extensive cell–cell contact through interdigitating membrane protrusions. By contrast, organoids treated with 1 mM MLCK inhibitor (ML7) cleared their lumens and their final ultrastructural organization was indistinguishable from simple cysts (one sample, 16 sections imaged).

ROCK inhibition prevents reversion to the single layered state and results reduced interior cell-cell contact

Pharmacologic inhibition of Rho kinase (ROCK) with Y-27632 results in a hyper-branched phenotype with reduced levels of E-cadherin at intercellular surfaces[7]. On the basis of the lower intensity and punctate appearance of E-cadherin staining following inhibition of ROCK, we hypothesized that Y-27632 treatment disrupts cell–cell contacts between luminal epithelial cells. Indeed, we observed dramatic changes in the localization of ZO-1 in ROCK-inhibitor-treated organoids (compare Fig. 3-8B–C’ with Fig. 3-8A,A’). Following ROCK inhibition, ZO-1 was frequently associated with small puncta (Fig. 3-8B’), but large regions that lacked ZO-1 immunoreactivity were also observed (Fig. 3-8C’). Consistent with these observations, we observed a striking reduction in intercellular contact in TEM images of ROCK-inhibited organoids (Fig. 3-8D–H’’’; two samples, 34 sections imaged). Lumens were no longer observed and cell–cell contacts were barely maintained on lateral surfaces (Fig. 3-

8D,F). We essentially observed a complete loss of luminal organization with no tight or adherens junctions. Instead of electron-dense lumens, there were electron-lucid intercellular spaces. Interior cells barely contacted each other and appeared completely unpolarized. Despite this dramatic loss of polarity and the reduction in cell–cell contact, we still observed occasional small desmosomes (Fig. 3-8E',E'',G'') and a well-organized basal tissue surface (Fig. 3-8H–H'''). This dramatic reduction in polarity and adhesion is reversible[7] and was not sufficient for dissemination of interior cells into the ECM. Treatment with H1152, an alternate ROCK inhibitor, also induced loss of the main lumen and extensive microlumens (Fig. 3-8I,J). However, some apico-basal polarity was maintained in H1152-treated organoids as PAR3 localized to the membrane of the microlumens (Fig. 3-8I,I'), whereas scribble localized to basolateral surfaces and was excluded from the microlumens (Fig. 3-8J,J'). We conclude that ROCK (or another Y27632-sensitive kinase) is required for maintenance of luminal continuity and lateral cell–cell adhesion within the luminal epithelial cell layer.

Terminal end buds in vivo have similar organization to mammary organoids.

Given the highly unusual ultrastructural organization of mammary epithelium during branching morphogenesis in 3D culture, we next asked whether the morphology of the interior cells of branching organoids matched the organization of interior ('body') cells of the normal in vivo structure for mammary ductal elongation, the TEB. We collected electron micrographs of sections through TEBs, including regions at the cell–ECM, lumen-facing and interior surfaces (Fig. 3-9; four samples, 60 sections imaged). Consistent with our in vitro results, we observed tight junctions connecting cells at surfaces facing lumens (Fig. 3-9B,B'). We also did not observe protrusions from the basal TEB surface into the ECM. As in the 3D cultures, there was considerable heterogeneity in cell and nuclear morphologies in the TEB

(Fig. 3-9C). Body cells of TEBs had a similar cellular organization to interior cells in 3D culture, with extensive interdigitating lateral membrane protrusions (Fig. 3-9D–F’’). The TEB was polarized at its apical and basal most tissue surfaces, with many morphologically unpolarized cells in the interior (Fig. 3-9C–F). Furthermore, the morphological polarity of cells lining the lumen was generally restricted to the lumen-facing surface, with interior surfaces adopting a round or mesenchymal morphology (Fig. 3-9G–G’’). We also observed microlumens within the multilayered region of the TEB, both by light (Fig. 3-1D) and electron microscopy (Fig. 3-9H).

Discussion

The mammary gland undergoes multiple rounds of epithelial morphogenesis during puberty, pregnancy, lactation and involution[40,41]. The mammary epithelium at rest has a simple organization, with a single luminal epithelial cell layer[36,35]. During early embryonic development and during puberty the elongating tips of mammary ducts are multilayered[3,4,7]. In this study, we used molecular markers and TEM to determine the polarity and adhesional status of this multilayered intermediate. Interior cell surfaces within the multilayered localized both apical (aPKC-ζ) and basolateral (scribble) molecular markers. Despite E-cadherin and β-catenin localization, we did not observe zonula adherens connecting interior cells. Instead points of cell–cell contact in the interior were connected by desmosomes and characterized by extensive interdigitating 3D membrane extensions. Interior cells were observed to extend protrusions and to migrate, but these behaviors were transient and spatially limited to the interior of the multilayer (Fig. 3-10).

3D primary organotypic culture recapitulates the normal junctional adhesion of the mammary epithelium

Without growth factor stimulation primary mammary organoids in 3D culture robustly form cysts with a highly polarized bilayered architecture and microvilli lining the lumen. The epithelium developed a complete apical junctional complex and displayed extensive desmosomal connections along lateral surfaces. This organization is consistent with the normal ultrastructure of the mammary epithelium in vivo[35], and is in contrast to the ultrastructural organization of MCF-10A acini cultured under similar 3D culture conditions. MCF-10A cysts do not form detectable tight junctions and instead appear to form their lumens through extensive desmosomal contacts[42]. Our primary 3D cultures therefore provide

a starting point for mechanistic evaluation of the relative importance of different junctional complexes and adhesion proteins.

Mammary epithelium adopts a low polarity state with few junctions during morphogenesis

During morphogenesis, the mammary epithelium was polarized at its apical (lumen-facing) and basal (ECM-contacting) tissue surfaces. However, even cells at the lumen or ECM border typically were polarized only on their apical- or basal-most cell surfaces. Cells in the interior were loosely connected and displayed dense interdigitating membrane protrusions. Some of these protrusions appeared morphologically similar to microvilli, despite their interior location. Other protrusions were intermingled with desmosomes in electron-lucid intercellular spaces, were several microns long, or were branched, all features uncharacteristic of classical microvilli. In volume reconstructions, these protrusions appeared as an interconnected 3D network of membrane extensions, rather than individual thin projections. Because we observed similar membrane protrusions on interior cells in TEBs from normal mammary glands, we conclude that these structures are transiently produced both in vivo and in vitro during normal mammary morphogenesis. These 3D membrane extensions increase the entangled surface area of adjacent cells and we speculate that they might thereby assist in maintaining intercellular adhesion among motile cells.

Tight junctions are only observed lining lumens

Tight junctions classically serve two functions: gate and fence. They function as a gate to enable selective control over paracellular permeability. They also function as a fence within the membrane, partitioning the apical from basolateral membrane regions[2]. Previous work has established that TJs can exist in stratified epithelia[43], but we found no evidence for TJs in the interior of the multilayer during morphogenesis except at the apical end of cells facing

lumens. Without TJs in the interior of the multilayer, it is consistent that the membranes appear to have an unresolved mix of apical and basolateral identity.

Mammary epithelial cells display extensive protrusive activity and individualistic cell migration within the multilayer

Elongating mammary buds maintain a smooth and highly organized basal-tissue–ECM surface both in vivo and in 3D culture. However, we observed extensive protrusions in the interior of the epithelium. We did not observe protrusions into the ECM at either the light or electron microscopy levels. These observations imply that there is a reduction in the epithelial character of mammary epithelial cells during morphogenesis, as protrusive migration is characteristic of mesenchymal cells. Strikingly, this reduction was spatially restricted to the multilayered region within elongated ducts and was reversible, with normal ducts eventually reverting to bilayered organization.

Epithelial organization during morphogenesis is similar in 3D culture and in vivo

The low intercellular adhesion, reduced polarity environment that we observed during morphogenesis in organotypic culture is highly similar to the organization of the in vivo mammary terminal end bud (TEB). The essential features of reduced intercellular adhesion, reduced apico-basal polarity, fewer intercellular junctions and stratified epithelial organization are all quite similar between organoids and TEBs. We observed tight junctions at the apical end of cells facing microlumens, and desmosomes connecting cells in the electron lucid intercellular spaces in both TEBs and ducts in 3D culture. Significantly, the low polarity environment is also similar to that observed in the mammary placode during embryonic development[3,44]. Whereas our data directly address only mouse mammary morphogenesis, immunohistochemistry of sections from pubertal human mammary epithelium, and human TEBs, indicates that a similar multilayered intermediate underlies

human mammary morphogenesis[45]. There are extensive previous TEM studies of simple bilayered mammary ducts[35,36], but we are aware of only one previous study that has used TEM to image TEBs during puberty[4]. In that study the authors observed membrane protrusions into intercellular spaces between interior cells within the TEB, consistent with our results. More recent TEM studies in the mammary gland have proposed that small light-staining cells are stem or progenitor cells[46,47,48,49]. We also observed variation in electron density, with smaller rounder cells typically staining more lightly, and larger elongated cells typically staining darker.

Collective epithelial migration has features of the epithelial to mesenchymal transition

A primary model for the cellular mechanism of normal and neoplastic epithelial morphogenesis is the epithelial to mesenchymal transition (EMT). Morphological hallmarks of this model include a reduction in epithelial organization and acquisition of motility. EMT has been proposed to explain the dissemination of previously adherent epithelial cells into the surrounding ECM and is thought to be a major cellular mechanism of metastasis in human breast cancer[50,51]. We did not observe migration of interior cells into the ECM either in 3D culture or in vivo. However, the reduced epithelial polarity and intercellular adhesion and increased motility that we observed during morphogenesis are consistent with models of a partial transient EMT[52]. However, we observed a striking confinement of these migratory cells to the interior of the multilayer. Furthermore, most models propose that EMT occurs at the epithelial–stromal or tumor–stromal border[53]. We see the opposite; the highest level of E-cadherin staining and the ultrastructurally highest degree of epithelial organization is at the luminal and basal surfaces of the tissue. It is the interior multilayered epithelial compartment, which is out of contact with ECM and stromal cells, that exhibited the largest reduction in

epithelial character. Furthermore, the cellular phenotype associated with inhibition of ROCK suggests that the luminal and lateral intercellular adhesions can be essentially eliminated without dissemination or loss of basal tissue organization.

Desmosomes are the most common junction connecting cells in the interior of the multilayered epithelium

Research in epithelial biology has focused on the adherens junction in part because E-cadherin is required very early in embryonic development[54] and disruption of the adherens junction can lead to disruption of the other adhesive junctions[55]. However, disruptions in desmosomal adhesion can also have severe phenotypes and can alter the function of classical cadherin junctions[56,57,58,59]. Desmosomes were the main intercellular junction that we observed in the interior of the multilayered epithelium both in 3D culture and in vivo. Desmosomes were also the only junction we observed connecting elongated, apparently migratory cells to their neighbors. A previous TEM study of cells in the interior of the elongating embryonic mammary bud found very few junctional complexes connecting interior cells, but did observe desmosomes[3]. The requirement for desmosomal adhesion has not been tested genetically in the mammary gland, but 3D culture studies suggest that desmosomal cadherins are essential to establish and maintain the correct apico-basal positions of luminal and myoepithelial cells[60]. Furthermore, desmosomal components are frequently mutated or silenced in breast cancer[61,62], and both p53 and p63 can regulate desmosomal adhesion[63,64,65].

Epithelial polarity and adhesion are altered during cancer progression

Both normal and neoplastic mammary epithelia lose polarity, reduce adhesion and shift from a simple to a multilayered organization. Importantly, normal mammary epithelia reduce the amount of polarity and adhesion in a highly restricted space for a limited period of time,

whereas mammary carcinomas persist in a state with lower polarity and adhesion. The reversibility of even very large changes in adhesion and polarity in normal epithelia suggest that tumors might also be able to 'correct' their organization and revert to a normal tubular architecture given the right set of molecular signals. In fact, previous work spanning over several decades has shown that human tumors can be 'normalized' by contact with embryonic mesenchyme and by contact with cell-type specific extracellular matrix proteins[66,67,68,69,70,71]. A previous ultrastructural study has examined ductal hyperplasias, ductal carcinoma in situ and infiltrating ductal carcinomas from human patients to determine the basis of the invasive switch in human breast cancer[72]. Importantly, the authors reported that: ''The most notable finding in our ultrastructural study of various types of breast lesions was an increased degree of cell membrane anomaly paralleling the increased degree of aggressiveness among these lesions… atypical ductal hyperplasia was characterized by abundant microvilli… [i]ntraductal carcinomas were recognizable by extremely complex cell interdigitations. Infiltrating ductal carcinomas were detectable by an overabundance of cellular microvilli''[72]. The morphological similarity between the complex interdigitations in the intraductal carcinomas in that study and in the normal mammary cells undergoing morphogenesis in our study is striking and suggests that at least some human breast cancers might recapitulate aspects of a normal developmental migration program. We have demonstrated in the present study that the ultrastructural organization of mammary epithelium during postnatal morphogenesis is highly similar to that during embryonic morphogenesis[3]. This observation provides an ultrastructural framework for the hypothesis that there is an embryonic program of partial EMT that can be reactivated during postnatal development and during cancer progression[73].

Materials and Methods

Organotypic culture

We generated epithelial fragments ('organoids') as previously described[7,12], using 5- to 8-week-old Charles River FVB mice as the source material. For ease of dissection, TEBs were isolated from a 5-week-old fluorescent reporter transgenic mouse (Sca-1::EGFP)[74]. Animals were housed and handled in accordance with approved IACUC protocols at UCSF or JHU. Briefly, to generate organoids we surgically isolated the mammary glands, minced them 50 times with a scalpel and dispersed the glands for 30 minutes in 50 ml collagenase solution at 37˚C, shaking at 100 rpm. The resulting mixture was then centrifuged at 520 g for 10 minutes at 25˚C. We aspirated away the supernatant and resuspended the pellet thoroughly in 4 ml DNase solution. We shook the tube by hand for 2 to 5 minutes at room temperature and then added 6 ml DMEM F12. We then centrifuged at 520 g for 10 minutes at 25˚C and aspirated the supernatant. To separate the epithelial organoids from the single cells we used differential centrifugation, a total of 4 times. For each round we resuspended the pellet thoroughly in 10 ml DMEM F12 and then pulsed the tube to 520 g (typically 33 seconds). The resulting pellet was then resuspended in the desired volume of growth factor reduced Matrigel (BD Biosciences) and plated in 24-well not tissue-culture treated plates (Falcon). Organoids were grown for 5–6 days and then fixed during the time active branching morphogenesis was ongoing.

Solutions and reagents for organotypic culture

DMEM (Dulbecco's modified Eagle's medium complete) F12 (Gibco). Collagenase solution consisted of: DMEM F12, fetal bovine serum (FBS, heat inactivated) (5% final), gentamicin

(50 mg/ml), insulin (5 mg/ml final, Sigma), trypsin (2 mg/ml, Gibco), collagenase A (2 mg/ml, Type IV from Clostridium histolyticum, Sigma). DNase I (Sigma) was resuspended at 4 U/ml in DMEM F12. Bovine serum albumin (BSA; Invitrogen) was resuspended at 2.5 mg/ml in D-PBS. Simple medium: DMEM F12, 16 Pen-Strep, 16 ITS (insulin, transferrin, sodium selenite; Sigma). Branching medium: simple medium plus 2.5 nM FGF2 (Sigma). ROCK inhibitor (Y27632; Chemicon) and Rac1 inhibitor (NSC23766; Calbiochem) were used as indicated. All inhibitor experiments were done in FGF2 medium.

Fixation strategy for ultrastructural analysis

We initially utilized conventional chemical processing and transmission electron microscopy (TEM) and observed minimally adherent cells, with highly convoluted membranes and extensive intercellular spaces. However, we encountered inadequate and irregular cytoplasmic and membrane preservation (not shown). These limitations in tissue preservation are often associated with room temperature dehydration and can be overcome by high-pressure freezing and subsequent freeze substitution[75]. However, fresh tissue microdissection and the exposure of unfixed tissues to relatively high levels of cryoprotectants (e.g. 20% glycerol), just prior to high-pressure freezing, can lead to physical damage or osmotic stress[76]. To avoid aggregation artifacts caused by the dehydration step in conventional protocols, yet guard against osmotic stress in fresh dissected tissue sample upon exposure to cryoprotectants, we adopted a conservative approach to sample preparation. We first prefixed in glutaraldehyde, then microdissected prefixed samples, then processed the samples for high-pressure freezing and freeze substitution[77]. Using this combination we were able to achieve highquality ultrastructural preservation across large sample regions. On separate samples, we also employed serial block face SEM to allow 3D reconstruction of selected

regions of interest to identify the intercellular membrane protrusions. Our focus was on the membrane organization and junctional complexes, both of which were well preserved in our samples. Given the highly heterogeneous epithelial environment in our samples, it was crucial to be able to process and image large areas of the samples to enable both low-magnification surveys of fields of cells and higher-resolution imaging of individual points of cell–cell contact. Three biologically independent sets of samples were examined for the main FGF2-treated branching organoids. Parallel samples were examined with conventional chemical processing TEM. The conclusions were consistent across all samples, but membrane preservation was better with high-pressure freezing and freeze-substitution prepared samples. All images presented are from samples subjected to high-pressure freezing.

High-pressure freezing

Samples were pre-fixed overnight in 4% glutaraldehyde in organoid medium. They were then subjected to high-pressure freezing in a BAL-TEC HPM-010 highpressure freezer (2100 bars for 5–7 milliseconds) (BAL-TEC, Carlsbad, CA) using 10% glycerol (v/v in cell culture medium) as the cryoprotectant in 200-mm deep aluminum planchettes.

Freeze substitution

Using the Leica automated freeze-substitution system AFS (Leica Microsystems, Vienna, Austria), cryofixed specimens were freeze-substituted in anhydrous acetone containing 1% osmium tetroxide and 0.1% uranyl acetate and after several rinses in pure acetone infiltrated with Epon-Araldite following established protocols[78,79,76]. Specimens were flat-embedded between two microscopy slides and polymerized at 60˚C over 1 to 2 days. Resin-embedded samples were remounted under a dissecting microscope for precise orientation.

Transmission electron microscopy

70–100-nm sections were collected on formvar-coated grids using a Reichert Ultracut E ultramicrotome (Leica). Sections were post-stained using 2% uranyl acetate in 70% methanol followed by Sato's lead citrate. The sections were imaged in an FEI Tecnai 12 TEM (FEI, Eindhoven, The Netherlands) operated at 120 kV.

Montaged TEM Images

Owing to the large size of the samples, it was frequently necessary to collect multiple TEM images of overlapping adjacent areas to cover the relevant field of view at the necessary resolution. Montages of electron microscopy images were reconstructed using the freely available TrakEM2 program[80,81,82]. Images were aligned at full 2048 by 2048 pixel resolution and contrast was adjusted across adjacent images using TrakEm2. A custom Python script was written to assist in reconstruction. The montage function in TrakEM2 was applied, with further manual alignment as necessary. Overlaps were linear blended, and montages were exported as tiff files.

Serial block face and focused ion bean SEM sample preparation

Mouse mammary organoids were chemically fixed with 2.5% glutaraldehyde. To produce enough back-scatter electrons for SBF-SEM imaging, the organoids were stained with an osmium-thiocarbohydrazide-osmium (OTO) method[83,84], in combination with microwave-assisted processing. Organoids were rinsed three times with 0.1 M sodium cacodylate buffer and then incubated with solution of reduced 2% osmium Collective epithelial cell migration 2651 Journal of Cell Sciencetetroxide (containing 1.5% potassium ferricyanide) in buffer. The samples were incubated using a Pelco Biowave microwave (Ted Pella Inc., Redding, CA) for 2 minutes at 150 watts of power. Following three rinses with buffer, the organoids

were microwave for 40 seconds at 150 W in 0.1% thiocarbohydrazide in doubledistilled water and then rinsed three times with water. Finally, they were microwaved for 1 minute at 150 watts with 2% osmium tetroxide and rinsed three times in water. To enhance preservation and contrast, the samples were highpressure frozen as described for the TEM samples and freeze substituted with a solution of 4% osmium tetroxide, 0.1% uranyl acetate and 5% water in acetone. Following five rinses in pure acetone samples were infiltrated with hard-forming Epon resin with accelerator according to the following schedule: 2 hours in 2:1 acetone:resin; 2 hours in 1:1; 4 hours in 1:2; and overnight in pure resin. Samples were flat-embedded as described for the TEM samples. Representative SBF-SEM and FIB-SEM data series have been uploaded to the 'The Cell: An Image Library' (run by the ASCB; http://www.cellimagelibrary.org/).

Focused ion beam SEM imaging

Resin-embedded samples were trimmed with a thin razor blade to expose the area of interest on both the top and one side of the block. This was then glued to a SEM stub using colloidal silver paint. Milling and imaging of the block was carried out using a FEI Strata 235 Dual Beam FIB (FEI, Hillsboro, OR). FIB milling at 50 pA generated a beam size of ,17 nm. 1k by 1k images were collected with a backscatter electron detector at 5 kV.

Antibody staining

Staining for E-cadherin (Zymed, 13-1900), ZO-1 (Chemicon, MAB1520), SMA (Sigma, F3777 or C6198), β-catenin (Santa Cruz Biotechnology, sc-7199), and aPKC-f (Santa Cruz Biotechnology, sc-216) was performed as previously reported[7]. Briefly, organoids were equilibrated in 25% sucrose in PBS for 1 hour, fixed in cold 1:1 methanol:acetone overnight at –20˚C, then reequilibrated in 25% sucrose in PBS for 1 hour. Samples were blocked 1 hour

with 5% serum, incubated with primary antibody (all 1:250 in PBS) for two hours to overnight and rinsed three times in PBS. For PAR3 (Millipore, catalog number 07-330), numb (Cell Signaling Technology, C29611) and scribble (Santa Cruz Biotechnology, sc-11049) staining, organoids were fixed in 4% PFA for 20 minutes and permeabilized in 0.5% Triton X-100 for 30 minutes. Samples were blocked in 10% serum for 3 hours, incubated with primary antibody (all 1:500 in 10% serum) for two hours to overnight and rinsed three times in 10% serum. Secondary Alexa-Fluor-conjugated antibodies (Molecular Probes, all 1:250 in PBS) were incubated with the organoids for 1–4 hours. Nuclei were stained with DAPI or propidium iodide (1:1000) (Molecular Probes). Antibody stains were performed at least three independent times, inspecting a minimum of 25 organoids in each condition each time.

Confocal imaging

Confocal imaging was performed on a Solamere Technology Group spinning disk confocal microscope as described previously[12], with a 406 CApochromat objective lens (Zeiss Microimaging). Acquisition of both fixed and time-lapse images was performed using a combination of mManager[85] and Piper (Stanford Photonics). Levels were adjusted in Adobe Photoshop to maximize clarity of the images. Level adjustments were always done on the entire image.

Single-cell labeling with adenoviral GFP

Epithelial fragments were prepared using the previously described organotypic culture method. Before resuspension in Matrigel 1000 organoids in 500 ml DMEM F12 were transferred to a 1.7 ml Eppendorf tube. The tube was then pulsed at 520 g for 30 seconds. Medium was removed from the pellet and organoids were resuspended in 50 ml DMEM F12.

Ad-CMV-GFP (Vector Biolabs, 1060) was then added at a ratio of 2000 or 10,000 plaque-forming units (pfu):organoid. Epithelial fragments were incubated with virus for 1.5 hours at 37˚C and washed three times in DMEM F12. Organoids were then resuspended in Matrigel and plated as described above.

Time-lapse microscopy

Time-lapse movies were recorded for 5–7 days during which time the temperature was held at 37˚C and humidity was held at 5%. Images were acquired every 10 minutes for a duration of 8–24 hours and 10–30 movies were collected in parallel. Imaris (Bitplane) was used for image analysis. CellTracker was used to label organoids as described previously (Ewald et al., 2008).

Image processing

Surface rendering and single-cell tracking were generated using the Imaris (Bitplane) IsoSurfaces function. Before surface rendering a gaussian smoothing filter with width of 1 voxel was applied and background signal was subtracted. A minimum intensity filter and a minimum voxel size filter were manually adjusted such that the rendered surface visually matched the surface area of individual cells. IsoSurfaces were tracked using the autoregressive motion algorithm with a maximum distance of 5 mm and a maximum gap of three frames. The mean cell speed was calculated as the total track length divided by the time.

References

1 Lauffenburger, D. A. and Horwitz, A. F. (1996). Cell migration: a physically integrated molecular process. Cell 84, 359-369.

2 Nelson, W. J. (2009). Remodeling epithelial cell organization: transitions between frontrear and apical-basal polarity. Cold Spring Harb. Perspect. Biol. 1, a000513.

3 Hogg, N. A., Harrison, C. J. and Tickle, C. (1983). Lumen formation in the developing mouse mammary gland. J. Embryol. Exp. Morphol. 73, 39-57.

4 Williams, J. M. and Daniel, C. W. (1983). Mammary ductal elongation: differentiation of myoepithelium and basal lamina during branching morphogenesis. Dev. Biol. 97, 274-290.

5 Hinck, L. and Silberstein, G. B. (2005). Key stages in mammary gland development: the mammary end bud as a motile organ. Breast Cancer Res. 7, 245-251.

6 Mailleux, A. A., Overholtzer, M., Schmelzle, T., Bouillet, P., Strasser, A. and Brugge, J. S. (2007). BIM regulates apoptosis during mammary ductal morphogenesis, and its absence reveals alternative cell death mechanisms. Dev. Cell 12, 221-234.

7 Ewald, A. J., Brenot, A., Duong, M., Chan, B. S. and Werb, Z. (2008). Collective epithelial migration and cell rearrangements drive mammary branching morphogenesis. Dev. Cell 14, 570-581.

8 Simian, M., Hirai, Y., Navre, M., Werb, Z., Lochter, A. and Bissell, M. J. (2001). The interplay of matrix metalloproteinases, morphogens and growth factors is necessary for branching of mammary epithelial cells. Development 128, 3117-3131.

9 Wiseman, B. S., Sternlicht, M. D., Lund, L. R., Alexander, C. M., Mott, J., Bissell, M. J., Soloway, P., Itohara, S. and Werb, Z. (2003). Site-specific inductive and inhibitory activities of MMP-2 and MMP-3 orchestrate mammary gland branching morphogenesis. J. Cell Biol. 162, 1123-1133. Yang, J. and Weinberg, R. A. (2008). Epithelial-mesenchymal transition: at the crossroads of development and tumor metastasis. Dev. Cell 14, 818-829.

10 Sternlicht, M. D., Sunnarborg, S. W., Kouros-Mehr, H., Yu, Y., Lee, D. C. and Werb, Z. (2005). Mammary ductal morphogenesis requires paracrine activation of stromal EGFR via ADAM17-dependent shedding of epithelial amphiregulin. Development 132, 3923-3933.

11 Fata, J. E., Mori, H., Ewald, A. J., Zhang, H., Yao, E., Werb, Z. and Bissell, M. J. (2007). The MAPK(ERK-1,2) pathway integrates distinct and antagonistic signals from TGFalpha and FGF7 in morphogenesis of mouse mammary epithelium. Dev. Biol. 306, 193-207.

12 Ewald, A. J. (2010). Practical considerations for long-term time-lapse imaging of epithelial morphogenesis in three-dimensional organotypic cultures. In Imaging in Developmental Biology (ed. R. Wong and J. Sharpe). New York: Cold Spring Harbor Laboratory Press.

13 Larsen, M., Wei, C. and Yamada, K. M. (2006). Cell and fibronectin dynamics during branching morphogenesis. J. Cell Sci. 119, 3376-3384.

14 Chi, X., Michos, O., Shakya, R., Riccio, P., Enomoto, H., Licht, J. D., Asai, N., Takahashi, M., Ohgami, N., Kato, M. et al. (2009). Ret-dependent cell

rearrangements in the Wolffian duct epithelium initiate ureteric bud morphogenesis. Dev. Cell 17, 199-209.
15 Daniel, C. W., De Ome, K. B., Young, J. T., Blair, P. B. and Faulkin, L. J., Jr (1968). The in vivo life span of normal and preneoplastic mouse mammary glands: a serial transplantation study. Proc. Natl. Acad. Sci. USA 61, 53-60.
16 Schneeberger, E. E. and Lynch, R. D. (2004). The tight junction: a multifunctional complex. Am. J. Physiol. Cell Physiol. 286, C1213-C1228.
17 Knudsen, K. A. and Wheelock, M. J. (2005). Cadherins and the mammary gland. J. Cell. Biochem. 95, 488-496.
18 Getsios, S., Huen, A. C. and Green, K. J. (2004). Working out the strength and flexibility of desmosomes. Nat. Rev. Mol. Cell Biol. 5, 271-281.
19 Feigin, M. E. and Muthuswamy, S. K. (2009). Polarity proteins regulate mammalian cell-cell junctions and cancer pathogenesis. Curr. Opin. Cell Biol. 21, 694-700.
20 Rosen, P. P. (2001). Rosen's Breast Pathology. Philadelphia, PA: Lippincott Williams and Wilkins.
21 Huang, L. and Muthuswamy, S. K. (2010). Polarity protein alterations in carcinoma: a focus on emerging roles for polarity regulators. Curr. Opin. Genet. Dev. 20, 41-50.
22 Berx, G., Cleton-Jansen, A. M., Strumane, K., de Leeuw, W. J., Nollet, F., van Roy, F. and Cornelisse, C. (1996). E-cadherin is inactivated in a majority of invasive human lobular breast cancers by truncation mutations throughout its extracellular domain. Oncogene 13, 1919-1925.
23 Hirohashi, S. (1998). Inactivation of the E-cadherin-mediated cell adhesion system in human cancers. Am. J. Pathol. 153, 333-339.
24 Conacci-Sorrell, M., Zhurinsky, J. and Ben-Ze'ev, A. (2002). The cadherin-catenin adhesion system in signaling and cancer. J. Clin. Invest. 109, 987-991.
25 Bogenrieder, T. and Herlyn, M. (2003). Axis of evil: molecular mechanisms of cancer metastasis. Oncogene 22, 6524-6536.
26 Derksen, P. W., Liu, X., Saridin, F., van der Gulden, H., Zevenhoven, J., Evers, B., van Beijnum, J. R., Griffioen, A. W., Vink, J., Krimpenfort, P. et al. (2006). Somatic inactivation of E-cadherin and p53 in mice leads to metastatic lobular mammary carcinoma through induction of anoikis resistance and angiogenesis. Cancer Cell 10, 437-449.
27 Jeanes, A., Gottardi, C. J. and Yap, A. S. (2008). Cadherins and cancer: how does cadherin dysfunction promote tumor progression? Oncogene 27, 6920-6929.
28 Derksen, P. W., Braumuller, T. M., van der Burg, E., Hornsveld, M., Mesman, E., Wesseling, J., Krimpenfort, P. and Jonkers, J. (2011). Mammary-specific inactivation of E-cadherin and p53 impairs functional gland development and leads to pleomorphic invasive lobular carcinoma in mice. Dis. Model. Mech. 4, 347-358.
29 Bilder, D., Li, M. and Perrimon, N. (2000). Cooperative regulation of cell polarity and growth by Drosophila tumor suppressors. Science 289, 113-116.
30 Pagliarini, R. A. and Xu, T. (2003). A genetic screen in Drosophila for metastatic behavior. Science 302, 1227-1231.
31 Pagliarini, R. A., Quin˜ones, A. T. and Xu, T. (2003). Analyzing the function of tumor suppressor genes using a Drosophila model. Methods Mol. Biol. 223, 349-382.

32 Lu, P., Ewald, A. J., Martin, G. R. and Werb, Z. (2008). Genetic mosaic analysis reveals FGF receptor 2 function in terminal end buds during mammary gland branching morphogenesis. Dev. Biol. 321, 77-87.
33 Wang, Z., Sandiford, S., Wu, C. and Li, S. S. (2009). Numb regulates cell-cell adhesion and polarity in response to tyrosine kinase signalling. EMBO J. 28, 2360-2373.
34 Go¨nczy, P. (2008). Mechanisms of asymmetric cell division: flies and worms pave the way. Nat. Rev. Mol. Cell Biol. 9, 355-366.
35 Pitelka, D. R., Hamamoto, S. T., Duafala, J. G. and Nemanic, M. K. (1973). Cell contacts in the mouse mammary gland. I. Normal gland in postnatal development and the secretory cycle. J. Cell Biol. 56, 797-818.
36 Ozzello, L. (1971). Ultrastructure of the human mammary gland. Pathol. Annu. 6, 1-59.
37 Stirling, J. W. and Chandler, J. A. (1976). The fine structure of the normal, resting terminal ductal-lobular unit of the female breast.
38 Keller, R. (2002). Shaping the vertebrate body plan by polarized embryonic cell movements. Science 298, 1950-1954.
39 Stubbs, J. L., Davidson, L., Keller, R. and Kintner, C. (2006). Radial intercalation of ciliated cells during Xenopus skin development. Development 133, 2507- 2515.
40 Hennighausen, L. and Robinson, G. W. (2005). Information networks in the mammary gland. Nat. Rev. Mol. Cell Biol. 6, 715-725.
41 Sternlicht, M. D. (2006). Key stages in mammary gland development: the cues that regulate ductal branching morphogenesis. Breast Cancer Res. 8, 201.
42 Underwood, J. M., Imbalzano, K. M., Weaver, V. M., Fischer, A. H., Imbalzano, A. N. and Nickerson, J. A. (2006). The ultrastructure of MCF-10A acini. J. Cell. Physiol. 208, 141-148.
43 Langbein, L., Grund, C., Kuhn, C., Praetzel, S., Kartenbeck, J., Brandner, J. M., Moll, I. and Franke, W. W. (2002). Tight junctions and compositionally related junctional structures in mammalian stratified epithelia and cell cultures derived therefrom. Eur. J. Cell Biol. 81, 419-435.
44 Nanba, D., Nakanishi, Y. and Hieda, Y. (2001). Changes in adhesive properties of epithelial cells during early morphogenesis of the mammary gland. Dev. Growth Differ. 43, 535-544.
45 Rudland, P. S. (1991). Histochemical organization and cellular composition of ductal buds in developing human breast: evidence of cytochemical intermediates between epithelial and myoepithelial cells. J. Histochem. Cytochem. 39, 1471-1484.
46 Smith, G. H. and Medina, D. (1988). A morphologically distinct candidate for an epithelial stem cell in mouse mammary gland. J. Cell Sci. 90, 173-183.
47 Chepko, G. and Smith, G. H. (1997). Three division-competent, structurally-distinct cell populations contribute to murine mammary epithelial renewal. Tissue Cell 29, 239-253.
48 Chepko, G. and Smith, G. H. (1999). Mammary epithelial stem cells: our current understanding. J. Mammary Gland Biol. Neoplasia 4, 35-52.
49 Smith, G. H. and Chepko, G. (2001). Mammary epithelial stem cells. Microsc. Res. Tech. 52, 190-203.

50 Kalluri, R. and Weinberg, R. A. (2009). The basics of epithelial-mesenchymal transition. J. Clin. Invest. 119, 1420-1428.
51 Polyak, K. and Weinberg, R. A. (2009). Transitions between epithelial and mesenchymal states: acquisition of malignant and stem cell traits. Nat. Rev. Cancer 9, 265-273.
52 O'Brien, L. E., Zegers, M. M. and Mostov, K. E. (2002). Opinion: Building epithelial architecture: insights from three-dimensional culture models. Nat. Rev. Mol. Cell Biol. 3, 531-537.
53 Lee, K., Gjorevski, N., Boghaert, E., Radisky, D. C. and Nelson, C. M. (2011). Snail1, Snail2, and E47 promote mammary epithelial branching morphogenesis. EMBO J. 30, 2662-2674.
54 Larue, L., Ohsugi, M., Hirchenhain, J. and Kemler, R. (1994). E-cadherin null mutant embryos fail to form a trophectoderm epithelium. Proc. Natl. Acad. Sci. USA 91, 8263-8267.
55 Gumbiner, B., Stevenson, B. and Grimaldi, A. (1988). The role of the cell adhesion molecule uvomorulin in the formation and maintenance of the epithelial junctional complex. J. Cell Biol. 107, 1575-1587.
56 Green, K. J. and Gaudry, C. A. (2000). Are desmosomes more than tethers for intermediate filaments? Nat. Rev. Mol. Cell Biol. 1, 208-216.
57 Vasioukhin, V., Bowers, E., Bauer, C., Degenstein, L. and Fuchs, E. (2001). Desmoplakin is essential in epidermal sheet formation. Nat. Cell Biol. 3, 1076-1085.
58 Den, Z. N., Cheng, X., Merched-Sauvage, M. and Koch, P. J. (2006). Desmocollin 3 is required for pre-implantation development of the mouse embryo. J. Cell Sci. 119, 482-489.
59 Lechler, T. and Fuchs, E. (2007). Desmoplakin: an unexpected regulator of microtubule organization in the epidermis. J. Cell Biol. 176, 147-154.
60 Runswick, S. K., O'Hare, M. J., Jones, L., Streuli, C. H. and Garrod, D. R. (2001). Desmosomal adhesion regulates epithelial morphogenesis and cell positioning. Nat. Cell Biol. 3, 823-830.
61 Klus, G. T., Rokaeus, N., Bittner, M. L., Chen, Y. D., Korz, D. M., Sukumar, S., Schick, A. and Szallasi, Z. (2001). Down-regulation of the desmosomal cadherin desmocollin 3 in human breast cancer. Int. J. Oncol. 19, 169-174.
62 Oshiro, M. M., Kim, C. J., Wozniak, R. J., Junk, D. J., Mun˜oz-Rodrı´guez, J. L., Burr, J. A., Fitzgerald, M., Pawar, S. C., Cress, A. E., Domann, F. E. et al. (2005). Epigenetic silencing of DSC3 is a common event in human breast cancer. Breast Cancer Res. 7, R669-R680.
63 Ihrie, R. A. and Attardi, L. D. (2005). A new Perp in the lineup: linking p63 and desmosomal adhesion. Cell Cycle 4, 873-876. Ingber, D. E. (2008). Can cancer be reversed by engineering the tumor microenvironment? Semin. Cancer Biol. 18, 356-364.
64 Cui, T., Chen, Y., Yang, L., Kno¨sel, T., Zo¨ller, K., Huber, O. and Petersen, I. (2011). DSC3 expression is regulated by p53, and methylation of DSC3 DNA is a prognostic marker in human colorectal cancer. Br. J. Cancer 104, 1013-1019. 2652 Journal of Cell Science 125 (11) Journal of Cell Science
65 Dusek, R. L. and Attardi, L. D. (2011). Desmosomes: new perpetrators in tumour suppression. Nat. Rev. Cancer 11, 317-323.

66 Streuli, C. H., Bailey, N. and Bissell, M. J. (1991). Control of mammary epithelial differentiation: basement membrane induces tissue-specific gene expression in the absence of cell-cell interaction and morphological polarity. J. Cell Biol. 115, 1383-1395.
67 Petersen, O. W., Rønnov-Jessen, L., Howlett, A. R. and Bissell, M. J. (1992). Interaction with basement membrane serves to rapidly distinguish growth and differentiation pattern of normal and malignant human breast epithelial cells. Proc. Natl. Acad. Sci. USA 89, 9064-9068.
68 Weaver, V. M., Petersen, O. W., Wang, F., Larabell, C. A., Briand, P., Damsky, C. and Bissell, M. J. (1997). Reversion of the malignant phenotype of human breast cells in three-dimensional culture and in vivo by integrin blocking antibodies. J. Cell Biol. 137, 231-245.
69 Nelson, C. M. and Bissell, M. J. (2006). Of extracellular matrix, scaffolds, and signaling: tissue architecture regulates development, homeostasis, and cancer. Annu. Rev. Cell Dev. Biol. 22, 287-309.
70 Hendrix, M. J., Seftor, E. A., Seftor, R. E., Kasemeier-Kulesa, J., Kulesa, P. M. and Postovit, L. M. (2007). Reprogramming metastatic tumour cells with embryonic microenvironments. Nat. Rev. Cancer 7, 246-255.
71 Weigelt, B. and Bissell, M. J. (2008). Unraveling the microenvironmental influences on the normal mammary gland and breast cancer. Semin. Cancer Biol. 18, 311-321.
72 Goldenberg, V. E., Goldenberg, N. S. and Sommers, S. C. (1969). Comparative ultrastructure of atypical ductal hyperplasia, intraductal carcinoma, and infiltrating ductal carcinoma of the breast. Cancer 24, 1152-1169.
73 Yang, j. and Weinberg, R.A. (2008). Epithelial-mesenchymal transition: at the cossroad of development and tumor metastasis. Dev. Cell 14(6), 818-29
74 Hanson, P., Mathews, V., Marrus, S. H. and Graubert, T. A. (2003). Enhanced green fluorescent protein targeted to the Sca-1 (Ly-6A) locus in transgenic mice results in efficient marking of hematopoietic stem cells in vivo. Exp. Hematol. 31, 159-167.
75 McDonald, K. L. and Auer, M. (2006). High-pressure freezing, cellular tomography, and structural cell biology. Biotechniques 41, 137-143.
76 Triffo, W. J., Palsdottir, H., McDonald, K. L., Lee, J. K., Inman, J. L., Bissell, M. J., Raphael, R. M. and Auer, M. (2008). Controlled microaspiration for high-pressure freezing: a new method for ultrastructural preservation of fragile and sparse tissues for TEM and electron tomography. J. Microsc. 230, 278-287.
77 Sosinsky, G. E., Crum, J., Jones, Y. Z., Lanman, J., Smarr, B., Terada, M., Martone, M. E., Deerinck, T. J., Johnson, J. E. and Ellisman, M. H. (2008). The Collective epithelial cell migration 2653 Journal of Cell Sciencecombination of chemical fixation procedures with high pressure freezing and freeze substitution preserves highly labile tissue ultrastructure for electron tomography applications. J. Struct. Biol. 161, 359-371.
78 McDonald, K. and Mu¨ller-Reichert, T. (2002). Cryomethods for thin section electron microscopy. Methods Enzymol. 351, 96-123.
79 McDonald, K. (2007). Cryopreparation methods for electron microscopy of selected model systems. Methods Cell Biol. 79, 23-56.
80 Cardona, A., Saalfeld, S., Preibisch, S., Schmid, B., Cheng, A., Pulokas, J., Tomancak, P. and Hartenstein, V. (2010). An integrated micro- and

macroarchitectural analysis of the Drosophila brain by computer-assisted serial section electron microscopy. PLoS Biol. 8, e1000502.

81 Saalfeld, S., Cardona, A., Hartenstein, V. and Tomanca´k, P. (2010). As-rigid-aspossible mosaicking and serial section registration of large ssTEM datasets. Bioinformatics 26, i57-i63.

82 Schmid, B., Schindelin, J., Cardona, A., Longair, M. and Heisenberg, M. (2010). A high-level 3D visualization API for Java and ImageJ. BMC Bioinformatics 11, 274.

83 Friedman, P. L. and Ellisman, M. H. (1981). Enhanced visualization of peripheral nerve and sensory receptors in the scanning electron microscope using cryofracture and osmium-thiocarbohydrazide-osmium impregnation. J. Neurocytol. 10, 111-131.

84 Willingham, M. C. and Rutherford, A. V. (1984). The use of osmium-thiocarbohydrazide-osmium (OTO) and ferrocyanide-reduced osmium methods to enhance membrane contrast and preservation in cultured cells. J. Histochem. Cytochem. 32, 455-460.

85 Edelstein, A., Amodaj, N., Hoover, K., Vale, R. and Stuurman, N. (2010). Computer control of microscopes using microManager. Curr. Protoc. Mol. Biol. 14, 20.

Figure 3-1: Normal mammary morphogenesis is accomplished by a stratified epithelium.

(A) Mammary ducts are elongated during puberty by specialized structures at the end of the duct, terminal end buds (TEBs). (Carmine Red stained 10-week-old mammary gland) (B) Resting mammary ducts have a bilayered organization, with luminal epithelial cells connected by extensive intercellular junctions, and basally located myoepithelial cells. (C) Normal ducts in vivo have simple epithelial organization when not actively growing. They localize zona occludens 1 (ZO-1) to the apico-lateral surface of the luminal epithelial cells and b-catenin to basolateral surfaces. (D) Mammary ducts are elongated during puberty by terminal end buds, stratified epithelial structures with many luminal cell layers. b-catenin localizes to all basolateral surfaces and is only excluded from lumen facing surfaces. ZO-1 localizes to the lumen lining surfaces of both the main lumen and isolated micro-lumens. (E-E'') Primary mammary ducts can be isolated and grown in 3D Matrigel gels. Without addition of growth factor all ducts form simple cysts. These cysts are bilayered, with a single luminal (Lum) cell layer and a single myoepithelial (Myo) layer. The lumen has electron dense secretory material (arrows), microvilli (MV), and tight junctions (TJ). Both luminal and myoepithelial cells are connected by desmosomes (Des). (F-H) Polarized cysts in 3D culture localize Par-3 to apical surfaces (F) and both Scribble (G) and Numb (H) to basolateral surfaces. All TEM images are from high pressure frozen, freeze-substituted samples that were pre-fixed with 4% glutaraldehyde.

Figure 3-1

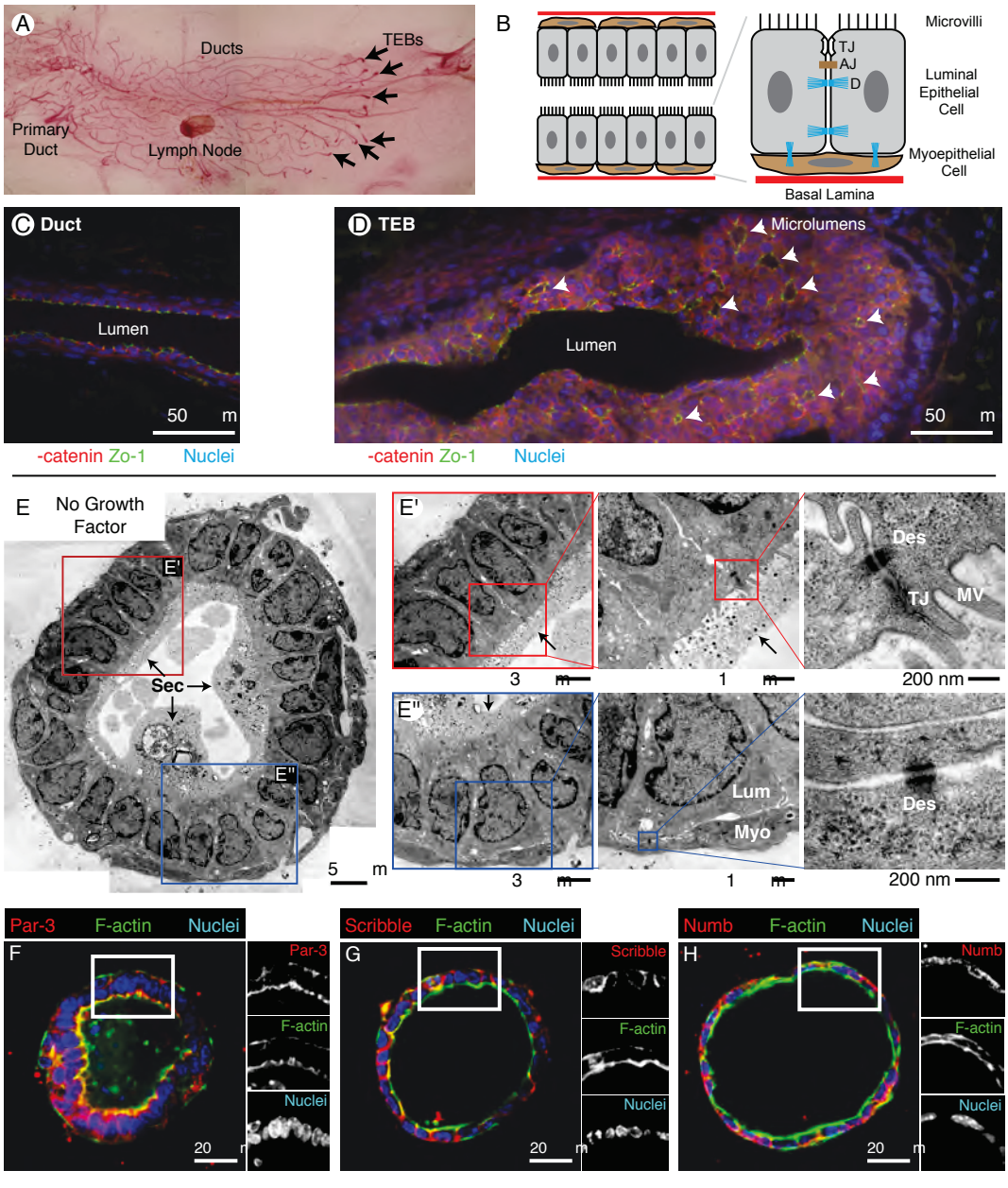
A
Ducts
TEBs
Primary Duct
Lymph Node
B
Microvilli
TJ
AJ
D
Luminal Epithelial Cell
Myoepithelial Cell
Basal Lamina
C Duct
Lumen
50 m
-catenin Zo-1 Nuclei
D TEB
Microlumens
Lumen
50 m
-catenin Zo-1 Nuclei
E No Growth Factor
E'
Sec
E"
5 m
E'
3 m
1 m
Des
TJ
MV
200 nm
E"
Lum
Myo
Des
3 m
1 m
200 nm
Par-3 F-actin Nuclei
F
Par-3
F-actin
Nuclei
20 m
Scribble F-actin Nuclei
G
Scribble
F-actin
Nuclei
20 m
Numb F-actin Nuclei
H
Numb
F-actin
Nuclei
20 m

Figure 3-2: During morphogenesis in 3D culture the mammary epithelium is transiently stratified.

(A-C') Within the multilayered epithelium of elongating buds in 3D culture, most interior cell surfaces were out of contact with the lumen or with the ECM. These interior surfaces stained positive for APKC-z (A), E-cadherin (B), β-catenin (C). Following morphogenesis, the mammary epithelium regained simple organization. In regions of simple organization, APKC-z localized to apical domains (A') and β-catenin localized to basolateral domains (C'). (D-E') We next used TEM to define the ultrastructural polarity of the tissue and observed that the basal tissue surface was smooth and lacks ECM-directed protrusions. (F-G''') Both elongated cells (F') and round unpolarized cells (F''') are present in the interior of the multilayer. Away from the basal tissue surface, the epithelial cells exhibit dense, inter-digitating membrane extensions (F''). We also observed division of round cells distant from either the ECM or lumen facing surfaces (F, green asterisk). (G-G''') Within the same branching structure, there are regions of simple epithelial organization with an electron dense lumen and tight junctions (TJ). All TEM images are from high pressure frozen, freeze-substituted samples that were pre-fixed with 4% glutaraldehyde. ED = electron-dense. EL = electron-lucid. TJ = tight junction.

Figure 3-2

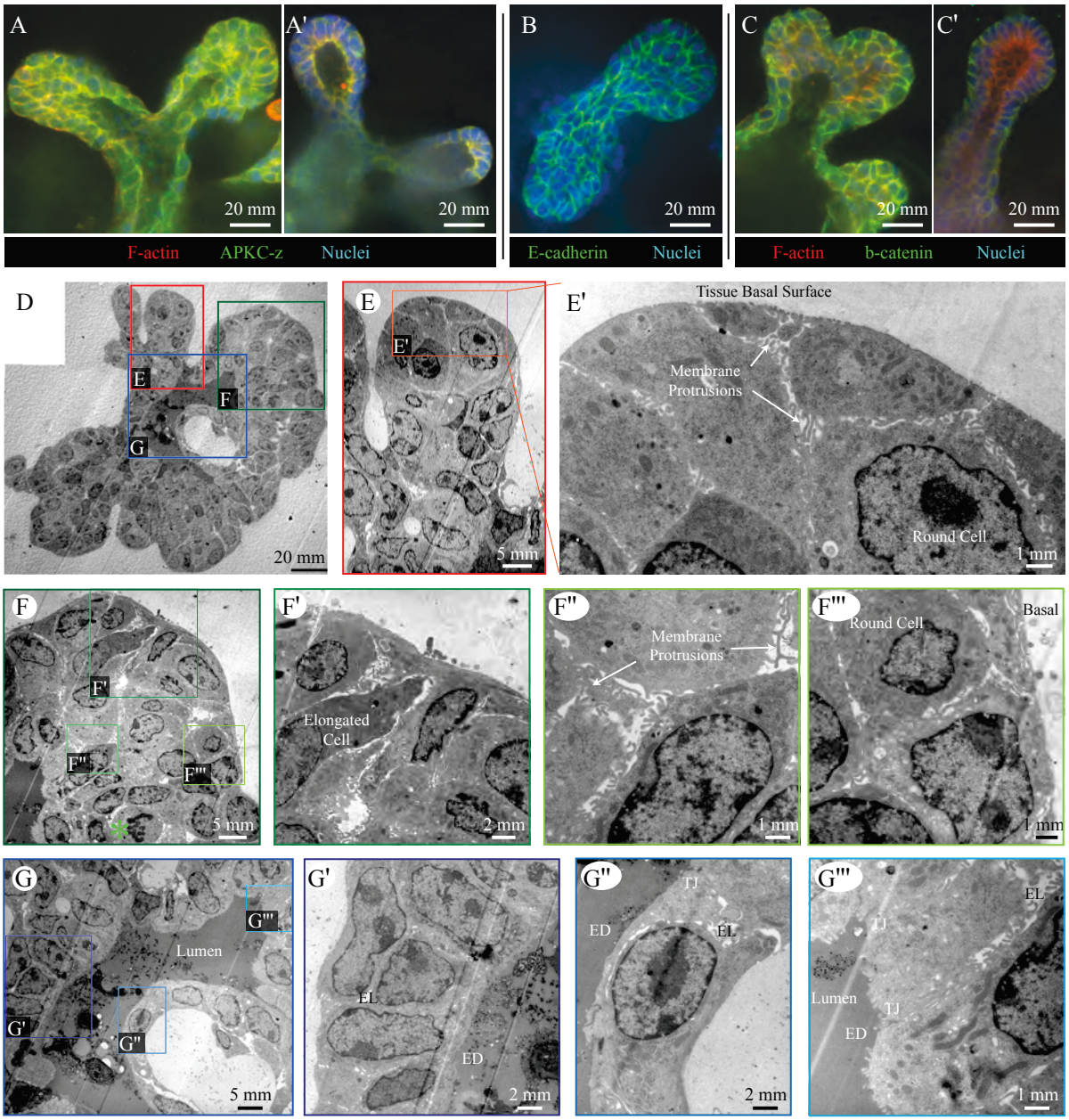
A
A'
B
C
C'
20 mm
F-actin
APKC-z
Nuclei
E-cadherin
Nuclei
F-actin
b-catenin
Nuclei
D
E
E'
F
G
5 mm
Tissue Basal Surface
Membrane Protrusions
Round Cell
1 mm
F'
F''
F'''
Elongated Cell
2 mm
Basal
G'
G''
G'''
Lumen
EL
ED
TJ

Figure 3-3: Morphogenesis in 3D culture is associated with a loss of molecular polarity.

(A-C) Interior cells are first evident in "complex cyst" structures. Within these structures interior cells display cytoplasmic localization of Par-3 (A), while Scribble and Numb localize to all interior cell surfaces (B-C). (D-F') In the multilayered region of elongating mammary end buds Par-3 is cytoplasmically localized (D), while Scribble and Numb localize to all interior surfaces. After morphogenesis is complete the epithelium regains simple epithelial organization and Par-3 is associated with the apical membrane (D'), while Scribble and Numb are localized to basolateral cell surfaces (E',F').

Figure 3-3

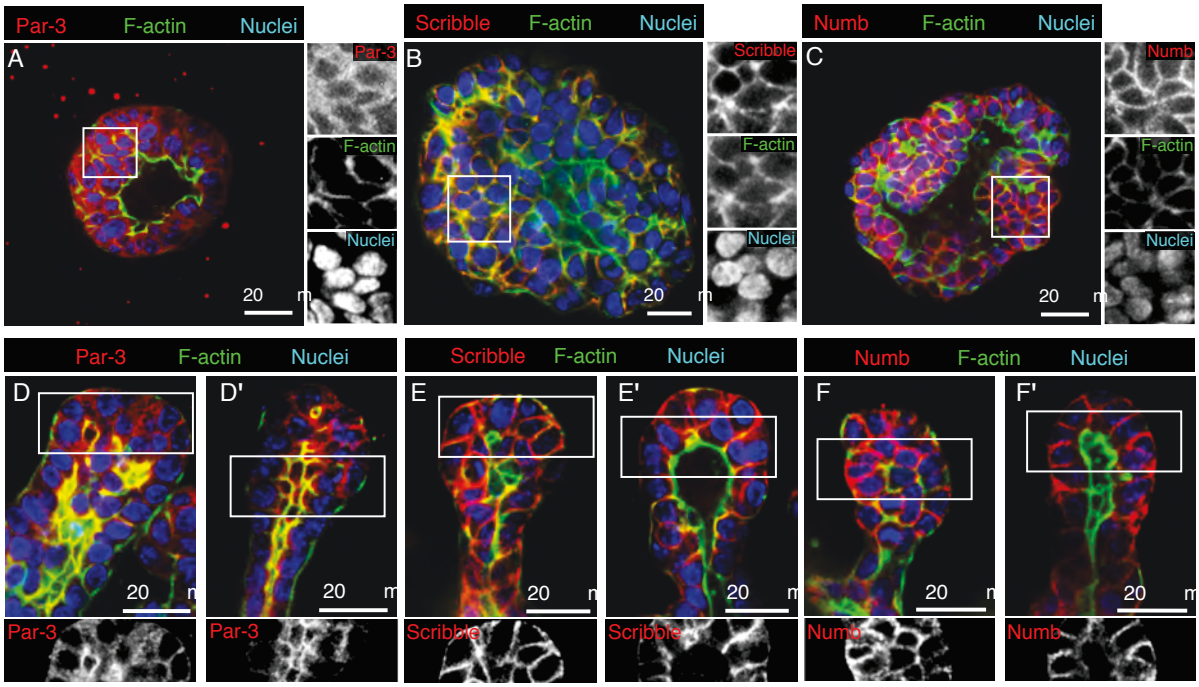
Par-3 F-actin Nuclei
A
Par-3
F-actin
Nuclei
20 m
Scribble F-actin Nuclei
B
Scribble
F-actin
Nuclei
20 m
Numb F-actin Nuclei
C
Numb
F-actin
Nuclei
20 m
Par-3 F-actin Nuclei
D
D'
20 m
Par-3
Scribble F-actin Nuclei
E
E'
20 m
Scribble
Numb F-actin Nuclei
F
F'
20 m
Numb

Figure 3-4: The multilayered region contains microlumens with tight junctions.

(A-A'') By light microscopy, ZO-1 (green) localizes both to the lining of the main lumen and to isolated microlumens located between luminal epithelial cells (arrowheads in 3D volume reconstruction). (B-B') Following morphogenesis simple epithelial organization is restored and a single clear lumen is observed. (C-D''') Using TEM there are two different intercellular spaces: electron-lucid spaces with extensive, irregular membrane protrusions, but without tight junctions (C') and electron-dense intercellular spaces with tight junctions, microvilli, and secretory material (red arrow in C'') (C''-D'''). (E) Serial block face scanning electron microscopy enabled 3D reconstruction of the microlumens and confirmed that they are multiple microns thick. All TEM images are from high-pressure frozen, freeze-substituted samples that were pre-fixed with 4% glutaraldehyde. The serial block face SEM image series from Panel E was uploaded to the ASCB's The Cell: An Image Library, CIL:39304.

Figure 3-4

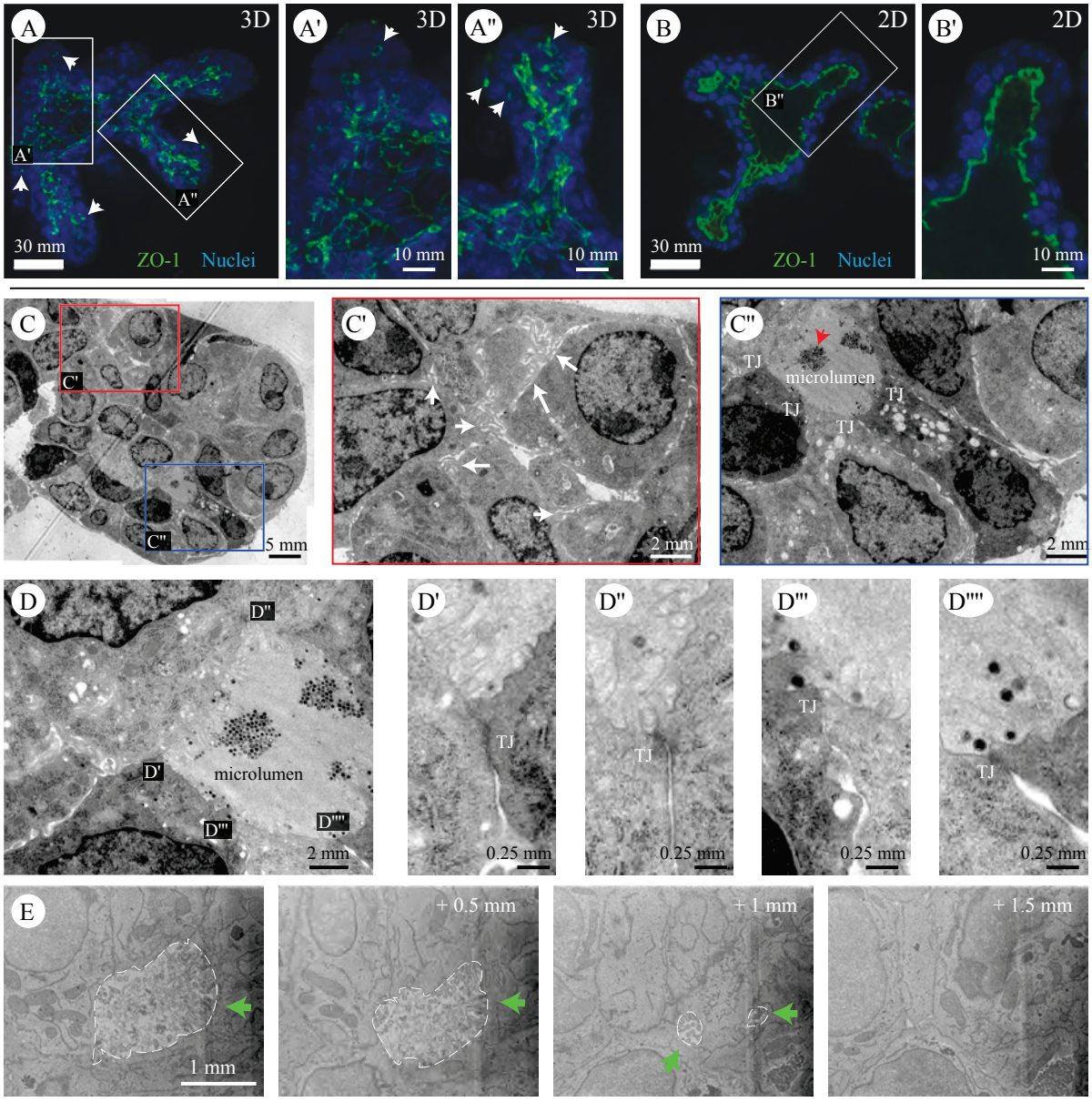
A
3D
A'
A"
30 mm
ZO-1
Nuclei
A'
3D
10 mm
A"
3D
10 mm
B
2D
B"
30 mm
ZO-1
Nuclei
B'
2D
10 mm
C
C'
C"
5 mm
C'
2 mm
C"
TJ
microlumen
TJ
TJ
TJ
2 mm
D
D"
D'
microlumen
D'''
D''''
2 mm
D'
TJ
0.25 mm
D"
TJ
0.25 mm
D'''
TJ
0.25 mm
D''''
TJ
0.25 mm
E
1 mm
+ 0.5 mm
+ 1 mm
+ 1.5 mm

Figure 3-5: Cell shape and lateral membrane organization are highly heterogeneous in the multilayered region.

(A-A'') Nearby regions in the same branching structure can have high (A') or low (A'') epithelial organization. (B-D) Lateral membrane protrusions within the multilayer were frequently interdigitated (B-B'), could be multiple microns in length (C-C') and were frequently branched (D). (E-F) Analysis of serial sections by TEM (E-E') and serial block face scanning electron microscopy (F) revealed that the lateral membrane protrusions extend through multiple sections and can morph between thin and broad and between linear and branched. (G-H'') Three-dimensional reconstructions of cell contact regions along interior lateral surfaces using serial block face SEM revealed densely interdigitating 3D membrane extensions. All TEM images are from high-pressure frozen, freeze-substituted samples that were pre-fixed with 4% glutaraldehyde. Serial block face SEM image series of these contact regions were uploaded to the ASCB's The Cell: An Image Library, CIL:39301-39304. Panel F corresponds to CIL:39303.

Figure 3-5

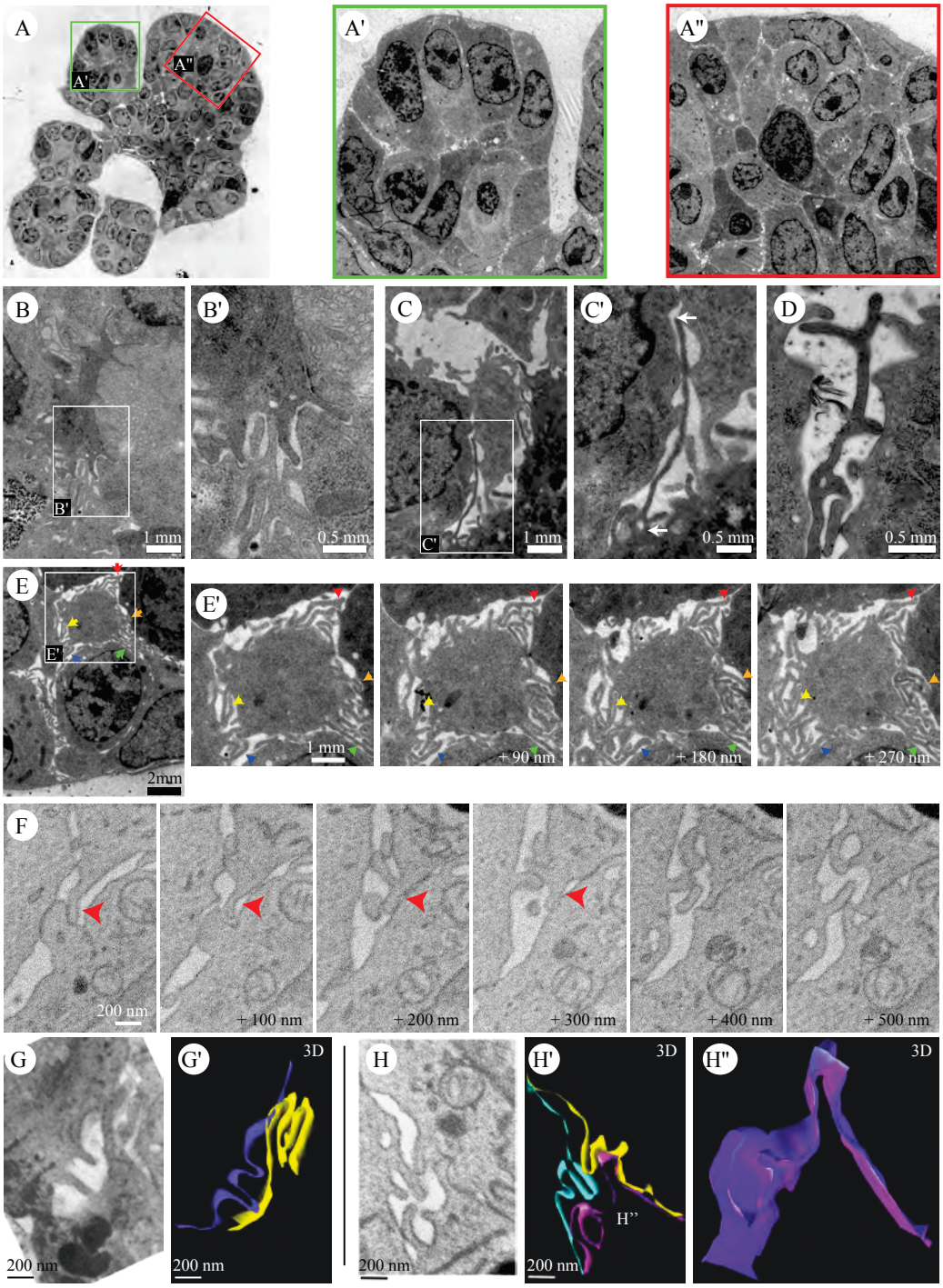
A
A'
A"
B
B'
C
C'
D
E
E'
F
G
G'
H
H'
H"
3D
1 mm
0.5 mm
2mm
+ 90 nm
+ 180 nm
+ 270 nm
200 nm
+ 100 nm
+ 200 nm
+ 300 nm
+ 400 nm
+ 500 nm
H''

Figure 3-6: Elongated cells are observed within the epithelial multilayer.

(A-A'') Electron-dense elongated cells are seen within the multilayered region. These cells frequently had long protrusions extending in a single direction between adjacent cells (A''). (B-C') Elongated cells were observed deep within the multilayer (A) and also within microns of the ECM (B). The only intercellular junctions observed on these cells were small desmosomes (C-C'). (D-D'') At the ECM border some cells appeared intermediate between columnar epithelial and elongated morphologies. They did not extend protrusions into the ECM. (E-F') Cells in extensive contact with the ECM had smooth basal surfaces, lateral desmosomes, but frequently displayed little morphologic polarity on their lateral surfaces. (G-H) Interior lateral surfaces displayed intermixed membrane protrusions and small desmosomes. All TEM images are from high pressure frozen, freeze-substituted samples that were pre-fixed with 4% glutaraldehyde.

Figure 3-6

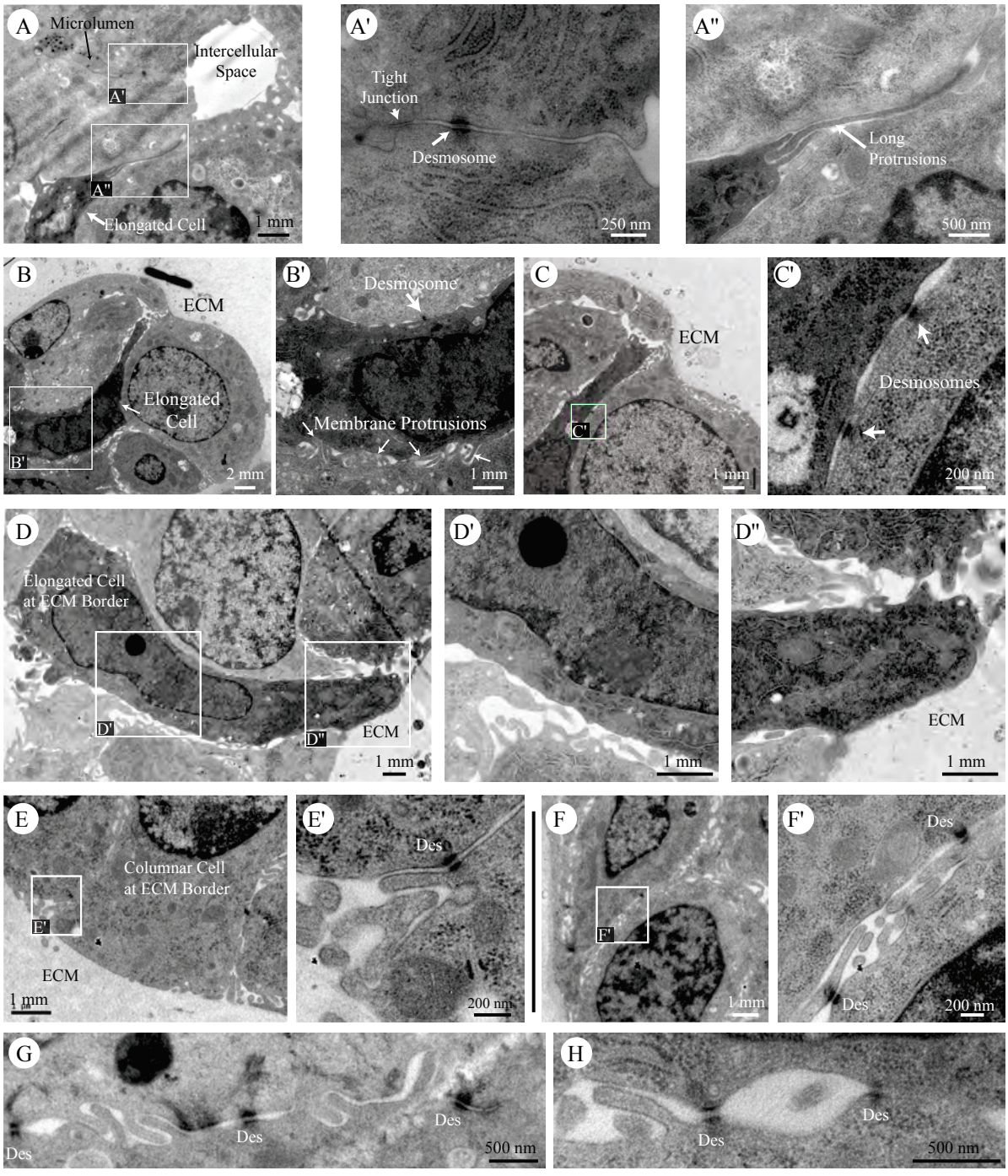
A
Microlumen
Intercellular Space
A'
A"
Elongated Cell
1 mm
A'
Tight Junction
Desmosome
250 nm
A"
Long Protrusions
500 nm
B
ECM
Elongated Cell
B'
2 mm
B'
Desmosome
Membrane Protrusions
1 mm
C
ECM
C'
1 mm
C'
Desmosomes
200 nm
D
Elongated Cell at ECM Border
D'
D"
ECM
1 mm
D'
1 mm
D"
ECM
1 mm
E
Columnar Cell at ECM Border
E'
ECM
1 mm
E'
Des
200 nm
F
F'
1 mm
F'
Des
Des
200 nm
G
Des
Des
Des
500 nm
H
Des
Des
500 nm

Figure 3-7: Interior cells are frequently migratory and protrusive within the multilayer.

All cells were labeled with Cell Tracker Red and a subset of cells were labeled with an adenovirally delivered cytoplasmic GFP. Images depict 3D reconstructions of the cytoplasm in individual GFP+ cells. (A) Interior cells were frequently highly migratory and could move in directions opposite to the direction of ductal elongation. (B) Interior cells extended and retracted cytoplasmic protrusions within the multilayer, but not into the lumen or ECM. (C) Individual cells migrated from the interior to basal positions in contact with the ECM, a process termed radial intercalation. (D-E) Cells in contact with the basal tissue surface (D) or both apical and basal tissue surfaces (D-E) extended cytoplasmic protrusions from all lateral surfaces.

Figure 3-7

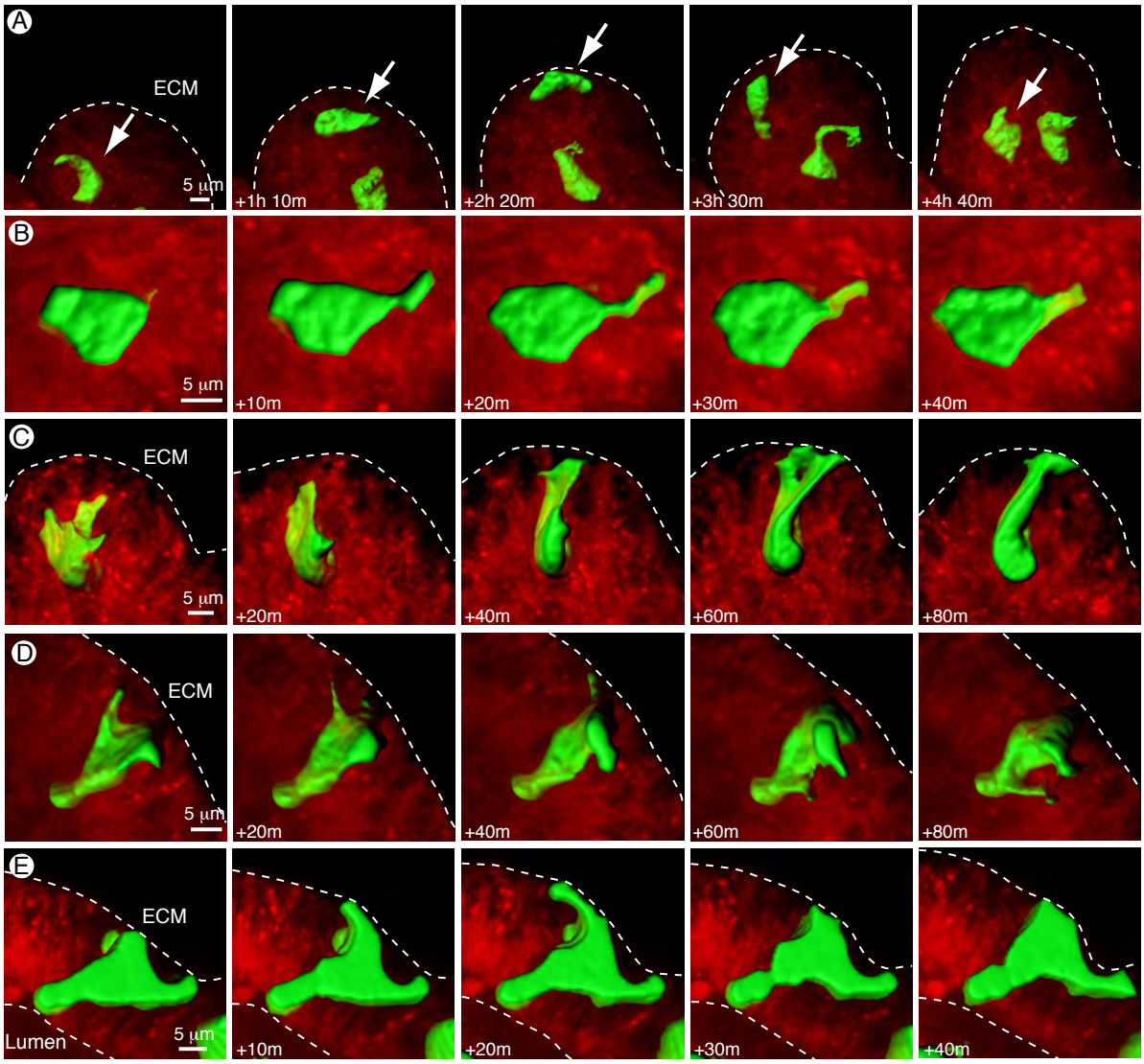

Cell Tracker Red Cytoplasmic GFP (3D Single Cell)

Figure 3-8: Treatment with Y-27632 results in disorganization and reduced cell-cell contact on lateral and apical surfaces. (**A-C'**)

Normal organoids have a stereotyped branching pattern, with a large ZO-1 lined lumen (A-A'). Treatment with Y-27632 results in rapid loss of the lumen, luminal epithelial disorganization, and localization of ZO-1 exclusively to small foci (B-B'). Large regions of Y-27632 treated epithelium were free of ZO-1 immunoreactivity (red = phalloidin, green = ZO-1, blue = nuclei). (**D-H'''**) Ultrastructural examination revealed a loss of electron dense luminal spaces and a large decrease in cell-cell contact along lateral cell surfaces. The basal tissue surface was still smooth and well organized (H-H'''). The only junctions we observed connecting cells in Y-27632 treated samples were small desmosomes (E',E'',G',G''). All TEM images are from high pressure frozen, freeze-substituted samples that were pre-fixed with 4% glutaraldehyde. (**I,I'**) Organoids treated with the ROCK inhibitor H1152 localized Par-3 to their microlumens (I = 3D reconstruction, I' = 2D optical section). (**J,J'**) Organoids treated with H1152 localized Scribble to lateral surfaces, but not to their microlumens (J = 3D reconstruction, J' = 2D optical section).

Figure 3-8

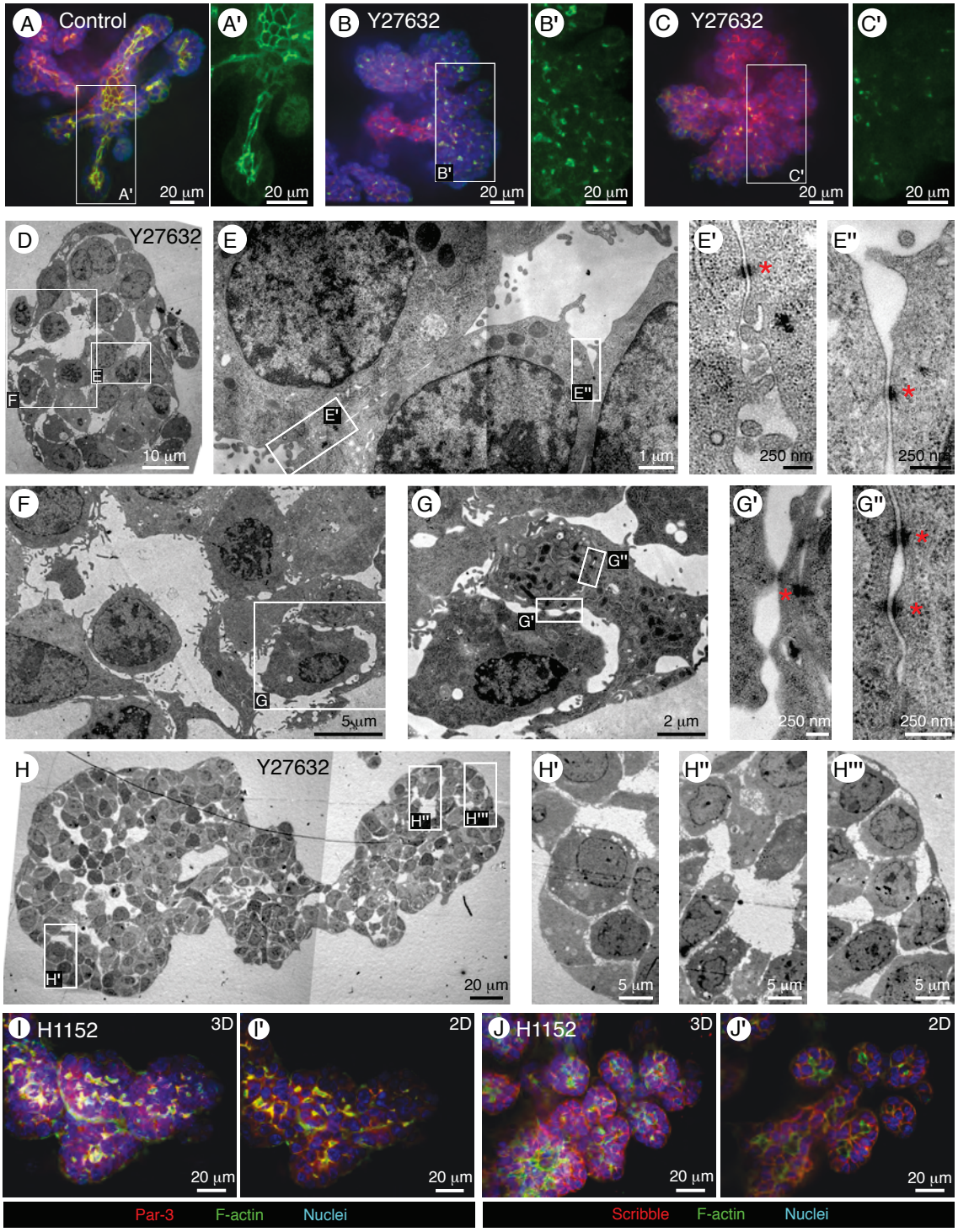
A Control
A'
20 μm
B Y27632
B'
C Y27632
C'
D Y27632
E
E'
E''
F
10 μm
1 μm
250 nm
G
G'
G''
5 μm
2 μm
H Y27632
H'
H''
H'''
I H1152
3D
I'
2D
J H1152
J'
Par-3
F-actin
Nuclei
Scribble

Figure 3-9: Terminal End Buds (TEBs) in vivo display reduced apico-basal polarity and extensive intercellular membrane protrusions. (**A**) Mammary epithelial ducts are elongated by terminal end buds (TEBs), shown here in a light micrograph, with boxes indicating regions that were subsequently imaged by TEM. (**B-B'**) TEBs contain a fluid filled lumen, with microvilli and tight junctions (B-B'). (**C-F''**) Cells within the multilayered region appeared morphologically unpolarized and displayed extensive intercellular protrusions. These protrusions were observed to interdigitate (D) and branch (F''). (**G-G''**) Cells at the apical or basal most tissue surface were polarized at the tissue boundary, but could be unpolarized and irregularly shaped a few microns away. (**H**) Microlumens within the body cell region had both microvilli and tight junctions (TJ). All TEM images are from high pressure frozen, freeze-substituted samples that were pre-fixed with 4% glutaraldehyde.

Figure 3-9

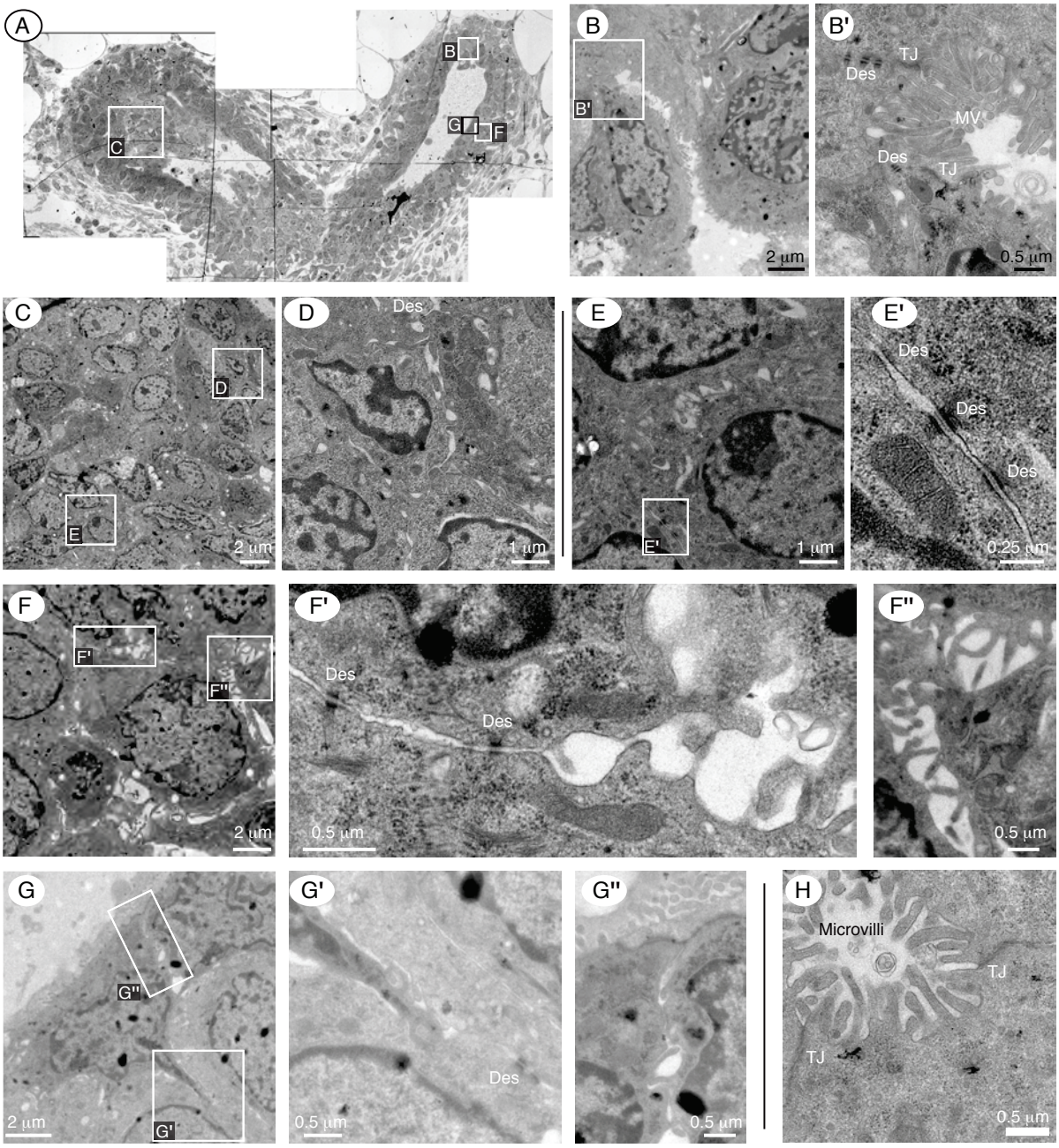
A
B
C
G
F
B
B'
2 μm
B'
TJ
Des
MV
Des
TJ
0.5 μm
C
D
E
2 μm
D
Des
1 μm
E
E'
1 μm
E'
Des
Des
Des
0.25 μm
F
F'
F''
2 μm
F'
Des
Des
0.5 μm
F''
0.5 μm
G
G''
G'
2 μm
G'
Des
0.5 μm
G''
0.5 μm
H
Microvilli
TJ
TJ
0.5 μm

Figure 3-10: Normal mammary epithelial morphogenesis is accomplished by a transiently stratified epithelium.

The transient multilayered epithelium associated with mammary morphogenesis is polarized as a tissue, but displays reduced apico-basal polarity and few intercellular junctions at points of cell-cell contact in the interior.

Figure 3-10

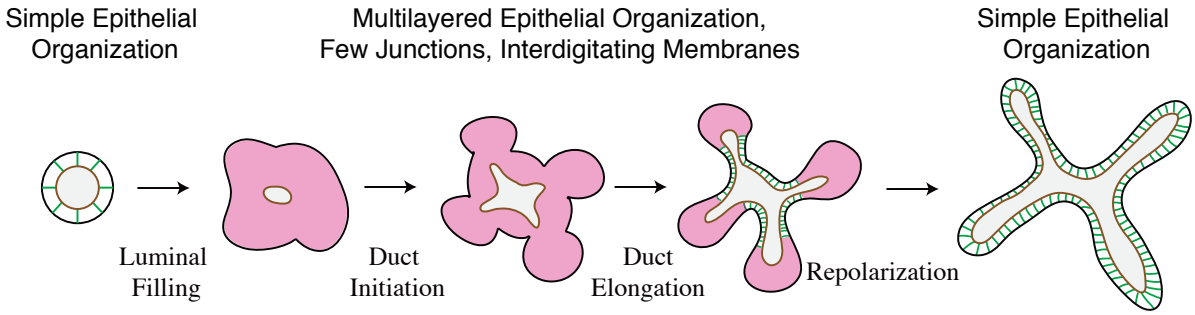
Simple Epithelial Organization
Multilayered Epithelial Organization, Few Junctions, Interdigitating Membranes
Simple Epithelial Organization
Luminal Filling
Duct Initiation
Duct Elongation
Repolarization

Chapter 4

Developmental stratification of the mammary epithelium occurs through symmetry-breaking vertical divisions of apically positioned luminal cells

(Modified from Huebner et al., Development 2014)

Abstract

Mammary ducts are elongated during development by stratified epithelial structures, known as terminal end buds (TEBs). TEBs exhibit reduced apico-basal polarity and extensive proliferation. A major unanswered question concerns the mechanism by which the simple ductal epithelium stratifies during TEB formation. We sought to elucidate this mechanism using real-time imaging of growth factor induced stratification in 3D cultures of primary epithelial organoids. We hypothesized that stratification could result from vertical divisions in either the apically positioned luminal epithelial cells or the basally positioned myoepithelial cells. Stratification initiated exclusively from vertical apical cell divisions, both in 3D culture and in vivo. During vertical apical divisions, only the mother cell retained tight junctions and segregated apical membranes. Vertical daughter cells initiated an unpolarized cell population located between the luminal and myoepithelial cells, similar to the unpolarized body cells in the TEB. Since stratification and loss of apico-basal polarity are early hallmarks of cancer, we next determined the cellular mechanism of oncogenic stratification. Expression of activated ErbB2 induced neoplastic stratification through analogous vertical divisions of apically positioned luminal epithelial cells. However, ErbB2-induced stratification was accompanied by tissue overgrowth and acute loss of both tight junctions and apical polarity. Expression of phosphomimetic MEK (MEK1DD), a major ErbB2 effector, also induced stratification through vertical apical cell divisions. However, MEK1DD expressing organoids exhibited normal levels of growth and retained apico-basal polarity. We conclude that both normal and neoplastic stratification are accomplished through receptor tyrosine kinase signaling dependent vertical cell divisions within the luminal epithelial cell layer.

Introduction

Simple epithelial cells are characterized by extensive intercellular junctions and strong polarity along the apico-basal axis[1,2]. This polarity is manifested both in specialized morphological features, such as apically localized microvilli, and by segregated plasma membrane domains with distinct apical and basolateral polarity proteins[3]. Yet these highly polarized cells emerge during development from less polarized, multilayered embryonic tissues. Early embryonic morphogenesis in the mammary and salivary glands is accomplished by a tissue with lower levels of polarity and adhesion than the mature epithelium in the adult organ[4,5]. A fundamental and unresolved question in biology is how epithelial tissues transition between these different states of organization and polarity[6]. These transitions are also of biomedical interest as epithelial tumors lose apico-basal polarity and simple organization early in cancer progression[7], leading to the hypothesis that metastasis may involve reactivation of an embryonic developmental program[8,9,10,11].

The mammary gland is a powerful model system for studying transitions between simple and stratified epithelial organization, and for the corresponding changes in apico-basal polarity. The mammary ductal network arises during embryogenesis when the mammary placode invades the mammary mesenchyme[12]. During this invasion process the mammary epithelium is multilayered and few cells have contact with a luminal space or possess mature apico-basal polarity[12,13]. At the end of fetal development the rudimentary ductal network repolarizes through unknown cellular mechanisms to form simple epithelial tubes with a inner luminal epithelial cell layer and a basally positioned

myoepithelial cell layer[12]. These tubes then remain essentially quiescent until the arrival of circulating steroid hormones at the onset of puberty[14].

Steroid hormone signals are mediated in the mammary gland through local receptor tyrosine kinase (RTK) interactions[15,16]. One of the morphological consequences of RTK activation during puberty is the appearance of stratified terminal end buds (TEBs) at the tips of mammary ducts[17]. Cells within the TEB have low levels of cell adhesion and incomplete apico-basal polarity within the stratified cell layers[18,19,20]. TEBs are the major site of proliferation during pubertal branching morphogenesis and accomplish ductal elongation[21,22]. Genetic ablation of RTKs results in impaired TEB formation and delayed or abrogated ductal elongation[16,14]. We sought to determine how the stratified organization of the TEB arises from a simple bilayered epithelial duct and how stratification relates to loss of apico-basal polarity.

Results

Growth factor signaling induces stratification of the mammary epithelium

We first sought to distinguish whether the stratified organization of the TEB emerged during puberty or persisted from embryonic development. We collected a series of mammary glands from mice at two to four weeks of age and classified the ends of the primary mammary ducts as either bilayered or stratified based on the number of luminal epithelial cell layers (Fig. 4-1A,B). We observed exclusively bilayered primary ducts prior to puberty (Week 2, Fig. 4-1B). We observed a mixture of bilayered and stratified end buds at the onset of puberty (Week 3, Fig. 4-1B). All end buds were stratified during early puberty (Week 4, Fig. 4-1B). These data are consistent with earlier studies that noted polarized mammary tubes at birth[12]. Accordingly, we conclude that the stratified organization of the TEB emerges from a polarized, bilayered mammary duct, in response to RTK signaling at the onset of puberty. The result of this transition is an increase in the number of luminal epithelial marker^{+} cell layers. However, the cellular origin of these new luminal cells remains unclear.

We next sought to elucidate the cellular mechanism of TEB stratification. The slow timescale and optical inaccessibility of mammary development in vivo make it very difficult to image the cellular basis of developmental events within the intact mammary gland. This challenge led us to develop 3D organotypic culture and imaging techniques to enable real-time analysis of the cellular basis of mammary development[23,18,19]. Briefly, we isolate the epithelial ducts from primary mammary glands through a combination of mechanical disruption and enzymatic digestion and explant the resulting “mammary

organoids" into 3D gels of extracellular matrix (ECM; Fig. 4-1C)[24]. Branching morphogenesis is induced in mammary organoids in response to RTK signaling through addition of FGF or EGF ligands[18,25].

Stratification resulted in generation of an internal luminal epithelial cell layer

We imaged FGF2 induced stratification in real-time in organoids expressing a transgenically encoded myoepithelial-cell-specific fluorescent reporter[26] and a ubiquitous plasma membrane localized td-Tomato[27]. We observed a monolayer of myoepithelial cells throughout stratification (Fig. 4-1D). In contrast, we observed a marked increase in the number of luminal epithelial cell layers, consistent with the 3D organization of the mammary TEB in vivo[18,20]. Mammary organoids therefore provide an observable model of developmental stratification.

During stratification, there was a large reduction in the volume of the lumen (Fig. 4-1D). Tight junctions are the apical most intercellular junction and mark polarized luminal epithelial cells. Tight junctions also regulate paracellular fluid permeability and partition apical and basolateral membrane[28]. Stratification could occur through an incursion of cells past the tight junctions and into the luminal space or through the de novo generation of a third cell layer between the luminal and myoepithelial cells. To distinguish these possibilities, we imaged stratification in organoids expressing a tight junction reporter in which a fusion protein of GFP with zona occludens 1 (ZO-1-GFP) is knocked-into the endogenous ZO-1 allele. We observed reduction in luminal volume within the organoid but ZO-1 was present at the lumen-facing surface of the most apical luminal epithelial

cells throughout stratification in all movies (Fig. 4-1E). We occasionally observed dead cells within the lumen but did not observe migration of viable cells past the tight junctions. Our data reveal that a polarized, apically positioned luminal epithelial cell layer was maintained and that new cells arose between the apical and basal cell populations. At the end of stratification, organoids were composed of three structurally distinct cell populations, with a basal monolayer of myoepithelial cells, an apical layer of polarized luminal epithelial cells and a new internal cell population (Fig. 4-1F). Internal epithelial cells lacked contact with either the lumen or the basement membrane.

Developmental stratification initiates from vertical divisions of luminal epithelial cells

We hypothesized that internal epithelial cells could be generated through vertical proliferation of either apically positioned luminal epithelial cells or basally positioned myoepithelial cells (Fig. 4-2A). To distinguish these possibilities we imaged the location and direction of cell divisions in both populations using a dual transgenic fluorescent reporter mouse with nuclear and plasma membranes labels[29,27]. We classified the original cell based on its location and refer to it as the mother cell. We refer to the product of the cell division as the daughter cell. We analyzed 189 cell divisions to determine the origin of internal epithelial cells. We classified cell divisions based on the eventual location of the daughter cell through multiple timepoints in three dimensions (3D). The additional information provided by the 3D volume was critical to classifying cell division orientation. Vertical cell divisions were defined as those in which the daughter cell ended

up in a different cell layer than the mother. Planar divisions were defined as those in which both the mother and the daughter cell occupied the same cell layer.

We observed frequent divisions in which an apically positioned luminal epithelial cell divided and only the mother cell remained in an apical position along the lumen lining surface (vertical apical, 68/189 total divisions, 68/99 apical divisions, Fig. 4-2B). These vertical apical cell divisions initiated stratification and produced internal daughter cells located between the polarized luminal and myoepithelial cell layers. Stratification was polyclonal as multiple vertical apical divisions were observed in the same organoid (8 of 12 movies, Fig. 4-2B-B''). We did not observe stratification-initiating vertical divisions in the basally positioned myoepithelial cells (vertical basal, 0/189 total divisions, 0/39 basal divisions). Internal cells were also proliferative, further driving the stratification process (Fig. 4-2C). Both apically positioned luminal epithelial cells and basally positioned myoepithelial cells exhibited planar cell divisions with both mother and daughter cell remaining in the same cell layer (Fig. 4-2D,E). The percentage of each type of cell division was quantified and vertical apical proliferation events were the most common during stratification (Fig. 4-2F). Altogether, more than 60% of proliferation during stratification resulted in the formation of an internal cell, either through vertical apical or internal cell proliferation.

To test if this mechanism of stratification was utilized in vivo, we fixed and sectioned mammary glands from 3-week-old mice and stained the tissue for nuclei and F-actin. We observed 15 examples of vertical apical proliferation events within TEBs in vivo (15/50

total divisions, Fig. 4-2G). Proliferation of internal cells was also observed in vivo, as well as planar proliferation of both apical and basal cells. No vertical basal proliferation events were observed in vivo. Quantification in vivo revealed that divisions resulting in an internal daughter cell accounted for ~70% of total proliferation (Fig. 4-2H). We conclude that the initiating step of developmental stratification is vertical division of luminal epithelial cells, both in 3D culture and in vivo.

Vertical apical divisions were accompanied by loss of polarity in the internal daughter

Vertical apical divisions produced a daughter cell located between the polarized luminal and myoepithelial cell layers. These internal epithelial cells displayed incomplete apicobasal polarity[18,19]. We next sought to determine when this asymmetry in polarity emerged relative to cell division, through time-lapse imaging of organoids expressing ZO-1-GFP. During planar apical cell divisions, ZO-1-GFP remained punctate and apically localized in both the mother and daughter cell (Fig. 4-3A). In contrast, during vertical apical cell divisions the ZO-1-GFP signal was only observed at the apical membrane of the mother cell (80/80 divisions, Fig. 4-3B). Accordingly, we conclude that the internal daughter cell is generated without ZO-1 containing tight junctions.

Tight junctions play a critical role in partitioning the apical from the basolateral membrane and enabling stable segregation of apical and basolateral polarity complexes[28]. At the apical surface the Par complex (Par-3, aPKC, and CDC42) regulates apical identity and is required for mammary morphogenesis[30]. Conversely the scribble complex

(scribble, lethal giant larvae and discs large) regulates basolateral identity and its loss promotes mammary tumorigenesis[31]. We next used antibodies to determine the localization of apical and basal polarity complexes during vertical apical cell divisions. Par-3 was localized at the apical membrane of the mother cell and within the cytosol of the internal daughter cell (Fig. 4-3C). Scribble was excluded from the apical membrane between the tight junctions and localized to the basolateral membranes of the mother cell and all cell membranes of the internal daughter cell (Fig. 4-3D). In Drosophila, the Numb protein localizes asymmetrically within the sensory organ precursor and directs differential cell fates for the two daughter cells[32]. During vertical apical divisions in the mammary epithelium, Numb localized in a crescent along the basal surface of the internal daughter cell (Fig. 4-3E). We conclude that the mother cell retains tight junctions and molecularly distinct apical and basolateral membranes during vertical apical cell divisions. In contrast, internal daughter cells lacked tight junctions, displayed cytosolic Par-3, and localized scribble throughout the plasma membrane. We conclude that the internal daughter cells of vertical apical divisions are generated without the apico-basal polarity or junctional complexes typical of polarized simple epithelial cells.

Oncogenic stratification initiates from vertical apical cell divisions

Stratification and loss of polarity in a simple epithelium are also early events in the progression of epithelial cancers[7,33]. We next sought to determine if oncogenic stratification utilized the same cellular mechanism as developmental stratification. To answer this question, we induced hyperplasia formation through expression of an activated form of ErbB2[34]. Activated ErbB2 was expressed under the control of a two

allele tetracycline regulation system (Fig. 4-4A). The first allele encoded the reverse tetracycline transactivator (rtTA), an internal ribosomal entry site (IRES), and EGFP, both down-stream of a loxP-flanked stop codon. The second allele coded the activated form of ErbB2 downstream of a tetracycline operator. Adenoviral delivery of Cre recombinase enabled mosaic expression of rtTA and EGFP and addition of doxycycline then led to ErbB2 expression (Fig. 4-4B). Tet regulated expression of activated ErbB2 drives epithelial stratification in vivo[34] and ErbB2 expression is sufficient to cause proliferation of human mammary epithelial cells[35].

Expression of activated ErbB2 was also sufficient to induce proliferation and epithelial stratification in mammary organoids. We next collected time-lapse movies of control and activated ErbB2 expressing organoids to elucidate the cellular mechanism of oncogenic stratification. Organoids grown without exogenous growth factor remained bilayered (Fig. 4-4C-C'). Expression of activated ErbB2 resulted in stratification and disorganized growth of organoids, even without exogenous growth factor (Fig. 4-4D-D'). We measured growth rates to quantify the extent of organoid growth following ErbB2 expression. Organoids expressing activated ErbB2 grew at a much faster rate than that observed in control organoids treated with growth factor (Fig. 4-4E). ErbB2 driven tissue growth was accomplished by an expansion in the number of luminal cell layers while the myoepithelium remained in a complete monolayer (Fig. 4-4F), smooth muscle actin staining, green).

To isolate the cellular mechanism responsible for oncogenic stratification, we next visualized the location and direction of cell divisions. Vertical apical cell divisions were frequently observed to initiate stratification in response to activated ErbB2 expression (Fig. 4-4G,H). We did not observe vertical basal cell divisions. Planar proliferation was observed in both apically positioned luminal epithelial cells and basally positioned myoepithelial cells (Fig. 4-4G). Internal epithelial cells were also highly proliferative. In total, approximately 60% of cell divisions observed in organoids expressing activated ErbB2 resulted in generation of an internal daughter cell (sum of vertical apical and internal divisions, Fig. 4-4G). We conclude that expansion of the luminal epithelial compartment following expression of activated ErbB2 is typically accomplished via vertical divisions of apically positioned luminal epithelial cells.

Developmental stratification resulted in generation of low-polarity internal epithelial cells, located between a polarized luminal epithelial cell layer and the myoepithelial cells (Fig. 4-4I,K). We next assayed for molecular polarity in stratified hyperplasias induced by expression of activated ErbB2. Par-3 and ZO-1 staining indicated that apical polarity was acutely disrupted by activated ErbB2, consistent with reports in epithelial cell lines[35]. Punctate ZO-1 was absent from the plasma membranes adjacent to luminal spaces and the ZO-1 that was detected was largely cytosolic (Fig. 4-4L). Similarly, Par-3 was absent from the lumen-facing surface of the plasma membrane (Fig. 4-4J). The majority of Par-3 was cytosolic in organoids expressing activated ErbB2. These results reveal that ErbB2 induced and developmental stratification both occur through vertical division of apical

cells and that ErbB2 activation additionally leads to unrestrained growth and loss of apico-basal polarity.

MEK1DD induced stratification initiates from vertical apical cell divisions

Developmental stratification is induced through ligand dependent RTK signaling while activated ErbB2 drives RTK signaling in a ligand-independent fashion. The tissue overgrowth and loss of polarity associated with activated ErbB2 could therefore result from continuous activation of downstream RTK pathway components. To determine if intrinsic stimulation of proliferation was sufficient to result in tissue overgrowth, we induced expression of an activated form of a mitogen-activated protein kinase (MAPK), a downstream effector of RTK signaling. We used a genetic approach to express a constitutively active mutant of MEK1 (MEK1DD)[36]. The transgenic mouse line was engineered to enable expression of MEK1DD and EGFP following Cre recombinase mediated excision of a lox-p-flanked stop site[36]. We used adenovirally delivered Cre to enable expression of MEK1DD in fluorescently labeled mosaic clones within primary mammary epithelial organoids.

Expression of MEK1DD was sufficient to induce proliferation and stratification in the absence of exogenous growth factor (Fig. 4-5A,B). Stratification resulted in multiple luminal epithelial layers and a monolayer of myoepithelial cells (Fig. 4-5C). MEK1DD expression induced a similar growth rate as that observed following addition of growth factor to control organoids (Fig. 4-5B). We next used time-lapse confocal microscopy to identify the cellular mechanism of stratification. MEK1DD induced stratification also

initiated from vertical apical cell divisions and we did not observe vertical basal divisions (Fig. 4-5D,E). In contrast to the loss of polarity observed following activated ErbB2 expression, MEK1DD expressing organoids maintained apical-basal polarity comparable to growth factor stimulated control organoids (Fig. 4-5F,G).

MEK and PI3 kinase are both required for activated ErbB2 induced proliferation

We demonstrated that both growth factor induced and ligand independent activation of RTK signaling induced stratification through vertical apical cell divisions. However, activated ErbB2 induced both higher levels of proliferation and loss of apico-basal polarity, when compared to expression of MEK1DD. ErbB2 signals through both the MAPK and PI3K/AKT pathways. We therefore tested which of these two pathways were responsible for the excess proliferation observed following expression of activated ErbB2. Organoids were allocated to a control and three experimental groups, all of which received doxycycline. Control organoids were infected with Adeno-GFP and therefore could not express the rtTA. Experimental organoids were infected with Adeno-Cre, leading to expression of an rtTA and activated ErbB2. A subset of experimental organoids were treated with either MEK inhibitor (U0126) or PI3K inhibitor (LY294002). After 3 days, organoids were fixed and stained for the mitosis marker phospho-histone H3 (PH3) and DAPI to mark all nuclei. The percentage of proliferating cells per organoid was calculated as the ratio of PH3 positive cells to total cells. Control organoids exhibited low levels of proliferation (Fig. 4-6B,C) and expression of activated ErbB2 induced a significant increase in proliferation (Fig. 4-6B,D). Addition of either MEK inhibitor or PI3K inhibitor decreased proliferation below the control baseline (Fig.

4-6B,E,F). We conclude that MEK and PI3K are independently required for ErbB2 induced proliferation.

Discussion

The mammary epithelium represents a unique model system in which to study transitions in epithelial architecture, as the postnatal mammary duct is polarized and simple, while the elongation of these ducts is accomplished by stratified TEBs[21,22]. These transitions occur in response to steroid hormone and RTK signaling[17]. While genetic requirements for ductal elongation have become increasingly clear[16], the cellular basis of the simple to stratified transition has remained obscure.

Our data reveal that developmental stratification initiates from vertical division of apically positioned luminal epithelial cells in 3D culture and in vivo in TEBs. We observed no stratification-inducing divisions within the basally positioned myoepithelial compartment. Internal daughter cells lacked tight junctions and molecularly segregated apical membrane domains. Generation of the internal cell layer was not clonal as multiple vertical apical divisions occurred in individual organoids. Stratification also initiated by vertical apical divisions in organoids expressing activated forms of ErbB2 or MEK1. However, expression of activated ErbB2 additionally induced tissue overgrowth and acute loss of apical polarity and required both MEK and PI3K activity. The differences in phenotypes between ErbB2 and MEK expression could result from this utilization of multiple proliferation pathways or from differences in levels of MEK activation. Alternately, ErbB2 itself could be involved in polarity loss through direct interactions between ErbB2 and Par6-aPKC[37].

Cell surface marker based epithelial isolation and transplantation studies defined the mammary epithelial populations capable of single cell, long-term repopulation. These studies suggested that long-term repopulating cells may express basal epithelial markers[38,39]. Accordingly, it was reasonable to expect a contribution of basal cells to stratification. One recent study revealed exclusively planar cell divisions within the basal, cap cell layer of the TEB, with no observed contribution of basal cells to the internal, body cell compartment[40]. Another recent study observed a minority of vertical basal cell divisions in stratified TEBs during ductal elongation[41]. Both of these studies were based on the analysis of fixed sections of the mammary gland. Cell division orientation can be difficult to analyze in 2D in fixed sections, as spindle orientation can rotate extensively during mitosis in vivo[42]. In contrast, we were able to follow the entire process of mitosis in 3D in real-time. However, our data do not exclude the possibility of infrequent contributions to the stratified body cell compartment from basally positioned stem cells. However, our data suggest that vertical apical divisions are the typical mechanism for initiation of epithelial stratification. We cannot distinguish whether vertical apical divisions are actively induced or whether a signal that would normally constrain cell divisions to the planar direction is repressed.

This mechanism of stratification from the apical side is in contrast to that observed in other epithelial organs in which stratification initiates exclusively from basally positioned cells[43]. Within the embryonic skin, stratification initiates when cells rotate their division axis from parallel with the ECM to perpendicular, thereby generating suprabasal cells[43]. Suprabasal cells proliferate and differentiate apically until terminal differentiation, cell

death and eventual sloughing off of the body[44]. The organization of the lung epithelium is also regulated by the angle of the mitotic spindle and oncogenic signals disrupt normal lung structure in part by changing spindle angle[45]. Oncogenic stimuli can also induce multilayered epithelial structures through migration of cells into the luminal space[46,47]. Accordingly, we anticipate that our observed mechanism of vertical apical cell divisions might be most common in cancers in which the driving molecular event is deregulated RTK signaling. 3D culture models of mammary cancer have also provided insight into the cellular response to ErbB2 activation. Ubiquitous expression of ErbB2 was sufficient to induce stratification in mature acini of non-transformed mammary epithelial cells (MCF10A)[35]. Mosaic expression of ErbB2 in mature MCF-10A acini resulted in cell migration into the lumen[46]. However, MCF-10A cells do not form tight junctions or establish bilayered tubes with defined luminal and myoepithelial cells[48]. The additional developmental constraints of tight junctions and myoepithelial-luminal epithelial cell interactions may prevent migration into the lumen, regulate the orientation of cell division, and determine the eventual location of the daughter cell.

We conclude that epithelial stratification can rapidly occur through vertical divisions of polarized, apically positioned luminal epithelial cells and that stratification is typically coincident with loss of tight junctions and apico-basal polarity in the internal daughters. Our data therefore reveal a readily accessible developmental program that can be activated to yield two characteristic features of epithelial cancers, stratification and loss of polarity.

Experimental Procedures

Transgenic Fluorescent Reporter Animals

Myoepithelial cells were visualized in real-time by transgenic expression of GFP under the control of the keratin-14 promoter[26]; these mice were a kind gift from Elaine Fuchs. Membranes were labeled by membrane-targeted mTomato, expressed from the rosa26 locus; mice were acquired from the Jackson Laboratory[27]. Transgenic mice expressing Histone-H2B-GFP were acquired from AK Hadjantonakis, Memorial Sloan Kettering, and were used to follow proliferation in real-time[29]. All mouse procedures were conducted in accordance with an approved protocol from the Institutional Animal Care and Use Committee, Johns Hopkins University.

ZO-1-GFP Knock-In Animals

Targeting constructs and ES cell electroporation were performed by the Duke Recombineering Core and Transgenic animal facilities. GFP was inserted in frame immediately before the stop codon of ZO-1. The resulting strain Tjm1tm1(IF-GFP)Lech was viable with no observed phenotype even when maintained as a homozygote.

Organotypic culture

Three-dimensional culture of primary mammary epithelium was performed as previously described[18,24]. Briefly, mammary glands were removed from 8-12 week old mice and tissue was minced 40-50 times with a scalpel. The epithelial compartment was separated from the stromal tissues through collagenase and DNAse digestion. Differential centrifugation was used to separate epithelial organoids from single cells. The final pellet

was suspended in growth factor reduced Matrigel (BD Biosciences) at a concentration of 2 organoids/μL and plated as 100μl drops in 24-well glass bottom plates (Greiner Bio One). Matrigel drops were allowed to solidify for 20 minutes at 37 degrees prior to addition of minimal media. Growth factor was added at the time of plating (FGF2, 2.5 nM), unless otherwise noted. Cell Tracker Red was added, when required, as previously described[18].

Adenoviral Gene Delivery

Organoids were treated with adenoviral-Cre or adenoviral-GFP (Vector Biolabs) prior to suspension in Matrigel. Following differential centrifugation, 1,000 organoids were transferred to a 1.7 ml Eppendorf tube and centrifuged at 520xg for 10 minutes. All but 100 μl of media was then removed from the Eppendorf tube. Viral particles were added to the organoid containing media and incubated for 1 hour. Two viral concentrations were used: 10,000 plaque-forming units (PFU) or 500 PFU per organoid. The high concentration of virus resulted in approximately 80% infection and the low concentration produced 2-10 infected cells per organoid. Following viral treatment, organoids were washed twice in DMEM-F12 and suspended in Matrigel as previously described.

Whole Gland and Organoid Antibody Staining

Whole mammary glands were removed from 2-4 week old mice and fixed in 4% PFA for 20 minutes. Tissue was embedded in O.C.T. compound (Tissue-Tek) and cut as 50 μm sections. Sectioned tissue was washed with PBS to remove excess O.C.T and permeabilized with 0.5% Triton X-100 for 30 minutes. Epithelium was stained with

DAPI (Invitrogen, 1:1000) to visualize nuclei and phalloidin (Invitrogen, 1:500) to visualize F-actin. Slides were washed in PBS and mounted. Organoid staining for Par-3 (Millipore, 07-330), numb (Cell Signaling Technology, C29611), scribble (Santa Cruz Biotechnology, sc-11049), ZO-1 (Chemicon, MAB1520), and SMA (Sigma, F3777) was performed as described in[19]. Briefly, organoids were fixed with 4% paraformaldehyde for 20 minutes and permeabilized in 0.5% Triton x-100 for 30 minutes. Organoids were blocked in 10% serum in PBS for 3 hours and then incubated with primary antibody (1:500 in 10% serum in PBS) for 2 hours. Organoids were washed three times with 10% serum in PBS and then incubated with Alexa Fluor conjugated secondary antibodies (Molecular Probes, 1:500) in 10% serum in PBS for 1 hour. DAPI (1:1000) and phalloidin (1:500) staining were performed concurrently with secondary antibodies. Three 10-minute PBS washes were applied and organoids were analyzed by confocal microscopy.

ErbB2 and MEK activation assays

A dual transgenic mouse line was used to conditionally and mosaically express constitutively activated ErbB2 in mammary epithelium. The first transgenic mouse coded both an rtTA and EGFP downstream a lox-P flanked stop codon[49]. The second allele coded an activated form of rat ErbB2 regulated by the tetracycline operator[34]. Both lines were acquired from the Jackson Lab. Adeno-Cre was added as described above, resulting in mosaic expression of rtTA and EGFP. Doxycycline was added at a concentration of 5 μg/ml at 24 h after plating to induce ErbB2 expression. ErbB2 expressing organoids were grown in the absence of exogenous growth factors. All ErbB2 experiments were

internally controlled with organoids from the same animal. Control organoids received Adeno-GFP in place of Adeno-Cre and were treated with doxycycline. In cases where ErbB2 expressing organoids were compared to growth factor stimulated organoids, growth factor was added 24 h after plating.

An activated mutant of MEK1, with serine to aspartic acid substitutions at residues S218 and S222 (MEK1DD), was expressed to drive constitutive MAPK signaling. MEK1DD was expressed under the control of the rosa26 promoter, upstream of an IRES-EGFP and downstream of a lox-P flanked stop codon. Mice were acquired from Jackson laboratories[36]. Addition of Adeno-Cre, as described above, resulted in expression of the MEK mutant and EGFP. Tissue expressing MEK1DD did not receive exogenous growth factors. MEK experiments were internally controlled with organoids from the same animal treated with Adeno-GFP instead of Adeno-Cre. Growth factor was added at the time of plating to compare with the MEK expressing organoids.

MEK and PI3 Kinase inhibition assays

The MEK inhibitor U0126 was acquired from Cell Signaling and used at the 10μM. PI3 Kinase was inhibited with 50μM of LY294002, which was obtained from Cell Signaling. Organoids were pretreated with MEK or PI3K inhibitors for 30 min prior to ErbB2 gene induction. Organoids were fixed 3 days after inhibitor addition and stained for the nuclear marker DAPI and the proliferation marker phospho-histone H3 (Cell Signaling, 9701). Percent proliferating cells per organoid was quantified as the number of phospho-histone H3 positive cells divided by the total number of cells in the organoid. A single factor

analysis of variance was used to determine statistical significance ($P<0.001$) and a minimum of 20 organoids per condition from 3 independent experiments was analyzed.

Confocal Microscopy

Still and time-lapse confocal images were collected using a Solamere Technology Group spinning disk confocal microscope[23] with a 40x LD-LCI C-Apochromat objective (Zeiss Microimaging). A combination of μManager[50] and Piper (Stanford Photonics) imaging software was used for imaging acquisition. Images were recorded with a 10-minute time interval for 8-16 hours. Temperature was held at 37 degrees and CO_2 was 5% throughout imaging. Imaris (Bitplane) and Adobe Photoshop were used to adjust brightness and contrast across the entire image field, to optimize image clarity.

Time-Lapse Differential Interference Contrast Microscopy

A Zeiss Cell Observer system with a Zeiss AxioObserver Z1 and an AxioCam MRM camera was used to collect differential interference contrast microcopy movies. Movies were collected with a 20-minute time interval. Imaging began upon addition of growth factor or gene induction and continued until approximately 5 days after growth stimulation. Temperature was maintained at 37 degrees and CO_2 was held at 5%.

References

1 Bryant, D.M., and Mostov, K.E. (2008). From cells to organs: building polarized tissue. Nat Rev Mol Cell Biol 9, 887-901.

2 Zegers, M.M., O'Brien, L.E., Yu, W., Datta, A., and Mostov, K.E. (2003). Epithelial polarity and tubulogenesis in vitro. Trends Cell Biol 13, 169-176.

3 Nelson, W.J. (2003). Adaptation of core mechanisms to generate cell polarity. Nature 422, 766-774.

4 Andrew D. J., E., A. J. (2010). Morphogenesis of epithelial tubes: Insights into tube formation, elongation, and elaboration. Dev Biol 341, 34-55.

5 Hsu, J.C., and Yamada, K.M. (2010). Salivary gland branching morphogenesis--recent progress and future opportunities. Int J Oral Sci 2, 117-126.

6 Nelson, W.J. (2009). Remodeling epithelial cell organization: transitions between front-rear and apical-Basal polarity. Cold Spring Harb Perspect Biol 1, a000513.

7 Ewing, J. (1933). Lectures on tumor pathology, 2nd edn (New York, Cornell University Medical School, Class of 1934).

8 Hanahan, D., and Weinberg, R.A. (2011). Hallmarks of cancer: the next generation. Cell 144, 646-674.

9 Thiery, J.P. (2002). Epithelial-mesenchymal transitions in tumour progression. Nature Reviews Cancer 2, 442-454.

10 Thiery, J.P., Acloque, H., Huang, R.Y., and Nieto, M.A. (2009). Epithelial-mesenchymal transitions in development and disease. Cell 139, 871-890.

11 Yang, J., and Weinberg, R.A. (2008). Epithelial-mesenchymal transition: at the crossroads of development and tumor metastasis. Dev Cell 14, 818-829.

12 Hogg, N.A., Harrison, C.J., and Tickle, C. (1983). Lumen formation in the developing mouse mammary gland. J Embryol Exp Morphol 73, 39-57.

13 Nanba, D., Nakanishi, Y., and Hieda, Y. (2001). Changes in adhesive properties of epithelial cells during early morphogenesis of the mammary gland. Dev Growth Differ 43, 535-544.

14 Sternlicht, M.D., Kouros-Mehr, H., Lu, P., and Werb, Z. (2006). Hormonal and local control of mammary branching morphogenesis. Differentiation 74, 365-381.

15 Hennighausen, L., and Robinson, G.W. (2005). Information networks in the mammary gland. Nat Rev Mol Cell Biol 6, 715-725.

16 McNally, S., and Martin, F. (2011). Molecular regulators of pubertal mammary gland development. Ann Med 43, 212-234.

17 Sternlicht, M.D. (2006). Key stages in mammary gland development: the cues that regulate ductal branching morphogenesis. Breast Cancer Res 8, 201.

18 Ewald, A.J., Brenot, A., Duong, M., Chan, B.S., and Werb, Z. (2008). Collective epithelial migration and cell rearrangements drive mammary branching morphogenesis. Dev Cell 14, 570-581.

19 Ewald, A.J., Huebner, R.J., Palsdottir, H., Lee, J.K., Perez, M.J., Jorgens, D.M., Tauscher, A.N., Cheung, K.J., Werb, Z., and Auer, M. (2012). Mammary collective cell migration involves transient loss of epithelial features and individual cell migration within the epithelium. J Cell Sci 125, 2638-2654.

20 Mailleux, A.A., Overholtzer, M., Schmelzle, T., Bouillet, P., Strasser, A., and Brugge, J.S. (2007). BIM regulates apoptosis during mammary ductal

morphogenesis, and its absence reveals alternative cell death mechanisms. Dev Cell 12, 221-234.

21 Hinck, L., and Silberstein, G.B. (2005). Key stages in mammary gland development: the mammary end bud as a motile organ. Breast Cancer Res 7, 245-251.

22 Williams, J.M., and Daniel, C.W. (1983). Mammary ductal elongation: differentiation of myoepithelium and basal lamina during branching morphogenesis. Dev Biol 97, 274-290.

23 Ewald, A.J. (2013). Practical considerations for long-term time-lapse imaging of epithelial morphogenesis in three-dimensional organotypic cultures. Cold Spring Harb Protoc 2013.

24 Nguyen-Ngoc, K.V., Shamir, E.R., Huebner, R.J., Beck, J.N., Cheung, K.J., and Ewald, A.J. (2013). 3D Culture Assays of Murine Mammary Branching Morphogenesis and Epithelial Invasion. Methods in Molecular Biology, In Press.

25 Fata, J.E., Mori, H., Ewald, A.J., Zhang, H., ^{Y18ao}, E., Werb, Z., and Bissell, M.J. (2007). The MAPK(ERK-1,2) pathway integrates distinct and antagonistic signals from TGFalpha and FGF7 in morphogenesis of mouse mammary epithelium. Dev Biol 306, 193-207.

26 Vaezi, A., Bauer, C., Vasioukhin, V., and Fuchs, E. (2002). Actin cable dynamics and Rho/Rock orchestrate a polarized cytoskeletal architecture in the early steps of assembling a stratified epithelium. Dev Cell 3, 367-381.

27 Muzumdar, M.D., Tasic, B., Miyamichi, K., Li, L., and Luo, L. (2007). A global double-fluorescent Cre reporter mouse. Genesis 45, 593-605.

28 Schneeberger, E.E., and Lynch, R.D. (2004). The tight junction: a multifunctional complex. American Journal of Physiology-Cell Physiology 286, C1213-C1228.

29 Hadjantonakis, A.K., and Papaioannou, V.E. (2004). Dynamic in vivo imaging and cell tracking using a histone fluorescent protein fusion in mice. BMC Biotechnol 4, 33.

30 McCaffrey, L.M., and Macara, I.G. (2009). The Par3/aPKC interaction is essential for end bud remodeling and progenitor differentiation during mammary gland morphogenesis. Genes Dev 23, 1450-1460.

31 Zhan, L., Rosenberg, A., Bergami, K.C., Yu, M., Xuan, Z., Jaffe, A.B., Allred, C., and Muthuswamy, S.K. (2008). Deregulation of scribble promotes mammary tumorigenesis and reveals a role for cell polarity in carcinoma. Cell 135, 865-878.

32 Rhyu, M.S., Jan, L.Y., and Jan, Y.N. (1994). Asymmetric distribution of numb protein during division of the sensory organ precursor cell confers distinct fates to daughter cells. Cell 76, 477-491.

33 Huang, L., and Muthuswamy, S.K. (2010). Polarity protein alterations in carcinoma: a f ocus on emerging roles for polarity regulators. Curr Opin Genet Dev 20, 41-50.

34 Xie, W., Chow, L.T., Paterson, A.J., Chin, E., and Kudlow, J.E. (1999). Conditional expression of the ErbB2 oncogene elicits reversible hyperplasia in stratified epithelia and up-regulation of TGFalpha expression in transgenic mice. Oncogene 18, 3593-3607.

35 Muthuswamy, S.K., Li, D., Lelievre, S., Bissell, M.J., and Brugge, J.S. (2001). ErbB2, but not ErbB1, reinitiates proliferation and induces luminal repopulation in epithelial acini. Nat Cell Biol 3, 785-792.
36 Srinivasan, L., Sasaki, Y., Calado, D.P., Zhang, B., Paik, J.H., DePinho, R.A., Kutok, J.L., Kearney, J.F., Otipoby, K.L., and Rajewsky, K. (2009). PI3 kinase signals BCR-dependent mature B cell survival. Cell 139, 573-586.
37 Aranda, V., Haire, T., Nolan, M.E., Calarco, J.P., Rosenberg, A.Z., Fawcett, J.P., Pawson, T., and Muthuswamy, S.K. (2006). Par6-aPKC uncouples ErbB2 induced disruption of polarized epithelial organization from proliferation control. Nat. Cell Biol. 8, 1235-1245.
38 Vaillant, F., Asselin-Labat, M.L., Shackleton, M., Lindeman, G.J., and Visvader, J.E. (2007). The emerging picture of the mouse mammary stem cell. Stem Cell Rev 3, 114-123.
39 Visvader, J.E., and Smith, G.H. (2011). Murine mammary epithelial stem cells: discovery, function, and current status. Cold Spring Harb Perspect Biol 3.
40 Taddei, I., Deugnier, M.A., Faraldo, M.M., Petit, V., Bouvard, D., Medina, D., Fassler, R., Thiery, J.P., and Glukhova, M.A. (2008). Beta1 integrin deletion from the basal compartment of the mammary epithelium affects stem cells. Nat Cell Biol 10, 716-722.
41 Regan, J.L., Sourisseau, T., Soady, K., Kendrick, H., McCarthy, A., Tang, C., Brennan, K., Linardopoulos, S., White, D.E., and Smalley, M.J. (2013). Aurora a kinase regulates mammary epithelial cell fate by determining mitotic spindle orientation in a notch-dependent manner. Cell Rep 4, 110-123.
42 Kieserman, E.K., and Wallingford, J.B. (2009). In vivo imaging reveals a role for Cdc42 in spindle positioning and planar orientation of cell divisions during vertebrate neural tube closure. J Cell Sci 122, 2481-2490.
43 Lechler, T., and Fuchs, E. (2005). Asymmetric cell divisions promote stratification and differentiation of mammalian skin. Nature 437, 275-280.
44 Fuchs, E. (2007). Scratching the surface of skin development. Nature 445, 834-842.
45 Tang, N., Marshall, W.F., McMahon, M., Metzger, R.J., and Martin, G.R. (2011). Control of mitotic spindle angle by the RAS-regulated ERK1/2 pathway determines lung tube shape. Science 333, 342-345.
46 Leung, C.T., and Brugge, J.S. (2012). Outgrowth of single oncogene-expressing cells from suppressive epithelial environments. Nature 482, 410-413.
47 Yagi, S., Matsuda, M., and Kiyokawa, E. (2012). Suppression of Rac1 activity at the apical membrane of MDCK cells is essential for cyst structure maintenance. EMBO Rep 13, 237-243.
48 Underwood, J.M., Imbalzano, K.M., Weaver, V.M., Fischer, A.H., Imbalzano, A.N., and Nickerson, J.A. (2006). The ultrastructure of MCF-10A acini. J Cell Physiol 208, 141-148.
49 Belteki, G., Haigh, J., Kabacs, N., Haigh, K., Sison, K., Costantini, F., Whitsett, J., Quaggin, S.E., and Nagy, A. (2005). Conditional and inducible transgene expression in mice through the combinatorial use of Cre-mediated recombination and tetracycline induction. Nucleic Acids Res 33, e51.

50 Edelstein, A., Amodaj, N., Hoover, K., Vale, R., and Stuurman, N. (2010). Computer control of microscopes using microManager. Curr Protoc Mol Biol Chapter 14, Unit14 20.

Figure 4-1: Mammary Stratification Generates an Internal Population of Luminal Epithelial Cell Lacking Tight Junctions

(A-A'') Terminal end buds from 2-4 week old mice were stained for F-actin (red) and nuclei (green). (B) Quantification of bilayered (gray) and stratified (black) end buds at 2, 3 and 4 weeks postnatal. (C) Schematic depicting organotypic culture. (D) Still images from a movie of an organoid undergoing stratification. Luminal epithelial cells are labeled red with a membrane localized td-Tomato and myoepithelial cells are labeled green with a genetically encoded GFP. Dashed line highlights the boundary of the luminal space. (E) Still images of an organoid undergoing stratification with ZO-1-GFP marking tight junctions and Cell Tracker Red staining the cytosol. (F) Cartoon depiction of mammary epithelial stratification showing the generation of an internal luminal epithelial cell population lacking tight junctions. Scale bars are 20μm.

Figure 4-1

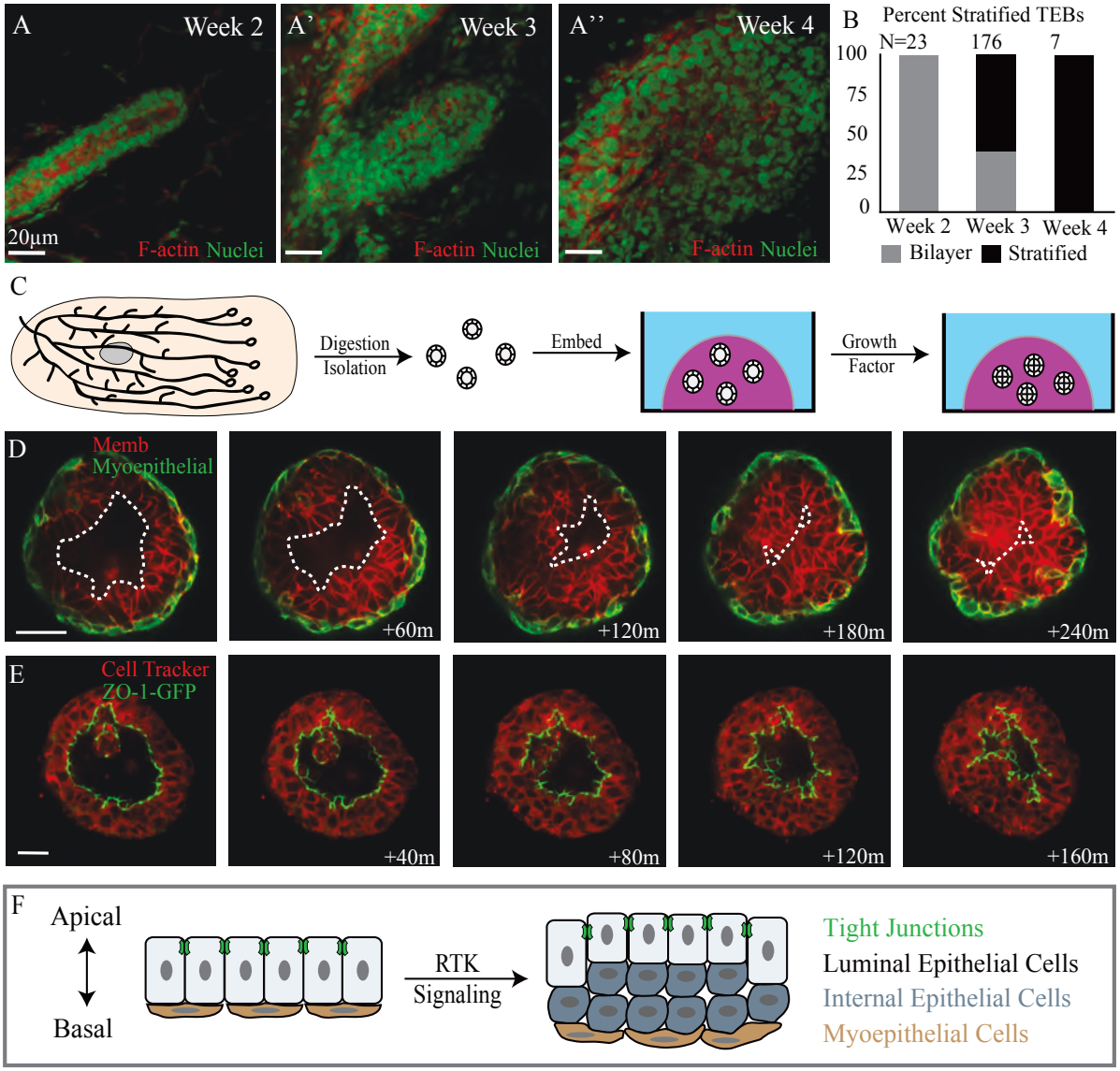
A
Week 2
20µm
F-actin Nuclei
A'
Week 3
F-actin Nuclei
A''
Week 4
F-actin Nuclei
B
Percent Stratified TEBs
N=23
176
7
100
75
50
25
0
Week 2
Week 3
Week 4
Bilayer
Stratified
C
Digestion
Isolation
Embed
Growth
Factor
D
Memb
Myoepithelial
+60m
+120m
+180m
+240m
E
Cell Tracker
ZO-1-GFP
+40m
+80m
+120m
+160m
F
Apical
Basal
RTK
Signaling
Tight Junctions
Luminal Epithelial Cells
Internal Epithelial Cells
Myoepithelial Cells

Figure 4-2: Vertical Apical Cell Divisions Initiated Mammary Stratification
(A) Schematic depicting the alternatives of stratification initiation by vertical apical versus vertical basal proliferation. (B-E) Frames from movies of organoids expressing nuclear (green) and membrane (red) markers were collected to visualize proliferation in real-time. (B) Image of an organoid prior to stratification. Arrows highlight apical cells that undergo vertical proliferation in B' and B''. (B'-B'') Movie frames showing two vertical apical cell divisions, each producing one apical mother cell and one internal daughter cell. Yellow dashed lines show apical mother cells, solid yellow lines highlight internal daughter cells and dashed white lines represent the border of the lumen. (C) Organoid that is partially stratified with inset on an internal cell that divides in C'. (C') Frames showing division of the internal cell highlighted in C, solid yellow lines outline the dividing nuclei. (D-E) Image of planar proliferation of apical and basal cells respectively, insets on dividing cells. (F) Quantification of the types of proliferation observed in organotypic culture. (G) Terminal end bud from 3-week-old mouse stained for F-actin (red) and nuclei (green). Inset highlights a vertical apical division. (G') Enlarged image of inset from G, arrows point to dividing nuclei and dashed white line shows border of lumen. (H) Quantification of the types of proliferation observed in vitro. Scale bars are 20μm.

Figure 4-2

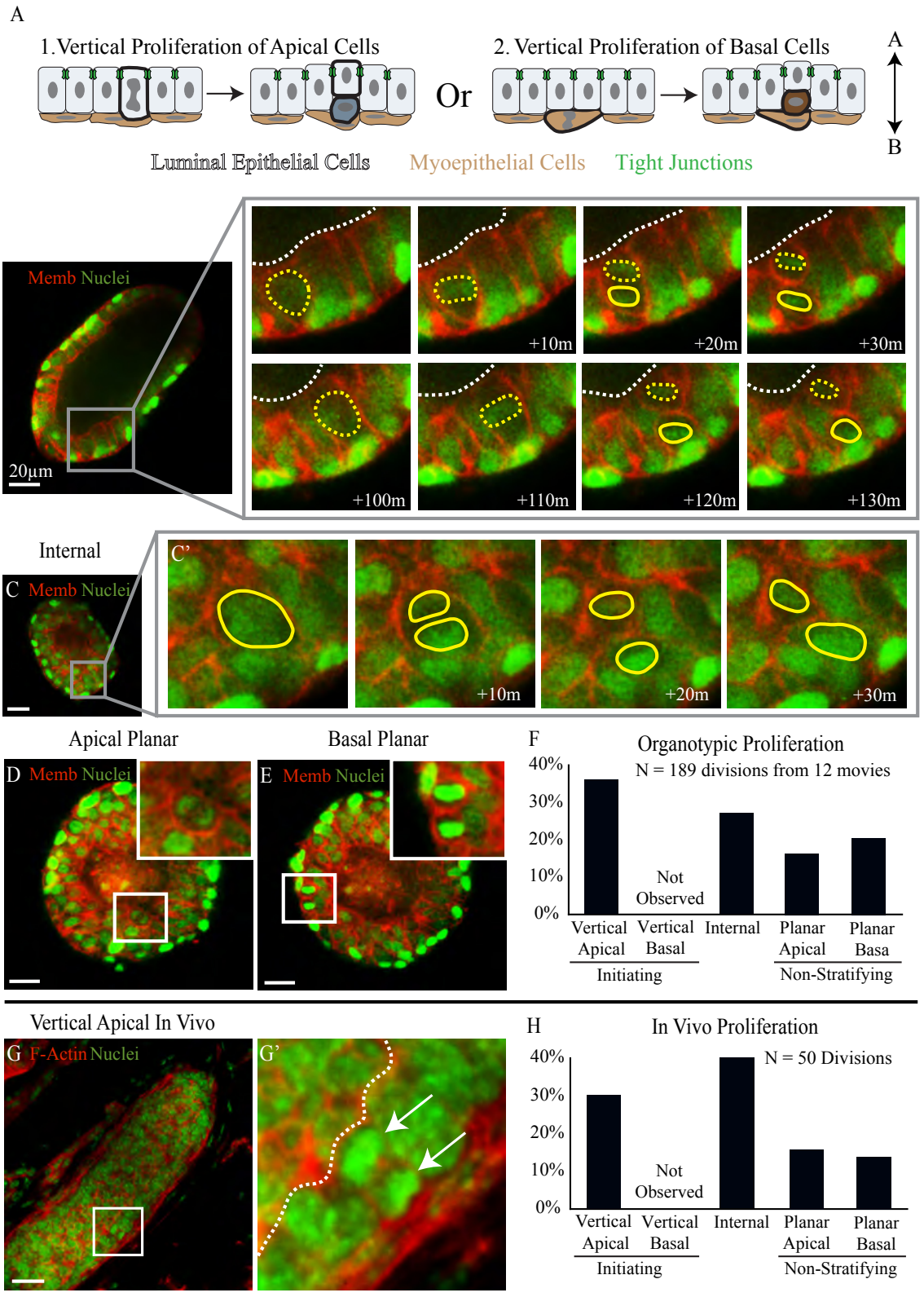
A
1. Vertical Proliferation of Apical Cells
Or
2. Vertical Proliferation of Basal Cells
A
B
Luminal Epithelial Cells
Myoepithelial Cells
Tight Junctions
Memb Nuclei
20µm
+10m
+20m
+30m
+100m
+110m
+120m
+130m
Internal
C Memb Nuclei
C'
+10m
+20m
+30m
Apical Planar
Basal Planar
D Memb Nuclei
E Memb Nuclei
F
Organotypic Proliferation
N = 189 divisions from 12 movies
40%
30%
20%
10%
0%
Not Observed
Vertical Apical
Vertical Basal
Internal
Planar Apical
Planar Basa
Initiating
Non-Stratifying
Vertical Apical In Vivo
G F-Actin Nuclei
G'
H
In Vivo Proliferation
N = 50 Divisions
40%
30%
20%
10%
0%
Not Observed
Vertical Apical
Vertical Basal
Internal
Planar Apical
Planar Basal
Initiating
Non-Stratifying

Figure 4-3: Vertical Apical Cell Divisions Result in Polarity Loss for Internal Daughter Cells

(A-B') Frames from movies of a ZO-1-GFP (green) expressing organoid counterstained with Cell Tracker Red. (A) An organoid undergoing stratification, inset highlights a cell that undergoes planar apical proliferation in A'. (A') Magnification of inset from A, arrows point to tight junctions, which were apically localized during apical proliferation. Yellow dashed lines highlight both the mother and the daughter cell. (B) Still image of an organoid with inset on an apical cell prior to vertical division shown in B'. (B') Images show the asymmetric localization of ZO-1 to the apically positioned mother cell during vertical apical cell division. Yellow dashed lines emphasize the mother cell; solid lines show the internal daughter cell and arrows point to the tight junctions. (C-E) Immuno-fluorescence staining of apical cells during vertical divisions. The luminal space is marked L, apical nuclei are highlighted with dashed yellow lines and internal nuclei are shown with solid yellow lines. Black and white images of the respective polarity proteins are shown in the upper right and a schematic depiction of the protein localization is included in the bottom right. (C) Par-3 was asymmetrically localized to the apical membrane of the mother cell during vertical division. (D) The basolateral polarity protein scribble was excluded from the ZO-1 defined apical domain but was present on all other basolateral surfaces. (E) Numb was enriched in the basolateral membranes of the daughter cell. (F) Cartoon depiction of the asymmetric localization of polarity proteins during vertical apical cell divisions. (G) Schematic depicting the cellular mechanism of mammary stratification-initiating with polarity breaking vertical apical cell divisions

followed by expansion of the low-polarity internal cell layer. Scale bars are 20μm unless otherwise noted.

Figure 4-3

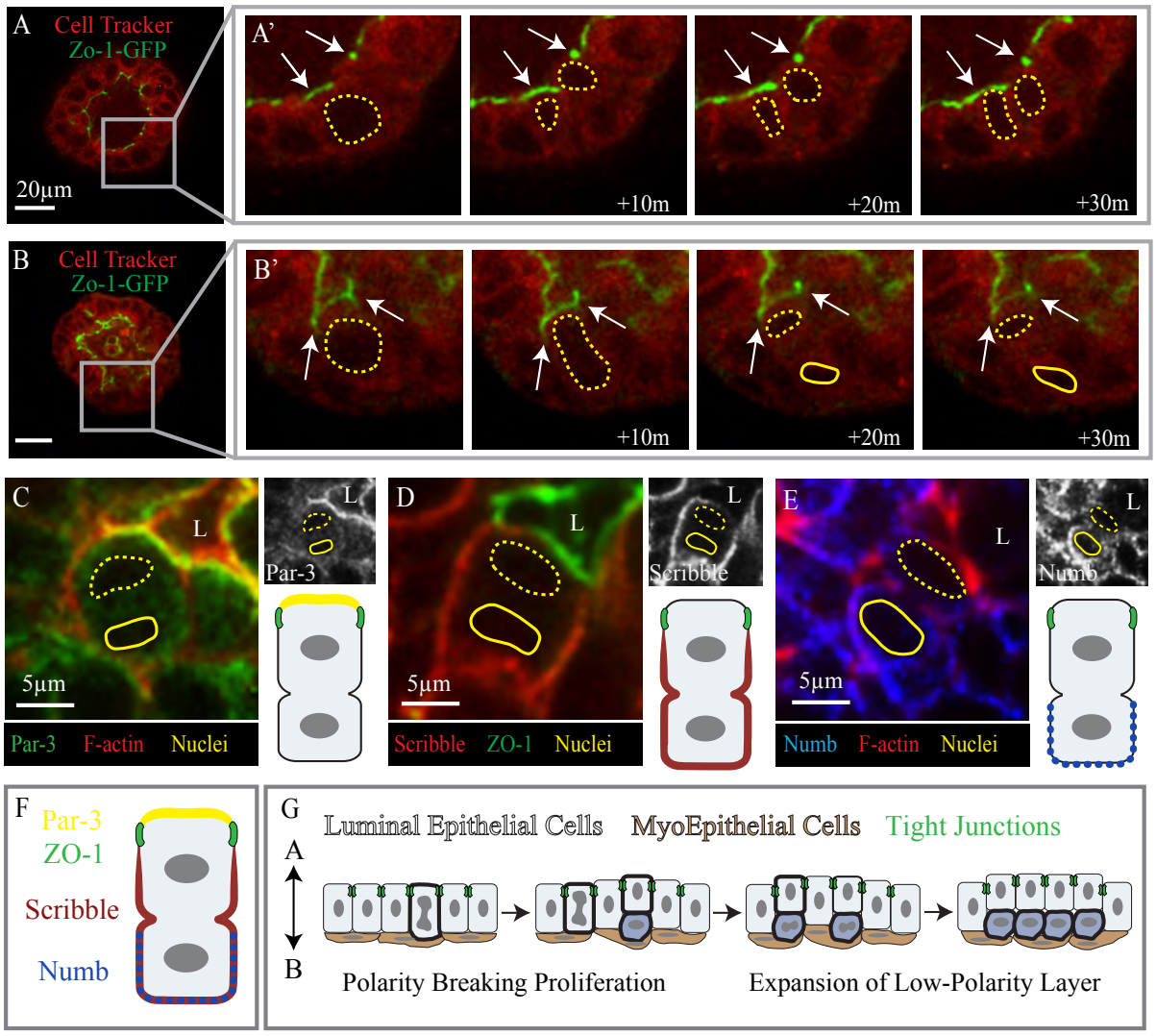
A
Cell Tracker
Zo-1-GFP
20µm
A'
+10m
+20m
+30m
B
Cell Tracker
Zo-1-GFP
B'
+10m
+20m
+30m
C
L
5µm
Par-3 F-actin Nuclei
Par-3
D
L
5µm
Scribble ZO-1 Nuclei
Scribble
E
L
5µm
Numb F-actin Nuclei
Numb
F
Par-3
ZO-1
Scribble
Numb
G
A
B
Luminal Epithelial Cells
MyoEpithelial Cells
Tight Junctions
Polarity Breaking Proliferation
Expansion of Low-Polarity Layer

Figure 4-4: Oncogenic Stratification Shares a Conserved Cellular Mechanism with Developmental Stratification

(A) Schematic of the transgenes used for conditional and mosaic expression of activated ErbB2. (B) Cartoon depicting the protocol followed to drive ErbB2 expression. (C-D') Still images from time-lapse movies of unstimulated organoids in the presence or absence of ErbB2 expression. (C-C') Organoids remained bilayered in the absence of ErbB2. (D-D') Expression of ErbB2 in 80-90% of cells resulted in rapid stratification and growth. (E) Organoid growth rates were quantified as the increase in organoid area normalized to the initial organoid size. Growth curves for organoids expressing activated ErbB2 without exogenous growth factor are shown in orange, for control organoids with growth factor are shown in green, and for control organoids without exogenous growth factor are shown in blue. (F) Organoids expressing ErbB2 in 80-90% of cells were fixed and stained for smooth muscle actin (SMA, green), 3 days after gene activation. SMA, a marker of myoepithelial cells, showed that ErbB2 induced stratification increased the number of luminal epithelial cell layers. (G) Quantification of the types of cell divisions observed in ErbB2 expressing organoids. (H) Mosiac expression of ErbB2 in 1-10% of cells, allowed observation of individual cellular responses to oncogene activation. ErbB2 expressing cells were labeled with GFP (green) and Cell Tracker Red was used to infer nuclear location. ErbB2 induced stratification initiated from vertical apical cell divisions. (I-L) Tissue was fixed and stained 3 days after addition of growth factor or activation of ErbB2 in 80-90% of cells. (I-J) Apical polarity was visualized by staining for Par-3 (green) as well as F-actin (red) and nuclei (blue). (I) Polarized apical membranes were present at the apical surfaces of tissue treated with growth factor. (J) Tissue expressing

ErbB2 lacked membrane localized Par-3. (K-L) ZO-1 staining (green) was used to observe tight junctions; tissue was also stained for F-actin (red) and nuclei (blue). (K) Growth factor treated organoids had ZO-1 localized to apical membranes. (L) Tight junctions were absent from apical membranes in cells expressing ErbB2, inset shows region of tissue lacking tight junctions. Scale bars are 20μm.

Figure 4-4

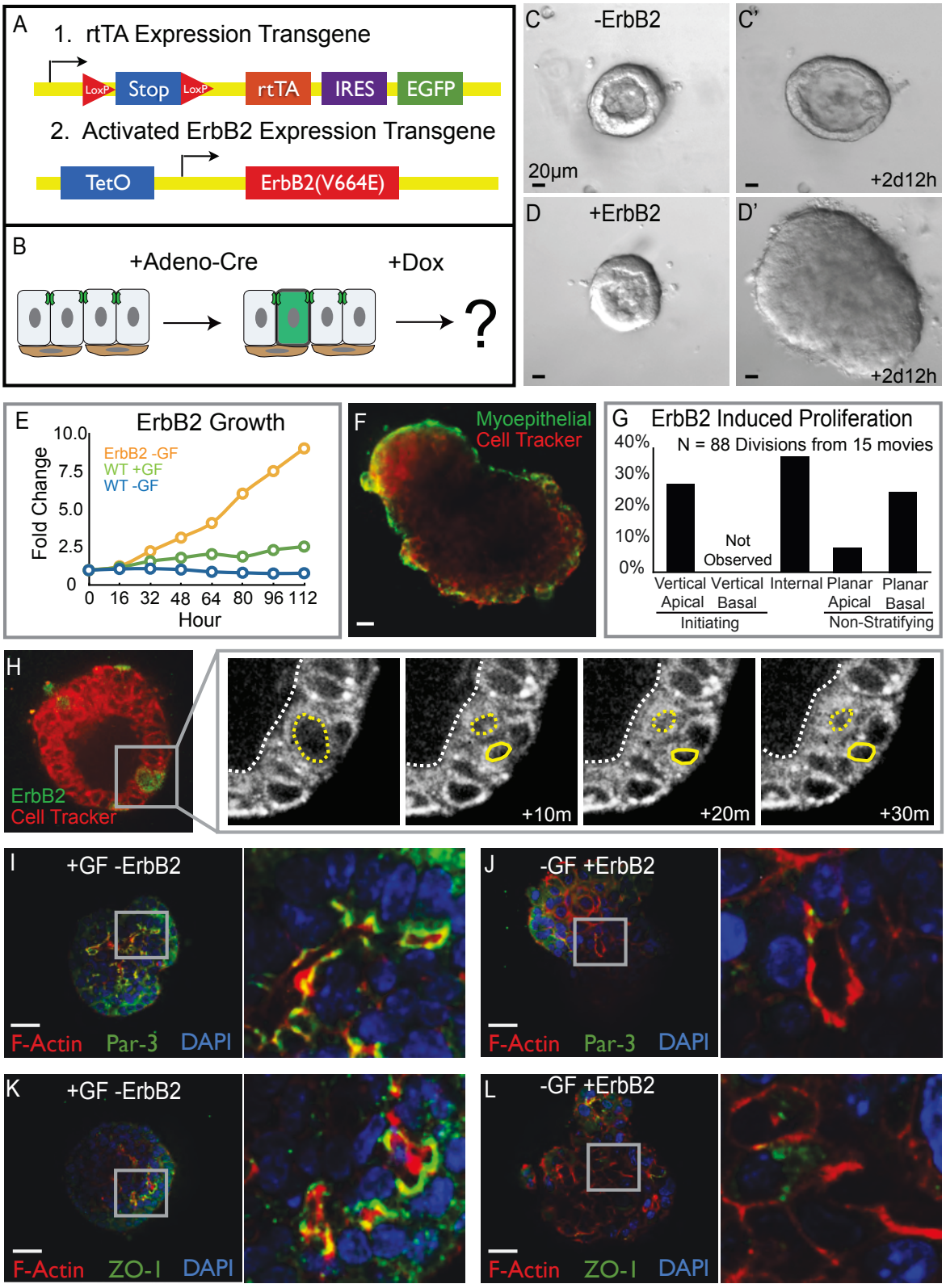
A
1. rtTA Expression Transgene
LoxP
Stop
LoxP
rtTA
IRES
EGFP
2. Activated ErbB2 Expression Transgene
TetO
ErbB2(V664E)
B
+Adeno-Cre
+Dox
?
C -ErbB2
20μm
C'
+2d12h
D +ErbB2
D'
+2d12h
E ErbB2 Growth
Fold Change
10.0
7.5
5.0
2.5
0
ErbB2 -GF
WT +GF
WT -GF
0 16 32 48 64 80 96 112
Hour
F
Myoepithelial
Cell Tracker
G ErbB2 Induced Proliferation
N = 88 Divisions from 15 movies
40%
30%
20%
10%
0%
Not
Observed
Vertical Apical
Vertical Basal
Internal
Planar Apical
Planar Basal
Initiating
Non-Stratifying
H
ErbB2
Cell Tracker
+10m
+20m
+30m
I +GF -ErbB2
F-Actin Par-3 DAPI
J -GF +ErbB2
F-Actin Par-3 DAPI
K +GF -ErbB2
F-Actin ZO-1 DAPI
L -GF +ErbB2
F-Actin ZO-1 DAPI

Figure 4-5: MEK1DD Induced Stratification through Vertical Apical Cell Divisions

(A) Still images from a time-lapse movie of organoids expressing a phosphomimetic form of MEK (MEK1DD). MEK1DD expression was sufficient to drive stratification. (B) Growth curves for organoids expressing MEK1DD without exogenous growth factor are shown in orange, for control organoids with growth factor in green and for organoids without exogenous growth factor in blue. (C) MEK1DD-expressing organoids were stained for SMA (green) and nuclei (blue) to visualize the myoepithelial cells. (D) Quantification of the types of proliferation observed in response to MEK1DD expression. (E) MEK1DD-induced stratification was initiated by vertical apical cell divisions; organoids were stained with Cell Tracker Red to infer nuclear position. (F) Organoids were stained for Par-3 (green) F-actin (red) and nuclei (blue) to visualize apical polarity. (G) Organoids were stained for scribble (green) F-actin (red) and nuclei (blue) to visualize basolateral polarity. Scale bars are 20μm.

Figure 4-5

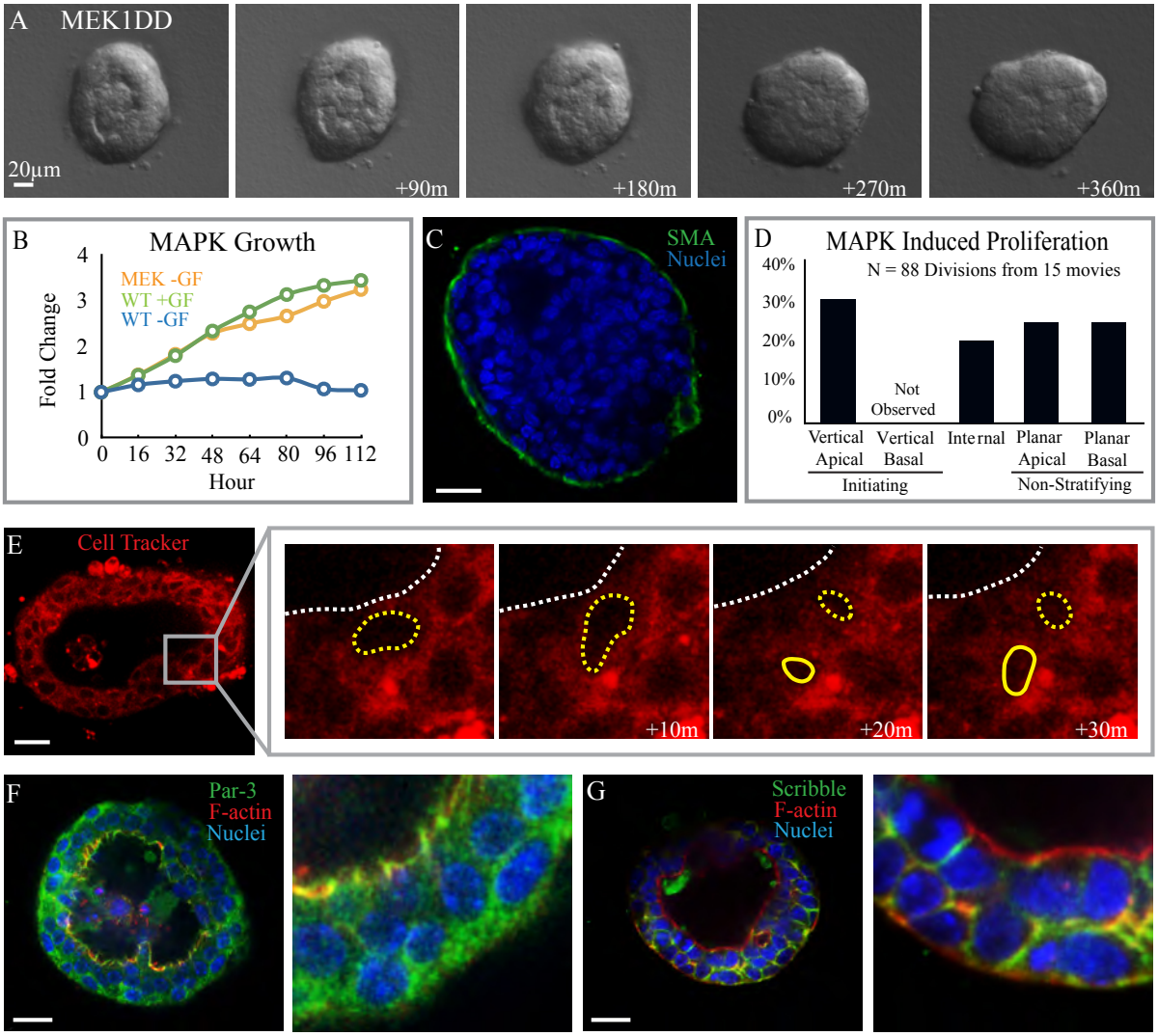
A MEK1DD
20µm
+90m
+180m
+270m
+360m
B
MAPK Growth
MEK -GF
WT +GF
WT -GF
Fold Change
Hour
0 16 32 48 64 80 96 112
C
SMA
Nuclei
D
MAPK Induced Proliferation
N = 88 Divisions from 15 movies
40%
30%
20%
10%
0%
Not Observed
Vertical Apical
Vertical Basal
Internal
Planar Apical
Planar Basal
Initiating
Non-Stratifying
E
Cell Tracker
+10m
+20m
+30m
F
Par-3
F-actin
Nuclei
G
Scribble
F-actin
Nuclei

Figure 4-6: MAPK and PI3 Kinase are both Required for ErbB2 Induced Proliferation

(A) Organoids were allocated to control and ErbB2 expressing experimental groups. Subset of the ErbB2 expressing organoids were treated with either MEK or PI3 kinase inhibitor. (B) Organoids were fixed 3 days after ErbB2 activation and stained for the proliferation marker phospho-histone H3 (pH-H3, red), DAPI (blue) and F-actin (green). Quantification of the effect of MEK and PI3 kinase inhibitors on organoids expressing mutant ErbB2. Percent proliferation was quantified as the number of phospho-histone-H3 positive cells divided by the total number of cells per organoid. Stars highlight conditions that were significantly different by ANOVA ($P<0.001$) than the activated ErbB2 mutant. (C) Control organoids displayed a low level of proliferation. (D) ErbB2 activation increased the number of pH-H3 positive cells. (E) MEK inhibition with U0126 (U) decreased proliferation below the level observed in control organoids. (F) Inhibition of the AKT pathway with the PI3 kinase inhibitor LY294002 (LY) decreased proliferation below the level of control organoids. Scale bars are 20μm.

Figure 4-6

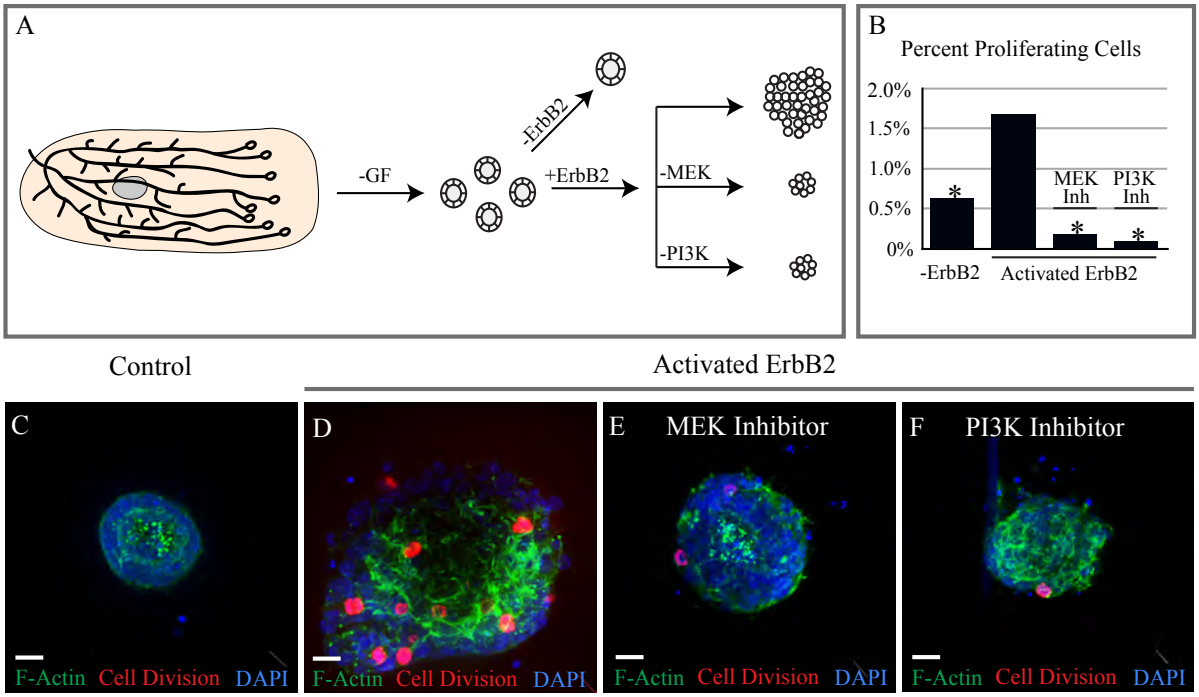
A
-GF
-ErbB2
+ErbB2
-MEK
-PI3K
B
Percent Proliferating Cells
2.0%
1.5%
1.0%
0.5%
0%
MEK Inh
PI3K Inh
-ErbB2
Activated ErbB2
Control
Activated ErbB2
C
D
E MEK Inhibitor
F PI3K Inhibitor
F-Actin Cell Division DAPI

Chapter 5

Spatially restricted MAPK signaling coordinates the polarization of cell migration during mammary branching morphogenesis

Abstract

We sought to resolve the cellular mechanisms driving mammary ductal elongation. We discovered that cells in the tips of tubes specifically displayed high pERK levels but did not require proliferation during elongation. Cells in this high pERK zone displayed elevated speed, elevated persistence, and anisotropic protrusions in the direction of elongation. Pharmacologic inhibition of either Rac or MEK blocked both cell migration and elongation. We next tested whether activation of these signaling pathways could initiate the elongation process in the absence of exogenous growth factors. Conditional induction of Rac activity had no gross phenotypic consequences. In contrast, conditional induction of MEK activity was sufficient to drive the initiation and elongation of new ducts. Our data reveal that mammary ductal elongation is fundamentally a Rac- and MEK-dependent collective cell migration. Furthermore, MEK activation alone is sufficient to induce collective motility within epithelial groups, a key feature of metastasis.

Introduction

Epithelial tubes provide the compartmentalization required for physiologic processes such as gas exchange, nutrient absorption, secretion, fluid transport, and waste elimination. While tubular organs are essential components of vertebrate and invertebrate animals, the cellular mechanisms that drive tube elongation remain incompletely understood[1]. Since mammalian organs generally increase in both size and structural complexity during development, researchers have for decades sought to understand the relative contributions of cell proliferation, cell shape change, and cell migration contribute to tubulogenesis in the lung, salivary gland, and kidney[1,2,3,4]. Recent advances, in primary organotypic culture and imaging technology have begun to shed light on the cellular processes that drive mammalian tube growth and development[5,6,7,8,9,10].

Mammary branching morphogenesis has provided a powerful model to study mammalian epithelial tube formation[11,12,13]. In vivo mammary epithelial development primarily occurs in the postnatal animal, triggered at the onset of puberty by rising steroid hormone levels[14,15]. Circulating hormones interact with local signaling networks, primarily through reciprocal interactions between different receptor tyrosine kinase pathways, resulting in the elongation and elaboration of the mammary ductal network[16,17]. The development of three-dimensional (3D) organotypic culture methods permitted key processes of mammary gland development to be recapitulated in vitro[11,12,18,19,20,21]. The "organoid assay", in which pieces of primary normal or cancerous epithelium are cultured in 3D gels of extracellular matrix (ECM) proteins[22], enables dynamic cell and tissue level analysis of both normal epithelial development and diseases states[11,23,24].

Time-lapse studies of mammary branching morphogenesis revealed that the tips of elongating ducts were composed of multilayered groups of highly migratory cells, without ECM-directed actin-based protrusions[12]. This unit of migration was significantly different from previously studied examples of tube development, such as the drosophila trachea[25] or zebrafish lateral line[26], which critically utilized highly protrusive leader cells[4,27]. In contrast, the basal surface of the tips of mammary epithelial tubes was smooth at both the light and ultrastructural level[21]. Cells at the leading edge exchanged positions creating a constantly changing elongation front[12]. Live-cell imaging of the mouse salivary gland and kidney revealed a smooth elongation front similar to the mammary epithelium, supporting the general relevance of this organizational state during mammalian tubulogenesis[9,28,29]. However, these studies collectively raise the question of how do mammalian epithelial tubes elongate in the absence key features, such as leading protrusions, common to so many migratory cells?

In this study, we use fluorescent reporter mice, 3D timelapse confocal microscopy, and cell tracking to visualize mammary branching morphogenesis in real-time. Consistent with prior studies, tube initiation and elongation occurs without overt ECM-directed protrusions. However, mammary epithelial cells were highly protrusive within the epithelium and selectively orient these protrusions, and preferentially migrate, in the direction of elongation. We used conditional activation and small molecule inhibitors to assess the role of specific signaling modules within receptor tyrosine kinase signaling pathways during elongation. These data revealed high levels of phospho-ERK (pERK) in the most migratory cells at the tips of elongating ducts. Morever, we demonstrated that

ERK signaling is required both for the single cell migration and for the elongation of the tissue as a whole. Surprisingly, mosaic activation of MEK was sufficient to induce initiation and elongation of new epithelial buds. These data provide a conceptual framework for epithelial tube elongation and provides novel insights into how receptor tyrosine kinase signaling regulates cell behaviors within intact tissues.

Results

Cells in the tips of elongating ducts display high pERK levels

Mammary epithelial ducts elongate during puberty, over distances of an inch or more in the mouse[14,15]. The mature ducts consist of a bilayered tube, with apically positioned luminal epithelial cells and basally positioned myoepithelial cells. However, elongation is accomplished by a multilayered group of highly proliferative cells at the tip of the duct, referred to as a terminal end bud (TEB)[15]. Direct observation of cell behaviors in the mammary gland is very challenging, as TEBs are surrounded by layers of light-scattering adipocytes. To overcome this optical inaccessibility, we used 3D organotypic culture to isolate and study primary mammary epithelium[22]. In brief, the mammary gland was surgically isolated and pieces of epithelial ducts ("organoids") were isolated through a combination of mechanical disruption, enzymatic digestion, and differential centrifugation[22]. These epithelial organoids were then embedded in a mixture of ECM proteins characteristic of the basement membrane and the stromal matrix (1:1 Matrigel:collagen I) and cultured with FGF2, conditions that we previously demonstrated support in vivo-like branching morphogenesis[30].

FGF2 stimulates receptor tyrosine kinase (RTK) signaling, which activates two canonical signaling modules; mitogen activated kinase (MAPK) and PI3K/AKT (Figure 5-1A)[31]. MAPK and PI3K/AKT have both distinct and overlapping roles. MAPK signaling has been shown to regulate proliferation, differentiation, apoptosis and cell migration[32], while PI3K/AKT signaling plays fundamental roles in cell survival, proliferation, metabolism,

and cell migration[33]. While we understand the molecular underpinnings of these signaling pathways, it is less clear how these modules regulate cell behaviors within multicellular tissues during development.

We first determined the localization of PI3K/AKT and MAPK signaling in elongating mammary ducts. Antibody staining against the phosphorylated form of AKT (pAKT) was used to determine the location of active PI3K/AKT signaling. We observed pAKT in the cytosol of all cells and enrichment in dividing cells (white arrow, Figure 1B). Antibody staining against phosphorylated ERK-1/2 (pERK), two downstream kinases in the $MAPK^{ERK-1,2}$ signaling module, was used to determine the location of active MAPK signaling[32]. In contrast to the uniform pAKT staining, strong pERK staining was specifically localized to the final few cell layers in the tip of elongating ducts (Figure 5-1C). As a control, organoids were stained for total ERK-1/2, which was diffusely present in the cytosol of all cells, indicating that the pattern of pERK likely reflected MAPK signaling activity, as opposed to the levels of ERK-1/2 proteins (Figure 5-1D). This observation suggested a unique and spatially restricted role for MAPK signaling during elongation and is consistent with elevated levels of ERK signaling seen at the tips of the Wolffian duct[34].

Proliferation was not required during ductal elongation

MAPK signaling is best known for its role in regulating cell proliferation[35] and so our first hypothesis was that the regions with elevated pERK corresponded to zones of localized proliferation that drove elongation. To test this hypothesis, we collected 3D

time-lapse movies of organoids with a genetically encoded nuclear marker (histone-H2B-GFP; H2B-GFP[36]). Since the H2B-GFP labeled the chromosomes, these movies allowed us to visualize mitosis in real-time. Widespread proliferation was observed in elongating branches but it was not confined to cells at the elongation front, suggesting that it was not correlated with the level of pERK. Furthermore, we observed that branches could initiate and elongate in the absence of local proliferation (Figure 5-1E). From these data we conclude that proliferation was neither specific to the region of elongation nor necessarily observed during the process of elongation.

We next sought to test the requirement for proliferation during ductal elongation, using aphidicolin, a DNA polymerase-α inhibitor that blocks entry into mitosis[37]. We allowed organoids to begin the branching process and then added either vehicle control or aphidicolin and imaged the resulting effects on ductal elongation (Figure 5-1F-G). Surprisingly, both vehicle and aphidicolin treated samples continued to elongate for up to two days after treatment (Figure 5-1H). We verified that aphidicolin was inhibiting proliferation in our system by treating branching organoids with aphidicolin for 24 hours and then staining for the mitosis marker phosphor-histone-H3 (pH-H3). In control organoids we observed an average of 4.3 cell divisions per organoid (N=22) (Figure 5-1I), while aphidicolin-treated organoids had 0 pH-H3+ cells in the 22 organoids examined (Figure 5-1J). We therefore conclude that proliferation is not required during mammary ductal elongation (Figure 5-1K).

Elongation correlated with an increase in cell motility

Having observed that localized proliferation was not required for branch elongation, we next hypothesized that elongation was primarily accomplished by cell migration. To test this hypothesis, we imaged organoids derived from transgenic mice in which the nuclei were labeled in green (H2B-GFP[36]) and the membranes in red (membrane TD-tomato)[38]. The combination of membrane and nuclear markers allowed us to track individual cell movements quantitatively using time-lapse confocal microscopy. We collected movies of organoids cultured in the absence of growth factor (no GF) and in organoids cultured with FGF2 at several stages: before elongation (Day 2), during active elongation (Day 4), or after completion of elongation (Day 7) (Figure 5-2A-D'). This approach allowed a direct comparison of cell movements at each stage of branching morphogenesis. Cell nuclei were tracked for 16 hours and 20 minutes with a 10-minute interval between movie frames. A minimum of 32 nuclei from three independent experiments was tracked for each condition.

We utilized the trajectories of the nuclear movements to compare two parameters: mean cell speed and cell persistence. Mean cell speed was measured as the total cell track length divided by the time of tracking. Persistence was quantified as track displacement divided by the total track length. Cells were minimally motile in the absence of FGF2 stimulation (Figure 5-2A-A'). Addition of FGF2 lead to a modest increase in cell motility even prior to ductal initiation (Figure 5-2B-B'). There was a second increase in cell motility during active elongation (Figure 5-2C-C'). Cell motility then decreased as ducts stopped elongating (Figure 5-2D-D'). The mean cell speed was significantly ($p<0.0001$) increased during active elongation (day 4) compared to the other conditions (No GF, Day

2, or 7) (Figure 5-2E). There was also a significant ($p<0.0001$) increase in cellular persistence during active elongation (Figure 5-2F). We conclude that FGF2 induces an increase in cell motility and that there is a burst in both cell speed and persistence during active elongation.

Elongating branches displayed regional differences in cell motility

Cells within elongating branches displayed a large range of mean cell speeds (Figure 5-2E). This led us to ask if the differences in cell speed were related to the cells' location within the epithelial group. To answer this question, we tracked cells at the leading edge (front cells), within the neck of the elongating branch (branch cells), or cells that were not in the branch (body cells) (Figure 5-3A-A'). We then quantified the mean cell speed and cellular persistence for each of these populations (Figure 5-3B-C). A minimum of 34 cells from 4 independent experiments was tracked for each condition. Cells were tracked for 16 hours and 20 minutes, with a 10-minute time interval between frames.

Front cells had a significant increase in cell speed ($p<0.0001$) compared to either branch or body cells and branch cells had increased cell speed ($p<0.01$) compared to body cells (Figure 5-3B). Similar regional differences have been described in the elongating mouse salivary gland indicating a conserved cellular mechanism for mammalian epithelial tube elongation[10]. Despite variations within individual branches (Figure 5-3A'), there were no consistent and significant regional differences in persistence, when analyzed across all movies. Taken together, out data reveal that the entire organoid displays increased

persistence during elongation, while cell speed is regionally enhanced in the cells in the high pERK elongation front.

Cells exchanged into and out of the high motility elongation front

We previously demonstrated qualitatively that cells within elongating branches could change relative positions[12]. Our novel identification of a high pERK, high motility cell region within the elongation front led us to revisit the issue of cell mixing quantitatively. We sought to test this hypothesis that cells could enter and exit the high motility elongation front. Cells were classified as at the elongation front if they were in the basal-most luminal cell layer adjacent to the ECM, at the tip of the elongating branch. We tracked cells in 3D over time and counted the frequency of cells entering into or exiting from this basal most cell layer. Of the 47 branch cells followed, we observed 4 (8.5%) that migrated into the elongation front (Figure 5-3D). Conversely, of the 51 front cells that we followed, 5 (10%) were observed to move into an interior position within the branch (Figure 5-3E). Our quantitative cell tracking therefore revealed that cells can exchange between front and interior positions but that most cells remained within their original compartment over the period of observation (Figure 5-3F).

Cell protrusions are anisotropic in the direction of branch elongation

Migratory epithelial cells form protrusions between other cells within the elongating branch but do not extend protrusions into the ECM[12,21]. Consistent with our model that elongation is fundamentally a cell migration process, we hypothesized that the high pERK, highly migratory cells would orient their protrusions in the direction of elongation

of the branch as a whole. To test this hypothesis, we labeled individual cells within the epithelium and collected 3D time-lapse confocal movies during elongation.

We quantified the orientation of protrusions by placing a transparent circular chart over a labeled cell, with 0 degrees in the direction of branch elongation. We then counted the number of cellular protrusions within each of 8 equally divided bins (Figure 5-4A). Protrusions within the 0-45 degree or 270-315 degree bin were in the direction of branch elongation, while protrusions within the 180-135 degree and 180-225 degree bins were opposing the direction of branch elongation. Our comparison was between cells within the main organoid body or within an actively elongating branch (Figure 5-4A).

During branch elongation, cells within the body of the organoid were highly motile and protrusive (Figure 5-4B-B'). However, the orientation of protrusions in these body cells was isotropic and showed no tendency to protrude in the direction of branch elongation (Figure 5-4C). Cells within elongating branches were also highly motile and protrusive (Figure 5-4D,D'). However, in contrast to cells within the body of the organoid, the orientation of protrusions in branch cells was highly anisotopic and corresponded to the direction of branch elongation (Figure 5-4D,D',E). We conclude that the cells at the tips of elongating branches display a coordination to both their migration and protrusive activity.

Rac signaling was required for cell motility and branch elongation

The Rho family of small GTPase has well defined roles in both single and collective cell migration[39]. In particular, Rac is required for the establishment of front-rear migratory cell polarity and in generating the actin-based protrusions at the leading edge of migrating cells[40]. Given the extensive, coordinated protrusions we observed during branch elongation, we hypothesized that Rac would be required both for mammary epithelial cell motility and mammary branch elongation. We tested this hypothesis by analyzing nuclear trajectories in elongating branches in the presence of a commercially available Rac inhibitor.

To establish a baseline of level of cell migration, time-lapse movies of nuclear GFP were collected for 4.5 hours during active branch elongation (Figure 5-5A,A'). Following this baseline imaging session, organoids were treated with Rac inhibitor for twelve hours. The same organoids were then imaged for an additional 4.5 hours (Figure 5-5B,B'). Nuclei trajectories and cell speeds were collected and calculated from the same region of each organoid. A total of 64 cells from 8 organoids and 3 independent experiments were analyzed (Figure 5-5C). Rac inhibition significantly resulted in a significant decrease in mean cell speed. Mean speed of cells treated with Rac inhibitor was indistinguishable from the mean speed of cells in the absence of growth factor (Figure 5-2E).

We concluded that Rac signaling was required for cell motility, but it remained unclear if Rac mediated cell migration was required for branch elongation. To test the requirement for Rac signaling in branching morphogenesis, we treated with either Rac inhibitor or vehicle control at day 1 of culture. Consistent with previous work, branch initiation was

completely blocked[12]. We next sought to test the requirement for Rac signaling during elongation, by adding Rac inhibitor or vehicle control at day 4 of culture (Figure 5-5D,E). Vehicle control treated organoids all continued elongating (Figure 5-5D,F). In contrast, organoids treated with Rac inhibitor during active branching stopped elongating and the mammary branches collapsed into the body of the organoid (Figure 5-5E,F). We conclude that Rac-dependent cell migration is required for branch elongation.

Rac signaling was not sufficient to induce mammary branch elongation

Previous studies have demonstrated that Rac activation can be sufficient to orient collective cell migration[41]. To test this, we utilized a transgenic mouse that allowed conditional expression of an active mutant of Rac1 (RacV12)[42]. The transgenic locus contained a floxed Stop, RacV12, an internal ribosomal entry site (IRES), and EGFP (Figure 5-5G). Cre recombinase activity therefore regulates expression of both RacV12 and EGFP. We utilized an adenovirally delivered Cre as it enabled us to modulate the number of fluorescently-labeled, RacV12-expressing cells by manipulating the viral titer (Figure 5-5H). To determine if Rac activity was sufficient to induce branching morphogenesis, we expressed the RacV12 in organoids cultured without exogenous growth factors. Cre was delivered at the onset of culture, with approximately 80% of cells transduced, using EGFP as a reporter for Rac expression. We then compared tissue growth and branching morphogenesis in time-lapse movies of control tissue in the presence of FGF2 and RacV12 expressing tissue in the absence of growth factor stimulation. FGF2 treated control organoids underwent normal branching morphogenesis (Figure 5-5I). In contrast, organoids expressing RacV12 did not branch or increase in size

(Figure 5-5J). We conclude that experimental induction of Rac activity is not sufficient to drive mammary branching morphogenesis.

MAPK signaling was required for cell motility and branch elongation

Since the most migratory cells at the tips of elongating branches had high pERK staining, we hypothesized that MAPK signaling would be required both for epithelial cell migration and branch elongation. We utilized a small molecule inhibitor of MEK and ERK (U0126) to test this hypothesis, in an analogous fashion as in our Rac inhibitor experiments.

We first collected time-lapse movies of nuclear GFP for 4.5 hours during active branch elongation (Figure 5-6A,A') and then treated with U0126 for twelve hours. The same organoids were then imaged for an additional 4.5 hours (Figure 5-6B,B'). Nuclear trajectories and cell speeds were collected and calculated from the same region of each organoid. A total of 64 cells from 8 organoids and 4 independent experiments were analyzed (Figure 5-6C). MAPK inhibition significantly resulted in a significant decrease in mean cell speed, to a level indistinguishable from cells in the absence of growth factor (Figure 5-2E).

We next treated organoids with U0126 at either day 1 or day 4 of culture and collected timelapse movies of tissue growth and branching morphogenesis. Time-lapse movies were collected for both the control and treated organoids. Control organoids branched as expected (Figure 5-6D), while addition of U0126 at day 1 completely blocked branching

morphogenesis, consistent with prior reports[11,20]. Strikingly, addition of U0126 during active branching at day 4 resulted in an acute arrest in elongation and regression of existing branches back into the body of the organoid (98% of organoids regressed; Figure 5-6E,F). We conclude that MAPK signaling is required both for cell migration and branch elongation during a period of culture in which proliferation is dispensable (Figure 51F-H), suggesting that MAPK has proliferation-independent roles in mammary branching morphogenesis.

Mosaic MAPK activity was sufficient to induce mammary branch morphogenesis

Since ERK signaling was highest in the most migratory cells and MAPK signaling was required for both cell migration and branch elongation, we hypothesized that experimental manipulation of MAPK activity would be sufficient to induce the initiation and elongation of mammary branches. To test this hypothesis, we utilized a transgenic mouse line that allowed conditional expression of a phospho-mimetic, constitutively-active mutant of MEK (MEK1DD)[42]. The transgenic locus encoded a floxed STOP cassette, MEK1DD, an IRES, and EGFP (Figure 5-7A). Using adenovirally delivered Cre, we conditionally and mosaically expressed MEK1DD in organoids cultured in the absence of exogenous growth factors (Figure 5-7B).

We collected time-lapse movies of three conditions: control organoids in the presence or absence of growth factor, and organoids expressing MEK1DD in the absence of growth factor (Figure 5-7C-E). We observed no branching in control organoids without growth factor and we observed branching in essentially all control organoids treated with FGF2

(0% vs. 90%; Figure 5-7E). Strikingly, experimental expression of MEK1DD was sufficient to induce initiation and elongation of mammary branches even in the absence of growth factor stimulation (40%; Figure 5-7D,E). We next sought to determine the location of MEK1DD expressing cells within the elongating branches, using the transgenic EGFP as a reporter in 3D confocal timelapse movies. We observed that MEK1DD induced branches were elongated by distinct clusters of EGFP expressing cells (Figure 5-7F). Taken together, we conclude that that MAPK signaling is necessary and sufficient to induce mammary branch elongation and that both wildtype and MEK1DD-induced branches are led clusters of cells with high levels of MAPK signaling.

Discussion

Our goal in this study was to establish a cellular and molecular framework for the process of branch initiation and elongation in the mammary gland. We first answered a long-standing question about the relative contributions of proliferation and cell migration, by showing that proliferation was not required during branch elongation. Branch initiation and elongation instead correlated with a marked increase in cell motility, which was specifically elevated in a subpopulation of cells at the branch tips. This high motility cell population correlated with high levels of MAPK signaling, as reported by pERK levels. Importantly, this region of active motility was dynamic, as we observed migration into and out of the elongation front. Individual cells were motile and protrusive within the epithelium, appearing almost mesenchymal in their behavior but the cellular protrusions were confined within the epithelial group and did not penetrate into the ECM. Cells within elongating branches exhibited a striking alignment of the direction of cellular protrusion with the direction of branch elongation. This coordination of protrusions and migration led us to test the requirement for Rac1 and we demonstrated that Rac activity was required for both cell migration and branch elongation. However, experimental activation of Rac1 was not sufficient to induce branching. MAPK signaling was also required for collective cell migration and branch elongation but, strikingly, mosaic expression of MEK1DD was sufficient to induce branching morphogenesis in the absence of exogenous growth factors.

The cell behavioral basis of tube elongation

From first principles, it is possible to conceptualize the process of tube elongation operating through essentially any combination of proliferation, migration, and cell shape change[1]. Two very well studied examples are the *Drosophila* trachea and *Drosophila* salivary gland. In the *Drosophila* trachea, there is no proliferation during branching morphogenesis and most of the elongation and ramification of the tubular network is accomplished by cell shape change[4,43]. In the *Drosophila* salivary gland there is a period of proliferation during the establishment and specification of the salivary gland[43]. The elongation of the tube is then accomplished by a combination of cell migration and cell shape change, with no proliferation observed during tube elongation[1,43]. The fact that proliferation does not occur during elongation in the *Drosophila* trachea or salivary gland has enabled exquisite genetic and time-lapse analyses of the cellular movements driving development of these organs without the complication of increasing cell number[44,45,46,47,48]. This proliferation followed by migration mechanism of tube elongation has also been observed during zebrafish kidney morphogenesis and so is utilized in vertebrates as well[49]. However, mammalian tubular organs exhibit profound proliferation-driven growth during development and so it had appeared that the principles uncovered in model systems were not sufficient to explain mammalian branching morphogenesis. In particular, mammary epithelial tubes elongate over centimeters in mice and much longer distances in large mammals and tube elongation is clearly accompanied by extensive proliferation. Furthermore, genetic manipulations that reduce the rate of proliferation in the mammary TEB slow the rate of tube elongation[50]. Despite clear in vivo evidence for its requirement, it remained unclear how exactly proliferation was contributing to mammary tube elongation. Proliferation has been shown to play

different roles during mammalian tubulogenesis, including regulation of lung tube shape[51], driving dispersal of cells in the ureteric bud[8], and inducing stratification of the mammary epithelium[11].

It was unknown how proliferation contributed to mammary branch elongation but it was reasonable to hypothesize that branches elongated exclusively through localized proliferation. We excluded this possibility by both observing branch initiation in the absence of proliferation and by observing continued branch elongation following aphidicolin treatment. Instead, we demonstrated that mammary tube elongation is accomplished by cell migration and we speculate that proliferation is utilized as a mechanism to produce migratory cells with lower apico-basal polarity and fewer intercellular junctions[11]. Inhibiting proliferation limits the generation of more of these cells but does prevent existing cells from contributing to tube elongation. Seen from this perspective, the model systems and mammalian organs differ in their timing of proliferation but share common mechanisms of cell migration and cell shape change as drivers of the elongation process.

Region specific cell migration within the epithelium

A surprising feature of mammary branching morphogenesis is that the epithelial cells are highly protrusive and motile within the epithelium but do not protrude into the ECM[12,21]. Individualistic cell motility has also been observed in the mouse salivary gland[9] and the mouse ureteric bud[29]. In the present study, we demonstrated that mammary epithelial cells within active branches are selectively protrusive in the elongation, which suggested

that coordinated cell migration is both required and potentially sufficient for branch formation. Consistent with this conceptual model, we identified a region of high pERK and high cell speed in the tips of elongating branches. High levels of cell motility in the elongation front have also been observed in the mouse salivary gland[10]. We next demonstrated that both cell migration and branch elongation required Rac and MAPK signaling. Strikingly, treatment with inhibitors to either pathway led to regression of existing mammary branches. Integrating our new data with published observations, we propose that RTK signaling induces the formation of highly motile epithelial cell clusters that elongate the epithelial tube but are unable to invade into the ECM, potentially due to the very limited ECM binding ability of luminal epithelial cells[52].

Localized MAPK signaling is sufficient to induce branch initiation and elongation

MAPK signaling is required for branching morphogenesis in the mouse submandibular gland[53], mouse kidney[54], rat lung[55], and mouse mammary gland[20]. In each of these tissues, general inhibition of MAPK signaling results in a decrease in tissue size, branch number, and proliferation. These previous studies demonstrated that MAPK regulates proliferation during tube development and that proliferation is required for mammalian branching morphogenesis. Using time-lapse imaging and MAPK inhibition during active branching, we have shown that MAPK signaling regulates cell motility during branch elongation at a time when proliferation is dispensable.

Our conclusion is consistent with results from Madin-Darby canine kidney (MDCK) acini[56]and MCF-10A mammary acini[57], each of which experience increased cell motility

in response to MAPK signaling. The relationship between cell migration, $MAPK^{ERK1,2}$ signaling and tubulogenesis appears to be deeply conserved as *branchless* is a master regulator of cell migration during Drosophila trachea formation and encodes an FGF ligand[58]. The key conceptual advance embodied in our paper is the dual demonstration that normal mammary elongation is led by clusters of motile, protrusive cells with high-pERK levels and that expression of MEK1DD is sufficient to induce branching morphogenesis. In particular, the sufficiency of MEK1DD to induce branch initiation and elongation is highly surprising because RTK signaling activates multiple pathways other than MEK and genetics has implicated members of the EGFR, FGFR, and MET receptor pathways in mammary branching morphogenesis[50]. Our data lead us to speculate that MAPK is the fundamental signaling node for mammary tube elongation and to suggest that spatial control of pERK may represent the key to generating directional growth despite a uniform concentration of growth factors. This perspective is consistent with the frequent activation of MAPK signaling in cancer[59] and suggests that high MAPK activity may be sufficient for initiating collective cell invasion during metastasis.

Experimental Procedures

Transgenic animals

A transgenic mouse line expressing a membrane-targeted tdTomato was used to label cell membranes; this line was acquired from the Jackson Laboratory[38]. A transgenic mouse line expressing H2B-GFP was used to label nuclei; this mouse line was a kind gift from AK Hadjantonakis, Memorial Sloan Kettering[36]. Transgenic mouse lines enabling conditional expression of RacV12 and MEK1DD were acquired from the Jackson Laboratory[42]. All animal experiments were conducted in accordance with protocols approved by the Institutional Animal Care and Use Committee, Johns Hopkins University, School of Medicine.

Organotypic culture

The organotypic culture methods used here are described in detail in[22]. In brief, mammary glands were isolated from 8-10 week old mice and minced using a scalpel. The epithelium was then separated from fat and stromal tissue by collagenase-trypsin digestion, DNase treatment, and differential centrifugation. Organoids were suspended in a 50:50 mixture of growth factor reduced Matrigel (BD Biosciences) and rat tail collagen 1 (Corning) and plated as 400µl drops containing an average of 1 org/µl. The organoid suspensions were plated on 24-well glass bottom plates (Greiner Bio One) sitting on a 37^{o}C hotplate to promote gel polymerization (as described in[22]). Plates were incubated for a 20 minutes at 37^{o}C to ensure gelation before addition of culture medium. Where indicated, organoids were treated with 2.5nM FGF2 to stimulate branching morphogenesis.

Organoid antibody staining

The organoid staining protocol is described in detail in[22]. Briefly, organoid-containing ECM gels were fixed in 4% PFA for 20 minutes and then washed 3 times in PBS. Organoids were then permeabilized in 0.5% Triton X-100 in PBS for 30 minutes to allow antibody access. 10% FBS in PBS was used as a blocking solution for 3 hours. Following block, organoids were incubated with primary antibodies for 2 hours in 10% FBS in PBS. Phospho-histone-H3, phospho-AKT, phospho-ERK, and total-ERK antibodies were acquired from Cell Signaling and used at 1:500. After incubation with primary antibodies organoids were washed 3 times in blocking solution. Organoids were then incubated with Alexa Fluor conjugated secondary antibodies (Molecular Probes, 1:500), phalloidin (Invitrogen, 1:500), and DAPI (Invitrogen, 1:1000) for 1 hour in blocking solution. Stained organoids were washed 3 times with PBS and analyzed by confocal microscopy.

Adenoviral gene delivery

Adenoviral-Cre or adenoviral-GFP (Vector Biolabs) were added after organoid isolation prior to suspension in ECM and plating. Isolated organoids were transferred to a 1.7ml Eppendorf tube and centrifuged at 520g for 10 minutes. The supernatant was removed and organoids were re-suspended in 100µl of DMEM-F12 (Gibco). Adenovirus was added at a concentration of 10,000 plaque-forming units per organoid to achieve gene expression in 50-80% of cells. Organoids were incubated with viral particles for one hour at 37^{o}. Following infection, organoids were washed twice with DMEM-F-12 and suspended in ECM for plating.

Time-lapse differential interference contrast microscopy

Differential interference contrast microscopy movies were collected on a Zeiss Cell Observer with a Zeiss AxioObserver Z1 and an AxioCam MRM camera (as described in[60]). Organoids were imaged for 5-7 days with a 20-minute time-interval and typically 100-200 movies collected in parallel. Time-lapse movies were started 24 hours after growth factor stimulation or gene induction. The environment was maintained at 37^{o} C and 5% CO_2 throughout imaging.

Confocal Microscopy

Images of fixed samples were acquired using a Zeiss LSM 780 confocal microscope with a 40x LD-LCI C-Apochromat objective using ZEN imaging software. Time-lapse images were acquired on a spinning disk confocal microscope from Solamere Technology Group using a 40x LD-LCl C-Apochromat lens[60]. The spinning disk microscope used a combined software package from μManager[61] and Piper (Stanford Photonics) to acquire images. Organoids were imaged from 4-16 hours with a 10-minute time interval in an environmentally controlled chamber with the temperature maintained at 37^{o} and CO_2 at 5%. Brightness and contrast were adjusted using Adobe Photoshop and Imaris (Bitplane) to maximize image clarity. Adjustments were always applied to the entire image.

Proliferation inhibition assay

Organoids were cultured in the presence of FGF2 and imaged using time-lapse differential interference contrast microscopy. Aphidicolin was used at a concentration of

1.25 nM and added during active elongation (day 4). Time-lapse movies were collected from the time of inhibitor addition until up to 2 days after aphidicolin treatment. Movies were analyzed to determine whether organoids continued elongating after inhibition. To verify that proliferation was inhibited, organoids were treated with aphidicolin at day 4 in culture. The treated organoids were fixed 24 hours after aphidicolin treatment and stained for the proliferation marker phospho-histone-H3, in 22 organoids from 3 independent experiments. No proliferation was observed aphidicolin treated samples.

Nuclei Tracking

Nuclei were tracked using the Imaris Spots function. Images were first smoothed using a 0.35 μm Gaussian filter. Cells were manually tracked by placing a Spot in the center of the cell nuclei within each frame in a movie and then using the Spots function to connect the nuclei over time. The Imaris OrthoSlicer function was used to move through the Z-dimension to enable tracking in 3D. The mean cell speed was quantified as the total track length divided by time of tracking and persistence was measured as the displacement divided by the total track length. A single factor analysis of variance (ANOVA) was used to determine statistical significance for mean speed and persistence.

Analysis of cellular protrusions

Mammary epithelial organoids were isolated and cultured, as described above. Organoids expressing membrane-targeted tdTomato were isolated and cultured. Time-lapse confocal images were captured every 15-20 minutes for 12-24 hours. 3D image analyses were conducted using Imaris (Bitplane). Protrusions data for sector charts was conducted by

drawing an 8-section pie with deviations every 45-degrees on a clear, overhead projector sheet. The 0 to 180-degree axis was aligned with the axis for bud initiation or branch elongation. This axis was used on each cell by placing and moving the the center of the overhead projector sheet over the center of mass for each cell. The number of protrusions per bin per cell was counted every 15-20 minutes for a minimum of 6 hours.

Protrusion data was statistically analyzed by creating sector charts using Mathematica (Wolfram), plotting the mean values for each bin and equally weighting each angle. Statistical analyses were performed on circular data using Oriana (Kovach Computing Services). Hotelling's test was used to determine the significance of a weighted mean direction. The null hypothesis is that there is no mean direction. Hotelling's paired test was used to determine the significance of the difference in the weighted mean direction between circular data. The null hypothesis is that there is no difference in the mean direction.

Rac and ERK/MEK inhibition assays

InSolution^{TM} Rac1 inhibitor (Calbiochem) was used at a concentration of 50μM and the small molecule MEK/ERK inhibitor U0126 (Cell signaling) was used at a concentration of 10μM. Organoids were cultured in the presence of FGF2 to induce branching morphogenesis. To assess for inhibition of cell motility organoids expressing histone H2B-GFP were imaged during active branch elongation. Elongating organoids were imaged for 4.5 hours prior to inhibitor treatment and the same organoids were imaged for 16.5 hours following inhibition. Mean speeds were then quantified and statistically

analyzed by a student t-test with a Mann-Whitney correction. To determine if Rac or ERK/MEK were required for branching we collected DIC movies of organoids beginning at 24 hours in culture and continuing through day 6 with a 20-minute time interval. Inhibitors were added at day 4 during active branching and organoids were assessed for their ability to continue elongating after inhibitor treatment.

Rac and MEK activation assays

Active Rac (RacV12) or MEK (MEK1DD) were expressed in organoids in the absence of growth factor. Active Rac and MEK were coded under the *rosa26* promoter, downstream of a floxed-stop cassette and upstream of an internal ribosomal entry site and EGFP. Adenoviral delivered Cre, described above, was used to mosaically and conditionally express the mutant proteins. The MEK and Rac experiments were internally controlled with organoids from the same animal treated with adeno-GFP in place of adeno-Cre. Control organoids were culture in the presence or absence of growth factor to serve as positive and negative controls respectively. Organoids expressing the mutant proteins were then assessed for the ability to initiate mammary branches both by time-lapse microscopy and by examining organoids after a week in culture.

References

1 Andrew D. J., E., A. J. Morphogenesis of epithelial tubes: Insights into tube formation, elongation, and elaboration. Dev. Biol. 341, 34-55, (2010).

2 Alescio, T. & Di Michele, M. Relationship of epithelial growth to mitotic rate in mouse embryonic lung developing in vitro. Journal of embryology and experimental morphology 19, 227-237, (1968).

3 Goldin, G. V. & Wessells, N. K. Mammalian lung development: the possible role of cell proliferation in the formation of supernumerary tracheal buds and in branching morphogenesis. J Exp Zool 208, 337-346, (1979).

4 Lubarsky, B. & Krasnow, M. A. Tube morphogenesis: making and shaping biological tubes. Cell 112, 19-28, (2003).

5 Shamir, E. R. & Ewald, A. J. Three-dimensional organotypic culture: experimental models of mammalian biology and disease. Nat Rev Mol Cell Biol 15, 647-664, (2014).

6 Kim, H. Y., Varner, V. D. & Nelson, C. M. Apical constriction initiates new bud formation during monopodial branching of the embryonic chicken lung. Development 140, 3146-3155, (2013).

7 Schnatwinkel, C. & Niswander, L. Multiparametric image analysis of lung-branching morphogenesis. Dev. Dyn. 242, 622-637, (2013).

8 Packard, A. *et al.* Luminal Mitosis Drives Epithelial Cell Dispersal within the Branching Ureteric Bud. Dev. Cell 27, 319-330, (2013).

9 Larsen, M., Wei, C. & Yamada, K. M. Cell and fibronectin dynamics during branching morphogenesis. J Cell Sci 119, 3376-3384, (2006).

10 Hsu, J. C. *et al.* Region-specific epithelial cell dynamics during branching morphogenesis. Dev Dyn 242, 1066-1077, (2013).

11 Huebner, R. J., Lechler, T. & Ewald, A. J. Developmental stratification of the mammary epithelium occurs through symmetry-breaking vertical divisions of apically positioned luminal cells. Development 141, 1085-1094, (2014).

12 Ewald, A. J., Brenot, A., Duong, M., Chan, B. S. & Werb, Z. Collective epithelial migration and cell rearrangements drive mammary branching morphogenesis. Dev Cell 14, 570-581, (2008).

13 Huebner, R. J. & Ewald, A. J. Cellular foundations of mammary tubulogenesis. Semin Cell Dev Biol 31, 124-131, (2014).

14 Sternlicht, M. D. Key stages in mammary gland development: the cues that regulate ductal branching morphogenesis. Breast Cancer Res 8, 201, (2006).

15 Hinck, L. & Silberstein, G. B. Key stages in mammary gland development: the mammary end bud as a motile organ. Breast Cancer Res 7, 245-251, (2005).

16 Sternlicht, M. D., Kouros-Mehr, H., Lu, P. & Werb, Z. Hormonal and local control of mammary branching morphogenesis. Differentiation 74, 365-381, (2006).

17 Hennighausen, L. & Robinson, G. W. Information networks in the mammary gland. Nat Rev Mol Cell Biol 6, 715-725, (2005).

18 Simian, M. *et al.* The interplay of matrix metalloproteinases, morphogens and growth factors is necessary for branching of mammary epithelial cells. Development 128, 3117-3131, (2001).

[19] Sternlicht, M. D. *et al.* Mammary ductal morphogenesis requires paracrine activation of stromal EGFR via ADAM17-dependent shedding of epithelial amphiregulin. Development 132, 3923-3933, (2005).
[20] Fata, J. E. *et al.* The MAPKERK-1,2 pathway integrates distinct and antagonistic signals from TGFα and FGF7 in morphogenesis of mouse mammary epithelium. Dev. Biol. 306, 193-207, (2007).
[21] Ewald, A. J. *et al.* Mammary collective cell migration involves transient loss of epithelial features and individual cell migration within the epithelium. J Cell Sci 125, 2638-2654, (2012).
[22] Nguyen-Ngoc, K. V. *et al.* 3D culture assays of murine mammary branching morphogenesis and epithelial invasion. Methods Mol Biol 1189, 135-162, (2015).
[23] Cheung, K. J., Gabrielson, E., Werb, Z. & Ewald, A. J. Collective invasion in breast cancer requires a conserved basal epithelial program. Cell 155, 1639-1651, (2013).
[24] Shamir, E. R. *et al.* Twist1-induced dissemination preserves epithelial identity and requires E-cadherin. J. Cell Biol. 204, 839-856, (2014).
[25] Ghabrial, A. S. & Krasnow, M. A. Social interactions among epithelial cells during tracheal branching morphogenesis. Nature 441, 746-749, (2006).
[26] Valentin, G., Haas, P. & Gilmour, D. The chemokine SDF1a coordinates tissue migration through the spatially restricted activation of Cxcr7 and Cxcr4b. Curr Biol 17, 1026-1031, (2007).
[27] Lecaudey, V. & Gilmour, D. Organizing moving groups during morphogenesis. Curr Opin Cell Biol 18, 102-107, (2006).
[28] Watanabe, T. & Costantini, F. Real-time analysis of ureteric bud branching morphogenesis in vitro. Dev. Biol. 271, 98-108, (2004).
[29] Chi, X. *et al.* Ret-dependent cell rearrangements in the Wolffian duct epithelium initiate ureteric bud morphogenesis. Dev Cell 17, 199-209, (2009).
[30] Nguyen-Ngoc, K. V. & Ewald, A. J. Mammary ductal elongation and myoepithelial migration are regulated by the composition of the extracellular matrix. J Microsc 251, 212-223, (2013).
[31] Schlessinger, J. Common and distinct elements in cellular signaling via EGF and FGF receptors. Science 306, 1506-1507, (2004).
[32] Dhillon, A. S., Hagan, S., Rath, O. & Kolch, W. MAP kinase signalling pathways in cancer. Oncogene 26, 3279-3290, (2007).
[33] Manning, B. D. & Cantley, L. C. AKT/PKB signaling: navigating downstream. Cell 129, 1261-1274, (2007).
[34] Hoshi, M., Batourina, E., Mendelsohn, C. & Jain, S. Novel mechanisms of early upper and lower urinary tract patterning regulated by RetY1015 docking tyrosine in mice. Development 139, 2405-2415, (2012).
[35] Seger, R. & Krebs, E. G. The MAPK signaling cascade. FASEB J 9, 726-735, (1995).
[36] Hadjantonakis, A. K. & Papaioannou, V. E. Dynamic in vivo imaging and cell tracking using a histone fluorescent protein fusion in mice. BMC Biotechnol 4, 33, (2004).
[37] Ikegami, S. *et al.* Aphidicolin prevents mitotic cell division by interfering with the activity of DNA polymerase-alpha. Nature 275, 458-460, (1978).

[38] Muzumdar, M. D., Tasic, B., Miyamichi, K., Li, L. & Luo, L. A global double-fluorescent Cre reporter mouse. Genesis 45, 593-605, (2007).
[39] Ridley, A. J. *et al.* Cell migration: integrating signals from front to back. Science 302, 1704-1709, (2003).
[40] Nobes, C. D. & Hall, A. Rho, rac and cdc42 GTPases: regulators of actin structures, cell adhesion and motility. Biochem Soc Trans 23, 456-459, (1995).
[41] Wang, X., He, L., Wu, Y. I., Hahn, K. M. & Montell, D. J. Light-mediated activation reveals a key role for Rac in collective guidance of cell movement in vivo. Nat Cell Biol 12, 591-597, (2010).
[42] Srinivasan, L. *et al.* PI3 kinase signals BCR-dependent mature B cell survival. Cell 139, 573-586, (2009).
[43] Kerman, B. E. & Andrew, D. J. Staying alive: dalmation mediated blocking of apoptosis is essential for tissue maintenance. Dev Dyn 239, 1609-1621, (2010).
[44] Ribeiro, C., Ebner, A. & Affolter, M. In vivo imaging reveals different cellular functions for FGF and Dpp signaling in tracheal branching morphogenesis. Dev Cell 2, 677-683, (2002).
[45] Kato, K., Chihara, T. & Hayashi, S. Hedgehog and Decapentaplegic instruct polarized growth of cell extensions in the Drosophila trachea. Development 131, 5253-5261, (2004).
[46] Cheshire, A. M., Kerman, B. E., Zipfel, W. R., Spector, A. A. & Andrew, D. J. Kinetic and mechanical analysis of live tube morphogenesis. Dev Dyn 237, 2874-2888, (2008).
[47] Affolter, M., Zeller, R. & Caussinus, E. Tissue remodelling through branching morphogenesis. Nat Rev Mol Cell Biol 10, 831-842, (2009).
[48] Lebreton, G. & Casanova, J. Specification of leading and trailing cell features during collective migration in the Drosophila trachea. J Cell Sci 127, 465-474, (2014).
[49] Vasilyev, A. *et al.* Collective Cell Migration Drives Morphogenesis of the Kidney Nephron. PLoS Biol. 7, e9, (2009).
[50] McNally, S. & Martin, F. Molecular regulators of pubertal mammary gland development. Ann Med 43, 212-234, (2011).
[51] Tang, N., Marshall, W. F., McMahon, M., Metzger, R. J. & Martin, G. R. Control of mitotic spindle angle by the RAS-regulated ERK1/2 pathway determines lung tube shape. Science 333, 342-345, (2011).
[52] Cerchiari, A. E. *et al.* A strategy for tissue self-organization that is robust to cellular heterogeneity and plasticity. Proc Natl Acad Sci U S A 112, 2287-2292, (2015).
[53] Kashimata, M. *et al.* The ERK-1/2 signaling pathway is involved in the stimulation of branching morphogenesis of fetal mouse submandibular glands by EGF. Dev Biol 220, 183-196, (2000).
[54] Fisher, C. E., Michael, L., Barnett, M. W. & Davies, J. A. Erk MAP kinase regulates branching morphogenesis in the developing mouse kidney. Development 128, 4329-4338, (2001).
[55] Kling, D. E. *et al.* MEK-1/2 inhibition reduces branching morphogenesis and causes mesenchymal cell apoptosis in fetal rat lungs. American journal of physiology. Lung cellular and molecular physiology 282, L370-378, (2002).

[56] O'Brien, L. E. *et al.* ERK and MMPs sequentially regulate distinct stages of epithelial tubule development. Dev Cell 7, 21-32, (2004).

[57] Pearson, G. W. & Hunter, T. Real-time imaging reveals that noninvasive mammary epithelial acini can contain motile cells. J Cell Biol 179, 1555-1567, (2007).

[58] Sutherland, D., Samakovlis, C. & Krasnow, M. A. branchless encodes a Drosophila FGF homolog that controls tracheal cell migration and the pattern of branching. Cell 87, 1091-1101, (1996).

[59] Whyte, J., Bergin, O., Bianchi, A., McNally, S. & Martin, F. Key signalling nodes in mammary gland development and cancer Mitogen-activated protein kinase signalling in experimental models of breast cancer progression and in mammary gland development. Breast Cancer Research 11, (2009).

[60] Ewald, A. J. Practical considerations for long-term time-lapse imaging of epithelial morphogenesis in three-dimensional organotypic cultures. Cold Spring Harb Protoc 2013, (2013).

[61] Edelstein, A., Amodaj, N., Hoover, K., Vale, R. & Stuurman, N. Computer control of microscopes using microManager. Curr Protoc Mol Biol Chapter 14, Unit14 20, (2010).

Figure 5-1: Proliferation is not required for mammary branch initiation

(A) Schematic depicting canonical growth factor induced receptor tyrosine kinase signaling. (B) Confocal section of a branch from an organoid expressing membrane targeted tdTomato (red) and stained for phospho-AKT (green) and nuclei (blue), arrow highlights a dividing cell. (C) Organoid branch expressing membrane tdTomato (red) stained for phospho-ERK (green) and nuclei (blue). (D) Mammary branch with membranes marked by tdTomato (red) and stained for total-ERK (green) and nuclei (Blue). (E) Confocal z-projection still images from a time-lapse movie of an organoid expressing histone H2B-GFP (green). Still images are focused on an organoid branch that initiates and elongates in the absence of proliferation. (F-G) Frames from time-lapse differential interference contrast microscopy movies of organoids undergoing branch elongation in the absence (F) or presence of aphidicolin (G). Control and treated organoids were obtained from the same mouse and 1.25 nM aphidicolin was used to inhibit proliferation. (H) Table showing the number and percentage of organoids that continued to elongate mammary branches after addition of vehicle or aphidicolin. (I-J) Confocal z-projections of organoids undergoing active branch elongation. Organoids are expressing membrane tdTomato (red) and stained for the proliferation marker phospho-histone-H3 (green). Organoids were fixed 24 hours after treatment with vehicle (I) or 1.25 nM aphidicolin (J). (K) Cartoon showing that proliferation is not required for branch elongation and instead elongation is driven by collective cell migration.

Figure 5-1

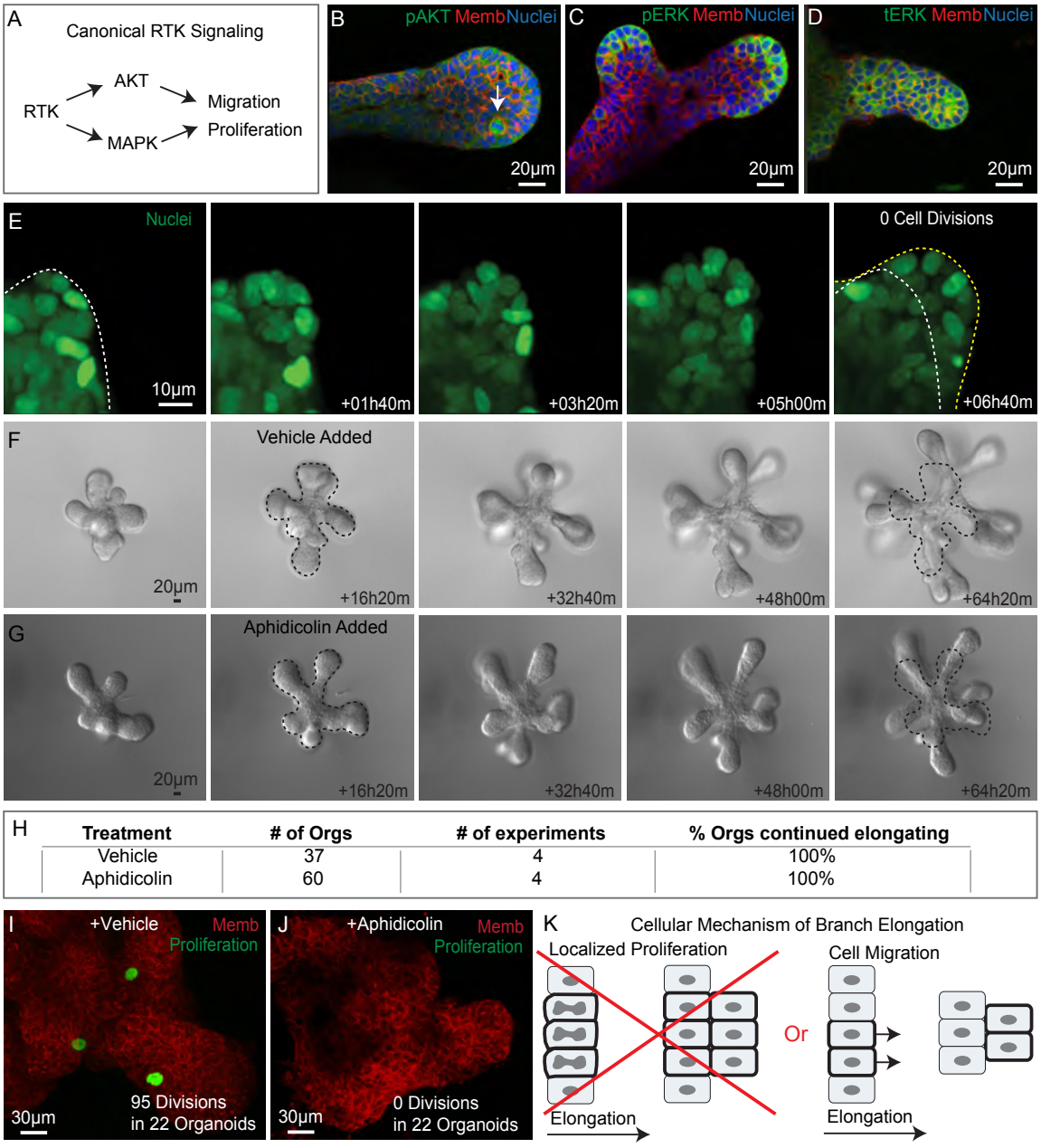

H

Treatment	# of Orgs	# of experiments	% Orgs continued elongating
Vehicle	37	4	100%
Aphidicolin	60	4	100%

Figure 5-2: Elongation occurs concurrently with an increase in cell motility

(A,B,C,D) Z-projection still images from time-lapse confocal movies of organoids expressing histone H2B-GFP (green) and membrane targeted tdTomato (red). (A',B',D') Tracks from cell nuclei from the respective time-lapse movies shown in A, B and D. Cells were tracked for 16 hours 40 minutes (100 frames) and a rainbow color scheme was used to indicate time, with purple indicating the beginning of the movie and red representing the end. (A-A') Nuclei were tracked in the absence of growth factor stimulation. (B-B') Cells were tracked two days after addition of growth factor. (C-C') Organoids underwent active branching 4 days after growth factor addition. (C') Still frames of tracked nuclei from time-lapse movie an actively elongating branch. Track tails represent the cellular movements from the previous 4 hours and 20 minutes. (D-D') Nuclei were tracked from branches after completion of elongation. (E) Mean cell speeds were quantified from organoids in the absence of growth factor (No GF), before branch formation (Day2), during branch elongation (Day4), or after branches finished elongating (Day7). Mean speed was measured as the total track length divided by time and samples were statistically compared using a single factor analysis of variance ($p<0.0001$). (F) Persistence is a measure of track straightness and was quantified as displacement divided by total track length. A single factor analysis of variance ($p<0.0001$) was used to compare persistence measurements from different days.

Figure 5-2

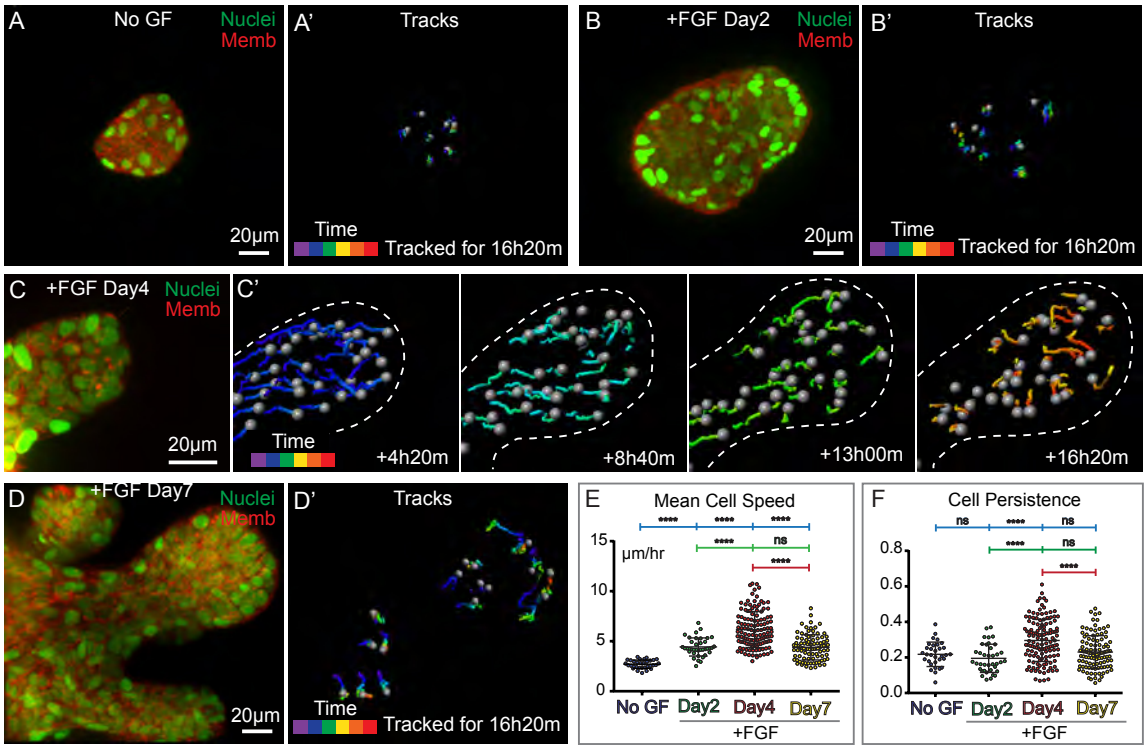
A
No GF
Nuclei
Memb
20μm
A'
Tracks
Time
Tracked for 16h20m
B
+FGF Day2
Nuclei
Memb
20μm
B'
Tracks
Time
Tracked for 16h20m
C
+FGF Day4
Nuclei
Memb
20μm
C'
Time
+4h20m
+8h40m
+13h00m
+16h20m
D
+FGF Day7
Nuclei
Memb
20μm
D'
Tracks
Time
Tracked for 16h20m
E
Mean Cell Speed
μm/hr
15
10
5
0
No GF
Day2
Day4
Day7
+FGF
F
Cell Persistence
0.8
0.6
0.4
0.2
0.0
No GF
Day2
Day4
Day7
+FGF

Figure 5-3: Elongating organoids had regions of differential cell motility

(A) Z-projection of the initial frame of a time-lapse confocal movie of an organoid expressing membrane tdTomato and histone H2B-GFP. Nuclei were tracked from three regions of elongating organoids. Cells contacting the ECM at the leading edge of the branch were considered front cells, cells in the neck of the branch were considered branch cells and cells behind the branch were considered body cells. Cells from these three regions were tracked for quantitative comparison. (A') Frame showing the total track length of cells marked in (A), cells were tracked for 16 hours 20 minutes. Front cell tracks are yellow, branch tracks are red, and body tracks are green. (B) Graphical representation of the mean cell speeds of front, branch, and body cells. A single factor of analysis of variance ($p<0.0001$) was used to statistically compare mean cell speeds. (C) Graph showing persistence measurements from the three cell regions. Persistence measurements were compared by a single factor of analysis of variance ($p<0.05$) and there was no significant difference in persistence between front, branch, or body cells. (D) Z-projection from the first frame of a time-lapse confocal movie. 3D reconstruction and an arrow highlight the nucleus of a branch cell. (D') Track of the branch cell highlighted in (D) showing that a branch cell could move to a front cell position. Dashed line highlights the surface of the organoid branch; track length represent the previous 4 hours 20 minutes of cell movement and track color represent relative time with respect to the length of the movie. (E) Frame shown in z-projection from the beginning of a time-lapse confocal movie. A front cell nucleus is 3D rendered and highlighted with an arrow. (E') The track from the cell highlighted in (E) showing that a front cell could move into the branch. Dashed line shows the outline of the branch; track length shows the previous

4 hours and 20 minutes of cell movement. Color of the track represent relative time from the start of the movie. (F) Table showing the position, front or branch, of cells at the beginning and end of nuclei tracking.

Figure 5-3

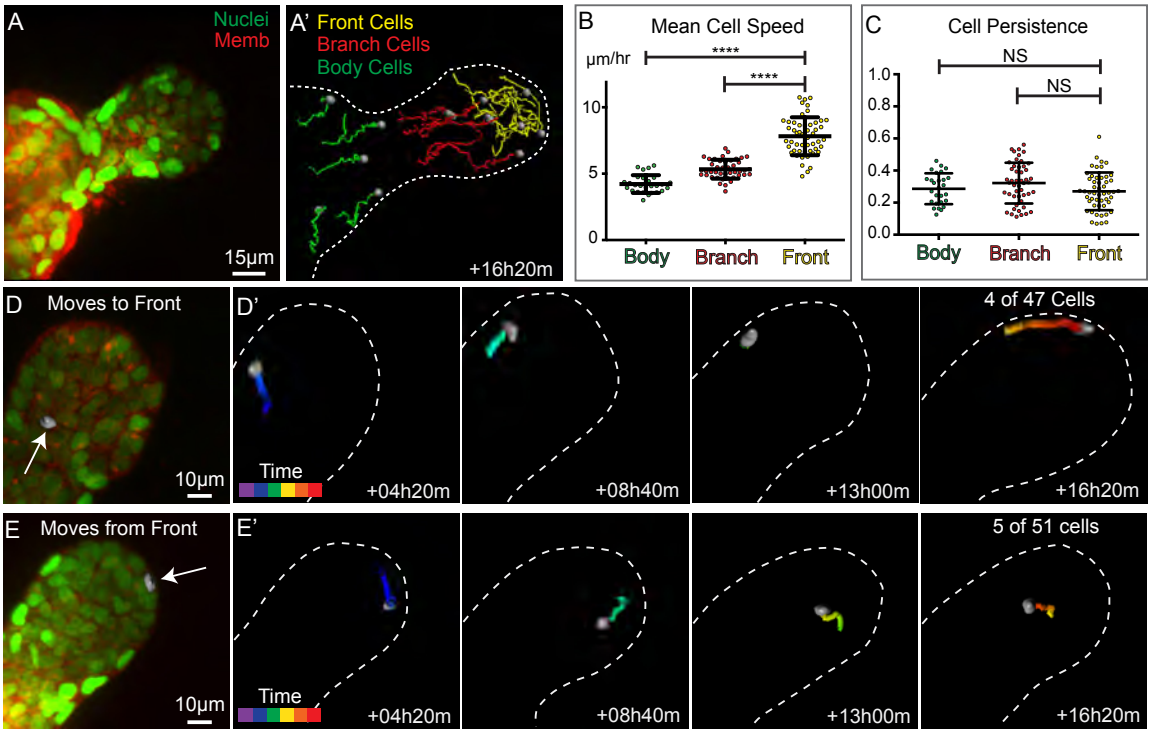

F

Initial Position	Final Position	# 0f Cells	% Cells
Front	Front	43	91.5%
Front	Branch	4	8.5%
Branch	Branch	46	90.2%
Branch	Front	5	9.8%

Figure 5-4: Cells were selectively protrusive in the direction of branch elongation

(A) Schematic demonstrating the overlay method for the circular sector chart. The horizontal axis line is aligned with the directional axis of elongation, moving from left to right. This axis is then used to overlay the circular sector chart on individual cells either within the body of the organoid (body cells), or on cells that are within or give rise to bud initiation or branch elongation (branch cells). (B) An example of a 3D maximum intensity projection is shown of isotropic body cell protrusions over time in an organoid actively undergoing branch elongation. Inset shows a zoomed, 3D rendered cell by Imaris. (C) The percent of protrusions per bin were counted over 3 experiments using 7 organoids, 32 body cells, and 1,244 total counted protrusions. Hotelling's test was used to determine the significance of mean direction; giving a p-value that was not significant (N.S.). (D) An example of a 3D maximum intensity projection is shown of anisotropic branch cell protrusions over time in an organoid actively undergoing branch elongation. Insets show a zoomed, 3D rendered cell by Imaris. (E) The percent of protrusions per bin were counted over 3 experiments using 6 organoids, 36 branch cells, and 1,579 total counted protrusions. Hotelling's test was used to determine the significance of mean direction ($p< 5E^{-5}$). Hotelling's paired test was used to compare the significant in difference of mean direction for the graph in C to the graph in E ($p< 5E^{-5}$).

Figure 5-4

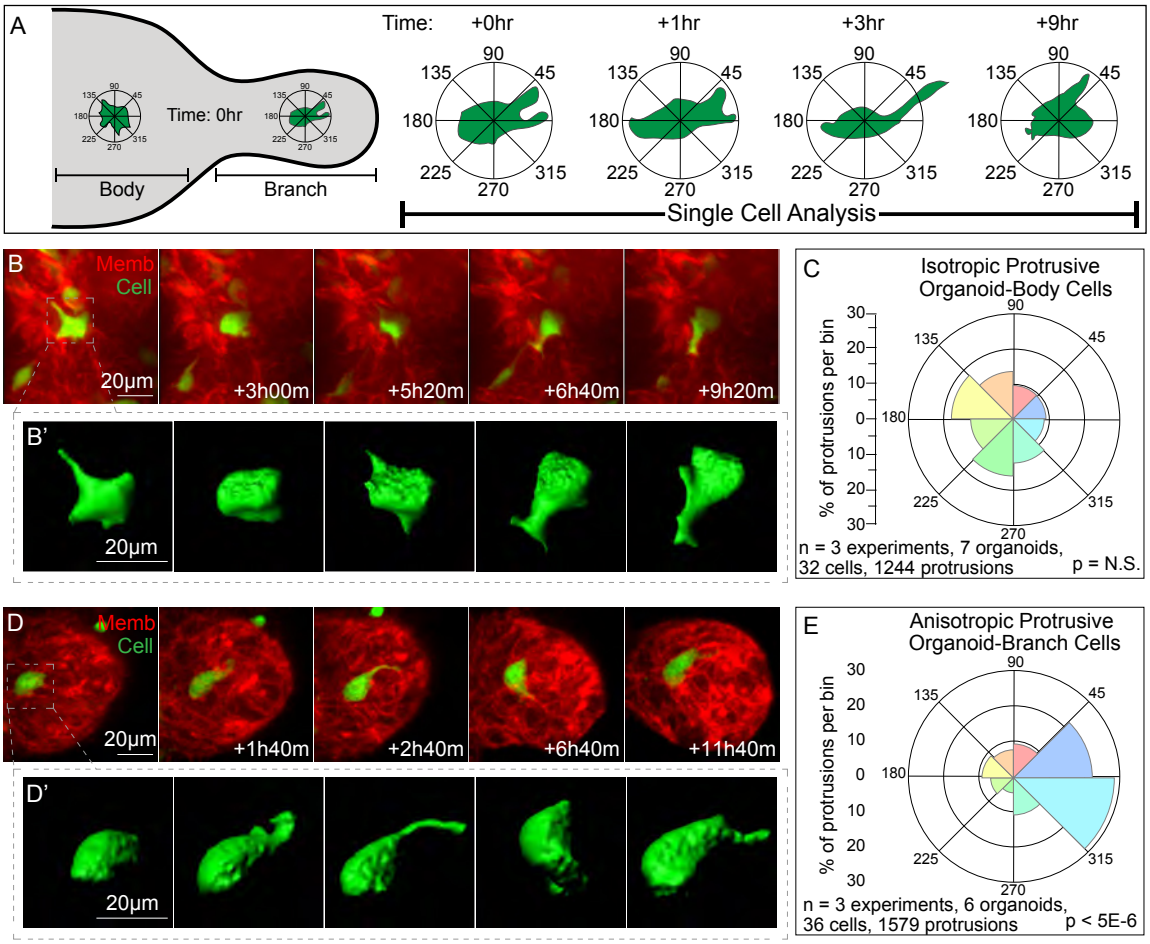
A
Time: 0hr
Body
Branch
Time: +0hr
+1hr
+3hr
+9hr
Single Cell Analysis
B
Memb
Cell
20μm
+3h00m
+5h20m
+6h40m
+9h20m
B'
20μm
C
Isotropic Protrusive
Organoid-Body Cells
% of protrusions per bin
n = 3 experiments, 7 organoids,
32 cells, 1244 protrusions
p = N.S.
D
Memb
Cell
20μm
+1h40m
+2h40m
+6h40m
+11h40m
D'
20μm
E
Anisotropic Protrusive
Organoid-Branch Cells
% of protrusions per bin
n = 3 experiments, 6 organoids,
36 cells, 1579 protrusions
p < 5E-6

Figure 5-5: Rac was required but not sufficient for cell motility and branch elongation

(A) Z-projection of the first frame of a time-lapse movie of an elongating branch. Movies were collected for 4 hours 30 minutes. (A') Frames showing tracked nuclei of cells from the organoid shown in A. Track length represents movements between frames and track color indicates the same cell in successive frames. (B) Z-projection of the organoid shown in A after treatment with Rac inhibitor. Time-lapse movies were collected for 16 hours 20 minutes after Rac inhibition. (B') Frames showing the final 4 hours and 30 minutes of nuclei tracking after Rac inhibition, these frames are shown to match the time interval in A'. Track length represents movements between frames and colors match cells between frames. (C) Quantification of the mean cell speed prior to and after Rac inhibition, cells were tracked for 4 hours and 30 minutes before inhibition and 16 hours 20 minutes after inhibition. Cells were tracked from the same organoid branch pre and post Rac inhibitor and a total of 64 cells were tracked for each condition from 8 organoids from 4 independent experiments. Significance was quantified with a Student's t-test ($p<0.0001$). (D-E) Time-lapse differential interference contrast microscopy movies were collected in the presence or absence of Rac inhibitor to determine if Rac was required for branch elongation. (D) Control organoids continued to elongate during the time of imaging. (E) Organoids were treated with Rac inhibitor during active branch and the treated organoids stopped elongating. (F) Table showing the percentage of organoids that continued to elongate after addition of vehicle or Rac inhibitor. (G) Schematic of the transgene used to express active Rac. An activating mutant of Rac, an internal ribosomal entry site and EGFP were coded downstream of a floxed STOP cassette. (H) Cartoon

depicting the method used to mosaically express the mutant Rac. Adeno-viral delivered cre allowed modulation of the number of cells expressing the mutant protein. (I-I') Frames from a time-lapse movie of control organoids treated with adeno-GFP grown in the presence of growth factor. (J-J') Images from a movie where the organoid was treated with a viral titer of adeno-cre that resulted in expression of mutant Rac in 50-80% of cells. Organoids expressing mutant Rac in the absence of growth factor did not form mammary branches.

Figure 5-5

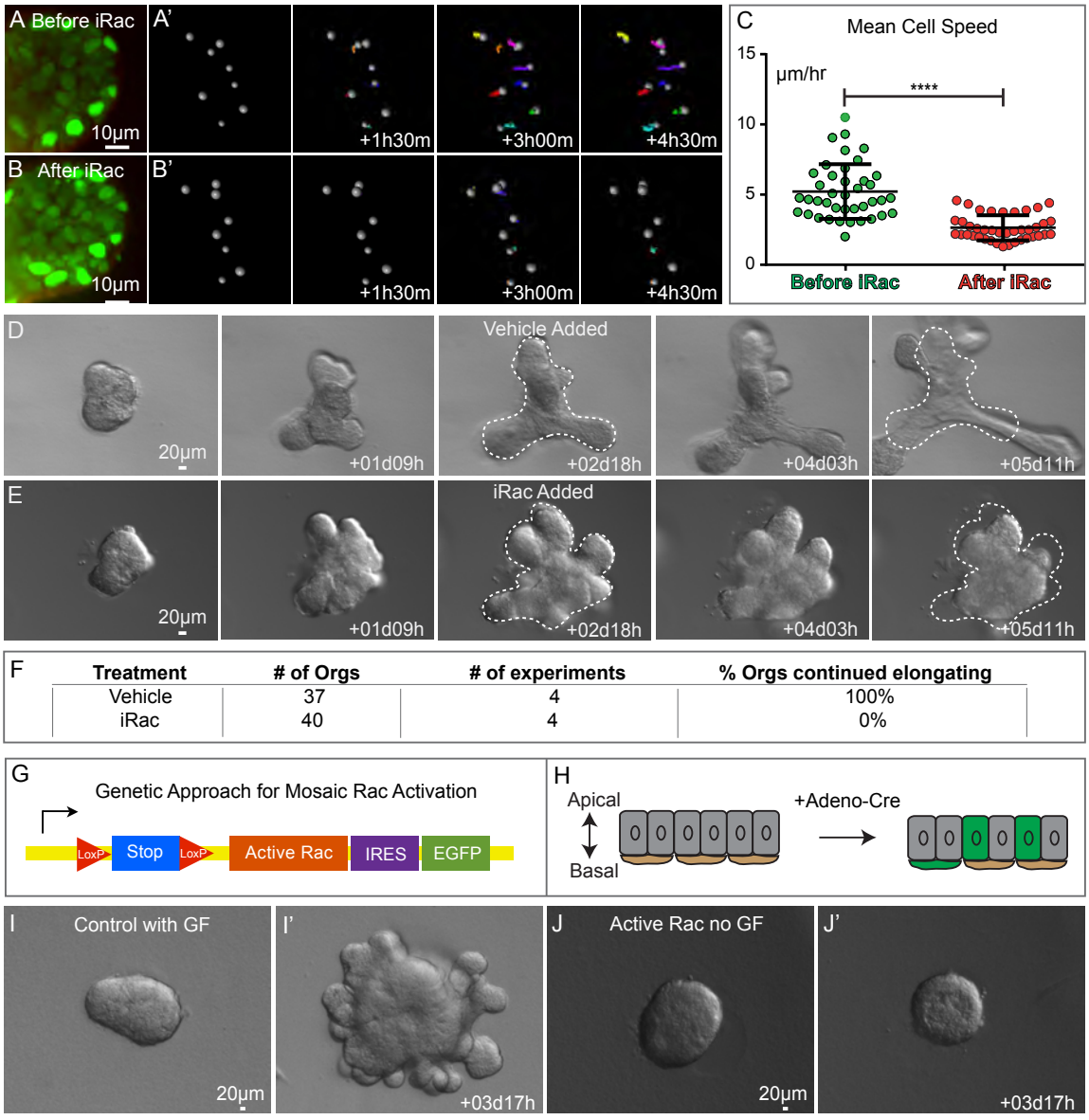

F

Treatment	# of Orgs	# of experiments	% Orgs continued elongating
Vehicle	37	4	100%
iRac	40	4	0%

Figure 5-6: ERK signaling was required for cell motility and branch elongation

(A) Image of the first frame of a time-lapse confocal movie of an actively elongating organoid branch. (A') Nuclei that were tracked from the movie shown in A; cells were tracked for 4 hours and 30 minutes prior to ERK inhibition. Tracks represent the cell movements between the frames and the colors represent the same cell tracked over multiple frames. (B) Still from the first frame of a time-lapse movie of the organoid shown in A after treatment with an ERK inhibitor. Nuclei were tracked for 16 hours 20 minutes after ERK inhibition. (B') Frames showing the final 4 hours and 30 minutes of nuclei tracking after ERK inhibition, these frames were chosen to match up with the time interval shown in A'. Track color shows the same cells over multiple frames and track length shows cell movements. (C) The mean cell speeds were quantified before and after inhibition of ERK signaling. Cells had a significantly increased mean speed before ERK inhibition; significance was tested using a student t-test ($p<0.0001$). (D-E) Still images from differential interference contrast movies of organoid branch elongation in the presence or absence of ERK inhibition. (D) Organoid treated with vehicle continued to elongate after treatment, dashed line represents the organoid area at them of vehicle addition. (E) ERK inhibitor was added as mammary branches were elongating, after ERK inhibition mammary branches stopped elongating. Dashed line shows the organoid area at time of ERK inhibition. (F) Table showing the number and percentage of organoids that continued elongating after addition of vehicle or ERK inhibitor.

Figure 5-6

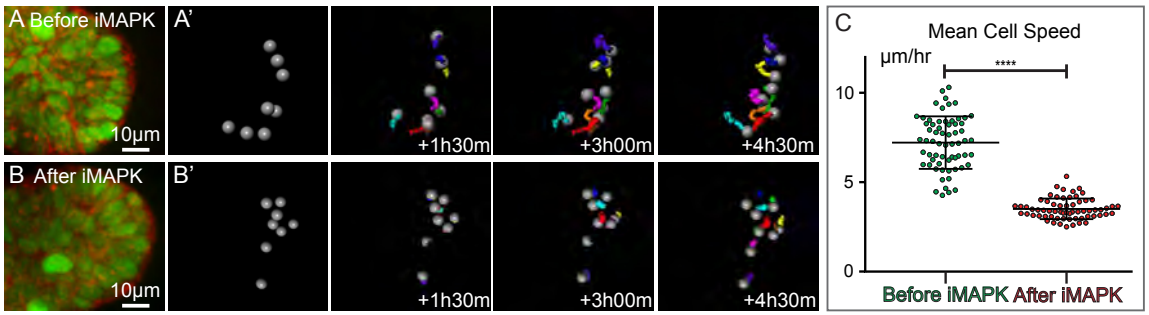

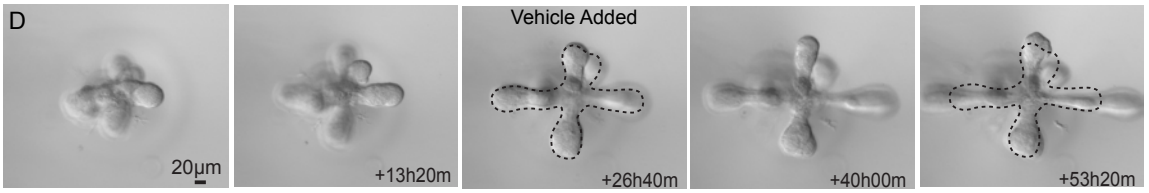

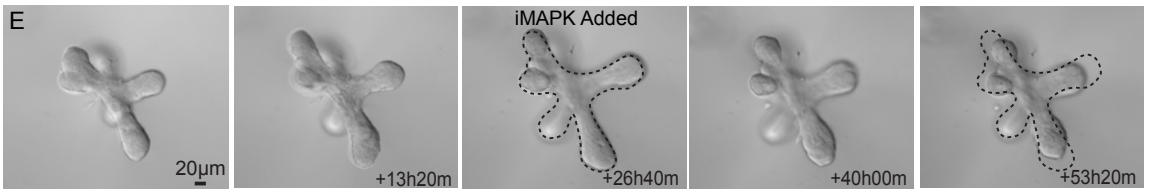

F

Treatment	# of Orgs	# of experiments	% Orgs continued elongating
Vehicle	37	4	100%
iMAPK	54	4	2%

Figure 5-7: MEK signaling was sufficient to initiate mammary branch elongation

(A) Diagram of the transgene used to mosaically express a constitutively active mutant of MEK (MEK1DD). MEK1DD an internal ribosomal entry site, and EGFP were coded downstream of a floxed STOP cassette. (B) Cartoon depicting the method used to mosaically express MEK1DD. (C-D) Frames from time-lapse movies of organoids in the absence of growth factor and in the presence or absence of mutant MEK1DD expression. (C) Organoids grown in the absence of growth factor did not form branches. (D) Organoid treated with adeno-cre to express MEK1DD in 50-80% of cells. The mutant MEK expressing organoids we grown in the absence of growth factor and were able to initiate mammary branches. (E) Graph representing the percentage of organoids that initiated branches in the presence or absence of growth factor or expressing MEK1DD. (F) Still frames from time-lapse confocal movies of organoids expressing mutant MEK (green), as indicated by EGFP expression, and treated with a cytosolic dye (red). MEK1DD positive cells functioned as the elongation front of branches in organoids mosaically expressing the mutant protein.

Figure 5-7

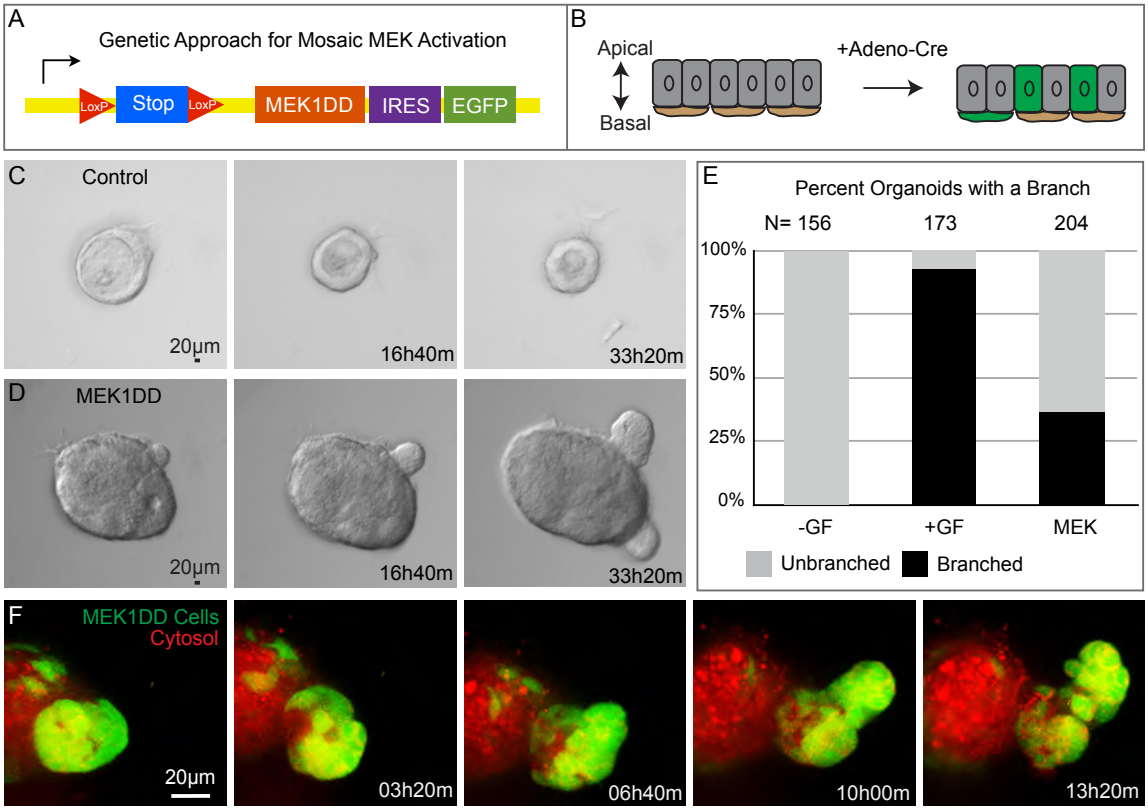
A
Genetic Approach for Mosaic MEK Activation
LoxP
Stop
LoxP
MEK1DD
IRES
EGFP
B
Apical
Basal
+Adeno-Cre
C
Control
20µm
16h40m
33h20m
D
MEK1DD
20µm
16h40m
33h20m
E
Percent Organoids with a Branch
N= 156
173
204
100%
75%
50%
25%
0%
-GF
+GF
MEK
Unbranched
Branched
F
MEK1DD Cells
Cytosol
20µm
03h20m
06h40m
10h00m
13h20m

Chapter 6

Conclusions

Epithelial tubes function as barriers creating the chemically distinct spaces used for gas and fluid exchange. To achieve this role, epithelial cells are connected with junctional complexes that provide integrity to the epithelium and make epithelial sheets impermeable to fluids and gases. Epithelial cells are also polarized, using a series of molecular complexes to distinguish between surfaces facing the luminal space, the extracellular matrix, or other cells. The structural complexity of epithelial cells makes it challenging to understand how individual cell behaviors, such as proliferation or cell migration, can achieve the large scale epithelial remodeling required for development of epithelial organs. Our work studying mouse mammary branching morphogenesis shows that one solution to this problem is to simply lose the structural complexity allowing cells the freedom to proliferate and migrate.

The primary mammary duct is established during embryogenesis and remains essentially quiescent until the onset of puberty[1]. Prior to puberty epithelial ducts are bilayered, with apical luminal epithelial cells and basal myoepithelial cells, and are polarized along the apico-basal axis[1,2]. Puberty results in release of circulating steroid hormones that stimulate local receptor tyrosine kinase (RTK) signaling which initiates mammary branching morphogenesis[3,4,5]. The first morphological evidence of branching morphogenesis is the formation of stratified epithelial structures known as terminal end buds (TEBs) at the ductal tips[3]. TEBs are the morphogenically active unit of the elongating mammary epithelium and impaired TEB formation blocks ductal elongation[3,5]. Despite extensive knowledge of the genetics and signaling pathways that drive mammary

duct elongation we have only recently begun to understand how the cells within the epithelium respond to these signals to achieve branching morphogenesis.

Organotypic culture and advances in time-lapse microscopy allowed the first real-time cellular resolution study of mammalian epithelial branching morphogenesis[6,7,8,9,10]. Two unexpected findings came from time-lapse study of mammary epithelial branch elongation. First, the elongation front of the epithelium is highly disorganized lacking apico-basal polarity[10]. Second, there are no clear leader cells and the elongation front lacked the forward directed protrusions that are characteristic of migrating cells[10]. These results indicated that the TEB was a novel epithelial structure and that the TEB was using a novel cellular mechanism to elongate the mammary duct. The bulk of this thesis work has focused on understanding the structure of the TEB and identifying the cellular mechanisms that underlie TEB formation and mammary duct elongation.

In Ewald et al., 2008 it was shown that the stratified mammary epithelium had miss-localized E-cadherin, β-catenin, APKC-ζ, and ZO-1 indicating incomplete apico-basal polarity. These results lead us to assess the cell adhesion in the stratified epithelium using transmission and scanning electron microscopy. At the ultra-structural level the stratified epithelium lacked tight junctions, had few desmosomes and had loose interdigitating membrane protrusions in place of tight cell-cell contacts[11]. Cells within the stratified epithelia lacked the simple cuboidal shape common of ductal epithelium and instead we observed heterogeneity in cell shape including cells that appeared to be protrusive and

migratory[11]. We next asked if cells were indeed migratory within epithelium by scatter labeling single cells with cytosolic EGFP and following the movements in real-time. Individual cells were highly motile within the epithelium displaying a front-rear polarity that is commonly associated with mesenchymal cell migration. These results were of particular interest because loss of apico-basal polarity and cell-adhesion as well as acquisition of cell motility is required for metastasis[12,13,14]. Here we showed that these metastatic features might be conserved from normal development and more interestingly that during development these processes were regulated such that they caused no danger to the animal.

We next sought to determine the cellular mechanisms that resulted in epithelial stratification and polarity-loss during TEB formation. Using time-lapse microscopy and immuno-fluorescence we determined that stratification was initiated through vertical divisions of apically localized luminal epithelial cells[15]. This result answered an ongoing question in the field as there had been conflicting reports that stratification was initiated by basal[16] or apical cells[17]. Stratification initiating from the apical side was also interesting because other epithelial organs such as the skin stratify exclusively through proliferation of basal-localized cells[18]. We next showed that the vertical apical cell divisions directly resulted in the loss of apico-basal polarity by generating a single unpolarized daughter cell with each cell division[15]. Finally we observed proliferation in the unpolarized cell population, which further drove stratification of the epithelium and TEB formation[15].

Epithelial stratification and polarity-loss are amongst the earliest steps of tumor progression[19,14] which lead us to ask if epithelium would stratify from the apical side in response to acute oncogene activation. To test this we conditionaly and mosaically expressed an activating mutant of the oncogene ErbB2[20]. The mutant ErbB2 was sufficent to stratify the epithelium and oncogene induced stratification was initiated by vertical divisions of apical cells[15]. ErbB2 has also been shown to result in stratification of non-transformed mammary epithelial cell (MCF-10A) acini[21] but ErbB2 induced stratification in of MCF-10A acini was achieved by cell migration and not proliferation[22]. The different results in these two systems are likely derived from the fact that MCF-10A acini lack myoepithelial cells and tight junctions[23]. This result showed a direct example of conservation of a developmental process during cancer progression.

Having established a mechanism for TEB formation we wanted to determine how cells within the TEB elongated the mammary ducts. The best understood examples of tublogenesis are the Drosophila trachea and salivary gland. Drosophila tubes are elongated by collective cell migration of a chain of cells attached to a specified protrusive leader cell[24,25]. A similar mechanism is observed during zebrafish kidney morphogenesis[26]. However, this mechanism was ruled out for the mammary duct elongation due to a lack of leader cells or ECM directed protrusions[10]. This left us with two logical mechanisms for how the mammary duct could elongate: localized

proliferation or a novel mechanism of collective cell migration that lacked protrusive leader cells.

To begin to distinguish between these mechanisms of duct elongation we probed signaling pathways downstream of RTK signaling. We found specific activation of the pro-proliferation mitogen activated protein kinase (MAPK) signaling pathway at the leading edge of elongating ducts. This led us to hypothesize that MAPK signaling was stimulating localized proliferation at the front, but this proved untrue as mammary ducts could continue to elongate in the absence of proliferation and even after inhibition of proliferation. Instead we observed that mammary ducts were elongated by collective cell migration and that there was a subset of hyper-motile cells at the elongation front. The localized MAPK signaling overlapped with the highly motile cell population so we used a small molecule inhibitor to test if MAPK was required for cell motility and duct elongation. Inhibition of MAPK signaling blocked both cell motility and duct elongation. We then tested if MAPK was sufficient to drive duct elongation by mosaically expressing a constitutively active mutant of a member of the MAPK cascade. Expression of the activated mutant was sufficient to drive elongation and the elongation front was composed of mutant cells.

MAPK signaling is required for branching morphogenesis of the mouse submandibular gland[27], mouse kidney[28], rat[29], and mouse mammary gland[9] but the cellular mechanism down stream of MAPK signaling was unknown. We report the novel finding that MAPK

signaling acts by stimulating cell motility, specifically at the elongation front, and that this motility is required for mammary branch elongation. This mechanism is potentially generalizable to other epithelial mammalian organs, as localized high motility cells have also been observed at the front of the elongating mouse salivary gland[30]. Similarly, localized MAPK signaling has been observed at the tip of the Wolffian duct where the ureteric bud initiates[31]. Finally, individual cell migration has been observed in the mouse salivary gland[32] and mouse ureteric bud[33]. In the future it will be interesting to see the degree to which other mammalian epithelial tubes have conserved mechanism of elongation as compared to what we observe in the mammary epithelium.

The overarching theme of this dissertation is that epithelia are dynamic, and not simply in a motile sense; cells also rearrange, dismantle, and rebuild junctions and apico-basal polarity. A second major theme is that the defining features of cancer, polarity-loss, proliferation, and cell migration, are also common features of mammary epithelial development. This produces the questions how are these cell behaviors regulated and safe in the developmental context and how is this regulation lost during tumor progression? This thesis has primarily focused on describing the cellular behaviors that drive branching morphogenesis and will hopefully provide a platform from which we can start dissecting the molecular mechanisms that drive mammary development. By better understanding the molecular biology of normal development we will gain insight into what is mis-regulated in cancer, which will hopefully generate new ideas for how we treat breast cancer.

References

1 Hogg, N. A., Harrison, C. J. and Tickle, C. (1983). Lumen formation in the developing mouse mammary gland. J. Embryol. Exp. Morphol. 73, 39-57.

2 Huebner, R. J. & Ewald, A. J. Cellular foundations of mammary tubulogenesis. Semin Cell Dev Biol 31, 124-131, (2014).

3 Sternlicht, M. D. (2006). Key stages in mammary gland development: the cues that regulate ductal branching morphogenesis. Breast Cancer Res. 8, 201.

4 Hennighausen, L. and Robinson, G. W. (2005). Information networks in the mammary gland. Nat. Rev. Mol. Cell Biol. 6, 715-725.

5 McNally, S., and Martin, F. (2011). Molecular regulators of pubertal mammary gland development. Ann Med 43, 212-234.

6 Simian, M., Hirai, Y., Navre, M., Werb, Z., Lochter, A. and Bissell, M. J. (2001). The interplay of matrix metalloproteinases, morphogens and growth factors is necessary for branching of mammary epithelial cells. Development 128, 3117-3131.

7 Wiseman, B. S., Sternlicht, M. D., Lund, L. R., Alexander, C. M., Mott, J., Bissell, M. J., Soloway, P., Itohara, S. and Werb, Z. (2003). Site-specific inductive and inhibitory activities of MMP-2 and MMP-3 orchestrate mammary gland branching morphogenesis. J. Cell Biol. 162, 1123-1133.

8 Sternlicht, M. D., Sunnarborg, S. W., Kouros-Mehr, H., Yu, Y., Lee, D. C. and Werb, Z. (2005). Mammary ductal morphogenesis requires paracrine activation of stromal EGFR via ADAM17-dependent shedding of epithelial amphiregulin. Development 132, 3923-3933.

9 Fata, J. E., Mori, H., Ewald, A. J., Zhang, H., Yao, E., Werb, Z. and Bissell, M. J. (2007). The MAPK(ERK-1,2) pathway integrates distinct and antagonistic signals from TGFalpha and FGF7 in morphogenesis of mouse mammary epithelium. Dev. Biol. 306, 193-207.

10 Ewald, A. J., Brenot, A., Duong, M., Chan, B. S. and Werb, Z. (2008). Collective epithelial migration and cell rearrangements drive mammary branching morphogenesis. Dev. Cell 14, 570-581.

11 Ewald, A.J., Huebner, R.J., Palsdottir, H., Lee, J.K., Perez, M.J., Jorgens, D.M., Tauscher, A.N., Cheung, K.J., Werb, Z., and Auer, M. (2012). Mammary collective cell migration involves transient loss of epithelial features and individual cell migration within the epithelium. J Cell Sci 125, 2638-2654.

12 Rosen, P. P. (2001). Rosen's Breast Pathology. Philadelphia, PA: Lippincott Williams and Wilkins.

13 Feigin, M. E. and Muthuswamy, S. K. (2009). Polarity proteins regulate mammalian cell-cell junctions and cancer pathogenesis. Curr. Opin. Cell Biol. 21, 694-700.

14 Huang, L. and Muthuswamy, S. K. (2010). Polarity protein alterations in carcinoma: a focus on emerging roles for polarity regulators. Curr. Opin. Genet. Dev. 20, 41-50.

15 Huebner, R.J., Lechler, T., and Ewald, A.J. (2014) Developmental stratification of mammary epithelium occurs through symmetry-breaking vertical divisions of apically positioned luminal cells. Development 141, 1085-1094.

16 Regan, J.L., Sourisseau, T., Soady, K., Kendrick, H., McCarthy, A., Tang, C., Brennan, K., Linardopoulos, S., White, D.E., and Smalley, M.J. (2013). Aurora a kinase regulates mammary epithelial cell fate by determining mitotic spindle orientation in a notch-dependent manner. Cell Rep 4, 110-123.
17 Taddei, I., Deugnier, M.A., Faraldo, M.M., Petit, V., Bouvard, D., Medina, D., Fassler, R., Thiery, J.P., and Glukhova, M.A. (2008). Beta1 integrin deletion from the basal compartment of the mammary epithelium affects stem cells. Nat Cell Biol 10, 716-722.
18 Lechler, T., and Fuchs, E. (2005). Asymmetric cell divisions promote stratification and differentiation of mammalian skin. Nature 437, 275-280.
19 Ewing, J. (1933). Lectures on tumor pathology, 2nd edn (New York, Cornell University Medical School, Class of 1934)
20 Xie, W., Chow, L.T., Paterson, A.J., Chin, E., and Kudlow, J.E. (1999). Conditional expression of the ErbB2 oncogene elicits reversible hyperplasia in stratified epithelia and up-regulation of TGFalpha expression in transgenic mice. Oncogene 18, 3593-3607.
21 Muthuswamy, S.K., Li, D., Lelievre, S., Bissell, M.J., and Brugge, J.S. (2001). ErbB2, but not ErbB1, reinitiates proliferation and induces luminal repopulation in epithelial acini. Nat Cell Biol 3, 785-792.
22 Leung, C.T., and Brugge, J.S. (2012). Outgrowth of single oncogene-expressing cells from suppressive epithelial environments. Nature 482, 410-413.
23 Underwood, J.M., Imbalzano, K.M., Weaver, V.M., Fischer, A.H., Imbalzano, A.N., and Nickerson, J.A. (2006). The ultrastructure of MCF-10A acini. J Cell Physiol 208, 141-148.
24 Lubarsky, B. & Krasnow, M. A. Tube morphogenesis: making and shaping biological tubes. Cell 112, 19-28, (2003).
25 Kerman, B. E. & Andrew, D. J. Staying alive: dalmation mediated blocking of apoptosis is essential for tissue maintenance. Dev Dyn 239, 1609-1621, (2010).
26 Vasilyev, A. *et al.* Collective Cell Migration Drives Morphogenesis of the Kidney Nephron. PLoS Biol. 7, e9, (2009).
27 Kashimata, M. *et al.* The ERK-1/2 signaling pathway is involved in the stimulation of branching morphogenesis of fetal mouse submandibular glands by EGF. Dev Biol 220, 183-196, (2000).
28 Fisher, C. E., Michael, L., Barnett, M. W. & Davies, J. A. Erk MAP kinase regulates branching morphogenesis in the developing mouse kidney. Development 128, 4329-4338, (2001).
29 Kling, D. E. *et al.* MEK-1/2 inhibition reduces branching morphogenesis and causes mesenchymal cell apoptosis in fetal rat lungs. American journal of physiology. Lung cellular and molecular physiology 282, L370-378, (2002).
30 Hsu, J. C. *et al.* Region-specific epithelial cell dynamics during branching morphogenesis. Dev Dyn 242, 1066-1077, (2013).
31 Hoshi, M., Batourina, E., Mendelsohn, C. & Jain, S. Novel mechanisms of early upper and lower urinary tract patterning regulated by RetY1015 docking tyrosine in mice. Development 139, 2405-2415, (2012).
32 Larsen, M., Wei, C. & Yamada, K. M. Cell and fibronectin dynamics during branching morphogenesis. J Cell Sci 119, 3376-3384, (2006).

33 Chi, X. *et al.* Ret-dependent cell rearrangements in the Wolffian duct epithelium initiate ureteric bud morphogenesis. Dev Cell 17, 199-209, (2009).

Robert J. Huebner

Johns Hopkins University School of Medicine
Department of Cell Biology
855 N. Wolfe St., 480.26 Rangos Bldg.
Baltimore, MD 21205
(410) 614-3382

508 Carroll Ave
Mt Airy, MD 21771
(443) 863-0949

Education:

University of Maryland, Baltimore County, Baltimore, Maryland, 2002-2006
- B.S. in Biological Science

Johns Hopkins University School of Medicine, Baltimore, Maryland, 2009-Present
- Ph.D. in Biochemistry, Cell and Molecular Biology, Department of Cell Biology.

Research experience:

Doctoral Research: Department of Cell Biology, Johns Hopkins University School of Medicine, 2009-Present
Advisor: Andrew J. Ewald
- The Ewald lab uses the mouse mammary gland as a model to investigate key steps in epithelial development and tumor progression.
  - Project 1: Identified a novel cell division that drove polarity-loss and epithelial stratification in response to developmental signaling and acute oncogene activation.
  - Project 2: Determined that mammary branch elongation was achieved through collective migration of high motility low-polarity epithelial cells and that MAPK signaling was required and sufficient for branch elongation.

Post-Bacc IRTA Fellow: Laboratory of Cell Biology, National Heart Lung and Blood Institute, National Institutes of Health, 2007-2009
Advisor: Julie Donaldson
- Identified novel proteins trafficking in the clathrin-independent Arf6 regulated endocytosis pathway

Undergraduate Honors Research: University of Maryland, Baltimore County, 2005-2006
Advisor: Nessly Craig
- Investigation of Ribosomal RNA maturation from primary transcripts to mature rRNAs

Awards and Honors:

- Society for Developmental Biology travel award, 2014
- Selected for a mini symposium talk at the 2013 American Society for Cell Biology annual meeting, New Orleans Louisiana.
- Lewis Travel Award, from JHUSOM Department of Cell Biology, 2013
- American Society for Cell Biology Travel award, 2013
- Selected for Short Platform Talk at 71st Annual Society of Developmental Biology International Meeting, Montreal Canada 2012.
- National Institutes of Health Post-Bacc Intramural Research Training Award Fellowship, 2007-2009
- University of Maryland, Baltimore County, Departmental Honors, 2006
- University of Maryland, Baltimore County, Academic Honors, 2006

Publications:

Robert J. Huebner and Andrew J. Ewald. Mammary branch elongation is achieved by localized MAPK signaling in high motility epithelial cell clusters. (In Review at Dev. Cell)

Kim-Vy Nguyen-Ngoc, Eliah R. Shamir, Robert J. Huebner, Jennifer N. Beck, Kevin J. Cheung, and Andrew J. Ewald (2015). 3D culture assays of murine mammary branching morphogenesis and epithelial invasion. Methods Mol. Biol. 1189; 135-62.

Robert J. Huebner and Andrew J. Ewald (2014). *Cellular foundations of mammary tubulogenesis.* Sem Cell Dev. Biol. 31: 124-131.

Robert J. Huebner, Terry Lechler and Andrew J. Ewald (2014). Developmental stratification of the mammary epithelium occurs through symmetry-breaking vertical divisions of apically positioned luminal cells. Development 141: 1058-1094.

Allison Suarez, Tasuku Ueno, Robert Huebner, J. Michael McCaffery and Takanari Inoue (2014). Bin/Amphiphysin/Rvs (BAR) family members bend membranes in cells. Sci. Rep. 4: 1-6.

Andrew J. Ewald, Robert J. Huebner, Hildur Palsdottir, Jessie K. Lee, Melissa J. Perez, Danielle M. Jorgens, Andrew N. Tauscher, Kevin J. Cheung, Zena Werb, and Manfred Auer (2012). Mammary collective cell migration involves transient loss of epithelial features and individual cell migration within the epithelium. JCS 125: 2638-2654.

Higginson, J.D, C.A. Ester, R.J. Huebner, N. Porat-Shliom, R. Weigert, W.W. Wu, R. Shen, and J.G. Donaldson (2009). Discovery of New Cargo Proteins that

Enter Cells Through Clathrin-Independent Endocytosis, Traffic 10: 590-599. Co-first author.

Presentations:

Talks

Robert J. Huebner, Terry Lechler and Andrew J. Ewald. Vertical division of luminal cells drives developmental and oncogene-induced mammary epithelial stratification. Presented at American Society for Cell Biology annual meeting. New Orleans, LA (2013).

Robert J. Huebner, Terry Lechler and Andrew J. Ewald. Asymmetric divisions of luminal cells produces low-polarity high motility cells that collectively migrate to form mammary ducts. Presented at: 71st annual Society of Developmental Biology international meeting. Montreal, Canada (2012)

Robert J. Huebner and Andrew J. Ewald. Normal and neoplastic stratification result from vertical divisions of luminal epithelial cells. Presented at: Johns Hopkins Biochemistry Cell and Molecular Biology annual retreat. Baltimore, MD (2012)

Posters

Robert J. Huebner and Andrew J. Ewald. Mammary ducts are elongated by MAPK induced high motility cell clusters. Presented at: 73rd annual Society of Developmental Biology meeting. Seattle, WA (2014).

Robert J. Huebner, Terry Lechler and Andrew J. Ewald. Asymmetric division of luminal cells drives normal and ErbB2 induced epithelial stratification. Presented at: 72nd annual Society of Developmental Biology international meeting. Cancun, Mexico (2013).

Robert J. Huebner, and Andrew J. Ewald. Annually presented at Johns Hopkins Safeway breast cancer research retreat. Baltimore, MD (2010-2013).

Robert J. Huebner, and Andrew J. Ewald. Annually presented at Johns Hopkins Biochemistry Cell and Molecular Biology annual retreat. Baltimore, MD (2010-2013).

C.A. Ester, R.J. Huebner, J. Higginson, N. Porat-Shilom, R. Weigert, and J.G. Donaldson. New trafficking routes for cargo proteins entering cells via clathrin-independent endocytosis. Poster presented at: American Society for Cell Biology annual meeting, San Francisco, CA (2008). Co-presenter

Research Courses:

2015 Cold Spring Harbor Xenopus Course